

DOCTORAL THESIS

Characterization of Bacterial Dye-Decolorizing Peroxidases

Hegne Pupart

TALLINN UNIVERSITY OF TECHNOLOGY
DOCTORAL THESIS
72/2024

Characterization of Bacterial Dye-Decolorizing Peroxidases

HEGNE PUPART



TALLINN UNIVERSITY OF TECHNOLOGY

School of Science

Department of Chemistry and Biotechnology

This dissertation was accepted for the defence of the degree of Doctor of Philosophy in Chemistry 20/11/2024

Supervisor: Dr. Tiit Lukk
School of Science, Department of Chemistry and Biotechnology
Tallinn University of Technology, Tallinn, Estonia

Co-supervisor: Assoc. Prof. Priit Väljamäe
Faculty of Science and Technology, Institute of Molecular and Cell Biology
University of Tartu, Tartu, Estonia

Co-supervisor: Dr. Priit Eek
School of Science, Department of Chemistry and Biotechnology
Tallinn University of Technology, Tallinn, Estonia

Opponents: Prof. Timothy Bugg
Faculty of Science, Engineering and Medicine, Department of Chemistry
University of Warwick, Coventry, United Kingdom

Prof. Ago Rinke
Faculty of Science and Technology, Institute of Chemistry
University of Tartu, Tartu, Estonia

Defence of the thesis: 20/12/2024, Tallinn

Declaration:

I hereby declare that this doctoral thesis, submitted for the doctoral degree at Tallinn University of Technology, is my original investigation and achievement, and has not been previously submitted for a doctoral or an equivalent academic degree.

Hegne Pupart



European Union
European Regional
Development Fund



Investing
in your future

signature

Copyright: Hegne Pupart, 2024

ISSN 2585-6898 (publication)

ISBN 978-9916-80-238-0 (publication)

ISSN 2585-6901 (PDF)

ISBN 978-9916-80-239-7 (PDF)

DOI <https://doi.org/10.23658/taltech.72/2024>

Printed by EVG Print

Pupart, H. (2024). *Characterization of Bacterial Dye-Decolorizing Peroxidases* [TalTech Press].
<https://doi.org/10.23658/taltech.72/2024>

TALLINNA TEHNIKAÜLIKOOL
DOKTORITÖÖ
72/2024

Bakteriaalsete värvi pleegitavate peroksüdaaside iseloomustamine

HEGNE PUPART



Contents

List of publications	7
Author's contribution to the publications	8
Introduction	9
Abbreviations	10
1 Review of the literature	12
1.1 Lignocellulose	12
1.1.1 Degradation in nature	13
1.1.2 Lignin as a feedstock	14
1.2 Peroxidases	15
1.2.1 Classification	16
1.2.2 General catalytic cycle	17
1.3 Dye-decolorizing peroxidases	18
1.3.1 Discovery	18
1.3.2 Classification	18
1.3.3 Overall structure	19
1.3.4 Catalytic cycle	20
1.3.5 Potential biological functions	22
1.3.6 Investigation of kinetics	23
2 Aims of the study	25
3 Materials and methods	26
4 Results	28
4.1 General characterization of ScDyPs (Publication I)	28
4.2 In-depth kinetic characterization of DyPs (Publications II & III)	28
4.2.1 Biphasic kinetics of ScDyPB (Publication III)	28
4.2.2 Kinetic study of ThDyP with substrate inhibition (Publication II)	30
4.2.3 Investigations of inactivation (Publications II & III)	31
4.2.4 Mechanism explaining substrate inhibition by both substrates (Publication II)	32
4.2.5 Structure of ThDyP (Publication II)	33
4.2.6 Investigations of positive cooperativity (Publication II)	34
4.2.7 Model explaining positive cooperativity together with substrate inhibition (Publication II)	35
4.2.8 Dependence of the activity on the concentration of ScDyPB (Publication III)	36
4.3 Analysis of the size distribution of ScDyPB (Publication III)	38
4.4 ScDyPs acting on organosolv lignin (Publication I)	39
5 Discussion	41
5.1 The non-conventional kinetics of DyPs	41
5.1.1 Substrate inhibition	41
5.1.2 Positive cooperativity	42
5.1.3 Biphasic kinetics	42
5.2 Oligomeric states of DyPs	43
5.2.1 Relationships between catalytic activity and degree of oligomerization of ScDyPB.	43
5.3 Activity on organosolv lignin	46
Conclusions	47

References	48
Acknowledgements.....	60
Abstract.....	61
Lühikokkuvõte.....	63
Appendix 1	65
Appendix 2	87
Appendix 3	115
Curriculum vitae.....	135
Elulookirjeldus.....	137

List of publications

Current thesis has been prepared based on the following publications:

- I **Pupart, H.**; Jõul, P.; Bramanis, M. I.; Lukk, T. Characterization of the Ensemble of Lignin-Remodeling DyP-Type Peroxidases from *Streptomyces coelicolor* A3(2). *Energies* **2023**, *16*, 1557. <https://doi.org/10.3390/en16031557>.
- II **Pupart, H.**; Lukk, T.; Väljamäe, P. Dye-decolorizing peroxidase of *Thermobifida halotolerance* displays complex kinetics with both substrate inhibition and apparent positive cooperativity. *Arch Biochem Biophys* **2024**, *754*, 109931. <https://doi.org/10.1016/j.abb.2024.109931>.
- III **Pupart, H.***; Vastšjonok, D.*; Lukk, T. and Väljamäe, P. Dye-Decolorizing Peroxidase of *Streptomyces coelicolor* (ScDyPB) Exists as a Dynamic Mixture of Kinetically Different Oligomers. *ACS Omega* **2024**, *9*, 3866–3876. <https://doi.org/10.1021/acsomega.3c07963>.

*These authors contributed equally.

Author's contribution to the publications

Contribution to the papers in this thesis are:

- I The author contributed to designing the experiments, performing experiments, analyzing the data, and writing the manuscripts, except cloning of ScDyPB.
- II The author contributed to designing the experiments, performing experiments, analyzing the data, and writing the manuscripts, except the derivation of rate equations.
- III The author contributed to designing the experiments, performing experiments, analyzing the data, and writing the manuscripts, except cloning of ScDyPB and derivation of rate equations.

Introduction

We live in a dynamic and demanding world where society heavily relies on fossil feedstocks. With the global population steadily increasing, the demand for energy continues to rise, but these resources are rapidly depleting. It is estimated that by 2060, all fossil feedstocks will be exhausted if current consumption patterns persist. Therefore, exploring sustainable alternatives and innovative approaches is crucial to meet the needs of the society and sustain our way of life. One promising strategy to reduce our reliance on fossil resources is transitioning to plant-based feedstocks and harnessing the potential of lignin – the nature’s primary source of aromatic chemistry. However, lignin presents a formidable challenge as a biopolymer due to its complex structure and rigid nature. To unlock its potential value, it is essential to improve its utilization efficiency by breaking it down into lower molecular weight fragments. Lignin depolymerization can be achieved by various lignin-degrading enzymes, serving as promising tools. Finding novel efficient enzymes for this purpose is of outmost importance. The Laboratory of Wood Chemistry is committed to the study of lignin and lignin-degrading enzymes. Our research predominately focuses on metalloenzymes sourced from soil bacteria, as well as those derived from microorganisms thriving in extreme conditions.

My research focuses on peroxidases, particularly on a subset known as dye-decolorizing peroxidases (DyPs). Although DyPs share many similarities with classic peroxidases, they also exhibit distinct features that set them apart. One notable aspect of DyPs is their demonstrated activity on lignin, representing an area of keen interest for our laboratory. This thesis aims to (i) explore novel enzymes with lignin-degrading activity, (ii) explain the complex non-Michaelis-Menten kinetics of DyPs, and (iii) investigate the relationship between the degree of oligomerization and catalytic activity.

Abbreviations

ABTS	2,2'-azino-bis(3-ethylbenzothiazoline-6-sulfonic acid)
APX	ascorbate peroxidase
AQ	anthraquinone
Cpd I	compound I
Cpd II	compound II
Cpd III	compound III
CcP	cytochrome c peroxidase
2,6-DMP	2,6-dimethoxyphenol
DLS	dynamic light scattering
DyP	dye-decolorizing peroxidase
E_0	total concentration of the enzyme
G	guaiacyl
GC-MS	gas chromatography-mass spectrometry
GPC	gel permeation chromatography
h	Hill coefficient
H	4-hydroxyphenyl
HDO	high degree of oligomerization
HRP	horseradish peroxidase
k_{cat}	catalytic constant
k_{cat}/K_M	catalytic efficiency
K_i	inhibition constant
K_M	Michaelis constant
LCB	lignocellulosic biomass
LiP	lignin peroxidase
LDO	low degree of oligomerization
LMW	low molecular weight
LRET	long-range electron transfer
MM	Michaelis-Menten
MnP	manganese peroxidase
Mw	weight-average molecular weight
<i>Mxg</i>	<i>Miscanthus x giganteus</i>
NaAc	sodium acetate
RB4	Reactive Blue 4
RB5	Reactive Black 5
RB19	Reactive Blue 19
Rz	Reinheitszahl
S	syringyl
[S]	substrate concentration
ScDyP	DyP from <i>Streptomyces coelicolor</i>
SEC	size exclusion chromatography

<i>ThDyP</i>	DyP from <i>Thermobifida halotolerans</i>
v	initial rate
V_{\max}	maximal velocity

1 Review of the literature

1.1 Lignocellulose

The plant cell wall contains lignocellulose, which is a network of three tightly interconnected biopolymers: cellulose (40–60% in weight), hemicellulose (20–35%), and lignin (15–40%) [1–3] (**Figure 1**). Cellulose and hemicelluloses are carbohydrate macromolecules. Cellulose is a linear homopolymer composed of β -D-glucopyranose molecules linked together by β -1,4-glycosidic bonds, whereas hemicelluloses are heteropolymers that can contain different 5- and 6-carbon monosaccharide units [1, 4]. Cellulose and hemicelluloses serve as the primary structural components responsible for the mechanical strength of the cell wall and for tethering cellulose microfibers, respectively [5, 6]. Lignin, a phenolic biopolymer, is also an essential component of the cell wall of vascular plants, contributing to their mechanical support, nutrient transport, rigidity, hydrophobicity, and resistance to degradation [7]. Swiss botanist Augustin Pyramus de Candolle, the first to introduce the term “lignin”, described it as the basis of all woody organisms [8].

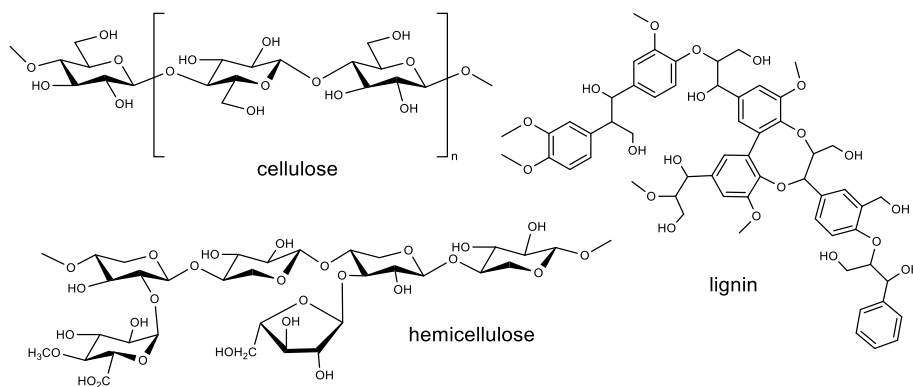


Figure 1. The biopolymers present in lignocellulose. The plant cell wall is primarily composed of cellulose, hemicelluloses, and lignin. Both cellulose and hemicelluloses are polysaccharides. Cellulose is made up of glucose molecules linked by β -1,4-glycosidic bonds. Hemicelluloses can consist of various 5- and 6-carbon monosaccharide units. An example shown here is xylan, a type of hemicellulose primarily composed of xylose residues. Lignin is a complex phenolic polymer, consisting of different units linked together by ether and carbon-carbon linkages. A hypothetical model of a lignin molecule is shown here.

Chemically, lignin is the most complex constituent of lignocellulose, constructed from three phenylpropanoid monomeric units: 4-hydroxyphenyl (H), guaiacyl (G), syringyl (S) [9, 10]. These units are derived from respective monolignol precursors, namely *p*-coumaryl alcohol, coniferyl alcohol, and sinapyl alcohol, which differ from each other by the lack of or the number of methoxy-groups attached to the benzene ring [9, 11] (**Figure 2**). The composition of precursors in lignin, as well as the lignin content itself, varies depending on the plant type [11]. Gymnosperm or softwood lignin primarily consists of coniferyl units (G-type lignin), while angiosperm or hardwood lignin comprises both coniferyl and sinapyl units (G/S-type lignin) [10–13]. Lignin from herbaceous plants includes the aforementioned subunits as well as *p*-coumaryl units (G/S/H-type

lignin) [11, 12]. These lignin units are predominately connected by ether and carbon-carbon linkages: β -O-4, β -5, β - β , β -1, 5-5, and 4-O-5 bonds [13]. Interestingly, other types of building blocks, such as flavonoids and hydroxystilbenes, have also been identified in the structure of lignin [14, 15].

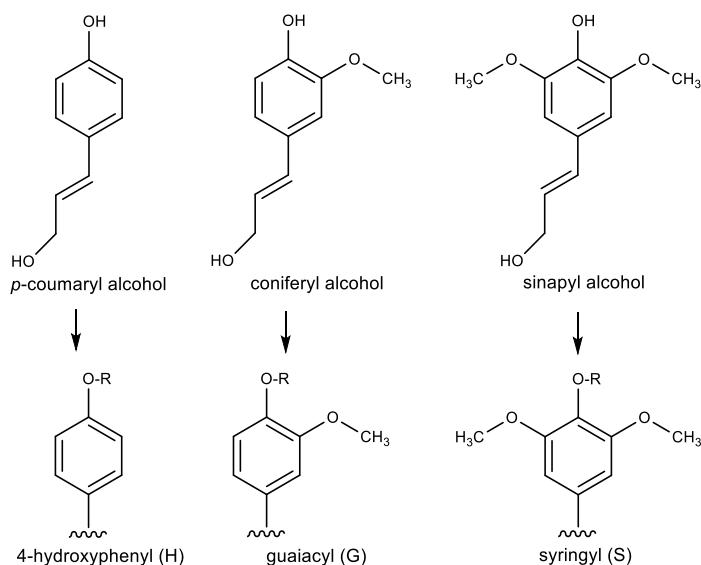


Figure 2. Monolignols and the structural units of lignin. Lignin biopolymer is derived from three main monolignols, *p*-coumaryl alcohol, coniferyl alcohol, and sinapyl alcohol and the resulting units from monolignols are 4-hydroxyphenyl (H), guaiacyl (G), and syringyl (S).

1.1.1 Degradation in nature

Lignocellulose degradation is a fundamental aspect of the global carbon cycle. In nature, the biodegradation of lignocellulose is made possible by the action of various cooperating microorganisms which employ a rich collection of enzymes [16, 17]. Enzymes involved in the process of the breakdown of biomass include laccases (EC 1.10.3.2), carbohydrate-active enzymes (CAZymes), and various peroxidases (EC 1.11.1.x) [18, 19]. Several fungal organisms possess the capability to degrade wood, causing white-rot, brown-rot, and soft-rot (named after the appearance of rotten wood) [20–22]. Fewer organisms can degrade lignin compared to the number of organisms that are able to degrade cellulose and hemicelluloses [16, 23]. Brown-rot fungi can metabolize cellulose and hemicellulose but only partially degrade lignin, harnessing extracellular non-enzymatic hydroxyl radicals via Fenton chemistry [22, 24, 25]. White-rot fungi, which constitute over 90% of all known wood-rotting species, such as *Trametes versicolor* [19, 20], are the most effective wood-decay fungi. They attack all compounds found in woods, employing extracellular enzymes [20, 25, 26]. White-rot fungi are also the only species known to mineralize lignin and other wood components to CO₂ and H₂O, making them the main means for lignin depolymerization in nature [19, 27]. Soft-rot fungi are the least studied compared to brown-rot and white-rot fungi. They can degrade polysaccharides, and some species are also capable of breaking down lignin, often utilizing laccases in the process [21, 28, 29]. In addition to fungi, various species from bacterial classes Actinomycetia, α -Proteobacteria, and γ -Proteobacteria are involved in

lignocellulose and lignin degradation; these are found in soil, termite guts, and wood-boring insects [20, 27, 30]. Genuses *Streptomyces* and *Rhodococcus* from class Actinomycetia are examples of Gram-positive bacteria harnessing lignin degradation abilities. For instance, *Streptomyces viridosporus* T7A has shown to degrade lignin as well as carbohydrates from grass, softwood, and hardwood [30, 31]. *Rhodococcus jostii* RHA1 can grow on wheat straw lignocellulose as a carbon source and break down lignin [32, 33].

1.1.2 Lignin as a feedstock

Lignocellulosic biomass (LCB) is an abundantly available renewable and sustainable material on Earth, representing a green carbon source. This characteristic renders LCB an attractive alternative to fossil carbon resources to produce bio-based fuels, energy, materials, and useful chemicals [3, 14, 34, 35]. Cellulose is already widely applied by the pulp and paper industries as well as biorefineries to produce cellulosic biofuel and bioproducts [14]. The lignin generated from these industrial activities is considered an undesirable by-product and is predominately used for on-site heat and power production, despite its potential as a feedstock [4, 14]. Annually, approximately 1.5–1.8 billion tons of technical lignin is produced [22], with only around 2% of lignin leftovers being utilized for commercial products [4, 36]. With the global shift towards a green economy, research into the utilization, conversion, and valorization of lignin is increasingly being pursued.

Lignin is not only the rate-limiting component for lignocellulose deconstruction in nature but also in industrial applications [3]. Lignin utilization is complicated due to several factors, including its complex and heterogeneous structure and close interaction with the carbohydrate components of the cell wall [12]. The chemical and physical properties of lignin are influenced by the plant tissue, its botanical source, and the methods (such as soda, sulfite, kraft, organosolv, hydrolysis) used for the extraction from LCB [1, 13]. Some of the pulping methods result in lignin with extensively modified structures, often involving rearrangements and modifications where ether linkages are cleaved and replaced by recalcitrant condensed C-C linkages. This complicates the depolymerization process, which is a crucial step in lignin applications [9]. Depolymerization can enhance the potential usage of lignin as the resulting fragments contain more reactive sites compared to untreated technical lignin [11]. Therefore, to enhance lignin utilization efficiency, it should be broken down into lower molecular weight fragments [37].

In nature, a diverse array of microbes possesses the capability to attack, convert, and degrade lignin [27]. Nature serves as a wellspring of inspiration for scientists and the natural decomposers of lignin – microorganisms and their enzymes – are extensively studied for the purpose of lignin depolymerization [37–39]. Most of the enzymes studied, such as laccases, manganese peroxidase (MnP, EC 1.11.1.13), and lignin peroxidase (LiP, EC 1.11.1.14), come from white-rot fungi [40–45]. In comparison to chemical processing, bioprocessing using microbes and enzymatic catalysis offers a cleaner and more efficient approach for lignin depolymerization and conversion. While bacteria are not as effective as fungi at degrading lignin, they exhibit greater environmental adaptability [39]. Compared to microbial degradation, enzymatic degradation of lignin *in vitro* can address the drawback of long culture times [46]. However, despite the promise of utilizing lignin-degrading or modifying enzymes for industrial applications, their use has remained at a relatively low technology readiness level and novel, efficient enzymes are being

sought for this purpose. Ongoing research on these enzymes, such as peroxidases, aims to assess their potential and address the challenges and barriers associated with scaling up to industrial levels and achieving commercial viability [36].

1.2 Peroxidases

The first recorded observations of the colored products generated in reactions catalyzed by peroxidases date back to the early 19th century and were described by Louis Antoine Planche [47]. However, the German-Swiss chemist Christian Friedrich Schönbein is regarded as the discoverer of peroxidases. In 1863, he observed peroxidase activity while treating a solution of guaiacol with extracts from plant and animal tissues and hydrogen peroxide (known at that time as “oxygenated water”), resulting in a blue color change in the solution [48–50]. Nonetheless, systematic research on peroxidases commenced with the studies of Robert Chodat and Alexei Nikolaevich Bach in the early 20th century, who investigated peroxidase from horseradish (*Armoracia rusticana*) [51]. Research on peroxidases was primarily focused on horseradish peroxidase (HRP, EC 1.11.1.7) until the 1940s. Yeast cytochrome c peroxidase (CcP, EC 1.11.1.5) was discovered in 1939, initially misidentified as an oxidase [52]. The discovery of most peroxidases did not occur until the 1970s [53–56].

In life, dioxygen (O₂) plays a crucial role in numerous chemical reactions and biological processes. However, the one-electron reduction of O₂ results in the production of the highly toxic superoxide ion (O₂^{•-}) [57]. This toxic species is neutralized by a cascade of enzymes, beginning with superoxide dismutase, which catalyzes the disproportionation of superoxide radicals to O₂ and H₂O₂ (Equation 1). Subsequently, catalases convert the excess peroxide generated to water and oxygen (Equation 2) to prevent cellular damage [58]. The concentration of peroxide is also regulated by peroxidases (peroxide reductases) (Equation 3), which catalyze the reduction of H₂O₂ to water while simultaneously oxidizing another substrate [59]. Undoubtedly, amongst enzymes, peroxidases are essential for living systems [60].



Heme peroxidases (EC 1.11.1) are ubiquitous H₂O₂-dependent enzymes found in plants, animal tissues, and microorganisms across all kingdoms of life [61]. These enzymes require protoporphyrin IX (heme) as a prosthetic group (**Figure 3A**). The presence of heme in peroxidases produces a strong absorption peak in the visible wavelength region around 400 nm, known as Soret band (**Figure 3B**). To estimate heme content, the Reinheitszahl (Rz) value is used, calculated as the ratio of absorbances at approximately 400 nm and 280 nm. With the aid of a redox cofactor, heme peroxidases catalyze the oxidation of various organic and inorganic compounds [61, 62]. Peroxidases are biotechnologically attractive enzymes, finding utility as a crucial component in clinical diagnostic kits and immunoassays [63, 64], biosensors [65], as reagents for organic synthesis, and in the treatment of waste waters [64].

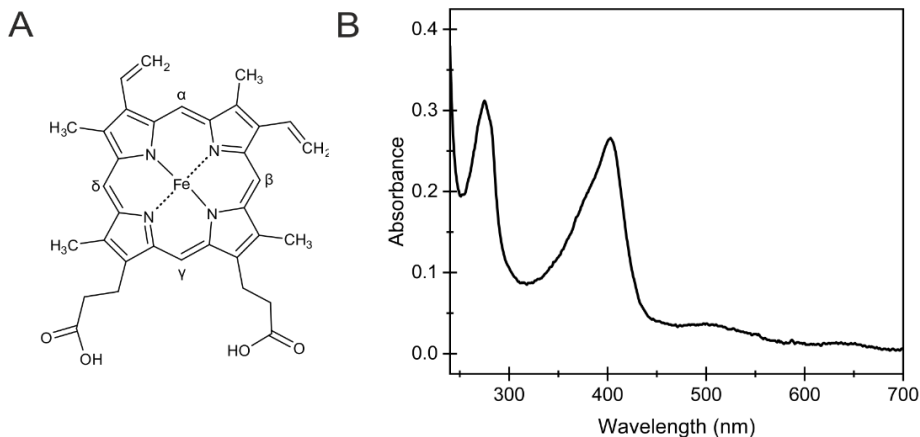


Figure 3. The structure of iron protoporphyrin IX (heme IX) and a typical heme peroxidase absorption spectrum. (A) Heme consists of an iron ion bound within a ring of four pyrrole groups, with two vinyl and two propionic acid side chains attached. Heme peroxidases use heme as a cofactor. The different edges of the heme are indicated with Greek letters, illustrating the nomenclature used in this thesis. **(B)** The absorption spectrum of HRP is characterised by an intense peak maximum at 403 nm, known as Soret band. The R_z value is the ratio of absorbances at 403 nm and 280 nm. This ratio is used to indicate the heme content.

1.2.1 Classification

There are four independently evolved heme peroxidase superfamilies, each with a distinct overall fold, active site, and catalytic functions [66, 67]: (i) the peroxidase-cyclooxygenase superfamily (annotated as PF03098 in the Pfam database), previously denoted as “animal heme-dependent peroxidases” [66, 67]; (ii) the peroxidase-peroxygenase superfamily (PF01328); (iii) the peroxidase-catalase superfamily (PF00141), formerly classified by Welinder as the “superfamily of bacterial, fungal, and plant heme peroxidases” [66, 68]; and (iv) the peroxidase-chlorite dismutase superfamily (Pfam Clan 0032) [69, 70]. Initially, this superfamily included protein families with related sequences and a common fold, namely dye-decolorizing peroxidases (DyPs) (PF04261), chlorite dismutases (ClDs, PF06778), and their evolutionary intermediates [66, 70]. This superfamily was termed CDE (ClD-DyP-EfeB). However, revised phylogenetic analyses revealed that EfeB is a DyP [66]. Depending on the database, the peroxidase-chlorite dismutase superfamily comprises 18–24 families [69] and is part of the larger dimeric $\alpha+\beta$ barrel structural superfamily (SCOPe 54909; Pfam database clade CL0032) [66, 69, 71]. The peroxidase-catalase superfamily of heme peroxidases encompasses three classes. Class I includes intracellular enzymes, such as ascorbate peroxidase (APX, EC 1.11.1.11) and yeast CcP. Class II incorporates secretory fungal enzymes, such as MnP and LiP. Class III includes extracellular plant peroxidases, like HRP [68, 72]. In the literature, these peroxidases of the peroxidase-catalase superfamily, but also peroxidases from other superfamilies, are often referred to as classic peroxidases [73, 74]. Thorough investigations have been conducted on these classic peroxidases, significantly contributing to our understanding of peroxidases, their catalytic mechanisms, and kinetics, thereby providing a foundation for contemporary research. Classic peroxidases serve as benchmarks for many other peroxidases in literature. Therefore, throughout this thesis, DyPs – the peroxidases of interest, are differentiated from classic peroxidases.

1.2.2 General catalytic cycle

Peroxidases follow the catalytic cycle of Poulos-Kraut [61] (**Figure 4**). The substituted-enzyme reaction, commonly referred to as a ping-pong reaction, occurs via three main stages: activation by peroxide and two consecutive oxidation steps. The peroxidase alternates between its ferrous resting state and a reactive high-valent ferryl heme iron species [69]. The heme molecule is oxidized by H_2O_2 to form compound I (Cpd I; $[\text{Fe}^{4+}=\text{O} \text{Por}^+]$). Cpd I is two electrons deficient compared to the enzyme in its resting state: one electron is removed from the iron, resulting in Fe(IV) , and the second one from the porphyrin ring, generating a porphyrin π cation radical (in HRP & APX) [75–79]. The existence of Cpd I allows for the binding of the reducing substrate, and Cpd I accepts an electron from the reductant, wherein porphyrin π cation radical is reduced to compound II (Cpd II; $[\text{Fe}^{4+}=\text{O}]\text{Por}$). Thereafter, Cpd II is reduced, and the peroxidase returns to its initial oxidation state. In total, two electrons are required to reduce Cpd I back to the resting state [62, 80]. A direct two-electron reduction of Cpd I to the resting state is also possible. An updated peroxidase mechanism incorporates a water molecule in the heme distal side, which determines whether the enzyme can undergo a one- or two-electron reduction. The direct two-electron reduction back to the resting state is favored by the dry form of the enzyme (water molecule is absent at the distal heme pocket). The wet form (water molecule is present) favors a one-electron reduction, leading to the initial reduction of Cpd I to Cpd II. Cpd II is then further reduced to form the resting state of the enzyme [81].

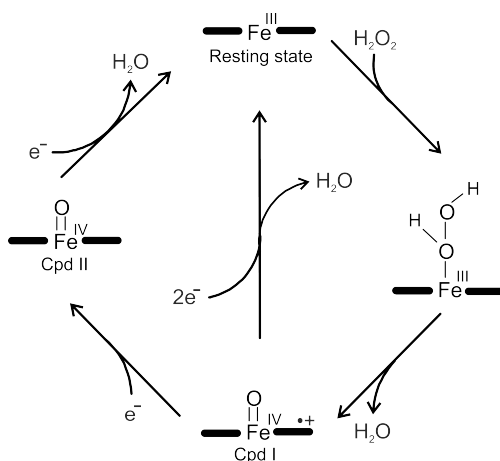


Figure 4. The overall catalytic cycle of peroxidases (Publication II, Fig. 2A). Generally, heme peroxidases proceed via a ferric iron resting state enzyme and reactive intermediates. H_2O_2 binds to the resting state of the enzyme. The resting enzyme in ferric form is oxidized due to the reaction with H_2O_2 , an H_2O molecule is produced, and Cpd I generated. Subsequently, by receiving an electron from the reducing substrate, Cpd I is reduced to Cpd II, and with the reception of another electron, the enzyme returns to its resting state. In the case of DyPs, a shunt pathway is also possible, wherein Cpd I can directly revert to the resting state enzyme through two-electron reduction.

The formation of Cpd I is considered the most crucial step in catalysis for heme peroxidases. A distal acid-base pair is essential for Cpd I formation to reposition a proton in the peroxide molecule [82]. Most heme peroxidases utilize a conserved His-Arg couple for that purpose [76].

1.3 Dye-decolorizing peroxidases

1.3.1 Discovery

In 1995, Kim et al. demonstrated that a basidiomycete *Bjerkandera adusta* (erroneously described as *Geotrichum candium*, later as *Thanatephorus cucumeris* albeit both misidentified) could degrade a variety of dyes, including anthraquinone- (AQ)-based dye Reactive Blue 5 (RB5), in solid and liquid cultures [83, 84]. Since there was no activity when the enzyme solution was added to RB5 without H₂O₂, they suggested that the enzyme responsible for the dye degradation activity is a peroxidase [83]. In 1999, the same enzyme was purified from *B. adusta* and tested on various dyes [83, 85]. The enzyme was confirmed to be a peroxidase and could decolorize seven AQ and azo dyes as well as three model compounds of RB5 [85]. In addition to dyes, this peroxidase catalyzed the oxidation of phenolic compounds, such as 2,6-dimethoxyphenol (2,6-DMP) and guaiacol, but not a non-phenolic substrate veratryl alcohol. The spectral characteristics of this peroxidase were like classic peroxidases, exhibiting a Soret absorption band maximum at 406 nm [80, 85, 86]. However, based on its molecular weight and substrate specificity, the purified peroxidase was believed to be a novel peroxidase distinct from classic peroxidases [85]. Comparison of its primary structure with other peroxidases confirmed the discovery of a unique peroxidase [87], and due to its rare ability to decolorize AQ dyes, it was named dye-decolorizing peroxidase [73].

Although DyPs were initially discovered in fungi in 2004, YwbN from *Bacillus subtilis* showed similarity to putative DyP peroxidases, though it was not identified as DyP at that time [88]. The following year, Ebihara et al. reported the existence of a peroxidase from a bacterium and noted its similarity to a DyP-type peroxidase [89]. Since then, several DyPs have been discovered, and it is known that DyPs are widely distributed across all domains of life, including Eukarya (protists, protozoans, fungi), Bacteria, and Archaea [90, 91].

1.3.2 Classification

DyPs exhibit no homology to classic peroxidases and are phylogenetically, structurally, and mechanistically distinct from them [59, 80]. Consequently, in 2007, DyP-type peroxidases were recognized as a new family of heme peroxidases [92]. DyPs can be classified in various ways, and several databases exist for classification of proteins. As mentioned earlier, DyPs belong to the superfamily of peroxidase-chlorite dismutase (Pfam Clan 0032) [69, 70]. According to the SCOP-extended (SCOPE) database (version 2.08), the family of DyP-type peroxidases (d.58.4.14, SCOP ID: 4003595) belongs to the superfamily of dimeric $\alpha+\beta$ barrel proteins (SCOP ID: 3000089). This superfamily is part of the ferredoxin-like fold (SCOP ID: 2000014) and the structural class of $\alpha+\beta$ proteins (SCOP ID: 1000003), where the secondary structure comprises segregated α -helices and β -strands [71, 93]. According to the InterPro database, which classifies proteins into families and predicts the presence of domains and important sites, the DyP-type peroxidase family (InterPro: IPR006314, Pfam entry PF04261) belongs to the Dim_A_B_barrel superfamily (Pfam clan: CL0032) [94]. RedoxiBase (formerly PeroxiBase) incorporates information about oxidoreductase superfamilies, where the existence of DyPs as a separate (super)family is represented (Dye-decolorizing Prx). In RedoxiBase, based on phylogenetic analysis and structural characteristics, DyPs are divided into four subfamilies (types): A, B, C, and D [95, 96]. Types A, B, and C are found in bacterial species, whereas type D DyPs are solely present in fungi [97]. Presumably, subfamily A evolved

first; evolution then led to the more sophisticated C and D subfamilies or alternatively towards the shortened subfamily B [66].

Type A DyPs possess a twin arginine translocation (Tat)-dependent signal sequence, directing the folded protein to function outside the cytoplasmic membrane of bacteria [59, 98]. Substrates for the Tat pathway often include redox enzymes requiring cofactor insertion in the cytoplasm and multimeric proteins that need to assemble into a complex before export [98]. The first DyP identified as a Tat-substrate was initially recognized as a novel class of Tat-dependently translocated hemoprotein [99]. DyPs studied from subfamily A include *TfuDyP* from actinomycete *Thermobifida fusca* [100], *DypA* from *R. jostii* RHA1 [101], *DtpAa* and *DtpA* from *Streptomyces lividans* [102, 103], *BsDyP* from *B. subtilis* [104], and *CboDyP* from alkaphilic cellulomonad *Cellulomonas bogoriensis* [105]. DyPs from subfamilies B & C are cytoplasmic, lacking the signal sequence [106]. Type B DyPs are the shortest in length. The representatives from subfamily B include *DypB* from *R. jostii* RHA1 [101, 107–110], *DtpB* from *S. lividans* [103], *PpDyP* from the soil bacterium *Pseudomonas putida* [111], and *VcDyP* from the pathogen *Vibrio cholera* [112]. DyPs from subfamily C are the least investigated ones [113]. An example of a subfamily C representative is *DrDyP* from the extremely radiation-resistant bacterium *Deinococcus radiodurans* [114]. In terms of structure, DyPs from subfamily D are more similar to those from subfamily C, but they generally lack the N-terminal pro-sequence that is typically present in subfamily C [113]. The first DyP discovered was from subfamily D, *DyP* from the basidiomycota *B. adusta* [85]. Distinguishing between the phylogenetic characteristics of subfamilies C and D can be challenging [115]. This has led to another classification of DyPs, based on structure-based sequence alignments, dividing DyPs into subfamilies I (Intermediate, previous subfamily A), P (Primary, previous subfamily B), and V (adVanced, previous subfamilies C & D) [113]. Although the newer classification is considered to be more accurate, the older one is still used in parallel. Throughout this thesis, the older classification is adopted.

1.3.3 Overall structure

Initially, the presence of β -strands in the structure of DyP was noted, highlighting the uniqueness of DyPs. Unlike classic peroxidases, DyPs lack a helix-rich structure and instead feature a β -sheet folding motif [116]. In 2005, the first complete crystal structure of DyP from *Thermus thermophilus* HB8, albeit in apo-form, was obtained [89]. DyPs are α + β proteins with a conserved tertiary structure comprising two similar domains. Within each domain, four-stranded antiparallel β -sheets form a β -barrel structure distal to the heme (**Figure 5**) [90, 117]. The β -sheet is flanked by α -helices in a ferredoxin-like fold ($\beta\alpha\beta\beta\alpha\beta$) [92, 117, 118]. While α -helices and β -sheets are mostly conserved, the loop regions connecting them vary [82]. It is believed that the N-terminal distal and C-terminal proximal domains evolved through ancestral gene duplication [118]. Both domains of DyP are involved in forming the active site of the peroxidase [117], primarily through the β -sheet of the proximal domain and also via the loop of the distal domain [97, 117]. The oligomeric state of DyPs has been investigated using various methods including gel filtration chromatography, analytical ultracentrifugation, blue native PAGE, and crystal structure analysis. These enzymes can exist as a monomer (**Figure 5A**), dimer (**Figure 5B**), or form multimeric assemblies, such as hexamer (**Figure 5C**) [85, 89, 99, 100, 104, 105, 112, 115, 117–134]. However, the relationship between the oligomeric organization and catalytic activity has yet to be explored.

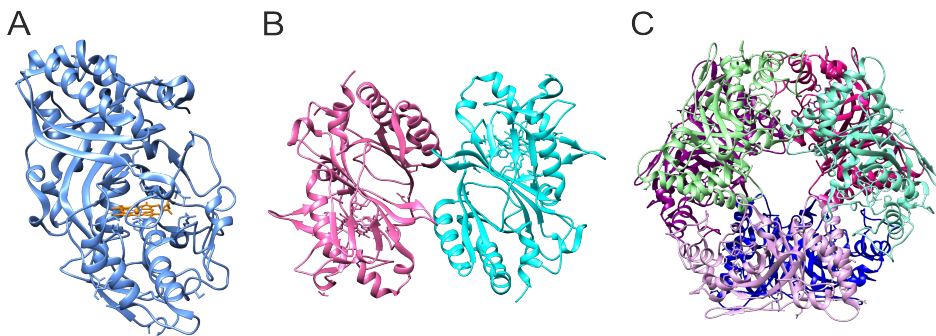


Figure 5. Different oligomeric states of DyPs. Representation of a monomeric AauDyP from *Auricularia auricula-judae*, wherein heme is indicated in orange (A), a dimeric TyrA from *Shewanella oneidensis* (B), and a hexameric BtDyP from *Bacteroides thetaiotaomicron* (C). PDB ID: 4AU9, 2IIZ, and 2GVK, respectively.

1.3.4 Catalytic cycle

In peroxidases, three substrate binding sites are recognized: the δ -edge and γ -edge of the heme and surface-exposed Tyr/Trp residues [135-137]. Different substrates may utilize different binding sites within the same peroxidase [77]. In DyPs, heme accessibility occurs through funnel-shaped channel(s) from the surface of the enzyme to the heme (**Figure 6A**) [78, 82]. These channels facilitate the movement of substrates. The size and shape of these channels can vary, influencing substrate specificity and reactivity [138]. The channels in DyPs are hydrophobic [82, 89, 117, 134]. The heme pocket can easily accommodate compounds that are not larger than a benzene ring with small substituents [78]. Bulky substrates cannot directly access the heme cavity; instead, these sterically demanding substrates utilize surface-exposed substrate-oxidation sites (Tyr/Trp residues). The long-range electron transfer pathway (LRET) is used, for instance, for the oxidation of Reactive Blue 19 [82, 91, 112, 131, 139–142]. In the active site, DyPs feature a proximal conserved His residue serving as a fifth axial iron ligand of the heme (**Figure 6B**). The central iron atom of heme is coordinated to N ϵ 2 of this His residue, similarly to classic peroxidases [69, 90, 92, 117]. In classic peroxidases, a strong hydrogen bond is established between the proximal His and the carboxylate of an adjacent, well conserved Asp [143, 144]. In DyPs, the proximal His forms a hydrogen bond with an acidic residue, creating an Fe-His-Asp/Glu triad [70, 89]. For instance, in DyP from *B. adusta*, Glu391 is hydrogen bonded to His308, thereby stabilizing Fe³⁺ and Fe⁴⁺ [92]. On the distal side of the heme, the highly conserved His, which acts as an acid-base catalyst in the formation of Cpd I in classic peroxidases, is absent [59, 92]. The heme-binding site of DyPs incorporates a collection of highly conserved residues, including a unique GXXDG motif [74, 100]. Initially, it was suggested that the conserved Asp, a weaker base than His, within the GXXDG motif takes over the role of the distal His found in classic peroxidases [145, 146]. Indeed, the studies with DyP from *B. adusta* demonstrated that the distal Asp171 functions similarly to the distal His in classic peroxidases [74, 92]. Arg329 in the C-terminus serves as the essential arginine. In other peroxidases, the essential arginine is usually located in the N-terminus, such as Arg38 in HRP [92]. The roles of Asp and Arg on the distal side of heme are not quite clear. A study on a B-type DyP from *R. jostii* RHA1 showed that Arg244 was necessary for Cpd I formation, while the distal Asp153 had

minimal effect on the activity of the DyP [147]. The distal Arg appears to be critical in type B DyPs, but not in A type DyPs [126]. Nevertheless, in BsDyP from *B. subtilis*, neither the conserved Asp nor the Arg were separately crucial for the peroxidase activity [148].

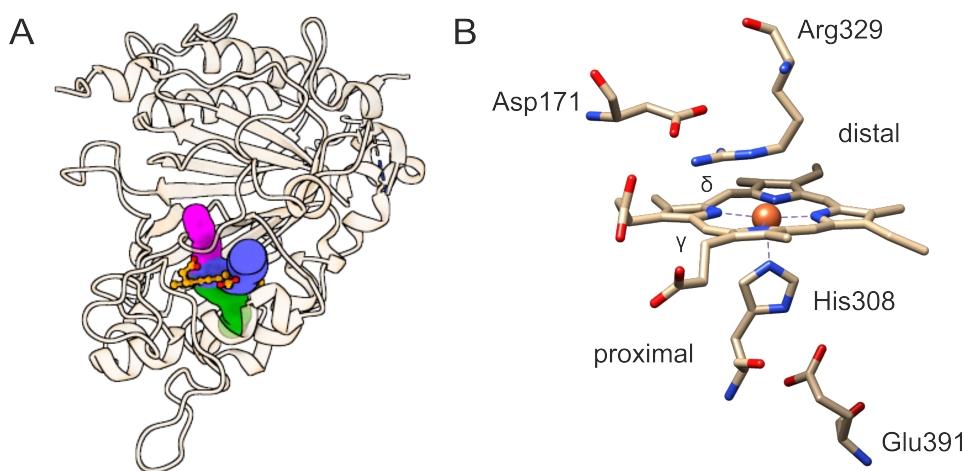


Figure 6. The heme along with its surrounding residues and channels in DyP. (A) In DyPs, heme accessibility is achieved through funnel-shaped channels that enable efficient substrate movement. The channels in DtpA from *S. lividans* (PDB ID: 6GZW) are illustrated here, using Cover 3.0.3 (minimum probe radius 1.4 Å). **(B)** In the active site of DyPs, the proximal His serves as the fifth axial iron ligand of the heme, forming an Fe-His-Glu triad. On the distal side of the heme, Asp and Arg residues are present, while the conserved His residue is absent. In DyP from *B. adusta* (PDB ID: 2D3Q), the distal Asp171 has been shown to function similarly to the distal His found in classic peroxidases. The proximal and distal sides of the heme are in the same orientation in both panels.

The catalytic cycle of DyPs closely resembles that of classic peroxidases, involving transitions between the enzyme in its resting state and interactive intermediates Cpd I and Cpd II. During these transitions, peroxide is reduced to water while another substrate is concurrently oxidized. To complete the catalytic cycle and return to the resting state, DyP requires two electrons from the reducing substrate. The first model for Cpd I formation in DyPs was proposed by Sugano et al. [92]. Over the years, the concept of Cpd I formation was further elucidated. In DyPs, a swinging mechanism can occur to accept the proton from H₂O₂ during the formation of Cpd I [149]. In DyPs, it has been shown that a wet heme pocket favors the one-electron reduction pathway, while a dry pocket favors the direct two-electron reduction of Cpd I to enzyme in its resting state [104, 109, 121, 129, 134, 148, 150, 151].

Several detailed studies of heme peroxidases have highlighted deviations from the typical peroxidase mechanism, particularly regarding the inactivation by H₂O₂ [72, 152–157]. In the absence of a reducing substrate and/or with excess H₂O₂, Cpd I reacts with H₂O₂, leading to enzyme inactivation. Some peroxidases have protective pathways, such as the compound III (Cpd III) pathway or a catalase-like pathway [153, 158]. When excess H₂O₂ reacts with Cpd II, the formation of Cpd III protects the enzyme by delaying inactivation [159]. For instance, in HRP, approximately 500 equivalents of H₂O₂ are needed to form Cpd III [160]. Notably, Cpd III is not part of the usual peroxidase cycle and only forms in the presence of excess peroxide [161]. In certain peroxidases,

the catalase-like pathway can reduce H₂O₂-induced inactivation [153]. Without reductants, H₂O₂ acts both as an oxidant (forming Cpd I) and as a reductant (serving as electron donor). HRP, for example, can decompose excess H₂O₂ through dismutation, producing O₂ [61, 153, 158, 162]. Conversely, APX does not exhibit significant catalase-like activity [72, 163]. Consequently, 625 molecules of H₂O₂ per active site are required for inactivation in HRP, while only 2.5 molecules of H₂O₂ are needed for APX [72]. However, even with catalase-like activity, peroxidases are not fully protected and still undergo inactivation by H₂O₂ [153].

The reducing substrate is the main protector of peroxidase by reducing the likelihood that H₂O₂ will react with Cpd I. Without it, many heme peroxidases are susceptible to H₂O₂ inactivation [72, 152–157]. Arnao et al. 1990 demonstrated this protective effect using 2,2'-azino-bis(3-ethylbenzothiazoline-6-sulfonic acid) (ABTS), showing that the peroxidase remains safeguarded as long as the ratio of [ABTS]/[H₂O₂] is sufficiently high. This ratio dictates the fate of the peroxidase, catalytic turnover, level of protection, and the protective pathway employed [164]. However, excessive H₂O₂ can still lead to inactivation, even when a reducing substrate is present. Once the ratio of reducing substrate to H₂O₂ drops, the enzyme becomes vulnerable to H₂O₂-induced inactivation [72].

1.3.5 Potential biological functions

Kim et al. 1999 provided the initial understanding of the overall substrate preferences of DyPs. DyPs can oxidize AQ and azo dyes (**Figure 7**), and phenolic substrates (2,6-DMP and guaiacol) without requiring Mn²⁺ (unlike MnP). However, they are unable to catalyze the oxidation of non-phenolic veratryl alcohol (unlike LiP) [85]. Despite being named after their dye-decolorizing ability [83, 85, 92], not all DyPs exhibit activity on dyes [100, 113]. The substrate spectrum of DyPs is much broader [86, 97]. Apart from dyes, DyPs catalyze the oxidation of substrates such as complex phenolic and non-phenolic molecules, lignin-related compounds, carotenoids, aromatic sulfides, and metal ions [85, 101, 165]. There are also notable catalytic differences among different subclasses [166]. While DyPs can catalyze the oxidation of synthetic dyes and xenobiotics, these dyes are likely not their natural substrates. Despite two decades of extensive research, the physiological role and biological substrate of DyPs remains largely unknown, although several potential physiological roles have been proposed [91].

The extracellular presence of fungal DyPs suggests a possible role in nonspecific detoxification, degrading extracellular substances to protect against hazardous materials such as xenobiotics [74]. Some of peroxidases (type A DyPs, such as *TfuDyP* from *T. fusca*, *YcdB* from *Escherichia coli*, etc.) are secreted into the periplasmic space of bacteria with the aid of the Tat-signal sequence [98–100, 167]. Proteins with Tat-signal are involved in a range of cellular activities, including anaerobic metabolism, cell envelope biogenesis, metal acquisition and detoxification, and virulence [98]. However, this function is unlikely for intracellular DyPs, such as *TyrA* and *BtDyP* [74].

The relatively high redox potential of some DyPs allows for the oxidation of lignin model compounds, suggesting a potential involvement in ligninolysis in nature [168]. Both bacterial as well as fungal DyPs have demonstrated the ability to oxidize non-phenolic as well as phenolic lignin model compounds. Examples include DyP from jelly fungus *A. auricula-judae* [168], DyPB from *R. jostii* RHA1 [107], DyP2 (type C) from *Amycolatopsis* sp. 75iv2 [119], *BsDyP* from *B. subtilis* KCTC2023 [169], *TfuDyP* from *T. fusca* [170], and *BaDyP* from *Bacillus amyloliquefaciens* [171]. Furthermore, some DyPs, such as DyPB

from *R. jostii* RHA1 [107], Dyp1B from *Pseudomonas fluorescens* Pf-5 [172], and *TfuDyP* have been tested on polymeric Kraft lignin and/or wheat straw lignocellulose [170]. Additionally, *IrlacDyP* from *Irpex lacteus* could transform the phenolic content of lignosulfonates [173].

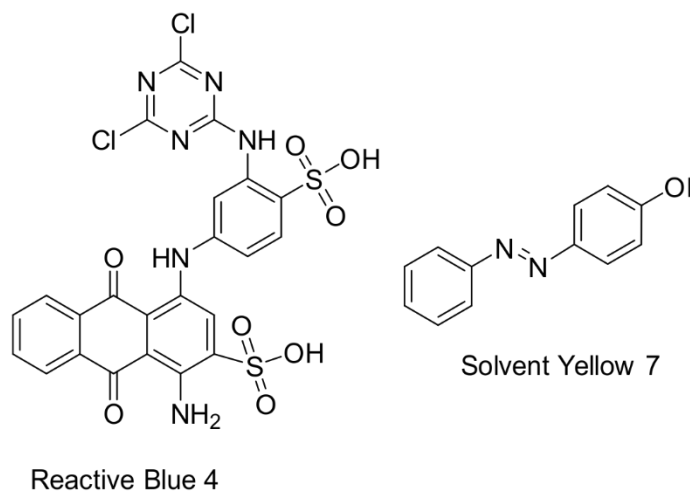


Figure 7. An example of AQ and azo dyes. In this figure are Reactive Blue 4 and Solvent Yellow 7, an orange-colored azo dye. AQ dyes contain a 3-ring aromatic core structure of 9,10-anthraquinone. Azo dyes contain a functional group $R-N=N-R'$, in which R and R' are usually aryl and substituted aryl groups.

1.3.6 Investigation of kinetics

The study of enzyme kinetics is essential for accurately characterizing enzymes. Numerous excellent kinetic studies on DyPs have investigated both transient-state kinetics and steady-state kinetics [102, 109, 115, 121, 134]. In conventional Michaelis-Menten (MM) kinetics, the initial rate of an enzyme-catalyzed reaction exhibits a hyperbolic dependence on substrate concentration. To determine kinetic parameters, the MM equation (Equation 4) is used, where v represents the initial rate, E_0 is the total concentration of the enzyme, V_{max} is the maximal velocity, $[S]$ is the substrate concentration, and K_M is the Michaelis constant.

$$\frac{v}{E_0} = \frac{V_{max}[S]}{K_M + [S]} \quad \text{Equation 4}$$

Kinetic studies of DyPs have revealed that these enzymes often exhibit atypical, non-MM kinetic behavior, characterized by non-hyperbolic plots of velocity versus $[S]$. This behavior may include substrate inhibition by H_2O_2 and/or by the reducing substrate [104, 115, 150, 174–176], and/or positive cooperativity [102, 109, 115, 121]. However, the underlying mechanisms of non-conventional kinetics remain poorly understood, complicating the study of DyPs and limiting our understanding of their potential. Substrate inhibition affects approximately 20–30% of all enzymes [177]. In some instances, it is considered an experimental artifact, often occurring at unnaturally high substrate concentrations [178]. Substrate inhibition is particularly common in multi-substrate enzyme reactions, where the substrate binds to an incorrect form of the

enzyme, leading to the formation of an enzyme-substrate complex that cannot generate a product [179]. Under substrate inhibition, the initial rate decreases at higher substrate concentrations, and the empirical equation of substrate inhibition (Equation 5) can be used, where k_{cat} and K_i represent the catalytic constant and inhibition constant, respectively.

$$\frac{v}{E_0} = \frac{k_{cat}[S]}{K_M + [S] + \frac{[S]^2}{K_i}} \quad \text{Equation 5}$$

Positive cooperativity is a characteristic feature of enzymes with multiple subunits or several binding sites. When the initial reaction velocity v exhibits a sigmoidal dependence on substrate concentration $[S]$ and includes a characteristic lag phase, it suggests the presence of apparent positive cooperativity. In this context, the empirical Hill equation (Equation 6) can be applied, where $K_{0.5}$ and h represent the concentration of substrate at half-maximal rate and the Hill coefficient, respectively.

$$\frac{v}{E_0} = \frac{k_{cat}[S]^h}{K_{0.5}^h + [S]^h} \quad \text{Equation 6}$$

2 Aims of the study

Lignin represents a primary reservoir of aromatic compounds in nature and is often regarded as a sustainable alternative to fossil-derived chemicals in the chemical industry. Efficient utilization of lignin requires its breakdown into lower molecular weight fragments, a process achievable by various enzymes, such as dye-decolorizing peroxidases (DyPs). Despite being studied for a quarter of a century, there are still unknown aspects about DyPs, including the relationship between oligomerization and catalytic activity. It is crucial to characterize these enzymes thoroughly to understand their potential in biotechnological and industrial applications and to utilize them effectively. Moreover, besides the challenges posed by lignin, the complex nature of DyPs presents additional hurdles. The characterization of DyPs is hindered by their non-Michaelis-Menten kinetics, exhibiting substrate inhibition and positive cooperativity.

The main aims of the thesis were as follows:

- To explore novel enzymes for lignin depolymerization.
- To reveal the mechanisms underlying the non-conventional kinetics (substrate inhibition and positive cooperativity) of DyPs.
- To clarify the relationships between the degree of oligomerization of DyPs and their catalytic activity.

3 Materials and methods

A brief description of the methods is provided below. Further details can be found in Publications I–III.

Cloning of DyPs

- Genes encoding DyPs were cloned into the pET15b vector, or codon-optimized genes, pre-cloned into the pET28a expression vector, were ordered from Twist Bioscience (Publications I–III).
- Transformation was performed by electroporation (Publications I–III).

Expression and purification of recombinant DyPs

- Recombinant DyPs from *Streptomyces coelicolor* (ScDyP) and *Thermobifida halotolerans* (ThDyP) were overexpressed in *E. coli* BL21 (DE3) as His₆-fusion proteins (Publications I–III).
- DyPs were purified using nickel-affinity chromatography (Publications I–III).
- The concentration of active enzyme was determined spectrophotometrically at 406 nm ($\epsilon_{406} = 100,000 \text{ M}^{-1} \text{ cm}^{-1}$) (Publications I–III).

Enzyme assays

- The concentration of H₂O₂ was determined spectrophotometrically at 240 nm using an extinction coefficient of $39.4 \text{ M}^{-1} \text{ cm}^{-1}$ (Publications II–III).
- Reactions were initiated by adding the enzyme from its working stock to the cuvette containing a mixture of the reducing substrate and H₂O₂ (Publications I–III).
- Non-enzymatic oxidation of substrates was tested by performing the measurements without the enzyme (Publications I–III).
- The optimal pH for the oxidation of ABTS and 2,6-DMP was determined for each ScDyP (Publication I).
- The kinetics of ScDyPs was studied with ABTS and 2,6-DMP (Publication I).
- The dependence of ABTS oxidation by ScDyPs on temperature was determined (Publication I).
- The stability of ScDyPs was assessed at 30 °C with ABTS (Publication I).
- ABTS, methylhydroquinone (MHQ), 2,6-dimethoxyhydroxyquinone (DMHQ), Reactive Blue 4 (RB4), and Reactive Blue 19 (RB19) were used as reducing substrates (Publication II).
- ABTS and MHQ were used for the kinetic characterization (Publication III).

Lignin experiments

- Ethanol organosolv lignin from bleached chemi-thermomechanical aspen pulp was extracted as described by Jöul et al. 2022. Ethanol organosolv lignin from *Miscanthus × giganteus* (Mxg-lignin) was provided by Stefan Bauer (Publication I).
- Lignin suspension at 1 mg/mL in HEPES buffer (50 mM, pH 8.0) with added 2 mM H₂O₂ was treated with 10 µM of ScDyPs and incubated for 24 h, 200 rpm, at 28 °C (Publication I).
- Gel permeation chromatography (GPC) was used to monitor changes in the molecular weight distribution of enzymatically treated lignins (Publication I).

- To analyze low molecular weight (LMW) compounds in *Mxg*- and aspen lignins treated with ScDyPs, as well as those without enzymatic treatment, gas chromatography-mass spectrometry (GC-MS) was used (Publication I).

Crystal structure

- *ThDyP* was crystallized using sitting-drop vapor diffusion crystallization screens (Publication II).
- X-ray diffraction data were collected at 100 K at the BL13-XALOC beamline, equipped with a PILATUS 6M detector at the ALBA synchrotron light source (Barcelona, Spain) (Publication II).
- The crystal structure of *ThDyP* was solved by molecular replacement using MOLREP in the CCP4 program suite, utilizing the coordinates of DyP from *Thermobifida cellulosilytica* (PDB ID: 4GS1) as the search model (Publication II).
- Initial model refinement was performed with REFMAC5, and iterative model building and refinement were carried out with COOT and phenix.refine (Publication II).

Oligomerization analysis

- The oligomerization state of *ThDyP* and ScDyPB was estimated by gel filtration chromatography (Publications II & III).
- Dynamic light scattering (DLS) analysis was used to determine the size distribution of ScDyPB (Publication III).

Inactivation studies

- For the time dependency of inactivation, *ThDyP* was pre-incubated with H₂O₂ or ABTS for a selected time. After pre-incubation, the residual ABTS oxidizing activity of *ThDyP* was measured using ABTS (Publication II).
- For the end-point inactivation, *ThDyP* was pre-incubated with H₂O₂ for 1 h or ABTS for 24 h, before measuring the residual ABTS oxidizing activity (Publication II).
- ScDyPB at pH 4.0 or at pH 7.5 was preincubated with H₂O₂. At selected times, an aliquot was withdrawn, and the activity was measured.

UV-vis absorption spectra

- The UV-vis absorption spectra of *ThDyP* and ScDyPB were recorded from 300 nm to 700 nm or from 250 to 700 nm, respectively (Publications II & III).
- The spectra of *ThDyP* were recorded in the presence of different molar equivalents of H₂O₂ (Publication II).
- The spectra of ScDyPB were recorded at pH 7.5 and pH 4.0 (Publication III).

4 Results

Four different DyPs from two Gram-positive bacteria were studied: two type A DyPs and a type B DyP from a soil-dwelling bacterium *S. coelicolor* (*ScDyP1A*, *ScDyP2A*, and *ScDyPB*) and a type A DyP from a bacterium *T. halotolerans* (*ThDyP*). The studied DyPs were characterized mostly using a common peroxidase substrate, ABTS, but also other reducing substrates such as AQ-based dyes and phenolic hydroquinones (Publication II, Scheme 1). *ScDyPs* were also tested on organosolv lignin derived from *Mxg* and aspen (Publication I).

4.1 General characterization of *ScDyPs* (Publication I)

For the ensemble of *ScDyPs*, the overall biochemical characterization included determining the optimal pH for the oxidation of ABTS, temperature dependency, and thermostability. The pH optima for *ScDyPs* were between 3.0–4.0 for the oxidation of ABTS (Publication I, Fig. 2; Publication III, Fig. 1C). For *ScDyPB*, the optimum pH for the oxidation on MHQ was similar to ABTS (Publication III, Fig. 1C). The optimal pH for 2,6-DMP was around 8.5 (data not shown). Temperature dependency and thermostability were assessed using ABTS as the electron donor. Oxidation reactions performed at 20–70 °C revealed that peroxidase activity for all DyPs decreased or started to decrease at 30 °C, with activity continuing to decline as the temperature increased further (Publication I, Fig. 3). The activity of *ScDyPs* at 30 °C decreased over time. In 24 h, *ScDyP2A* lost approximately half of its activity, while *ScDyP1A* and *ScDyPB* retained about 80% of their activity. After 48 h, only *ScDyP1A* maintained over half of its activity (approximately 70%), while the other two DyPs retained around 30% of their activity (Publication I, Fig. 4).

ScDyPs were studied kinetically. Steady-state kinetics measurements of *ScDyPs* were performed to determine the apparent kinetic parameters for ABTS. The kinetic curves of ABTS oxidation displayed characteristics of substrate inhibition by ABTS (Publication I, Fig. S2). Consequently, the kinetics were analyzed using the empirical equation for substrate inhibition (Equation 5). *ScDyPB* exhibited the lowest apparent K_M value of 80 μM for ABTS and the highest k_{cat} (49 s^{-1}), resulting in the highest catalytic efficiency (k_{cat}/K_M) (607 $\text{mM}^{-1}\cdot\text{s}^{-1}$) for ABTS oxidation. The K_i value of 0.4 mM for *ScDyPB* was smaller compared to *ScDyPAs*, indicating a stronger inhibitory effect by ABTS (Publication I, Table 3, Fig. S2). *ScDyP2A* and *ScDyPB* could catalyze the oxidation of 2,6-DMP, but they exhibited approximately 140- and 200-fold lower apparent k_{cat}/K_M compared to the oxidation of ABTS, respectively (data not shown). Additionally, the oxidation of 2,6-DMP also demonstrated substrate inhibition (Publication I, Fig. S3).

4.2 In-depth kinetic characterization of DyPs (Publications II & III)

The in-depth kinetic characterization of DyPs incorporated the investigations of biphasic kinetics, substrate inhibition, inactivation by H_2O_2 and ABTS, and apparent positive cooperativity of DyPs.

4.2.1 Biphasic kinetics of *ScDyPB* (Publication III)

A closer investigation of the kinetics of *ScDyPB* with ABTS showed that the dependency of the rates on H_2O_2 concentration adhered to typical MM kinetics (Figure 8B; Publication III, Fig. S2B, eq S1, Fig. 4B). Conversely, varying ABTS concentration revealed substrate

inhibition by ABTS, which became more prominent at lower H₂O₂ concentrations (**Figure 8A**; Publication III, Fig. 4A, Fig. S2A for the zoom-in of the series with low H₂O₂ concentrations). Unexpectedly, the data did not conform solely to ping-pong peroxidase kinetics with substrate inhibition by ABTS. Neither the MM equation (Equation 4) nor the empirical equation of substrate inhibition (Equation 5) could adequately describe these kinetics. The dependence of the rates of ABTS oxidation for H₂O₂ on the concentration of ABTS revealed a drop in the rates in the ABTS concentration range of 0.1–0.2 mM (**Figure 8A**; Publication III, Fig. 4A).

These results could be explained by the presence of biphasic kinetics. Let's assume that ScDyPB exhibits activity in two distinct, kinetically separate forms: enzyme form I (E^I) follows MM kinetics, and enzyme form II (E^{II}) which is substrate-inhibited by ABTS. By adopting this assumption, this kinetic phenomenon could be elucidated by combining the two steady-state rate equations (Equation 7).

$$\begin{aligned}
 \frac{v_i}{E_0} = & \frac{\frac{[E^I]}{E_0} k_{cat}^I [ABTS] [H_2O_2]}{K_{M(ABTS)}^I [H_2O_2] + K_{M(H_2O_2)}^I [ABTS] + [ABTS] [H_2O_2]} + \\
 & + \frac{\frac{[E^{II}]}{E_0} k_{cat}^{II} [ABTS] [H_2O_2]}{K_{M(ABTS)}^{II} [H_2O_2] + K_{M(H_2O_2)}^{II} [ABTS] \left(1 + \frac{[ABTS]}{K_i(ABTS)}\right) + [ABTS] [H_2O_2]}
 \end{aligned} \quad \text{Equation 7}$$

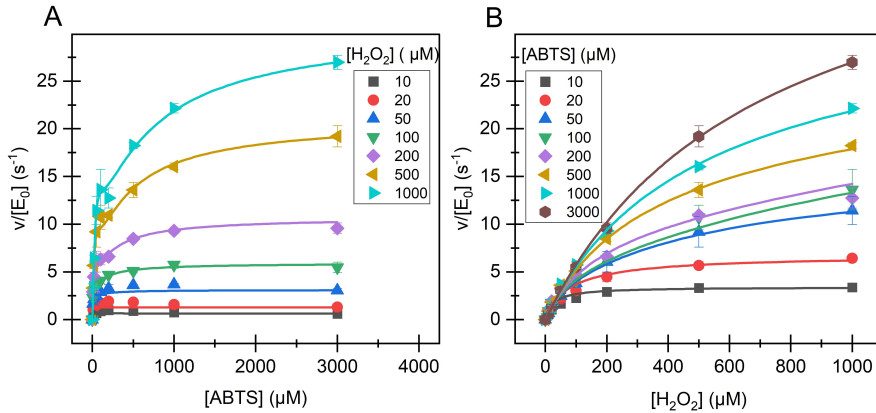


Figure 8. Kinetics of ScDyPB with ABTS. The dependence of the initial rates of the oxidation of ABTS on the concentration of (A) ABTS and (B) H₂O₂. The solid lines in (A) and (B) represent the global non-linear regression of the data according to Equation 8. The concentration of the substrate held constant in each series is shown in the respective plot. Data are presented as average values from three independent experiments (n = 3).

Equation 7 successfully captured the relationship between the rate of ABTS oxidation by ScDyPB and the concentration of ABTS and the observed drop in ABTS oxidation rates after 0.1 mM ABTS (**Figure 8A**; Publication III, Fig. 4A). We performed a global non-linear regression analysis of the data in **Figure 8A** (Publication III, Fig. 4A) using Equation 7 and predicted the kinetic parameters for E^I, [E^I]k_{cat}^I/[E]₀, K_{M(ABTS)}^I, and K_{M(H₂O₂)}^I values of 59 ± 3 s⁻¹, 1.0 ± 0.12 mM, and 0.89 ± 0.06 mM, respectively (for the fit, see Publication III,

Fig. S4A). While we could predict the kinetic parameters for E^I, the interdependence among the parameters prevented us from determining the kinetic parameters for E^{II}. However, by assuming that both enzyme forms share identical kinetic parameter values, with the distinction lying solely in the presence of substrate inhibition for form E^{II}, Equation 7 could be simplified to Equation 8. Subsequently, conducting a global non-linear regression analysis of the same data from **Figure 8A** (Publication III, Fig. 4A) according to Equation 8 allowed us to estimate the relative proportions of enzyme forms I and II as 0.18 ± 0.01 and 0.82 ± 0.01, respectively. Furthermore, it enabled to predict the common kinetic parameters for both forms, 327 ± 28 s⁻¹, 0.95 ± 0.09 mM, and 0.89 ± 0.06 mM, for k_{cat} , $K_{M(ABTS)}$, and $K_{M(H_2O_2)}$, respectively. The estimate of the $K_{i(ABTS)}$ was 4.12 ± 0.36 μM.

$$\frac{v_i}{E_0} = \frac{\frac{[E^I]}{E_0} k_{cat} [ABTS] [H_2O_2]}{K_{M(ABTS)} [H_2O_2] + K_{M(H_2O_2)} [ABTS] + [ABTS] [H_2O_2]} + \frac{\left(1 - \frac{[E^I]}{E_0}\right) k_{cat} [ABTS] [H_2O_2]}{K_{M(ABTS)} [H_2O_2] + K_{M(H_2O_2)} [ABTS] \left(1 + \frac{[ABTS]}{K_{i(ABTS)}}\right) + [ABTS] [H_2O_2]} \quad \text{Equation 8}$$

4.2.2 Kinetic study of *ThDyP* with substrate inhibition (Publication II)

The kinetics of *ThDyP* were investigated using ABTS, two hydroquinones (MHQ and DMHQ), and two AQ-based dyes (RB4 and RB19) (Publication II, Scheme 1). Similar to *ScDyPs*, the relationship between the initial rate of ABTS oxidation and the concentrations of ABTS or H₂O₂ was not hyperbolic (**Figure 9**; Publication II, Fig. 1A or Fig. 1B, respectively), exhibiting substrate inhibition. The substrate inhibition by ABTS was more pronounced at lower H₂O₂ concentrations (1.0–10 μM) (**Figure 9A**; Publication II, Fig. 1A). The substrate inhibition by H₂O₂ was intensified, as [ABTS] decreased (Publication II, Fig. 1B). The series of kinetic data showing substrate inhibition by ABTS or H₂O₂ could be analyzed using non-linear regression analysis according to the empirical equation for substrate inhibition (Equation 5). The kinetic parameters for H₂O₂ and ABTS are shown in Publication II, Table S1 and Table S2, respectively. The determined K_M^{app} and K_i^{app} (data from **Figure 9B**, Publication II, Fig. 1B) were used to determine the optimal substrate concentration $[H_2O_2]_{opt}$ using Equation 9 and was shown to increase proportionally with [ABTS] (Publication II, Fig. S2).

$$[S]_{opt} = \sqrt{K_M^{app} K_i^{app}} \quad \text{Equation 9}$$

ThDyP showed significantly lower activity with the other tested reducing substrates compared to ABTS. Nevertheless, inhibition by H₂O₂ was observed with these substrates, except with DMHQ (**Figure 9D, F**; Publication II, Fig. 1D, F). The inhibition by the reducing substrate was only evident with RB4 (**Figure 9E**; Publication II, Fig. 1E), but not with other substrates (**Figure 9C, E**; Publication II, Fig. 1C, E).

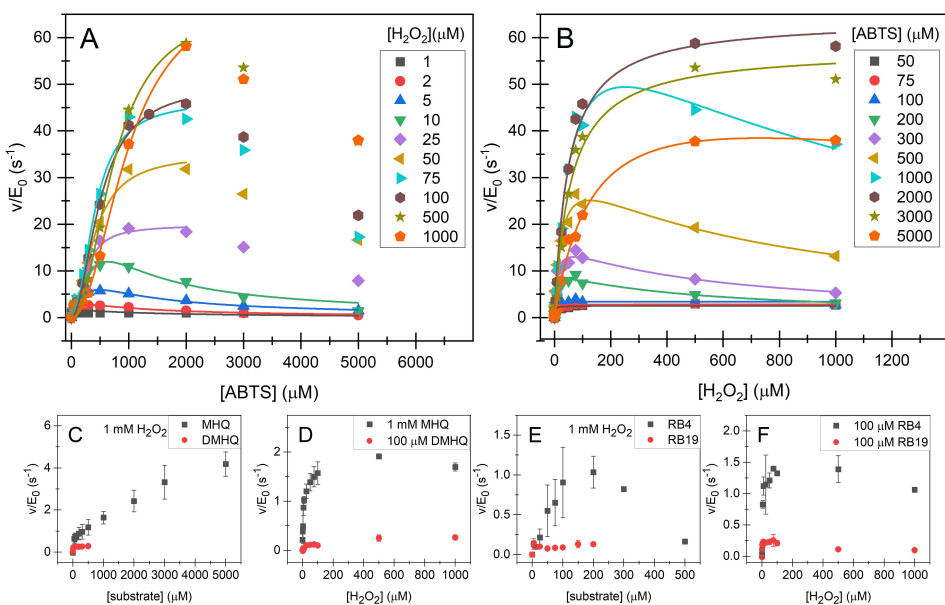


Figure 9. Kinetics of *ThDyP*. The dependence of initial rates of *ThDyP*-catalyzed oxidation of ABTS on the concentration of (A) ABTS and (B) H_2O_2 . Panels (C) and (E) show the dependence of the initial rates of the oxidation of hydroquinones and anthraquinone dyes on the concentration of hydroquinone and anthraquinone dye, respectively, while panels (D) and (F) show the dependence on H_2O_2 concentration. The solid lines in (A) represent non-linear regression of the data. For the series with $[\text{H}_2\text{O}_2]$ ranging from 1.0 to 10 μM , the regression follows Equation 5. For the series with $[\text{H}_2\text{O}_2]$ of 25 μM and above (with datasets limited to a maximum [ABTS] of 2 mM), it follows Equation 6. The solid lines in (B) represent non-linear regression of the data according to Equation 5. The substrate and its constant concentration in each series are indicated within the plot. Data represent average values from two experiments.

4.2.3 Investigations of inactivation (Publications II & III)

We explored the potential inactivation of *ThDyP* and *ScDyPB* by H_2O_2 , as well as *ThDyP* inactivation by ABTS (Publications II & III). The enzyme was pre-incubated with H_2O_2 or ABTS in the absence of the other substrate, and the residual activity was tested with ABTS. The residual activity of *ThDyP* declined over the pre-incubation period; however, after 30 min, it stabilized at a plateau, where the final value depended on the concentration of H_2O_2 (Publication II, Fig. S3A). We observed that *ThDyP* was fully inactivated by an average of only 4.6 ± 0.9 H_2O_2 molecules (Publication II, Fig. 3A). Titration of *ThDyP* with H_2O_2 led to a decrease in the absorbance of the Soret band at 405 nm, ultimately leading to its total disappearance (Publication II, Fig. S4). These observations suggest that a non-productive complex forms between Cpd I and H_2O_2 . *ScDyPB* was irreversibly inactivated by H_2O_2 (Publication III, Fig. S3). The rate of inactivation rose with increasing concentrations of H_2O_2 , yielding second-order rate constants of 4.9 ± 0.3 and 6.2 ± 0.9 $\text{M}^{-1} \text{s}^{-1}$ for H_2O_2 -induced inactivation of *ScDyPB* at pH 4.0 and 7.5, respectively (Publication III, Fig. S3).

ABTS-triggered inactivation was less effective. Pre-incubation with ABTS led to a time-dependent reduction in the residual activity of *ThDyP* (Publication II, Fig. S3B), and *ThDyP* was fully inactivated only when the ABTS to *ThDyP* ratio reached 250 (Publication II, Fig. 3B). ABTS oxidation in the absence of H_2O_2 was slow, producing a maximum of

approximately 10 oxidized ABTS molecules per *ThDyP* molecule (Publication II, Fig. S5), indicating that ABTS oxidation without added H₂O₂ and *ThDyP* inactivation are not interconnected. Nonetheless, the inactivation of *ThDyP* by ABTS in the absence of H₂O₂ implies the existence of a non-productive complex involving the resting state of *ThDyP* and ABTS. The inactivation of DyPs by H₂O₂ in the absence of ABTS suggests the possibility of Cpd I-H₂O₂ complex formation.

4.2.4 Mechanism explaining substrate inhibition by both substrates (Publication II)

The formation of non-productive complexes between the resting enzyme and ABTS, and between Cpd I and H₂O₂, was assumed to explain substrate inhibition by the reducing substrate and H₂O₂, respectively (Figure 10; Publication II, Fig. 2B). We exploited the knowledge that in enzymes exhibiting the ping-pong mechanism, substrates binding to the wrong form of the enzyme lead to inhibition. Additionally, we provided experimental supporting evidence that substrate inhibition by H₂O₂ or ABTS may be due to the formation of a non-productive complex with Cpd I or the *ThDyP* resting state, respectively (Publication II).

We proposed a mechanism to explain inhibition of DyPs or heme-peroxidases in general by both substrates – reducing substrate and H₂O₂ (Figure 10; Publication II, Fig. 2B). This mechanism was solved, and the rate equation was derived using rapid equilibrium as well as steady-state assumptions, both resulting in equivalent equations. In Equation 10, E_0 and $[P]$ represent the total concentration of the enzyme and the concentration of one-electron-oxidized product, respectively. The k_{cat} and equilibrium binding constants in Equation 10 are defined in Figure 10 (Publication II, Fig. 2B).

$$\frac{v}{E_0} = -\frac{d[H_2O_2]}{dt} = 2\frac{d[P]}{dt} = \frac{k_{cat}[S][H_2O_2]}{[S][H_2O_2] + \frac{k_{cat}K_{H_2O_2}}{k_{ox}}[S]\left(1 + \frac{[S]}{K_{i(S)}}\right) + \frac{k_{cat}K_{S1}}{k_{red1}}[H_2O_2]\left(1 + \frac{[H_2O_2]}{K_{i(H_2O_2)}}\right) + \frac{k_{cat}K_{S2}}{k_{red2}}[H_2O_2]} \quad \text{Equation 10}$$

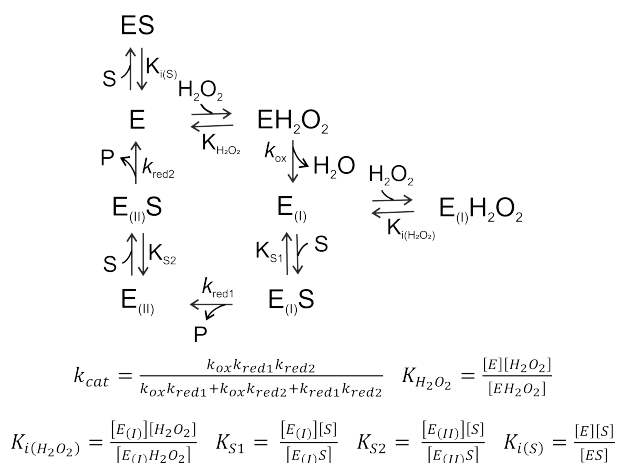


Figure 10. The kinetic mechanism explaining the substrate inhibition of heme peroxidase by both reducing substrate (S) and H₂O₂. E, E_(I), and E_(II), represent the enzyme in the resting state, Cpd I, and Cpd II, respectively. The k_{cat} and the equilibrium dissociation constants used to derive the rate equations are defined within the figure.

4.2.5 Structure of ThDyP (Publication II)

The crystal structure of ThDyP was solved, aiding in clarifying the complex kinetics of ThDyP. Similar to other solved structures of DyPs, ThDyP adopts a ferredoxin-like fold, consisting of two four-stranded antiparallel β -sheets and peripheral α -helices connected by loop regions (**Figure 11**; Publication II, Fig. 4A). Each monomer of ThDyP contains three heme access channels. The largest of them, the propionate pocket, is depicted in the inset (**Figure 11**; Publication II, Fig. 4A). Channel modelling indicates that this access route is wide and open enough for ABTS to reach and directly interact with the heme. This corroborates that competitive binding of ABTS and H₂O₂ to the resting state heme of ThDyP may cause substrate inhibition of ThDyP by ABTS (**Figure 10**; Publication II, Fig. 2B).

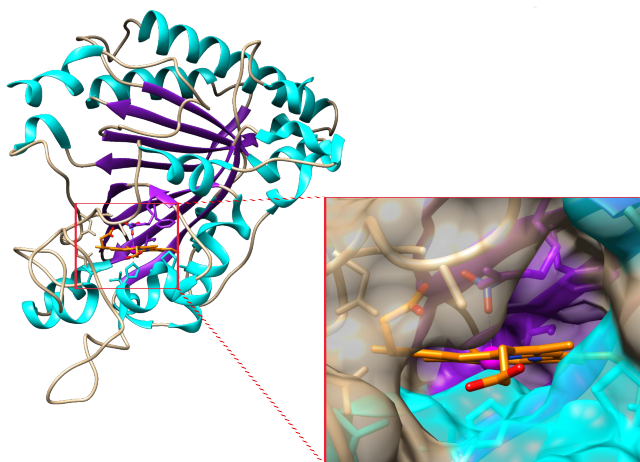


Figure 11. Structure of ThDyP. The structure of the ThDyP monomer (PDB ID: 8CK9). α -helices, β -sheets, and loops are shown in cyan, purple, and tan, respectively. The heme is shown in orange-red-blue stick representation and the iron as a magenta sphere. The inset highlights the propionate pocket of ThDyP, which is proposed as the main heme-access channel for reducing substrates.

4.2.6 Investigations of positive cooperativity (Publication II)

The atypicality of ABTS oxidation kinetics was not solely limited to substrate inhibition by ABTS, but further complicated by apparent positive cooperativity of ABTS. Apparent positive cooperativity was observed only at higher H_2O_2 concentrations (25–1000 μM) and not at lower H_2O_2 concentrations (1.0–10 μM) (**Figure 9A**; Publication II, Fig. 1A). Additionally, it was not seen in the oxidation of other reducing substrates (hydroquinones and dyes). Varying H_2O_2 concentration did not lead to the observation of positive cooperativity (**Figure 9B**; Publication II, Fig. 1B). Kinetics displaying positive cooperativity was analyzed using non-linear regression analysis of the data according to the empirical Hill equation (Equation 6). Data points showing substrate inhibition were excluded from the analysis of this kinetics data. An average h value of 2.0 ± 0.1 (Publication II, Fig. S1) was measured for the series made at different H_2O_2 concentrations. The kinetic parameters for H_2O_2 and ABTS are shown in Publication II, Table S1 and Table S2, respectively.

According to the classic understanding of cooperativity, multiple binding sites and subunits could explain this phenomenon. In the case of ThDyP, the catalysis of the oxidation of ABTS can occur directly in the heme cavity (**Figure 9A**; Publication II, Fig. 4A) or potentially at surface sites of the enzyme via LRET. Additionally, PISA analysis of the crystal structure model suggests that ThDyP forms a dimeric structure. The theoretical molecular weight of ThDyP is 45 kDa. The results of gel filtration aligned with the findings of PISA analysis, revealing a prominent peak with an apparent molecular weight of 76 kDa (Publication II, Fig. S7). Therefore, dimeric structure of ThDyP could explain the observed cooperativity with the h value of 2.

4.2.7 Model explaining positive cooperativity together with substrate inhibition (Publication II)

While classic explanations of cooperativity could not be entirely ruled out, it is noteworthy that apparent positive cooperativity was observed exclusively with ABTS (**Figure 9A**; Publication II, Fig. 1A). In comparison to other tested reducing substrates, ABTS is a one-electron donor, while hydroquinones and dyes are two-electron donors. It is important to note that the reduction of Cpd I back to the resting state enzyme requires two electrons, and DyPs can also utilize the shunt pathway. In this pathway, Cpd II is bypassed, allowing Cpd I to revert directly to the resting state enzyme through a two-electron reduction (**Figure 4**; Publication II, Fig. 2A). However, this mechanism is only feasible with substrates that can donate two electrons, which excludes ABTS (Publication II, Scheme 1). We proposed that the apparent positive cooperativity is due to the formation of a productive complex involving two single-electron-donating substrates, like ABTS (**Figure 12A**; Publication II, Fig. 5). As in Figure 10, this model also assumes that substrate inhibition arises from the competitive binding of ABTS and H₂O₂ to the resting state heme of *ThDyP* (**Figure 10**; Publication II, Fig. 5A). This mechanism was solved, yielding a rate equation (Equation 11). The k_{cat} and equilibrium constants are defined in **Figure 12A**; Publication II, Fig. 5A.

$$\frac{v}{E_0} = -\frac{d[H_2O_2]}{dt} = 2\frac{d[P]}{dt} = \frac{k_{cat}[S]^2[H_2O_2]}{[S]^2[H_2O_2] + \frac{k_{cat}K_{H_2O_2}}{k_{ox}}[S]^2\left(1 + \frac{[S]}{K_{i(S)}}\right) + \frac{k_{cat}K_{SS}K_S}{k_{red}}[H_2O_2]\left(1 + \frac{[H_2O_2]}{K_{i(H_2O_2)}}\right) + \frac{k_{cat}K_{SS}}{k_{red}}[S][H_2O_2]} \quad \text{Equation 11}$$

In equation 11, [P] denotes the concentration of the one-electron-oxidized product. In the series where positive cooperativity with ABTS was observed, this equation appropriately describes the results related to the oxidation of ABTS (**Figure 11**; Publication II, Fig. 5B). The squared term of substrate concentration in the nominator accounts for the ability of Equation 11 to accommodate the apparent positive cooperativity. Our experimental findings, which yielded an h value of 2 (Publication II, Fig. S1), support the notion that the oxidation of ABTS involves the simultaneous binding of two ABTS molecules.

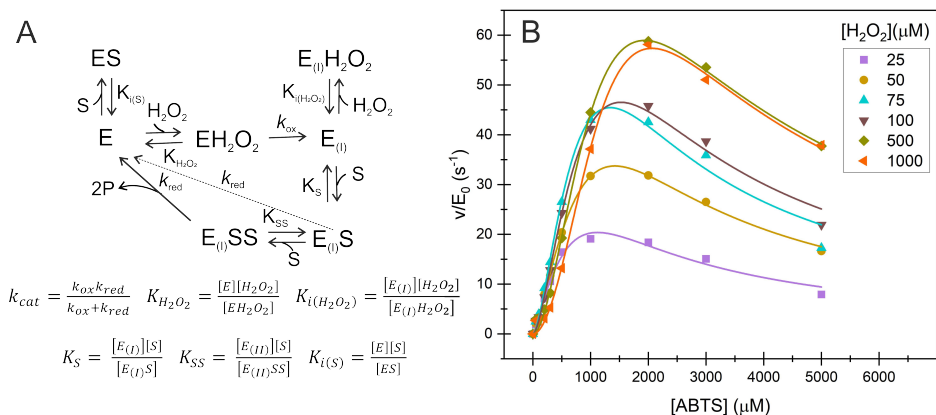


Figure 12. Kinetic mechanism of ThDyP catalysis. (A) In this mechanism, Cpd II does not form, and Cpd I is directly reduced back to the resting state via a simultaneous two-electron transfer from the substrate. For single-electron donors like ABTS, this involves the formation of a Cpd I complex with two substrate molecules ($E_{(I)}SS$) (the reduction pathway indicated by the solid arrow). In contrast, for two-electron donating substrates such as hydroquinones and anthraquinone dyes, the $E_{(I)}SS$ complex is not required (k_{red} pathway indicated by the dashed arrow). The rate and equilibrium dissociation constants used to derive Equation 11 and Equation 12 are detailed in the panel. (B) The data are shown from **Figure 8** (Publication II, Fig. 1A), excluding the series with $[H_2O_2] \leq 10 \mu M$ where positive cooperativity was not observed, for clarity. The solid lines represent the non-linear regression analysis of the dependence of the initial rates of ABTS oxidation on $[ABTS]$ according to Equation 11.

Positive cooperativity was not observed with other tested reducing substrates, which differ from ABTS by their ability to donate two electrons. For these substrates, there is no requirement for the enzyme complex with two substrate molecules. The route indicated by the dashed arrow can be used (**Figure 12A**; Publication II, Fig. 5A), leading to a simplified Equation 12.

$$\begin{aligned}
 \frac{v}{E_0} &= -\frac{d[H_2O_2]}{dt} = \frac{d[P]}{dt} = \\
 &= \frac{k_{cat}[S][H_2O_2]}{[S][H_2O_2] + \frac{k_{cat}K_{H_2O_2}}{k_{ox}}[S] \left(1 + \frac{[S]}{K_{i(S)}}\right) + \frac{k_{cat}K_S}{k_{red}}[H_2O_2] \left(1 + \frac{[H_2O_2]}{K_{i(H_2O_2)}}\right)} \quad \text{Equation 12}
 \end{aligned}$$

Note that in Equation 12, $[P]$ represents the concentration of the two-electron-oxidized product. Equation 12 lacks the squared term of substrate concentration in the numerator and thus cannot account for positive cooperativity. Compatibly, no positive cooperativity was observed in the oxidation of two-electron-donating substrates (MHQ, DMHQ, RB4, and RB19) by ThDyP (**Figure 9C, E**; Publication II, Fig. 1C, E).

4.2.8 Dependence of the activity on the concentration of ScDyPB (Publication III)

Activity measurements were conducted with two substrates, ABTS and MHQ, using different concentrations and pH in the enzyme working stock (enzyme stock solution to be diluted in the cuvette) (**Figure 13**; Publication III, Fig. 2). In activity measurements with ABTS, significantly higher activities were observed when the reaction was initiated with enzyme stock solution prepared in sodium acetate (NaAc) at pH 4.0 compared to Tris-HCl

pH 7.5 buffer (**Figure 13A**; Publication III, Fig. 2A). When varying the concentration of the enzyme in the working stock while keeping the concentration in the cuvette constant, the activity plateaued as the concentration of ScDyPB in the working stock increased. The apparent half-saturating concentration of ScDyPB in the pH 4.0 working stock was $0.03 \mu\text{M}$, approximately 13-times lower than that in the pH 7.5 working stock (**Figure 13C**; Publication III, Fig. 2C).

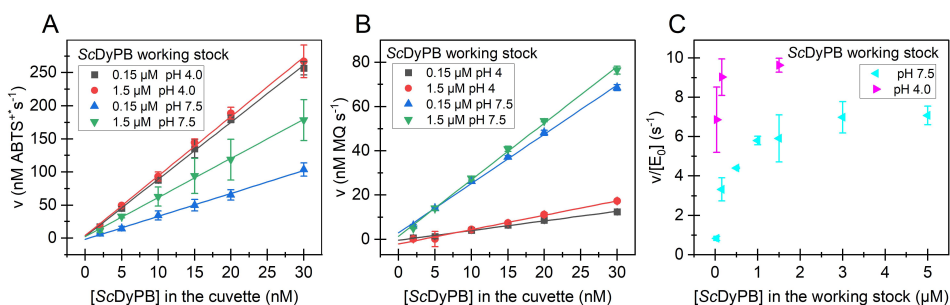


Figure 13. Dependence of the enzymatic activity on the concentration of ScDyPB in the cuvette and working stock. All reactions were performed in NaAc buffer (50 mM, pH 4.0). **(A)** and **(B)** show the rates of the oxidation of ABTS and MHQ, respectively, at varying concentrations of ScDyPB in the cuvette. The concentration of ScDyPB in the working stock and its pH are indicated in the figure. Solid lines represent linear regression of the data. **(C)** shows the dependence of the ABTS-oxidizing activity of ScDyPB on its concentration in the working stock. The pH of the working stock is indicated in the figure. The concentration of ScDyPB in the cuvette was 15 nM. Working stocks of ScDyPB, with concentrations ranging from 30 nM to 5 μM , were prepared at pH 4.0 and pH 7.5. Data are presented as average values from three independent experiments ($n = 3$).

The higher activity observed in reactions initiated from working stocks with higher enzyme concentrations can be attributed to the enzyme being active as an oligomer. Control experiments (Publication III, Fig. S1) suggested that the equilibrium established between different oligomerization states is not rapidly achieved, at least not within the timeframe of the reaction occurring in the cuvette, and that the higher oligomeric state is maintained during activity measurements. These results imply that the higher oligomeric state is favored for the oxidation of ABTS (**Figure 13C**; Publication III, Fig. 2C) and that its formation is enhanced by lower pH (**Figure 13A, C**; Publication III, Fig. 2A, C). Unlike with ABTS, higher activity with MHQ was noted when the enzyme stock was prepared in Tris-HCl buffer at pH 7.5, suggesting that increased oligomeric forms may reduce MHQ oxidizing activity and that lower oligomeric forms are preferred for MHQ oxidation. However, no enzyme working stock concentration-dependent effect was observed when using MHQ as the reducing substrate (**Figure 13B**; Publication III, Fig. 2B). It is thus possible that different forms of ScDyPB may be responsible for the oxidation of ABTS and MHQ.

The pH of the ScDyPB working stock had distinct effects on the oxidizing activity of ABTS and MHQ (**Figure 13A, B**; Publication III, Fig. 2A, B). In addition to pH, we investigated the influence of various additives in the enzyme's working stock. Among these, only the addition of 1.0 M ammonium sulfate significantly affected oxidation of ABTS and MHQ. Specifically, ammonium sulfate led to an approximately twofold increase in ABTS oxidation rate, while MHQ oxidation decreased roughly fourfold (Publication III, Fig. 3). The contrasting effects of ammonium sulfate on the catalytic activities with ABTS and

MHQ mirrored the opposite pH effects observed in the working stock (**Figure 13A, B**; Publication III, Fig. 2A, B), once again suggesting the involvement of different oligomeric forms of ScDyPB in the oxidation of ABTS and MHQ.

4.3 Analysis of the size distribution of ScDyPB (Publication III)

Our objective was to determine the potential oligomeric forms of ScDyPB under different conditions. Both size exclusion chromatography (SEC) and DLS analyses confirmed that ScDyPB exists as a mixture of oligomeric forms of varying sizes. SEC analysis showed that ScDyPB exists as a mixture of monomers (36 kDa) and trimers at pH 7.5, along with a notably larger molecular species likely corresponding to aggregates (**Figure 14A**).

DLS analysis indicated that the oligomeric composition of ScDyPB is complex, existing as a diverse blend of particles ranging in size from 9 nm to over 4 μm . The core dimensions of a ScDyPB monomer (PDB ID: 4GU7) are 6 x 5 x 4 nm. The majority of ScDyPB was observed as oligomers with an average size of approximately 10 nm (**Figure 14C**; Publication III, Fig. 5C, Table 1). Additionally, DLS analysis confirmed that the presence of ammonium sulfate led to an increase in the average size of ScDyPB oligomers (**Figure 14C**; Publication III, Fig. 5C, Table 1). The size of ScDyPB oligomers was highest at pH 7.5 in the presence of ammonium sulfate, followed by pH 4.0 and pH 7.5 without ammonium sulfate (**Figure 14B, C**; Publication III, Fig. 5B, C, Table 1). However, while DLS provided estimates of average sizes of different oligomeric forms (approximately 10 nm) under various conditions, it was not possible to precisely identify the exact oligomeric states of ScDyPB.

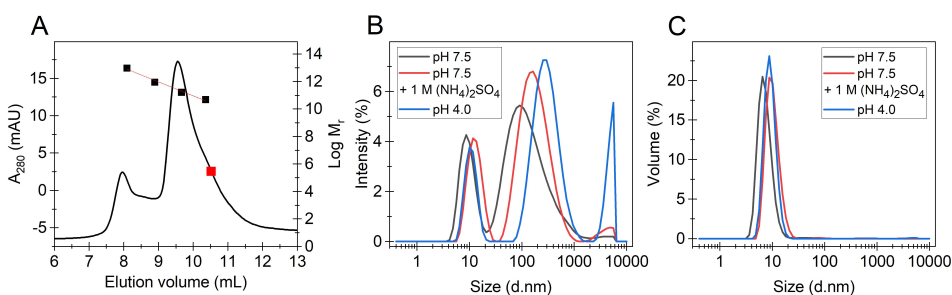


Figure 14. Analysis of the size distribution of ScDyPB. (A) Gel filtration chromatogram of ScDyPB at pH 7.5. Black squares indicate the elution volumes of standard proteins: ferritin (440 kDa), aldolase (158 kDa), conalbumin (75 kDa), and ovalbumin (44 kDa). The red line represents the linear regression of the mobility of these standard proteins used for calibration, and the red square marks the expected elution volume of the ScDyPB monomer. **(B, C)** DLS analysis of ScDyPB at pH 4.0, at pH 7.5, and at pH 7.5 supplemented with 1.0 M ammonium sulfate, as indicated in the plots, based on intensity **(B)** and volume **(C)**. Each trace represents the average of at least four consecutive scans.

4.4 ScDyPs acting on organosolv lignin (Publication I)

The ligninolytic activities of three ScDyPs were assessed using two different organosolv lignins sourced from perennial grass *Mxg* and aspen (*Populus tremula*). The lignins were incubated with ScDyPs for 24 h, then centrifuged, and the resulting pellets were analyzed with GPC to determine the molecular weight distributions of both enzymatically treated and untreated lignins. Additionally, the supernatants from the lignin treatments were analyzed using GC-MS to identify the most prominent LMW compounds.

Given that enzymatic treatment with ScDyPs showed no discernible effect at acidic pH, a range of pH conditions, from acidic to alkaline, was tested. The enzymes exhibited the highest activity on lignin within the pH range of 7.5 to 8.5, with optimal activity observed around pH 8.5 (data not shown). GPC results of ScDyP-treated lignins highlighted differences among the subfamilies of DyPs on *Mxg* and aspen lignin (**Figure 15**; Publication I, Table 4, Fig. 5). Treatment with ScDyPs from subfamily A had no significant impact on the molecular weight distribution of *Mxg*-lignin; however, these DyPs were effective at depolymerizing aspen lignin, with ScDyP2A showing the highest activity and resulting in approximately a 20% reduction in the weight-average molecular weight (Mw). In contrast, ScDyP1A was less efficient. Treatment with ScDyPB did not affect the Mw of aspen lignin but did increase the polymerization of *Mxg*-lignin by up to 19%.

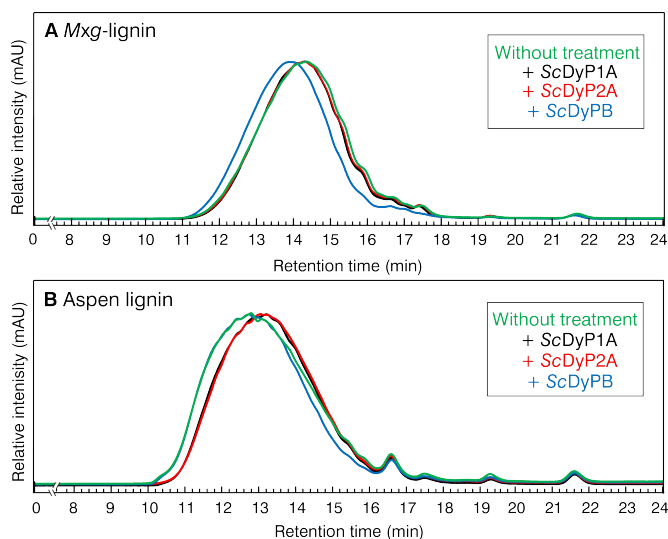


Figure 15. GPC analysis of lignin. (A) GPC chromatogram of *Mxg*-lignin and (B) aspen organosolv lignin treated with ScDyP1A (black), ScDyP2A (red), and ScDyPB (blue). 1 mg/mL of lignin in HEPES buffer (50 mM, pH 8.0) was treated with 10 μ M of ScDyPs, 2 mM H₂O₂ for 24 h, at 28 °C. The reaction mixtures and controls were centrifuged, lyophilized, dissolved in tetrahydrofuran, and analyzed using GPC.

Based on the GC-MS results, the soluble LMW fraction of *Mxg*-lignin predominately consisted of H-units, with fewer G-units, and a minor presence of S-units. In contrast, aspen lignin was predominately composed of S-units, with fewer G-units, and a minimal proportion of H-units (as determined by the integrated peak area). When comparing the supernatants of enzymatically treated lignin with those of untreated lignin, treatment with all ScDyPs produced similar effects. The enzymatic treatment reduced the amount

of LMW compounds in the supernatants of both organosolv lignins (Publication I, Table 5). Notably, *ScDyPB* had the most significant impact on monolignols. After the treatment with *ScDyPB*, 91–98% of the peak area disappeared or was undetected altogether in the *Mxg*-lignin supernatant. Overall, *ScDyPs* can be considered lignin-active enzymes capable of remodeling organosolv lignin.

5 Discussion

5.1 The non-conventional kinetics of DyPs

Even a quarter-century after their discovery, DyPs continue to captivate researchers, offering numerous opportunities for further investigation. The challenge in understanding DyPs lies in elucidating the molecular mechanisms responsible for their non-MM kinetics. Several studies, including Publications I–III, demonstrate that the kinetics of DyPs can be complex. This complexity is exemplified by substrate inhibition by H_2O_2 (Publications I–III), substrate inhibition by the reducing substrate (Publications II and III), and apparent positive cooperativity (Publication II). In publications II–III, we aimed to understand the molecular mechanisms behind the substrate inhibition, apparent positive cooperativity, and the observed apparent biphasic kinetics.

5.1.1 Substrate inhibition

The in-depth kinetics of ABTS oxidation by *Th*DyP presents a complex example of atypical DyP kinetics, demonstrating both substrate inhibition and positive cooperativity. Substrate inhibition refers to the reduction in enzymatic activity due to an excess of substrate, which occurs after the maximum turnover rate has been reached. For enzymes that follow ping-pong kinetics, substrate inhibition occurs when the substrate binds to the wrong form of the enzyme. In the case of heme peroxidases, the wrong form for the reducing substrate is the resting state, while for H_2O_2 , it is Cpd I (or Cpd II). In *Th*DyP, the initial rates of oxidation of ABTS exhibited substrate inhibition by both ABTS and H_2O_2 (**Figure 9**; Publication II, Fig. 1A and Fig. 1B, respectively). Substrate inhibition by ABTS was also observed in *Sc*DyPs (Publication I, Table 3, **Figure 8A**; Publication III, Fig. 4A). Inactivation of *Th*DyP by H_2O_2 indicates that it binds to Cpd I (Publication II, Fig. 3A). Our findings suggest that ABTS and H_2O_2 compete for Cpd I. Therefore, the substrate inhibition by H_2O_2 results from the formation of a non-productive complex between Cpd I and H_2O_2 (Publication II and III). We propose that the wide heme access channel allows direct contact with the heme. In that case, ABTS binds to the resting state of the enzyme and competes with H_2O_2 for binding to the resting state, leading to substrate inhibition (Publication II). Substrate inhibition by one substrate became more pronounced at lower concentrations of the other substrate: inhibition by ABTS at lower H_2O_2 concentrations (**Figure 9A**; Publication II, Fig. 1A) (**Figure 8A**; Publication III, Fig. 4A, Fig. S2A) and by H_2O_2 at lower ABTS concentrations (**Figure 9B**; Publication II, Fig. 1B). This is another characteristic kinetic feature of enzymes that exhibit a ping-pong mechanism.

It has been shown that ABTS can protect the enzyme from H_2O_2 inactivation only when the ratio of ABTS to H_2O_2 remains high [164]. In the case of *Th*DyP, inactivation requires approximately 4.6 ± 0.9 molecules of H_2O_2 (Publication II, Fig. 3A). To our knowledge, the presence of the Cpd III pathway or catalase-like activity has not been demonstrated in DyPs, including *Sc*DyPs and *Th*DyP (Publications I–III). Therefore, DyPs lack this form of enzyme protection. As a result, the stoichiometry of inactivation in DyPs is more comparable to that of enzymes that also do not exhibit catalase activity [72].

5.1.2 Positive cooperativity

The classic explanation of cooperativity involves multiple active sites or is associated with multimeric enzymes. It is a phenomenon in which the binding of a substrate to one active site of a protein affects the binding affinity and/or turnover of subsequent substrate molecule at the other active site (cooperation between binding sites). In cytochrome P450, it has been shown that the reason behind cooperativity is the simultaneous binding of multiple substrates [180]. A measure of the degree or extent of cooperativity in enzyme-substrate binding is represented by h value. If $h = 1$, there is no cooperativity; however, if $h > 1$, it indicates positive cooperativity. Furthermore, when the $h = 2$, a maximum of two active sites or subunits are involved. In the case of *ThDyP*, an average h value of 2.0 ± 0.1 was observed (Publication II, Fig. S1). The structure of *ThDyP* is dimeric (Publication II). Therefore, the classic explanations of positive cooperativity remain valid, the dimeric structure, along with the presence of multiple binding sites and the possible binding of ABTS to these sites, provide a plausible explanation for the observed positive cooperativity. However, we proposed an alternative mechanism. No one has yet demonstrated the existence of allosteric inhibitors and activators for DyPs, which are typically associated with conventional cooperative enzymes. Additionally, positive cooperativity was not observed with two-electron-donating substrates. Therefore, we suggested an explanation for the apparent cooperativity: the kinetic mechanism assumes that Cpd II is not formed and two ABTS molecules must bind to Cpd I simultaneously. The apparent positive cooperativity arises from the formation of a productive complex involving two one-electron-donating substrates (**Figure 12**; Publication II, Fig. 5). In Equation 11, the squared term of ABTS concentration in the nominator accounts for the apparent positive cooperativity and defines the h value of 2.

5.1.3 Biphasic kinetics

The oxidation of ABTS by *ScDyPB* is particularly interesting, as it exhibits biphasic kinetics. Biphasic kinetics have been attributed to the presence of multiple enzyme binding sites with distinct K_M and V_{max} values [181], or, as observed in versatile peroxidase, to the existence of both low- and high-efficiency catalytic sites [182]. Unfortunately, the mechanisms mentioned above could not account for the kinetics of ABTS oxidation by *ScDyPB*, specifically small “kink” in the initial rates versus [ABTS] curves observed around the ABTS concentrations of 0.1–0.2 mM (**Figure 8A**; Publication III, Fig. 4A). We proposed that *ScDyPB* exists in two kinetically distinct, independent enzyme forms. The simplest kinetic model that could describe the observed “kink”, was the combination of classic ping-pong kinetics (form I) and ping-pong kinetics with substrate inhibition by ABTS (form II). It was represented as a sum of two steady-state rate equations. By assuming that the two enzyme forms differ only by the presence of substrate inhibition by ABTS in form II, we were able to estimate the relative abundance of each enzyme form using global non-linear regression analysis according to Equation 8 (Publication III). The non-substrate-inhibited form (0.18 ± 0.01) had much lower abundance compared to the inhibited form (0.82 ± 0.01). Biphasic kinetics were also observed at pH 4.0 as well as at pH 7.5, which suggests that *ScDyPB* exists in two enzyme forms at different pH values.

5.2 Oligomeric states of DyPs

Type A DyPs have been reported to exist as monomers and dimers [99, 100, 104, 121, 126, 183], but also as tetramers and octamers [121]. In our research, we demonstrated that the most probable oligomeric state of *ThDyP* (a type A DyP), based on crystal structure and SEC analysis, is a dimer (Publication II). Although the impact of the oligomeric form of *ThDyP* on its catalytic activity was not examined, the heme is not situated at the oligomerization interface, and its accessibility is not hindered by oligomerization. Crystal interface analysis using PISA, which predicts the native oligomeric state of the enzyme, suggests that *ScDyP1A* (PDB ID: 4GRC) and *ScDyP2A* (PDB ID: 4GT2) also exist as dimers, however, the presence of other oligomeric forms remains to be determined.

Type B DyPs have been found to form assemblies ranging from monomers to hexamers [108, 112, 117, 118, 120, 127, 128, 133, 134]. According to PISA analysis, *ScDyPB* (PDB ID: 4GU7) exists as a hexamer (a trimer of dimers). Although DLS analysis was unable to determine the exact oligomeric state of *ScDyPB* (Publication III), it confirmed SEC results indicating that *ScDyPB* exists as a mixture of different oligomeric forms. SEC analysis revealed that *ScDyPB* has a molecular weight corresponding to something between a dimer and a trimer (91 kDa), with a portion also corresponding to a larger molecular weight (450 kDa). This finding aligns with a recent study by Lučić et al. 2024, which used analytical ultracentrifugation and cryo-EM to show that *DtpB*, a homologous DyP, primarily exists as a hexamer, but dimers and dodecamers are also present [184]. In Publication III, this larger form was thought to be an aggregate; however, it cannot be excluded that the larger molecular weight may correspond to a dodecamer. This suggests that *ScDyPB* may exist as both a dimer (theoretical size: 73 kDa) and a dodecamer (theoretical size: 436 kDa). As there is no gene for an encapsulin protein encoded in *S. lividans* as well as in *S. coelicolor*, these results illustrate that no encapsulin is required to form such high oligomeric assembly, as was previously suggested [108].

Additionally, we demonstrated that the average size of *ScDyPB* was affected by pH and the presence of ammonium sulfate (**Figure 14**; Publication III, Fig. 5, Table 1). According to DLS analysis, the presence of ammonium sulfate increased the average size of *ScDyPB* (Publication III, Table 1), indicating that hydrophobic interactions may contribute to the formation of oligomers. Changes in the protein's net charge (e.g., induced by changes in pH) can cause electrostatic repulsion and disrupt hydrogen bonding. The average size of *ScDyPB* also varied with pH, with a higher average size observed at pH 4.0, suggesting that lower pH favors higher oligomeric states. This finding contradicts the results of gel filtration for an A-type DyP from *B. subtilis* *BsDyP*, which existed in similar oligomeric forms at both neutral and pH 4.0 [123].

5.2.1 Relationships between catalytic activity and degree of oligomerization of *ScDyPB*

Although the existence of DyPs in different oligomeric forms is well reported, a very little is known about the relationships between the degree of oligomerization and catalytic activity. The activity of *ScDyPB* depended on the concentration of the enzyme working stock used for starting the reaction and the substrate used for the activity measurement (**Figure 13**; Publication III, Fig. 2). When higher activity is observed using a higher enzyme stock concentration, it suggests that the enzyme is active as an oligomer as the formation of higher oligomeric forms is favored. This was seen only with ABTS, the higher working

stock concentration did not result in increased MHQ oxidizing activity. The presence of 1 M ammonium sulfate in the working stock increased the ABTS oxidizing activity but decreased the MHQ oxidizing activity (Publication III, Fig. 3). Furthermore, the activity of ScDyPB depended on the pH of the enzyme working stock, and the effects were differential depending on the substrate used. The ABTS oxidizing activity was higher when the enzyme was prepared in a working stock at pH 4.0 compared to pH 7.5 (**Figure 12**; Publication III, Fig. 2A). Conversely, the opposite trend was observed with MHQ, where higher activity was seen when the enzyme was from the working stock prepared at pH 7.5 (**Figure 12**; Publication III, Fig. 2B). As mentioned previously, DLS analysis indicates that the lower pH and the presence of ammonium sulfate promote a higher oligomeric state of DyP (**Figure 14**; Publication III, Fig. 5, Table 1). Therefore, higher oligomeric forms appear to favor ABTS oxidation, which is promoted by the lower pH of the working stock, whereas lower oligomeric forms favor MHQ oxidation. These results suggest that different oligomeric forms may play distinct roles in the catalysis of ABTS and MHQ oxidation. The findings from these activity measurements (**Figure 13**, **Figure 14**; Publication III, Fig. 2, Fig. 3), along with the analysis of size distribution of ScDyPB, allowed us to propose a model involving different oligomeric forms.

Our model (**Figure 16**; Publication III, Fig. 6B) is based on four key assumptions:

- (i) ScDyPB exists in two enzyme forms: one with a high degree of oligomerization (HDO) and another with a low degree of oligomerization (LDO).
- (ii) ABTS can be oxidized via LRET at the surface binding site, whereas the oxidation of MHQ requires direct contact with Cpd I.
- (iii) ABTS causes substrate inhibition by competing with H₂O₂ for binding to the heme resting state, thereby hindering the formation of Cpd I.
- (iv) Both ABTS and MHQ can directly access the heme and Cpd I only in the LDO form. H₂O₂ can access the heme in both LDO and HDO forms of ScDyPB.

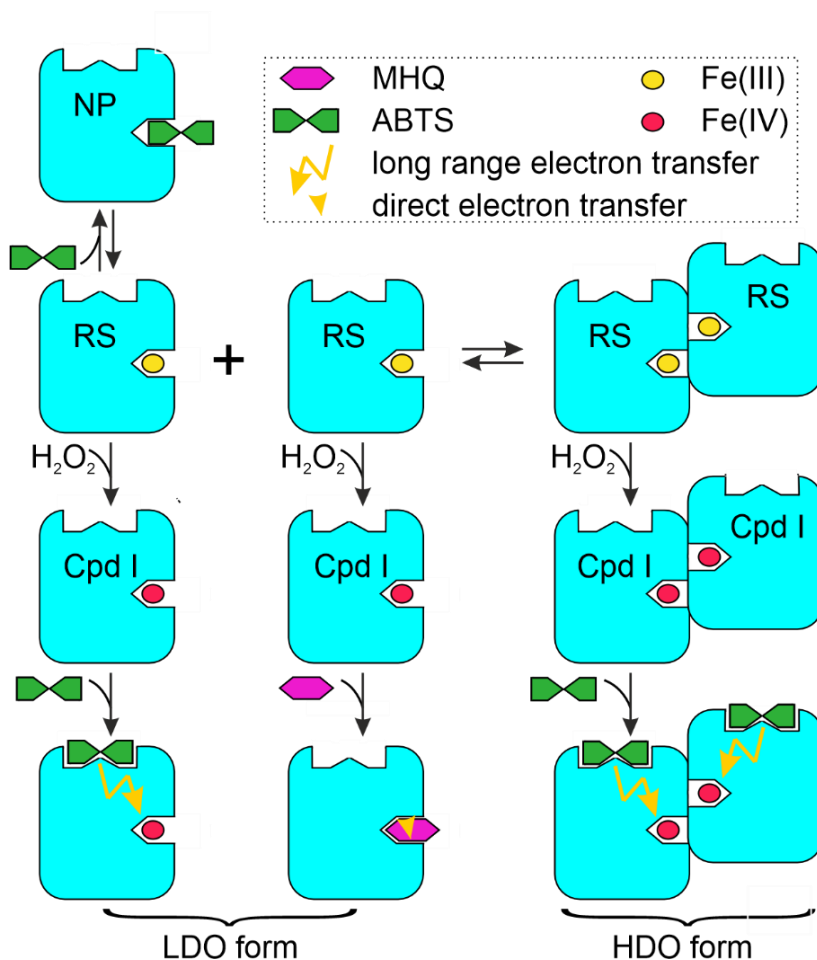


Figure 16. The schematic representation of mechanism for the oxidation of ABTS and MHQ by ScDyPB, as proposed in Publication III. ScDyPB exists as an equilibrium of two kinetically different, LDO and HDO forms. For the sake of simplicity, the LDO and HDO forms are represented as monomers and dimers, respectively.

ScDyPB has a channel leading to the heme that is accessible to reducing substrates in the LDO form. The proposed model assumed that this access is obstructed in the HDO form. Although oxidation of ABTS can occur in the HDO form, the oxidation of MHQ is only possible in the LDO form and is suppressed in the HDO form. Non-productive binding of ABTS to the enzyme's resting state, leading to substrate inhibition by ABTS, occurs only in the LDO form. Consequently, the oxidizing activity of ABTS increases as substrate inhibition is relieved in the HDO form. In this model, HDO and LDO forms would correspond to enzyme forms I and II in Equation 7, respectively. However, since the heme access channel is blocked in the HDO form, the oxidizing activity of MHQ decreases. It is important to note that potential substrate inhibition by MHQ and the direct oxidation of ABTS (without using LRET) were not considered in this model for simplicity, as they do not influence the overall outcome. Although consistent with our results, this mechanism would require further studies.

A recent study by Lučić et al. 2024 on the oligomeric states of DyPs from *S. lividans* and their impact on substrate oxidation provides some insights. *S. lividans* is highly similar to *S. coelicolor*, with the type B DyP, DtpB, sharing 94% similarity to ScDyPB. DtpB exists as a mixture of hexamer, dimer, and dodecamer. In DtpB, the access channels to and from the heme are accessible in different oligomeric states, including the dodecamer. However, it was proposed that the low activity of DtpB with synthetic dyes may partly be attributed to their inability to pass through the access channels in the hexamer, preventing them from approaching the heme, as well as to the absence of a LRET pathway [184]. If the HDO form corresponds to a hexamer, the heme is still accessible, as the heme is not positioned at the oligomerization interface (Publications II & III). However, if the heme is accessible to the reducing substrate in the dodecamer of ScDyPB, then the HDO form cannot correspond to a dodecamer. Further studies on the catalytic activity of DyPs with varying degrees of oligomerization are needed to determine whether our proposed model is true.

5.3 Activity on organosolv lignin

S. coelicolor is a Gram-positive bacterium known for utilizing laccases for lignin degradation [2]. We hypothesized that an ensemble of DyPs might also be necessary for lignin degradation. To test this hypothesis, we characterized three ScDyPs and assessed their effects on lignin. Our results demonstrated that ScDyPs were active on lignin. ScDyPAs were capable of depolymerizing lignin derived from aspen biomass, while the opposite effect was observed with ScDyPB. The treatment of *Mxg* biomass-derived lignin with ScDyPB led to lignin polymerization (**Figure 15**; Publication I, Fig. 5). This outcome is not uncommon due to the involvement of reactive radical species [185].

ScDyPB, which exhibited the highest activity in oxidizing ABTS, had the greatest impact on monolignols, significantly reducing the amount of these LMW compounds in the supernatant of *Mxg*-lignin. Only 2–9% of the peak area was retained after treatment or, in some cases, was even rendered undetectable. Most likely, as the soluble LMW compounds are oxidized and the generated radicals combine with insoluble lignin, these compounds remain in the pellet fraction after centrifugation. These results suggest that ScDyPs could be an effective tool for removing LMW phenolic compounds. While GC-MS analysis did not determine the complete content of monolignols, it provided a potential explanation for the results of size distribution analysis. Since *Mxg*-lignin contains more H-units than aspen lignin, it seems that a higher number of H-units enhances (re)polymerization by increasing crosslinking potential. In summary, DyPs from *S. coelicolor* can be considered lignin-active enzymes capable of remodeling organosolv lignin. Even if their application on lignin may not be highly effective, DyPs could replace classic peroxidases for other applications, such as dye degradation or even immunoassays [186].

Conclusions

This thesis contributes to the understanding of DyPs by studying A- and B-type DyPs from the Gram-positive bacteria *S. coelicolor* and *T. halotolerans*, providing novel insights into the relationship between the oligomeric state and kinetic properties, as well as the mechanisms underlying the non-conventional kinetics of these enzymes and their activity on lignin.

The main conclusions are as follows:

- Non-productive complexes with H₂O₂ and reducing substrate are responsible for substrate inhibition.
- Productive complex with two single-electron donating substrate molecules may be responsible for apparent positive cooperativity observed with *ThDyP*.
- *ScDyPB* exists as a mixture of enzyme forms with different degrees of oligomerization and different kinetic properties.
- *ScDyPs* can modify organosolv lignin; *ScDyPB* can polymerize grassy biomass-derived lignin and *ScDyPAs* can depolymerize hardwood-derived lignin.

References

1. Kumar, A., Anushree, Kumar, J. & Bhaskar, T. (2020) Utilization of lignin: A sustainable and eco-friendly approach, *J Energy Inst.* **93**, 235-271.
2. Majumdar, S., Lukk, T., Solbiati, J. O., Bauer, S., Nair, S. K., Cronan, J. E. & Gerlt, J. A. (2014) Roles of small laccases from *Streptomyces* in lignin degradation, *Biochemistry.* **53**, 4047-4058.
3. Zoghلامي, A. & Paes, G. (2019) Lignocellulosic Biomass: Understanding Recalcitrance and Predicting Hydrolysis, *Front Chem.* **7**, 874.
4. Cao, L., Yu, I. K. M., Liu, Y., Ruan, X., Tsang, D. C. W., Hunt, A. J., Ok, Y. S., Song, H. & Zhang, S. (2018) Lignin valorization for the production of renewable chemicals: State-of-the-art review and future prospects, *Bioresour Technol.* **269**, 465-475.
5. Rongpipi, S., Ye, D., Gomez, E. D. & Gomez, E. W. (2018) Progress and Opportunities in the Characterization of Cellulose - An Important Regulator of Cell Wall Growth and Mechanics, *Front Plant Sci.* **9**, 1894.
6. Scheller, H. V. & Ulvskov, P. (2010) Hemicelluloses, *Annu Rev Plant Biol.* **61**, 263-289.
7. Liu, Q., Luo, L. & Zheng, L. (2018) Lignins: Biosynthesis and Biological Functions in Plants, *Int J Mol Sci.* **19**, 335.
8. de Candolle, A. P. (1813) *Théorie élémentaire de la botanique; ou, Exposition des principes de la classification naturelle et de l'art de décrire et d'étudier les végétaux*, Déterville, Paris.
9. Koranyi, T. I., Fridrich, B., Pineda, A. & Barta, K. (2020) Development of 'Lignin-First' Approaches for the Valorization of Lignocellulosic Biomass, *Molecules.* **25**, 2815.
10. Vanholme, R., De Meester, B., Ralph, J. & Boerjan, W. (2019) Lignin biosynthesis and its integration into metabolism, *Curr Opin Biotechnol.* **56**, 230-239.
11. Chio, C., Sain, M. & Qin, W. (2019) Lignin utilization: A review of lignin depolymerization from various aspects, *Renew Sust Energy Rev.* **107**, 232-249.
12. Becker, J. & Wittmann, C. (2019) A field of dreams: Lignin valorization into chemicals, materials, fuels, and health-care products, *Biotechnol Adv.* **37**, 107360.
13. Ralph, J., Lapierre, C. & Boerjan, W. (2019) Lignin structure and its engineering, *Curr Opin Biotechnol.* **56**, 240-249.
14. Abu-Omar, M. M., Barta, K., Beckham, G. T., Luterbacher, J. S., Ralph, J., Rinaldi, R., Román-Leshkov, Y., Samec, J. S. M., Sels, B. F. & Wang, F. (2021) Guidelines for performing lignin-first biorefining, *Energy Environ Sci.* **14**, 262-292.
15. del Río, J. C., Rencoret, J., Gutiérrez, A., Elder, T., Kim, H. & Ralph, J. (2020) Lignin Monomers from beyond the Canonical Monolignol Biosynthetic Pathway: Another Brick in the Wall, *ACS Sustain Chem Eng.* **8**, 4997-5012.
16. Cragg, S. M., Beckham, G. T., Bruce, N. C., Bugg, T. D., Distel, D. L., Dupree, P., Etxabe, A. G., Goodell, B. S., Jellison, J., McGeehan, J. E., McQueen-Mason, S. J., Schnorr, K., Walton, P. H., Watts, J. E. & Zimmer, M. (2015) Lignocellulose degradation mechanisms across the Tree of Life, *Curr Opin Chem Biol.* **29**, 108-119.
17. Wilhelm, R. C., Singh, R., Eltis, L. D. & Mohn, W. W. (2019) Bacterial contributions to delignification and lignocellulose degradation in forest soils with metagenomic and quantitative stable isotope probing, *ISME J.* **13**, 413-429.
18. Guo, H., Zhao, Y., Chang, J. S. & Lee, D. J. (2023) Enzymes and enzymatic mechanisms in enzymatic degradation of lignocellulosic biomass: A mini-review, *Bioresour Technol.* **367**, 128252.

19. Janusz, G., Pawlik, A., Sulej, J., Swiderska-Burek, U., Jarosz-Wilkolazka, A. & Paszczynski, A. (2017) Lignin degradation: microorganisms, enzymes involved, genomes analysis and evolution, *FEMS Microbiol Rev.* **41**, 941-962.
20. Bugg, T. D., Ahmad, M., Hardiman, E. M. & Rahmanpour, R. (2011) Pathways for degradation of lignin in bacteria and fungi, *Nat Prod Rep.* **28**, 1883-1896.
21. Sanchez, C. (2009) Lignocellulosic residues: biodegradation and bioconversion by fungi, *Biotechnol Adv.* **27**, 185-194.
22. Tribot, A., Amer, G., Abdou Alio, M., de Baynast, H., Delattre, C., Pons, A., Mathias, J.-D., Callois, J.-M., Vial, C., Michaud, P. & Dussap, C.-G. (2019) Wood-lignin: Supply, extraction processes and use as bio-based material, *Eur Polym J.* **112**, 228-240.
23. Bugg, T. D. H. (2024) The chemical logic of enzymatic lignin degradation, *Chem Commun.* **60**, 804-814.
24. Castano, J., Zhang, J., Zhou, M., Tsai, C. F., Lee, J. Y., Nicora, C. & Schilling, J. (2021) A Fungal Secretome Adapted for Stress Enabled a Radical Wood Decay Mechanism, *mBio.* **12**, e0204021.
25. Peng, Q., Lin, L., Tu, Q., Wang, X., Zhou, Y., Chen, J., Jiao, N. & Zhou, J. (2023) Unraveling the roles of coastal bacterial consortia in degradation of various lignocellulosic substrates, *mSystems.* **8**, e0128322.
26. Shin, S. K., Ko, Y. J., Hyeon, J. E. & Han, S. O. (2019) Studies of advanced lignin valorization based on various types of lignolytic enzymes and microbes, *Bioresour Technol.* **289**, 121728.
27. Li, C., Chen, C., Wu, X., Tsang, C. W., Mou, J., Yan, J., Liu, Y. & Lin, C. S. K. (2019) Recent advancement in lignin biorefinery: With special focus on enzymatic degradation and valorization, *Bioresour Technol.* **291**, 121898.
28. Goodell, B., Winandy, J. E. & Morrell, J. J. (2020) Fungal Degradation of Wood: Emerging Data, New Insights and Changing Perceptions, *Coatings.* **10**, 1210.
29. Shary, S., Ralph, S. A. & Hammel, K. E. (2007) New insights into the ligninolytic capability of a wood decay ascomycete, *Appl Environ Microbiol.* **73**, 6691-6694.
30. Antai, S. P. & Crawford, D. L. (1981) Degradation of softwood, hardwood, and grass lignocelluloses by two streptomyces strains, *Appl Environ Microbiol.* **42**, 378-380.
31. Zeng, J., Singh, D., Laskar, D. D. & Chen, S. (2012) Degradation of native wheat straw lignin by *Streptomyces viridosporus* T7A, *Int J Environ Sci Technol.* **10**, 165-174.
32. Mycroft, Z., Gomis, M., Mines, P., Law, P. & Bugg, T. D. H. (2015) Biocatalytic conversion of lignin to aromatic dicarboxylic acids in *Rhodococcus jostii* RHA1 by re-routing aromatic degradation pathways, *Green Chem.* **17**, 4974-4979.
33. Sainsbury, P. D., Hardiman, E. M., Ahmad, M., Otani, H., Seghezzi, N., Eltis, L. D. & Bugg, T. D. (2013) Breaking down lignin to high-value chemicals: the conversion of lignocellulose to vanillin in a gene deletion mutant of *Rhodococcus jostii* RHA1, *ACS Chem Biol.* **8**, 2151-2156.
34. Herold-Majumdar, O. M., Loureiro, P. E. G., Ullrich, R. & Felby, C. (2020) The reaction of lignin model compounds during enzymatic bleaching with a *Curvularia verruculosa* haloperoxidase: impact on chlorination, *Holzforschung.* **74**, 156-165.
35. Watkins, D., Nuruddin, M., Hosur, M., Tcherbi-Narteh, A. & Jeelani, S. (2015) Extraction and characterization of lignin from different biomass resources, *J Mater Res Technol.* **4**, 26-32.
36. Chan, J. C., Paice, M. & Zhang, X. (2020) Enzymatic Oxidation of Lignin: Challenges and Barriers Toward Practical Applications, *ChemCatChem.* **12**, 401-425.

37. Hamalainen, V., Gronroos, T., Suonpaa, A., Heikkila, M. W., Romein, B., Ihalainen, P., Malandra, S. & Birikh, K. R. (2018) Enzymatic Processes to Unlock the Lignin Value, *Front Bioeng Biotechnol.* **6**, 20.
38. Reshmy, R., Athiyaman Balakumaran, P., Divakar, K., Philip, E., Madhavan, A., Pugazhendhi, A., Sirohi, R., Binod, P., Kumar Awasthi, M. & Sindhu, R. (2022) Microbial valorization of lignin: Prospects and challenges, *Bioresour Technol.* **344**, 126240.
39. Weng, C., Peng, X. & Han, Y. (2021) Depolymerization and conversion of lignin to value-added bioproducts by microbial and enzymatic catalysis, *Biotechnol Biofuels.* **14**, 84.
40. Biko, O. D. V., Viljoen-Bloom, M. & van Zyl, W. H. (2020) Microbial lignin peroxidases: Applications, production challenges and future perspectives, *Enzyme Microb Technol.* **141**, 109669.
41. Eggert, C., Temp, U. & Eriksson, K. E. (1997) Laccase is essential for lignin degradation by the white-rot fungus *Pycnoporus cinnabarinus*, *FEBS Lett.* **407**, 89-92.
42. Hofrichter, M. (2002) Review: lignin conversion by manganese peroxidase (MnP), *Enzyme Microb Technol.* **30**, 454-466.
43. Lundell, T. K., Makela, M. R. & Hilden, K. (2010) Lignin-modifying enzymes in filamentous basidiomycetes--ecological, functional and phylogenetic review, *J Basic Microbiol.* **50**, 5-20.
44. Munk, L., Sitarz, A. K., Kalyani, D. C., Mikkelsen, J. D. & Meyer, A. S. (2015) Can laccases catalyze bond cleavage in lignin?, *Biotechnol Adv.* **33**, 13-24.
45. Wong, D. W. (2009) Structure and action mechanism of ligninolytic enzymes, *Appl Biochem Biotechnol.* **157**, 174-209.
46. Zhang, C., Xin, Y., Wang, Y., Guo, T., Lu, S. & Kong, J. (2015) Identification of a Novel Dye-Decolorizing Peroxidase, EfeB, Translocated by a Twin-Arginine Translocation System in *Streptococcus thermophilus* CGMCC 7.179, *Appl Environ Microbiol.* **81**, 6108-6119.
47. Planche, L. A. (1810) Note sur la sophistication de la résine de jalap et sur les moyens de la reconnaître, *Bull Pharmacie.* **2**, 578-580.
48. Flohe, L. (2020) Looking Back at the Early Stages of Redox Biology, *Antioxidants.* **9**, 1254.
49. Paul, K. G. (1987) Peroxidases: past and present, *J Oral Pathol.* **16**, 409-411.
50. Schönbein, C. F. (1863) Über die katalytische Wirksamkeit organischer Materien und deren Verbreitung in der Pflanzen-und Thierwelt, *J Prakt Chem.* **98**, 323-344.
51. Bach, A. & Chodat, R. (1903) Untersuchungen über die Rolle der Peroxyde in der Chemie der lebenden Zelle. IV. Ueber Peroxydase, *Ber Deutsch Chem.* **36**, 600-605.
52. Altschul, A. M., Abrams, R. & Hogness, T. R. (1940) Cytochrome C Peroxidase, *J Biol Chem.* **136**, 777-794.
53. Glenn, J. K. & Gold, M. H. (1985) Purification and characterization of an extracellular Mn(II)-dependent peroxidase from the lignin-degrading basidiomycete, *Phanerochaete chrysosporium*, *Biochim Biophys Acta.* **242**, 329-341.
54. Groden, D. & E., B. (1979) H₂O₂ destruction by ascorbate-dependent systems from chloroplasts, *Biochim Biophys Acta.* **546**, 426-435.
55. Kelly, G. J. & Latzko, E. (1979) Soluble ascorbate peroxidase: detection in plants and use in vitamim C estimation, *Naturwissenschaften.* **66**, 617-619.
56. Tien, M. & Kirk, T. K. (1983) Lignin-Degrading Enzyme from the Hymenomycete *Phanerochaete chrysosporium* Burds, *Science.* **221**, 661-663.

57. Hayyan, M., Hashim, M. A. & AlNashef, I. M. (2016) Superoxide Ion: Generation and Chemical Implications, *Chem Rev.* **116**, 3029-3085.
58. Halliwell, B. (2006) Superoxide Dismutase, Catalase and Glutathione Peroxidase: Solutions to the Problems of Living with Oxygen, *New Phytologist.* **73**, 1075-1086.
59. Silveira, C. M., Moe, E., Fraaije, M., Martins, L. O. & Todorovic, S. (2020) Resonance Raman view of the active site architecture in bacterial DyP-type peroxidases, *RSC Adv.* **10**, 11095-11104.
60. Dunford, H. B. & Stillman, J. S. (1976) On the function and mechanism of action of peroxidases, *Coordination Chemistry Reviews.* **19**, 187-251.
61. Poulos, T. L. & Kraut, J. (1980) The stereochemistry of peroxidase catalysis, *J Biol Chem.* **255**, 8199-8205.
62. Poulos, T. L. (2010) Thirty years of heme peroxidase structural biology, *Arch Biochem Biophys.* **500**, 3-12.
63. Ingram, D. T., Lamichane, C. M., Rollins, D. M., Carr, L. E., Mallinson, E. T. & Joseph, S. W. (1998) Development of a colony lift immunoassay to facilitate rapid detection and quantification of Escherichia coli O157:H7 from agar plates and filter monitor membranes, *Clin Diagn Lab Immunol.* **5**, 567-573.
64. Veitch, N. C. (2004) Horseradish peroxidase: a modern view of a classic enzyme, *Phytochemistry.* **65**, 249-259.
65. Ramos, M. C., Torijas, M. C. & Navas Diaz, A. (2001) Enhanced chemiluminescence biosensor for the determination of phenolic compounds and hydrogen peroxide, *Sens Actuators B.* **73**, 71-75.
66. Zamocky, M., Hofbauer, S., Schaffner, I., Gasselhuber, B., Nicolussi, A., Soudi, M., Pirker, K. F., Furtmuller, P. G. & Obinger, C. (2015) Independent evolution of four heme peroxidase superfamilies, *Arch Biochem Biophys.* **574**, 108-119.
67. Zamocky, M., Jakopitsch, C., Furtmuller, P. G., Dunand, C. & Obinger, C. (2008) The peroxidase-cyclooxygenase superfamily: Reconstructed evolution of critical enzymes of the innate immune system, *Proteins.* **72**, 589-605.
68. Welinder, K. G. (1992) Superfamily of plant, fungal and bacterial peroxidases, *Curr Opin Struct Biol.* **2**, 388-393.
69. Celis, A. I. & DuBois, J. L. (2015) Substrate, product, and cofactor: The extraordinarily flexible relationship between the CDE superfamily and heme, *Arch Biochem Biophys.* **574**, 3-17.
70. Goblirsch, B., Kurker, R. C., Streit, B. R., Wilmot, C. M. & DuBois, J. L. (2011) Chlorite dismutases, DyPs, and EfeB: 3 microbial heme enzyme families comprise the CDE structural superfamily, *J Mol Biol.* **408**, 379-398.
71. Fox, N. K., Brenner, S. E. & Chandonia, J. M. (2014) SCOPe: Structural Classification of Proteins--extended, integrating SCOP and ASTRAL data and classification of new structures, *Nucleic Acids Res.* **42**, D304-D309.
72. Hiner, A. N., Rodríguez-López, J. N., Arnao, M. B., Lloyd Raven, E., García-Cánovas, F. & Acosta, M. (2000) Kinetic study of the inactivation of ascorbate peroxidase by hydrogen peroxide, *Biochem J.* **348**, 321-328.
73. Singh, R. & Eltis, L. D. (2015) The multihued palette of dye-decolorizing peroxidases, *Arch Biochem Biophys.* **574**, 56-65.
74. Sugano, Y. (2009) DyP-type peroxidases comprise a novel heme peroxidase family, *Cell Mol Life Sci.* **66**, 1387-1403.

75. Dolphin, D., Forman, A., Borg, D. C., Fajer, J. & Felton, R. H. (1971) Compounds I of catalase and horse radish peroxidase: pi-cation radicals, *Proc Natl Acad Sci U S A.* **68**, 614-618.
76. Jones, P. & Dunford, H. B. (2005) The mechanism of Compound I formation revisited, *J Inorg Biochem.* **99**, 2292-2298.
77. Raven, E. L. (2003) Understanding functional diversity and substrate specificity in haem peroxidases: what can we learn from ascorbate peroxidase?, *Nat Prod Rep.* **20**, 367-381.
78. Strittmatter, E., Wachter, S., Liers, C., Ullrich, R., Hofrichter, M., Plattner, D. A. & Piontek, K. (2013) Radical formation on a conserved tyrosine residue is crucial for DyP activity, *Arch Biochem Biophys.* **537**, 161-167.
79. Patterson, W. R., Poulos, T. L. & Goodin, D. B. (1995) Identification of a porphyrin pi cation radical in ascorbate peroxidase compound I, *Biochemistry.* **34**, 4342-4345.
80. Poulos, T. L. (2014) Heme enzyme structure and function, *Chem Rev.* **114**, 3919-3962.
81. Jones, P. (2001) Roles of water in heme peroxidase and catalase mechanisms, *J Biol Chem.* **276**, 13791-13796.
82. Strittmatter, E., Liers, C., Ullrich, R., Wachter, S., Hofrichter, M., Plattner, D. A. & Piontek, K. (2013) First crystal structure of a fungal high-redox potential dye-decolorizing peroxidase: substrate interaction sites and long-range electron transfer, *J Biol Chem.* **288**, 4095-4102.
83. Kim, S. J., Ishikawa, K., Hirai, M. & Shoda, M. (1995) Characteristics of a newly isolated fungus, *Geotrichum candidum* Dec 1, which decolorizes various dyes, *J Ferment Bioeng.* **79**, 601-607.
84. Ruiz-Duenas, F. J., Fernandez, E., Martinez, M. J. & Martinez, A. T. (2011) *Pleurotus ostreatus* heme peroxidases: an in silico analysis from the genome sequence to the enzyme molecular structure, *C R Biol.* **334**, 795-805.
85. Kim, S. J. & Shoda, M. (1999) Purification and characterization of a novel peroxidase from *Geotrichum candidum* dec 1 involved in decolorization of dyes, *Appl Environ Microbiol.* **65**, 1029-1035.
86. Catucci, G., Valetti, F., Sadeghi, S. J. & Gilardi, G. (2020) Biochemical features of dye-decolorizing peroxidases: Current impact on lignin degradation, *Biotechnol Appl Biochem.* **67**, 751-759.
87. Sugano, Y., Sasaki, K. & Shoda, M. (1999) cDNA cloning and genetic analysis of a novel decolorizing enzyme, peroxidase gene *dyp* from *Geotrichum candidum* Dec 1, *J Biosci Bioeng.* **87**, 411-417.
88. Jongbloed, J. D., Grieger, U., Antelmann, H., Hecker, M., Nijland, R., Bron, S. & van Dijk, J. M. (2004) Two minimal Tat translocases in *Bacillus*, *Mol Microbiol.* **54**, 1319-1325.
89. Ebihara, A., Okamoto, A., Kousumi, Y., Yamamoto, H., Masui, R., Ueyama, N., Yokoyama, S. & Kuramitsu, S. (2005) Structure-based functional identification of a novel heme-binding protein from *Thermus thermophilus* HB8, *J Struct Funct Genomics.* **6**, 21-32.
90. Strittmatter, E., Plattner, D. A. & Piontek, K. (2014) Dye-Decolorizing Peroxidase (DyP) in *Encyclopedia of Inorganic and Bioinorganic Chemistry* pp. 1-13.
91. Sugano, Y. & Yoshida, T. (2021) DyP-Type Peroxidases: Recent Advances and Perspectives, *Int J Mol Sci.* **22**, 5556.
92. Sugano, Y., Muramatsu, R., Ichiyanagi, A., Sato, T. & Shoda, M. (2007) DyP, a unique dye-decolorizing peroxidase, represents a novel heme peroxidase family: ASP171 replaces the distal histidine of classical peroxidases, *J Biol Chem.* **282**, 36652-36658.

93. Chandonia, J. M., Guan, L., Lin, S., Yu, C., Fox, N. K. & Brenner, S. E. (2022) SCOPe: improvements to the structural classification of proteins - extended database to facilitate variant interpretation and machine learning, *Nucleic Acids Res.* **50**, D553-D559.
94. Paysan-Lafosse, T., Blum, M., Chuguransky, S., Grego, T., Pinto, B. L., Salazar, G. A., Bileschi, M. L., Bork, P., Bridge, A., Colwell, L., Gough, J., Haft, D. H., Letunic, I., Marchler-Bauer, A., Mi, H., Natale, D. A., Orengo, C. A., Pandurangan, A. P., Rivoire, C., Sigrist, C. J. A., Sillitoe, I., Thanki, N., Thomas, P. D., Tosatto, S. C. E., Wu, C. H. & Bateman, A. (2023) InterPro in 2022, *Nucleic Acids Res.* **51**, D418-D427.
95. Fawal, N., Li, Q., Savelli, B., Brette, M., Passaia, G., Fabre, M., Mathe, C. & Dunand, C. (2013) PeroxiBase: a database for large-scale evolutionary analysis of peroxidases, *Nucleic Acids Res.* **41**, D441-D444.
96. Savelli, B., Li, Q., Webber, M., Jemmat, A. M., Robitaille, A., Zamocky, M., Mathe, C. & Dunand, C. (2019) RedoxiBase: A database for ROS homeostasis regulated proteins, *Redox Biol.* **26**, 101247.
97. Colpa, D. I., Fraaije, M. W. & van Bloois, E. (2014) DyP-type peroxidases: a promising and versatile class of enzymes, *J Ind Microbiol Biotechnol.* **41**, 1-7.
98. Lee, P. A., Tullman-Ercek, D. & Georgiou, G. (2006) The bacterial twin-arginine translocation pathway, *Annu Rev Microbiol.* **60**, 373-395.
99. Sturm, A., Schierhorn, A., Lindenstrauss, U., Lilie, H. & Bruser, T. (2006) YcdB from *Escherichia coli* reveals a novel class of Tat-dependently translocated hemoproteins, *J Biol Chem.* **281**, 13972-13978.
100. van Bloois, E., Torres Pazmino, D. E., Winter, R. T. & Fraaije, M. W. (2010) A robust and extracellular heme-containing peroxidase from *Thermobifida fusca* as prototype of a bacterial peroxidase superfamily, *Appl Microbiol Biotechnol.* **86**, 1419-1430.
101. Roberts, J. N., Singh, R., Grigg, J. C., Murphy, M. E., Bugg, T. D. & Eltis, L. D. (2011) Characterization of dye-decolorizing peroxidases from *Rhodococcus jostii* RHA1, *Biochemistry.* **50**, 5108-5119.
102. Chaplin, A. K., Wilson, M. T. & Worrall, J. A. R. (2017) Kinetic characterisation of a dye decolourising peroxidase from *Streptomyces lividans*: new insight into the mechanism of anthraquinone dye decolourisation, *Dalton Trans.* **46**, 9420-9429.
103. Lucic, M., Chaplin, A. K., Moreno-Chicano, T., Dworkowski, F. S. N., Wilson, M. T., Svistunenko, D. A., Hough, M. A. & Worrall, J. A. R. (2020) A subtle structural change in the distal haem pocket has a remarkable effect on tuning hydrogen peroxide reactivity in dye decolourising peroxidases from *Streptomyces lividans*, *Dalton Trans.* **49**, 1620-1636.
104. Santos, A., Mendes, S., Brissos, V. & Martins, L. O. (2014) New dye-decolorizing peroxidases from *Bacillus subtilis* and *Pseudomonas putida* MET94: towards biotechnological applications, *Appl Microbiol Biotechnol.* **98**, 2053-2065.
105. Habib, M. H., Rozeboom, H. J. & Fraaije, M. W. (2019) Characterization of a New DyP-Peroxidase from the Alkaliphilic Cellulomonad, *Cellulomonas bogoriensis*, *Molecules.* **24**, 1208.
106. Sutter, M., Boehringer, D., Gutmann, S., Gunther, S., Prangishvili, D., Loessner, M. J., Stetter, K. O., Weber-Ban, E. & Ban, N. (2008) Structural basis of enzyme encapsulation into a bacterial nanocompartment, *Nat Struct Mol Biol.* **15**, 939-947.
107. Ahmad, M., Roberts, J. N., Hardiman, E. M., Singh, R., Eltis, L. D. & Bugg, T. D. (2011) Identification of DypB from *Rhodococcus jostii* RHA1 as a lignin peroxidase, *Biochemistry.* **50**, 5096-5107.
108. Rahmanpour, R. & Bugg, T. D. (2013) Assembly in vitro of *Rhodococcus jostii* RHA1 encapsulin and peroxidase DypB to form a nanocompartment, *FEBS J.* **280**, 2097-2104.

109. Shrestha, R., Jia, K., Khadka, S., Eltis, L. D. & Li, P. (2021) Mechanistic Insights into DyPB from *Rhodococcus jostii* RHA1 Via Kinetic Characterization, *ACS Catalysis*. **11**, 5486-5495.
110. Singh, R., Grigg, J. C., Qin, W., Kadla, J. F., Murphy, M. E. & Eltis, L. D. (2013) Improved manganese-oxidizing activity of DypB, a peroxidase from a lignolytic bacterium, *ACS Chem Biol*. **8**, 700-706.
111. Mendes, S., Brissos, V., Gabriel, A., Catarino, T., Turner, D. L., Todorovic, S. & Martins, L. O. (2015) An integrated view of redox and catalytic properties of B-type PpDyP from *Pseudomonas putida* MET94 and its distal variants, *Arch Biochem Biophys*. **574**, 99-107.
112. Uchida, T., Sasaki, M., Tanaka, Y. & Ishimori, K. (2015) A Dye-Decolorizing Peroxidase from *Vibrio cholerae*, *Biochemistry*. **54**, 6610-6621.
113. Yoshida, T. & Sugano, Y. (2015) A structural and functional perspective of DyP-type peroxidase family, *Arch Biochem Biophys*. **574**, 49-55.
114. Frade, K. S. T., Fernandes, A. C. P., Silveira, C. M., Frazao, C. & Moe, E. (2018) A novel bacterial class V dye-decolourizing peroxidase from the extremophile *Deinococcus radiodurans*: cloning, expression optimization, purification, crystallization, initial characterization and X-ray diffraction analysis, *Acta Crystallogr F Struct Biol Commun*. **74**, 419-424.
115. Zitare, U. A., Habib, M. H., Rozeboom, H., Mascotti, M. L., Todorovic, S. & Fraaije, M. W. (2021) Mutational and structural analysis of an ancestral fungal dye-decolorizing peroxidase, *FEBS J*. **288**, 3602-3618.
116. Sato, T., Hara, S., Matsui, T., Sasaki, G., Saijo, S., Ganbe, T., Tanaka, N., Sugano, Y. & Shoda, M. (2004) A unique dye-decolorizing peroxidase, DyP, from *Thanatephorus cucumeris* Dec 1: heterologous expression, crystallization and preliminary X-ray analysis, *Acta Crystallogr D Biol Crystallogr*. **60**, 149-152.
117. Zubieta, C., Joseph, R., Krishna, S. S., McMullan, D., Kapoor, M., Axelrod, H. L., Miller, M. D., Abdubek, P., Acosta, C., Astakhova, T., Carlton, D., Chiu, H. J., Clayton, T., Deller, M. C., Duan, L., Elias, Y., Elsliger, M. A., Feuerhelm, J., Grzechnik, S. K., Hale, J., Han, G. W., Jaroszewski, L., Jin, K. K., Klock, H. E., Knuth, M. W., Kozbial, P., Kumar, A., Marciano, D., Morse, A. T., Murphy, K. D., Nigoghossian, E., Okach, L., Oommachen, S., Reyes, R., Rife, C. L., Schimmel, P., Trout, C. V., van den Bedem, H., Weekes, D., White, A., Xu, Q., Hodgson, K. O., Wooley, J., Deacon, A. M., Godzik, A., Lesley, S. A. & Wilson, I. A. (2007) Identification and structural characterization of heme binding in a novel dye-decolorizing peroxidase, TyrA, *Proteins*. **69**, 234-243.
118. Zubieta, C., Krishna, S. S., Kapoor, M., Kozbial, P., McMullan, D., Axelrod, H. L., Miller, M. D., Abdubek, P., Ambing, E., Astakhova, T., Carlton, D., Chiu, H. J., Clayton, T., Deller, M. C., Duan, L., Elsliger, M. A., Feuerhelm, J., Grzechnik, S. K., Hale, J., Hampton, E., Han, G. W., Jaroszewski, L., Jin, K. K., Klock, H. E., Knuth, M. W., Kumar, A., Marciano, D., Morse, A. T., Nigoghossian, E., Okach, L., Oommachen, S., Reyes, R., Rife, C. L., Schimmel, P., van den Bedem, H., Weekes, D., White, A., Xu, Q., Hodgson, K. O., Wooley, J., Deacon, A. M., Godzik, A., Lesley, S. A. & Wilson, I. A. (2007) Crystal structures of two novel dye-decolorizing peroxidases reveal a beta-barrel fold with a conserved heme-binding motif, *Proteins*. **69**, 223-233.
119. Brown, M. E., Barros, T. & Chang, M. C. (2012) Identification and characterization of a multifunctional dye peroxidase from a lignin-reactive bacterium, *ACS Chem Biol*. **7**, 2074-2081.

120. Cagide, C., Marizcurrena, J. J., Valles, D., Alvarez, B. & Castro-Sowinski, S. (2023) A bacterial cold-active dye-decolorizing peroxidase from an Antarctic *Pseudomonas* strain, *Appl Microbiol Biotechnol.* **107**, 1707-1724.
121. Chen, C., Shrestha, R., Jia, K., Gao, P. F., Geisbrecht, B. V., Bossmann, S. H., Shi, J. & Li, P. (2015) Characterization of Dye-decolorizing Peroxidase (DyP) from *Thermomonospora curvata* Reveals Unique Catalytic Properties of A-type DyPs, *J Biol Chem.* **290**, 23447-23463.
122. Contreras, H., Joens, M. S., McMath, L. M., Le, V. P., Tullius, M. V., Kimmey, J. M., Bionghi, N., Horwitz, M. A., Fitzpatrick, J. A. & Goulding, C. W. (2014) Characterization of a *Mycobacterium tuberculosis* nanocompartment and its potential cargo proteins, *J Biol Chem.* **289**, 18279-18289.
123. Dhankhar, P., Dalal, V., Sharma, A. K. & Kumar, P. (2023) Structural insights at acidic pH of dye-decolorizing peroxidase from *Bacillus subtilis*, *Proteins.* **91**, 508-517.
124. Johjima, T., Ohkuma, M. & Kudo, T. (2003) Isolation and cDNA cloning of novel hydrogen peroxide-dependent phenol oxidase from the basidiomycete *Termitomyces albuminosus*, *Appl Microbiol Biotechnol.* **61**, 220-225.
125. Lauber, C., Schwarz, T., Nguyen, Q. K., Lorenz, P., Lochnit, G. & Zorn, H. (2017) Identification, heterologous expression and characterization of a dye-decolorizing peroxidase of *Pleurotus sapidus*, *AMB Express.* **7**, 164.
126. Liu, X., Du, Q., Wang, Z., Zhu, D., Huang, Y., Li, N., Wei, T., Xu, S. & Gu, L. (2011) Crystal structure and biochemical features of EfeB/YcdB from *Escherichia coli* O157: ASP235 plays divergent roles in different enzyme-catalyzed processes, *J Biol Chem.* **286**, 14922-14931.
127. Ogola, H. J., Kamiike, T., Hashimoto, N., Ashida, H., Ishikawa, T., Shibata, H. & Sawa, Y. (2009) Molecular characterization of a novel peroxidase from the cyanobacterium *Anabaena* sp. strain PCC 7120, *Appl Environ Microbiol.* **75**, 7509-7518.
128. Pfanzagl, V., Nys, K., Bellei, M., Michlits, H., Mlynek, G., Battistuzzi, G., Djinovic-Carugo, K., Van Doorslaer, S., Furtmuller, P. G., Hofbauer, S. & Obinger, C. (2018) Roles of distal aspartate and arginine of B-class dye-decolorizing peroxidase in heterolytic hydrogen peroxide cleavage, *J Biol Chem.* **293**, 14823-14838.
129. Rai, A., Klare, J. P., Reinke, P. Y. A., Englmaier, F., Fohrer, J., Fedorov, R., Taft, M. H., Chizhov, I., Curth, U., Plettenburg, O. & Manstein, D. J. (2021) Structural and Biochemical Characterization of a Dye-Decolorizing Peroxidase from *Dictyostelium discoideum*, *Int J Mol Sci.* **22**, 6265.
130. Scheibner, M., Hulsdau, B., Zelena, K., Nimtz, M., de Boer, L., Berger, R. G. & Zorn, H. (2008) Novel peroxidases of *Marasmius scorodoni* degrade beta-carotene, *Appl Microbiol Biotechnol.* **77**, 1241-1250.
131. Shrestha, R., Chen, X., Ramyar, K. X., Hayati, Z., Carlson, E. A., Bossmann, S. H., Song, L., Geisbrecht, B. V. & Li, P. (2016) Identification of Surface-Exposed Protein Radicals and A Substrate Oxidation Site in A-Class Dye-Decolorizing Peroxidase from *Thermomonospora curvata*, *ACS Catal.* **6**, 8036-8047.
132. Sugawara, K., Nishihashi, Y., Narioka, T., Yoshida, T., Morita, M. & Sugano, Y. (2017) Characterization of a novel DyP-type peroxidase from *Streptomyces avermitilis*, *J Biosci Bioeng.* **123**, 425-430.
133. Yoshida, T., Ogola, H. J., Amano, Y., Hisabori, T., Ashida, H., Sawa, Y., Tsuge, H. & Sugano, Y. (2016) *Anabaena* sp. DyP-type peroxidase is a tetramer consisting of two asymmetric dimers, *Proteins.* **84**, 31-42.

134. Shrestha, R., Huang, G., Meekins, D. A., Geisbrecht, B. V. & Li, P. (2017) Mechanistic Insights into Dye-Decolorizing Peroxidase Revealed by Solvent Isotope and Viscosity Effects, *ACS Catal.* **7**, 6352-6364.
135. Blodig, W., Doyle, W. A., Smith, A. T., Winterhalter, K., Choinowski, T. & Piontek, K. (1998) Autocatalytic formation of a hydroxy group at C beta of trp171 in lignin peroxidase, *Biochemistry.* **37**, 8832-8838.
136. Dhankhar, P., Dalal, V., Singh, V., Sharma, A. K. & Kumar, P. (2021) Structure of dye-decolorizing peroxidase from *Bacillus subtilis* in complex with veratryl alcohol, *Int J Biol Macromol.* **193**, 601-608.
137. Gumiero, A., Murphy, E. J., Metcalfe, C. L., Moody, P. C. & Raven, E. L. (2010) An analysis of substrate binding interactions in the heme peroxidase enzymes: a structural perspective, *Arch Biochem Biophys.* **500**, 13-20.
138. Kingsley, L. J. & Lill, M. A. (2015) Substrate tunnels in enzymes: structure-function relationships and computational methodology, *Proteins.* **83**, 599-611.
139. Gray, H. B. & Winkler, J. R. (2021) Functional and protective hole hopping in metalloenzymes, *Chem Sci.* **12**, 13988-14003.
140. Linde, D., Pogni, R., Canellas, M., Lucas, F., Guallar, V., Baratto, M. C., Sinicropi, A., Saez-Jimenez, V., Coscolin, C., Romero, A., Medrano, F. J., Ruiz-Duenas, F. J. & Martinez, A. T. (2015) Catalytic surface radical in dye-decolorizing peroxidase: a computational, spectroscopic and site-directed mutagenesis study, *Biochem J.* **466**, 253-262.
141. Linde, D., Ruiz-Duenas, F. J., Fernandez-Fueyo, E., Guallar, V., Hammel, K. E., Pogni, R. & Martinez, A. T. (2015) Basidiomycete DyPs: Genomic diversity, structural-functional aspects, reaction mechanism and environmental significance, *Arch Biochem Biophys.* **574**, 66-74.
142. Nys, K., Furtmuller, P. G., Obinger, C., Van Doorslaer, S. & Pfanzagl, V. (2021) On the Track of Long-Range Electron Transfer in B-Type Dye-Decolorizing Peroxidases: Identification of a Tyrosyl Radical by Computational Prediction and Electron Paramagnetic Resonance Spectroscopy, *Biochemistry.* **60**, 1226-1241.
143. Finzel, B. C., Poulos, T. L. & Kraut, J. (1984) Crystal structure of yeast cytochrome c peroxidase refined at 1.7-Å resolution, *J Biol Chem.* **259**, 13027-13036.
144. Goodin, D. B. & McRee, D. E. (1993) The Asp-His-Fe triad of cytochrome c peroxidase controls the reduction potential, electronic structure, and coupling of the tryptophan free radical to the heme, *Biochemistry.* **32**, 3313-3324.
145. Banci, L. (1997) Structural properties of peroxidases, *J Biotechnol.* **53**, 253-263.
146. Passardi, F., Cosio, C., Penel, C. & Dunand, C. (2005) Peroxidases have more functions than a Swiss army knife, *Plant Cell Rep.* **24**, 255-265.
147. Singh, R., Grigg, J. C., Armstrong, Z., Murphy, M. E. P. & Eltis, L. D. (2012) Distal heme pocket residues of B-type dye-decolorizing peroxidase: arginine but not aspartate is essential for peroxidase activity, *J Biol Chem.* **287**, 10623-10630.
148. Mendes, S., Catarino, T., Silveira, C., Todorovic, S. & Martins, L. O. (2015) The catalytic mechanism of A-type dye-decolourising peroxidase BsDyP: neither aspartate nor arginine is individually essential for peroxidase activity, *Catal Sci Technol.* **5**, 5196-5207.
149. Yoshida, T., Tsuge, H., Konno, H., Hisabori, T. & Sugano, Y. (2011) The catalytic mechanism of dye-decolorizing peroxidase DyP may require the swinging movement of an aspartic acid residue, *FEBS J.* **278**, 2387-2394.

150. Brissos, V., Tavares, D., Sousa, A. C., Robalo, M. P. & Martins, L. O. (2017) Engineering a Bacterial DyP-Type Peroxidase for Enhanced Oxidation of Lignin-Related Phenolics at Alkaline pH, *ACS Catalysis*. **7**, 3454-3465.
151. Lucic, M., Wilson, M. T., Tosha, T., Sugimoto, H., Shilova, A., Axford, D., Owen, R. L., Hough, M. A. & Worrall, J. A. R. (2022) Serial Femtosecond Crystallography Reveals the Role of Water in the One- or Two-Electron Redox Chemistry of Compound I in the Catalytic Cycle of the B-Type Dye-Decolorizing Peroxidase DtpB, *ACS Catal.* **12**, 13349-13359.
152. Bao, X., Huang, X., Lu, X. & Li, J. J. (2014) Improvement of hydrogen peroxide stability of *Pleurotus eryngii* versatile ligninolytic peroxidase by rational protein engineering, *Enzyme Microb Technol.* **54**, 51-58.
153. Hernández-Ruiz, J., Arnao, M. B., Hiner, A. N., García-Cánovas, F. & Acosta, M. (2001) Catalase-like activity of horseradish peroxidase: relationship to enzyme inactivation by H₂O₂, *Biochem J* **354**, 107-114.
154. Hiner, A. N., Hernandez-Ruiz, J., Rodriguez-Lopez, J. N., Garcia-Canovas, F., Brisset, N. C., Smith, A. T., Arnao, M. B. & Acosta, M. (2002) Reactions of the class II peroxidases, lignin peroxidase and *Arthromyces ramosus* peroxidase, with hydrogen peroxide. Catalase-like activity, compound III formation, and enzyme inactivation, *J Biol Chem.* **277**, 26879-26885.
155. Paumann-Page, M., Furtmuller, P. G., Hofbauer, S., Paton, L. N., Obinger, C. & Kettle, A. J. (2013) Inactivation of human myeloperoxidase by hydrogen peroxide, *Arch Biochem Biophys.* **539**, 51-62.
156. Perez Galende, P., Hidalgo Cuadrado, N., Kostetsky, E. Y., Roig, M. G., Villar, E., Shnyrov, V. L. & Kennedy, J. F. (2015) Kinetics of Spanish broom peroxidase obeys a Ping-Pong Bi-Bi mechanism with competitive inhibition by substrates, *Int J Biol Macromol.* **81**, 1005-1011.
157. Saez-Jimenez, V., Acebes, S., Guallar, V., Martinez, A. T. & Ruiz-Duenas, F. J. (2015) Improving the oxidative stability of a high redox potential fungal peroxidase by rational design, *PLoS One.* **10**, e0124750.
158. Arnao, M. B., Acosta, M., del Río, J. A., Varón, R. & García-Cánovas, F. (1990) A kinetic study on the suicide inactivation of peroxidase by hydrogen peroxide, *Biochim Biophys Acta* **1041**, 43-47.
159. Bagger, S. & Williams, R. J. P. (1971) Intermediates in the Reaction Between Hydrogen Peroxide and Horseradish Peroxidase, *Acta Chem Scand.* **25**, 976-982.
160. Nakajima, R. & Yamazaki, I. (1980) The conversion of horseradish peroxidase C to a verdohemoprotein by a hydroperoxide derived enzymatically from indole-3-acetic acid and by m-nitroperoxybenzoic acid, *J Biol Chem.* **255**, 2067-2071.
161. Adediran, S. A. & Lambeir, A. M. (1989) Kinetics of the reaction of compound II of horseradish peroxidase with hydrogen peroxide to form compound III, *Eur J Biochem.* **186**, 571-576.
162. Hiner, A. N., Hernández-Ruiz, J., García-Cánovas, F., Smith, A. T., Arnao, M. B. & Acosta, M. (1995) A comparative study of the inactivation of wild-type, recombinant and two mutant horseradish peroxidase isoenzymes C by hydrogen peroxide and m-chloroperoxybenzoic acid, *Eur J Biochem.* **234**, 506-512.
163. Miyake, C. & Asada, K. (1996) Inactivation Mechanism of Ascorbate Peroxidase at Low Concentrations of Ascorbate; Hydrogen Peroxide Decomposes Compound I of Ascorbate Peroxidase, *Plant Cell Physiol.* **37**, 423-430.

164. Arnao, M. B., Acosta, M., del Río, J. A. & García-Cánovas, F. (1990) Inactivation of peroxidase by hydrogen peroxide and its protection by a reductant agent, *Biochim Biophys Acta*. **1038**, 85-89.
165. Lončar, N., Colpa, D. I. & Fraaije, M. W. (2016) Exploring the biocatalytic potential of a DyP-type peroxidase by profiling the substrate acceptance of *Thermobifida fusca* DyP peroxidase, *Tetrahedron*. **72**, 7276-7281.
166. Silva, D., Rodrigues, C. F., Lorena, C., Borges, P. T. & Martins, L. O. (2023) Biocatalysis for biorefineries: The case of dye-decolorizing peroxidases, *Biotechnol Adv*. **65**, 108153.
167. van der Ploeg, R., Mader, U., Homuth, G., Schaffer, M., Denham, E. L., Monteferrante, C. G., Miethke, M., Marahiel, M. A., Harwood, C. R., Winter, T., Hecker, M., Antelmann, H. & van Dijk, J. M. (2011) Environmental salinity determines the specificity and need for Tat-dependent secretion of the YwbN protein in *Bacillus subtilis*, *PLoS One*. **6**, e18140.
168. Liers, C., Bobeth, C., Pecyna, M., Ullrich, R. & Hofrichter, M. (2010) DyP-like peroxidases of the jelly fungus *Auricularia auricula-judae* oxidize nonphenolic lignin model compounds and high-redox potential dyes, *Appl Microbiol Biotechnol*. **85**, 1869-1879.
169. Min, K., Gong, G., Woo, H. M., Kim, Y. & Um, Y. (2015) A dye-decolorizing peroxidase from *Bacillus subtilis* exhibiting substrate-dependent optimum temperature for dyes and beta-ether lignin dimer, *Sci Rep*. **5**, 8245.
170. Rahmanpour, R., Rea, D., Jamshidi, S., Fulop, V. & Bugg, T. D. (2016) Structure of *Thermobifida fusca* DyP-type peroxidase and activity towards Kraft lignin and lignin model compounds, *Arch Biochem Biophys*. **594**, 54-60.
171. Yang, J., Gao, T., Zhang, Y., Wang, S., Li, H., Li, S. & Wang, S. (2019) Degradation of the phenolic beta-ether lignin model dimer and dyes by dye-decolorizing peroxidase from *Bacillus amyloliquefaciens*, *Biotechnol Lett*. **41**, 1015-1021.
172. Rahmanpour, R. & Bugg, T. D. (2015) Characterisation of Dyp-type peroxidases from *Pseudomonas fluorescens* Pf-5: Oxidation of Mn(II) and polymeric lignin by Dyp1B, *Arch Biochem Biophys*. **574**, 93-98.
173. de Eugenio, L. I., Peces-Pérez, R., Linde, D., Prieto, A., Barriuso, J., Ruiz-Dueñas, F. J. & Martínez, M. J. (2021) Characterization of a Dye-Decolorizing Peroxidase from *Irpex lacteus* Expressed in *Escherichia coli*: An Enzyme with Wide Substrate Specificity Able to Transform Lignosulfonates, *Journal of Fungi*. **7**, 325.
174. Avram, A., Sengupta, A., Pfromm, P. H., Zorn, H., Lorenz, P., Schwarz, T., Nguyen, K. Q. & Czermak, P. (2018) Novel DyP from the basidiomycete *Pleurotus sapidus*: substrate screening and kinetics, *Biocatalysis*. **4**, 1-13.
175. Rodrigues, C. F., Borges, P. T., Scocozza, M. F., Silva, D., Taborda, A., Brissos, V., Frazao, C. & Martins, L. O. (2021) Loops around the Heme Pocket Have a Critical Role in the Function and Stability of BsDyP from *Bacillus subtilis*, *Int J Mol Sci*. **22**, 10862.
176. Yoshida, T., Tsuge, H., Hisabori, T. & Sugano, Y. (2012) Crystal structures of dye-decolorizing peroxidase with ascorbic acid and 2,6-dimethoxyphenol, *FEBS Lett*. **586**, 4351-4356.
177. Adkar, B. V., Bhattacharyya, S., Gilson, A. I., Zhang, W. & Shakhnovich, E. I. (2019) Substrate inhibition imposes fitness penalty at high protein stability, *Proc Natl Acad Sci U S A*. **116**, 11265-11274.
178. Kokkonen, P., Beier, A., Mazurenko, S., Damborsky, J., Bednar, D. & Prokop, Z. (2021) Substrate inhibition by the blockage of product release and its control by tunnel engineering, *RSC Chem Biol*. **2**, 645-655.

179. Cornish-Bowden, A. (1999) *Fundamentals of Enzyme Kinetics (revised ed.)*, Portland Press Ltd., London.
180. Denisov, I. G., Frank, D. J. & Sligar, S. G. (2009) Cooperative properties of cytochromes P450, *Pharmacol Ther.* **124**, 151-167.
181. Korzekwa, K. R., Krishnamachary, N., Shou, M., A., O., Parise, R. A., Rettie, A. E., Gonzalez, F. J. & Tracy, T. S. (1998) Evaluation of atypical cytochrome P450 kinetics with two-substrate models: evidence that multiple substrates can simultaneously bind to cytochrome P450 active sites, *Biochemistry.* **37**, 4137-4147.
182. Morales, M., Mate, M. J., Romero, A., Martinez, M. J., Martinez, A. T. & Ruiz-Duenas, F. J. (2012) Two oxidation sites for low redox potential substrates: a directed mutagenesis, kinetic, and crystallographic study on *Pleurotus eryngii* versatile peroxidase, *J Biol Chem.* **287**, 41053-41067.
183. Dhankhar, P., Dalal, V., Mahto, J. K., Gurjar, B. R., Tomar, S., Sharma, A. K. & Kumar, P. (2020) Characterization of dye-decolorizing peroxidase from *Bacillus subtilis*, *Arch Biochem Biophys.* **693**, 108590.
184. Lucic, M., Allport, T., Clarke, T. A., Williams, L. J., Wilson, M. T., Chaplin, A. K. & Worrall, J. A. R. (2024) The oligomeric states of dye-decolorizing peroxidases from *Streptomyces lividans* and their implications for mechanism of substrate oxidation, *Protein Sci.* **33**, e5073.
185. Kim, K. H. & Kim, C. S. (2018) Recent Efforts to Prevent Undesirable Reactions From Fractionation to Depolymerization of Lignin: Toward Maximizing the Value From Lignin, *Front Energy Res.* **6**, 92.
186. Morales-Urrea, D., Lopez-Cordoba, A. & Contreras, E. M. (2023) Inactivation kinetics of horseradish peroxidase (HRP) by hydrogen peroxide, *Sci Rep.* **13**, 13363.

Acknowledgements

This work was conducted at the Department of Chemistry and Biotechnology at Tallinn University of Technology (TalTech) and the Institute of Molecular and Cell Biology at University of Tartu. The research was supported by the European Regional Development Fund and the Estonian Research Council (MOBTT60, RESTA11, PRG1540, and TEM-TA49).

I would like to express my deepest gratitude to all the kind and wonderful people who have supported me throughout my studies and during the preparation of this thesis.

First and foremost, I am profoundly grateful to my supervisors. Tiit Lukk, thank you for giving me the opportunity to work with dye-decolorizing peroxidases and for introducing me to the world of crystallography. Priit Väljamäe, I sincerely appreciate your warm welcome to Tartu, your invaluable guidance in enzymology, and your detailed and constructive feedback on my thesis. Priit Eek, thank you for your support and insightful feedback during the final stages of my work. I also want to express my gratitude to my previous supervisors – Taavi Ivan, Asko Uri, Jinghui Luo, Karin Valmsen, and Peep Palumaa – whose guidance has been invaluable over the years. Thank you all!

I am truly fortunate to have colleagues who are also great friends. I would like to thank all my colleagues at TalTech and the University of Tartu, as well as everyone who has contributed to my research with valuable advice, guidance, or assistance. I am grateful for your willingness to listen and help. You are the best! Darja, thank you for studying ScDyPB with me. Piia, I appreciate your assistance with GC-MS and your patience in answering my questions. Kairit and Eve-Ly, thank you for always being there to help and discuss. Vello, thank you for reviewing my thesis and offering helpful advice. Silja, I really appreciate your willingness to assist with experimental tasks. PhD students at TalTech (Maarja, Kannan, Tran) and at the University of Tartu (Sirelin, Kaspar, Vlad, Silva), thank you for being such wonderful company. To my colleagues in Tartu, especially Maie, Rya, Aivar, Jürgen, Tiina T., and Margus, thank you for contributing to a pleasant and enriching environment during my time there.

I would also like to extend my heartfelt gratitude to my friends and family. I am incredibly fortunate to have you in my life. To my dear friends who have remained steadfast throughout my PhD journey – especially Alla, Diana, Krete, and Sandra – thank you for your constant support. Avery, thank you for dedicating time to read my thesis and help with language corrections. Jaanika, I am so grateful for your presence, especially during the final stages of writing. Eno, thank you for being by my side and for loving and supporting me the best way you could. I would also like to thank the Noorsalu family, especially Sirje, for embracing me into your family and providing support during my studies. *Aitäh Noorsalude perele, eriti Sirjele, et võtsite mind oma perekonda ja olite mulle õpingute ajal toeks.*

Last but not least, I want to express my profound gratitude to my family – mom, dad, and my grandparents – for your endless encouragement, love, and support throughout my studies, the entire PhD journey, and the preparation of this thesis. I could not have accomplished this without you. Thank you for believing in me, even when I doubted myself. Your love and support mean the world to me. *Kallis pere, mu armsad ema, isa ja vanavanemad. Tänan teid südamest julgustamise, armastuse ja toetuse eest nii õpingute kui ka doktoritöö kirjutamise ajal! Ma ei oleks saanud seda teha ilma teieta. Aitäh, et uskusite minusse isegi siis, kui ma seda ise teha ei suutnud. Nii kallid olete!*

Abstract

Characterization of bacterial dye-decolorizing peroxidases

Lignocellulosic biomass is widely distributed in nature and serves as a renewable carbon source. It consists of three biopolymers: cellulose, hemicellulose, and lignin. Cellulose is extensively utilized in the wood and paper industries, as well as in biorefineries. During these industrial processes, lignin is generated as a by-product and is typically burned for energy production. To date, the potential of polyphenolic lignin as a starting material for the chemical industry has been recognized. However, the utilization of lignin is complicated by its complex and heterogeneous structure. In nature, lignin is broken down by various fungi and bacteria that use a rich collection of enzymes. These same enzymes could be harnessed in industrial processes to break down lignin into smaller fragments, facilitating its further use. Dye-decolorizing peroxidases (DyPs) continue to attract research interest due to their ability to degrade lignin. In my research, I studied four different bacterial dye-decolorizing peroxidases (DyPs): three DyPs from the soil bacterium *Streptomyces coelicolor* (ScDyP1A, ScDyP2A, ScDyPB) and one from the bacterium *Thermobifida halotolerans* (ThDyP).

DyPs are heme-dependent enzymes that catalyze the oxidation of various substrates using hydrogen peroxide. These enzymes operate via a ping-pong mechanism, alternating between the resting state and the reactive intermediate states known as compound I (Cpd I) and compound II (Cpd II). Enzyme kinetics is crucial for characterizing and understanding the potential of enzymes. While enzymes are typically described using Michaelis-Menten kinetics, the kinetics of DyPs is often more complex and exhibits substrate inhibition as well as apparent positive cooperativity. One of the aims of my doctoral thesis was to investigate molecular mechanisms underlying the unusual kinetics of DyPs. 2,2'-azino-bis(3-ethylbenzothiazoline-6-sulfonic acid) (ABTS) was used as the main model substrate, along with dyes and hydroquinones. Oxidation of ABTS was substrate inhibited by ABTS in the case of both ThDyP and ScDyPB, whereas substrate inhibition by H₂O₂ was observed only in the case of ThDyP. The irreversible inactivation of DyPs upon incubation with H₂O₂ in the absence of a reducing substrate suggests that a non-productive complex forms between H₂O₂ and Cpd I. A non-productive complex also forms between ABTS and the resting state ThDyP. We concluded that non-productive complexes between ABTS and the resting state of the enzyme, as well as between H₂O₂ and Cpd I / Cpd II, are responsible for the substrate inhibition. The kinetics of ThDyP was further complicated by the presence of apparent positive cooperativity. This cooperativity was observed with a substrate capable of donating only one electron (ABTS), but not with substrates that can donate two electrons (such as hydroquinones and dyes). We proposed a hypothesis that the positive cooperativity arises from the need for ThDyP to bind two ABTS molecules simultaneously. We solved the crystal structure of ThDyP (PDB: 8CK9), which, along with gel filtration chromatography results, indicates that ThDyP exists as a dimer in its native form. Therefore, the usual cooperative mechanisms involving the true "cooperation" between two subunits cannot be excluded.

DyPs can exist as monomers as well as larger oligomers. However, very little is known about the relationships between the degree of oligomerization and catalytic activity of DyPs. To investigate whether such a connection exists, we conducted a comprehensive kinetic and size distribution analysis of ScDyPB, using ABTS and methylhydroquinone (MHQ) as reducing substrates. For both substrates, there was an unusual activity dependence of enzyme reactions on the concentration and pH of the enzyme working

stock used to initiate the reactions. In addition, the effects on enzyme activity were opposite depending on the substrate (ABTS or MHQ). For example, lowering the pH of the enzyme working stock from 7.5 to 4.0 resulted in an increase in ABTS oxidation activity, while the oxidation activity of MHQ decreased. We proposed that the oxidation of these substrates involves different mechanisms. MHQ is oxidized in direct contact with heme, while the oxidation of ABTS can also occur on the protein surface through the electron transfer pathway between the protein surface and heme. The dependency of the rate of the oxidation of ABTS on its concentration was best described by a model in which ScDyPB exists as two kinetically distinct enzyme forms. Both forms operate via the ping-pong mechanism, but one is substrate-inhibited by ABTS, while the other is not. Gel filtration chromatography and dynamic light scattering revealed that ScDyPB exists as a mixture of molecules of different sizes. We proposed a simplified model in which ScDyPB exists as an equilibrium mixture of low and high oligomerization forms with different kinetic properties. Moreover, the equilibrium of these two forms is influenced by the concentration of the enzyme in solution and the pH. This work paves the way for a better understanding of the role of oligomerization in DyPs.

DyPs are of particular interest to our research group due to their ability to act on lignin. We tested ScDyPs on organosolv lignins derived from both hardwood and herbaceous biomass. The lignin was dissolved and incubated overnight with ScDyPs, after which we analyzed the size distribution and molecular weight changes of the lignins using gel permeation chromatography. Our results showed that ScDyPB treatment led to the polymerization of lignin from herbaceous plants, while treatment of hardwood lignin with ScDyPAs resulted in a decrease in molecular weight. Additionally, we examined the soluble fractions of lignin from these same treatments using gas chromatography-mass spectrometry. We observed a reduction in the amount of soluble monolignols in the lignin supernatant following ScDyP treatment. These findings demonstrate that ScDyPs are effective in utilizing lignin as a substrate.

Lühikokkuvõte

Bakteriaalsete värvi pleegitavate peroksüdaaside iseloomustamine

Lignotselluloosne biomass on looduses laialdaselt levinud taastuv süsinikuallikas, mis koosneb kolmest biopolümeerist: tselluloosist, hemitselluloosist ja ligniinist. Tselluloosi kasutatakse puidu- ja paberitööstuses ning biorafineerimistehastes. Nende tööstusprotsesside käigus tekib kõrvalproduktina ligniin, mis enamasti põletatakse energia tootmiseks. Polüfenoolne ligniin on keemiatööstuse jaoks (alg)materjalina väärtuslik allikas, kuid selle kasutamist raskendab tema keeruline ja heterogeenne struktuur. Looduses lagundavad ligniini mitmed seened ning bakterid, kasutades selleks erinevate ensüümide abi. Neid samu ensüüme saaks rakendada tööstuslikes protsessides, et ligniini teha väiksemateks fragmentideks ja hõlbustada sellega ligniini edasist kasutamist. Värvi pleegitavad peroksüdaasid (DyP-d) on jäänud teadlaste huviorbiiti just tänu oma võimele lagundada ligniini. Oma doktoritöös uurisin nelja erinevat bakteriaalset DyP peroksüdaasi: kolm DyP-d mullabakterist *Streptomyces coelicolor* (ScDyP1A, ScDyP2A, ScDyPB) ja üks bakterist *Thermobifida halotolerans* (ThDyP).

DyP-d on heem-sõltuvad ensüümid, mis katalüüsivad mitmete erinevate substraatide oksüdatsiooni, kasutades selleks vesinikperoksiidi. Need ensüümid töötavad ping-pong mehhanismi alusel, kus DyP hüpleb edasi-tagasi puhkeoleku ja reaktiivsete vaheolekute, ühend I (Cpd I) ja ühend II (Cpd II), vahel. Nende ensüümide iseloomustamiseks ning nende potentsiaali mõistmiseks kasutatakse ensüümkineetikat. Kui tavapäraselt saab ensüüme kirjeldada Michaelis-Menteni kineetika abil, siis DyP-de kineetika teeb keeruliseks nii tihti esinev substraatinhibitsioon kui ka näiline positiivne kooperatiivsus. Minu doktoritöö üheks eesmärgiks oli välja selgitada, millised molekulaarsed mehhanismid tingivad DyP-de ebahariliku kineetika. Põhilise mudelsubstraadina kasutasime ühendit 2,2'-asiino-bis(3-etuülbensotiasoliin-6-sulfoonhape) (ABTS), kuid ka värve ja hüdrokiinoone. Nii ThDyP kui ka ScDyPB puhul inhibeeris ABTS iseenda oksüdeerimist, H₂O₂ põhjustas substraatinhibitsiooni ainult ThDyP puhul. DyP-de pöördumatu inaktiveerumine inkubeerimisel H₂O₂-ga redutseeriva substraadi puudumisel viitas sellele, et ThDyP ja ScDyPB puhul moodustub H₂O₂ ja Cpd I vahel mitte-produktiivne kompleks. Samuti tekib mitte-produktiivne kompleks ABTS-i ja puhkeolekus ThDyP vahel. Kokkuvõttes järeldasime, et substraatinhibitsiooni põhjustavad mitte-produktiivsed kompleksid ABTS-i ja ensüümi puhkeoleku vahel ning H₂O₂ ja Cpd I / Cpd II vahel. ThDyP kineetika tegi veel keerukamaks näiline positiivne kooperatiivsus. Kooperatiivsus esines substraadi puhul, mis on võimeline loovutama vaid ühe elektroni (ABTS), kuid mitte nende substraatidega, mis saavad loovutada kaks elektroni (hüdrokiinoonid ja värvid). Pakkusime välja hüpoteesi, mille kohaselt on positiivse kooperatiivsuse põhjuseks ThDyP vajadus seostada samaaegselt kaks ABTS-i molekuli. Lahendasime ThDyP kristallstruktuuri (PDB: 8CK9). Kristallstruktuuri ning ka geelfiltratsiooni põhjal esineb ThDyP natiivsel kujul dimeerina, seega ei ole välistatud ka tavapärased, kahe subühiku koostööl põhinevad kooperatiivsuse mehhanismid.

DyP-d võivad esineda nii monomeeridena kui ka suuremate oligomeeridena. Varasemalt puudusid uuringud DyP-de oligomerisatsiooni ja katalüütilise aktiivsuse seose kohta. Selleks et välja selgitada, kas selline seos esineb, viisime läbi põhjalikuma ScDyPB kineetilise kui ka suuruse jaotuse analüüsi. Redutseerivate substraadidena

kasutasime ABTS-i ja metüülhüdrokinooni (MHQ). Mõlema substraadi puhul sõltus aktiivsus reaktsioonide käivitamiseks kasutatud ensüümi vahelahjenduse kontsentratsioonist ning pH-st. Lisaks oli mõju ensüümreaktsioonide aktiivsusele vastupidised, sõltuvalt kasutatud substraadist (ABTS või MHQ). Näiteks põhjustas ensüümi vahelahjenduse pH alandamine 7,5-lt 4,0-le aktiivsuse suurenemist ABTS-i oksüdatsioonil, samas kui MHQ oksüdeerimise aktiivsus hoopis langes. Saadud tulemuste põhjal pakkusime välja, et nende substraatide oksüdatsioonil kasutatakse erinevaid mehhanisme. MHQ oksüdeeritakse vahetus kontaktis heemiga, kuid ABTS-i oksüdeerimine on võimalik ka valgu pinnal, kasutades elektronide ülekande ahelat valgu pinna ja heemi vahel. Kiiruse sõltuvus ABTS-i kontsentratsioonist oli kõige paremini kirjeldatav mudeliga, mille kohaselt ScDyPB esineb kahe kineetiliselt erineva ensüümvormina. Mõlemad vormid töötavad ping-pong mehhanismi alusel, kuid üks neist on ABTS-i poolt substraatinhibeeritud, teine mitte. Geelfiltratsioonkromatograafia ning dünaamilise valguse hajumise abil selgitasime välja, et ScDyPB esineb eri suurusega molekulide seguna. Pakkusime välja lihtsustatud mudeli, milles ScDyPB esineb madala ja kõrge oligomerisatsioonistmega vormide tasakaalulise seguna, millel on erinevad kineetilised omadused. Saadud tulemustega on tehtud esimesed sammud, et DyP-de oligomerisatsiooni rolli paremini mõista.

DyP-d on meie uurimisrühma jaoks huvipakkuvateks ensüümideks nende aktiivsuse tõttu ligniinil. Katsetasime ScDyP-sid lehtpuu ning rohhtaime biomassidest pärit organosolv-ligniinidel. Lahustatud ligniini inkubeerisime üle öö ScDyP-de juuresolekul. Ligniini molekulmassi jaotust ja ensüümtöötuse mõju sellele analüüsisime geelpermetatsioonkromatograafiaga. Nendest tulemustest lähtus, et ScDyPB töötuse tulemusena rohthaime ligniin polümeeriseerub. Vastupidist efekti nägime lehtpuu ligniini töötlemisel ScDyPA-dega, mille tulemusel ligniini molekulmass vähenes. Samast töötusest pärit ligniini lahustuvat fraktsiooni analüüsisime gaasikromatograafia-massispektromeetriaga. Nägime, et ScDyP-de toimel väheneb monolignoolide hulk ligniini lahustuvas fraktsioonis. Tehtud katsed näitasid, et ScDyP-d on võimelised kasutama ligniini substraadina.

Appendix 1

Publication I

Pupart, H.; Jõul, P.; Bramanis, M. I.; Lukk, T. Characterization of the Ensemble of Lignin Remodeling DyP-Type Peroxidases from *Streptomyces coelicolor* A3(2). *Energies* **2023**, *16*, 1557. <https://doi.org/10.3390/en16031557>.

Article

Characterization of the Ensemble of Lignin-Remodeling DyP-Type Peroxidases from *Streptomyces coelicolor* A3(2)

Hegne Pupart, Piia Jõul , Melissa Ingela Bramanis and Tiit Lukk * 

Department of Chemistry and Biotechnology, Tallinn University of Technology, Akadeemia tee 15, 12618 Tallinn, Estonia

* Correspondence: tiit.lukk@taltech.ee

Abstract: Lignin is Nature’s major source of aromatic chemistry and is by many seen as the green entry-point alternative to the fossil-based chemical industry. Due to its chemically recalcitrant structure, the utilization of lignin is challenging, wherein enzymes might be the key to overcome this challenge. Here, we focus on the characterization of dye-decolorizing peroxidases from *Streptomyces coelicolor* A3(2) (ScDyPs) in the context of enzymatic modification of organosolv lignins from aspen and *Miscanthus × giganteus*. In this study, we show that the ScDyPB can remodel organosolv lignins from grassy biomass, leading to higher molecular weight species, while ScDyPAs can deconstruct hardwood lignin, leading to an overall reduction in its molecular weight. Additionally, we show that ScDyPB is effective in polymerizing low-molecular-weight phenolics, leading to their removal from the solution.

Keywords: lignin remodeling; DyP-type peroxidases; Actinobacteria



check for updates

Citation: Pupart, H.; Jõul, P.; Bramanis, M.I.; Lukk, T.

Characterization of the Ensemble of Lignin-Remodeling DyP-Type Peroxidases from *Streptomyces coelicolor* A3(2). *Energies* **2023**, *16*, 1557. <https://doi.org/10.3390/en16031557>

Academic Editor: Jeong-Hun Park

Received: 30 December 2022

Revised: 21 January 2023

Accepted: 25 January 2023

Published: 3 February 2023



Copyright: © 2023 by the authors. Licensee MDPI, Basel, Switzerland. This article is an open access article distributed under the terms and conditions of the Creative Commons Attribution (CC BY) license (<https://creativecommons.org/licenses/by/4.0/>).

1. Introduction

Lignocellulosic biomass (LCB) is Earth’s most abundant renewable raw material [1]. This sustainable feedstock makes an attractive alternative to fossil-based resources to obtain bio-based materials, second-generation biofuels, bioenergy, value-added products, and chemicals [2–4]. LCB comprises three biopolymers: cellulose, hemicellulose, and lignin, with a typical ratio of 4:3:3, which varies among different species [5,6].

Lignin represents the second most abundant natural polymer after cellulose and constitutes the most abundant phenolic biopolymer on Earth [7]. Therefore, lignin is by many seen as a green entry-point alternative to fossil-based sources for the chemical industry [8,9]. The content of lignin varies significantly among hardwoods, softwoods, and herbaceous plants, wherein the highest content of lignin is in softwoods and the lowest in grasses [10].

Lignin is constructed from three monolignols—coniferyl alcohol, sinapyl alcohol, and *p*-coumaryl alcohol—which differ by the degree of methoxylation. When incorporated into lignin, those monolignols make up guaiacyl (G), syringyl (S), and hydroxyphenyl (H) units, respectively (Figure 1) [7,11]. The composition and type of lignin depend on the plant type. While softwood lignins primarily comprise guaiacyl units (G-type lignin), hardwood lignins also contain syringyl units (G/S-type lignin). Lignins in grassy biomass are built up from all three sub-units and, in addition to the previous two, contain substantial amounts of hydroxyphenyl units (G/S/H-type lignin) [10,12].

Since monolignol coupling involves radicals, there are many possibilities for linkages between lignin monomers. These sub-units are primarily connected by ether and carbon-carbon linkages, wherein β -aryl ether (β -O-4) linkages are the most common ones in softwood and hardwood lignins, approximately 50% and 60%, respectively (Figure 1). C-C linkages are less common in hardwood than in softwood lignins, as the additional methoxy groups, chiefly in the S units, hamper the formation of these linkages [12,13].

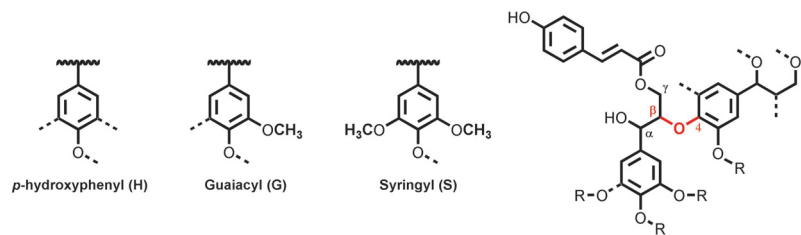


Figure 1. Lignin monomers with potential branchpoints marked with a dashed line; a structure of a possible lignin fragment containing the β -O-4 aryl ether linkage.

In addition to the source of lignin, the composition and molecular weight depend on the extraction method [12]. Most of the technical lignins are obtained by recovery as an industrial by-product [14]. The pulp and paper industries are the primary producers of technical lignin generating 50–70 million tons annually [15]. In contrast to the more traditional Kraft process, organosolv pulping utilizes organic solvents to dissolve lignin from the biomass [12]. It is a potent method for biorefineries for the utilization of biomass from hard- and softwoods as well as from grasses [12,16,17]. Organosolv lignin is highly pure, homogeneous, sulfur-free, with low content of carbohydrates and ash, and has a low molecular weight and dispersity. It is highly similar to native lignin, containing fewer modifications, and has an increased number of aryl ether linkages. So far, this technology has only reached pilot and demonstration scale, and not the industrial scale, mainly due to the high cost of solvent recovery [6,12,18].

Approximately only 2% of industrial lignin leftovers are used for commercial products [4,19]. Instead of being a mere by-product, lignin could be a useful co-product to produce valuable chemicals, such as vanillin [20]. Structurally extensively modified technical lignins with rearranged structures hinder its depolymerization into smaller fragments, a crucial and critical step for lignin utilization [21,22].

In nature, lignin decomposition is accomplished by numerous organisms, such as white-, brown-, and soft-rot fungi [23], and several Gram-positive and Gram-negative bacteria, mostly Actinobacteria and Proteobacteria [24]. In addition to other Streptomycetes, *Streptomyces coelicolor* has been identified as a lignin-degrading bacterial species, which harbors genes responsible for the catabolism of naturally occurring phenolics [25].

Lignin degraders, in nature, employ sophisticated metabolic and enzyme systems to attack and depolymerize lignin. Lignin-modifying enzymes, the key enzymes in lignin depolymerization, are phenol oxidases (laccases, EC 1.10.3.2) and heme-containing peroxidases—lignin-modifying peroxidases (LMPs): lignin peroxidase (LiP, EC 1.11.1.14), manganese(-dependent) peroxidase (MnP, EC 1.11.1.13), and versatile peroxidase (VP, EC 1.11.1.16). LMPs are part of the fungal class II heme-containing peroxidases in the catalase-peroxidase superfamily. These three ligninolytic peroxidases share noticeably high sequence identity and similarities in their structure [26,27].

Dye-decolorizing peroxidases (DyPs) also belong to LMPs but are phylogenetically unrelated to other LMPs (LiP, MnP, and VP). These peroxidases have heme as the attached prosthetic group and require hydrogen peroxide as the co-substrate that is reduced to water during its catalytic cycle [28]. DyPs (EC 1.11.1.19), systematically reactive-blue-5: hydrogen-peroxide oxidoreductases, were first identified in the fungus *Bjerkandera adusta* (previously *Geotrichum candidum* 1 Dec) in 1999 [29], later in bacteria [26]. Because of their distinctive structural and catalytic characteristics, DyPs form a new group of heme peroxidases [30]. They were named based on their ability to degrade and decolorize anthraquinone and azo dyes, such as Reactive Blue 5 [29,31,32]. The substrate specificity of DyPs is broad; in addition to dyes, they also oxidize other typical peroxidase substrates such as 2,2'-azino-bis(3-ethylbenzothiazoline-6-sulfonic acid) (ABTS) and 2,6-dimethoxyphenol (2,6-DMP) [26,33]. DyPs can oxidize phenolic [34] and non-phenolic lignin fragments without requiring a mediator [35,36].

According to the phylogenetic analysis of genomic sequences, DyPs have been classified into four sub-families in PeroxiBase. Sub-families A, B, and C contain predominately bacterial peroxidases, while sub-family D peroxidases are from fungi [37]. A newer classification was proposed in 2015, which divides DyPs into classes P (primitive, former class B), I (intermediate, former class A), and V (advanced, former classes C and D) [38]. DyP-type peroxidases are more or less considered bacterial counterparts to fungal LMPs [39]. The ability to decompose lignin has been identified from several DyPs. It includes peroxidases from fungi *Auricularia auricula-judae* [35], *Irpex lacteus* [40], and bacterial species such as *Rhodococcus jostii* [41], *Thermobifida fusca* [42], and *Pseudomonas fluorescens* [43]. *S. coelicolor* A3(2) genome was sequenced in 2002 [44] and has three genes encoding DyPs, two A-type DyPs and a B-type DyP. We hypothesize that this bacterium requires dye-decolorizing peroxidases to metabolize lignin.

Here, we cloned, expressed, and purified all three DyPs encoded by *S. coelicolor* A3(2). The H₂O₂-dependent activity of the enzymes were characterized using a soluble model substrate ABTS as well as water-insoluble organosolv lignins from *Miscanthus × giganteus* and aspen. The activity of DyPs on ABTS did not correlate with their ability in modifying lignin, a phenomenon that may reflect different pH optima observed with these two substrates. Furthermore, different DyPs had distinctly different effects in lignin modification. Treatment of lignins with type-A DyPs, ScDyP1A and ScDyP2A, resulted in depolymerization of lignin, whereas treatment with ScDyPB increased the molecular weight of lignin.

2. Materials and Methods

In order to conserve space, portions containing detailed information about the experiments can be found in the Supplementary Materials.

2.1. Gene Cloning

Genes encoding dye-decolorizing peroxidases (DyPs) (accession numbers: NP_626524.1, NP_628147.1, and NP_631251.1 for locus tags SCO2276 (ScDyP1A), SCO3963 (ScDyP2A), and SCO7193 (ScDyPB), respectively) were amplified from *Streptomyces coelicolor* A3(2) genomic DNA using the oligonucleotide primers with restriction endonuclease sites for NdeI and XhoI, respectively (Table S1). Plasmid DNAs were purified by alkaline lysis. The amplified genes (1263 bp, 1338 bp, and 951 bp for SCO2276, SCO3963, and SCO7193, respectively) were cloned into pET15b expression vector coding for an N-terminal His₆-tag followed by thrombin protease site. Additionally, codon-optimized genes for SCO2276 and SCO3963 were obtained and pre-cloned into the pET28a expression vector (Twist Bioscience, San Francisco, CA, USA). Each clone (codon-optimized) carried the Kan resistance gene, N-terminal His₆-tag, and thrombin cleavage site.

2.2. Overexpression

Recombinant ScDyPs were overproduced in *E. coli* BL21 (DE3) as His₆-fusion proteins (without the N-terminal 40-amino acid putative twin-arginine translocation (Tat) signal peptides in the case of ScDyPAs). The overnight starter cultures were used for inoculation. The culture media (LB prepared in tap water) supplemented with antibiotics was incubated at 37 °C until the OD₆₀₀ reached 0.6–0.8. The overexpression of recombinant protein was induced by 1 mM isopropyl-β-D-1-thiogalactopyranoside. The culture was grown overnight, at 30 °C and 180 rpm. The cells were harvested at 4000 g, 15 min, and 4 °C.

2.3. Purification

The harvested cells were resuspended in buffer A (20 mM Tris-HCl, pH 7.5, 0.5 M NaCl, 5 mM imidazole) and lysed using sonication (Bandelin Sonopuls, Bandelin GmbH & Co, Berlin, Germany) or high-pressure homogenization (Emulsiflex-C5, Avestin, Ottawa, ON, Canada). The lysed cells were centrifuged at 35,000 g for 1 h, at 4 °C. The supernatant was loaded onto the HisTrap FF column (GE Healthcare, Chicago, IL, USA). The column was washed with 10 column volumes (CV) of 10% buffer B (20 mM Tris-HCl, pH 7.5, 0.5 M NaCl,

0.5 M imidazole) to remove non-specifically bound proteins. The His₆-tagged protein was eluted with the linear gradient of imidazole of 10 to 100% buffer B (20 CV). The fractions were analyzed with SDS-PAGE, and the protein of interest was pooled. His₆-tag was cleaved by overnight incubation with thrombin (2 U per 1 mg protein) at 4 °C. The heme reconstitution was conducted with hemin (2-fold molar excess) at room temperature for 2 h using 20 mg/mL hemin (98%, porcine, Acros Organics, Fair Lawn, NJ, USA) dissolved in DMSO. The protein was exchanged to 20 mM Tris-HCl buffer (pH 7.5) containing 0.1 M NaCl (HiPrep 26/10 Desalting column) (GE Healthcare); the resulting protein fractions were pooled and concentrated using centrifugal filters with a molecular weight cutoff of 10 kDa (Sartorius, Göttingen, Germany). The protein was flash-frozen in liquid nitrogen and stored at −80 °C.

2.4. Determination of Enzyme Concentration

The total protein concentration was determined spectrophotometrically at 280 nm (UV-2700 UV-Visible Spectrophotometer, Shimadzu, Japan). The extinction coefficient ϵ_{280} nm values, calculated using the ExPASy ProtParam tool (<https://web.expasy.org/protparam/>, accessed on 15 August 2022), were 51,450; 38,960; and 18,450 M^{−1}cm^{−1}, for ScDyP1A, ScDyP2A, and ScDyPB, respectively. To estimate the total protein concentration before heme reconstitution, the buffer was exchanged using ultrafiltration filters to prevent concentration overestimation due to imidazole absorption.

The amount of active enzyme (with heme in the active site) was calculated using characteristic absorbance at 406 nm ($\epsilon_{406} = 100,000$ M^{−1} cm^{−1}) for heme proteins [45]. The total and the active enzyme content was calculated before and after the reconstitution with hemin. The heme content of DyPs was evaluated by Reinheitszahl value (Rz, A_{406}/A_{280}). In all experiments, the enzymes were dosed based on the active enzyme concentration.

2.5. Enzyme Assays

All enzyme assays with ABTS (ChemCruzTM, Santa Cruz, CA, USA) were performed in triplicate using Shimadzu UV-2700 UV-Visible Spectrophotometer at room temperature (except for the investigation of temperature dependence). All measurements with 100 nM ScDyP1A, 50 nM ScDyP2A, or 15 nM ScDyPB were used. Oxidation of ABTS was carried out with 1 mM H₂O₂, and the formation of ABTS cation radical was measured at 420 nm ($\epsilon_{420} = 36,000$ M^{−1} cm^{−1}). A fresh stock solution of H₂O₂ was prepared daily before use. The stock of 2,6-DMP (Acros Organics, Fair Lawn, NJ, USA) was prepared in dimethylformamide. The oxidation of 2,6-DMP was measured at 470 nm ($\epsilon_{470} = 53,200$ M^{−1} cm^{−1}) [46]. Optimal pH and temperature dependence parameters were determined (Supplementary Materials). The data analysis was carried out using OriginPro 2021 software (OriginLab, Northampton, MA, USA).

2.6. Organosolv Extraction of Lignin

Ethanol organosolv lignin from bleached chemi-thermomechanical aspen pulp was extracted as described in Jõul et al., 2022 [16]. Ethanol organosolv lignin from *Miscanthus × giganteus* (Mxg-lignin) was provided by Stefan Bauer [17]. Klason analysis was conducted as described in Jõul et al., 2022 [16] to determine the total lignin content for aspen (86.8 ± 0.7%) and Mxg (85.0 ± 1.1%) lignins, respectively.

2.7. Enzymatic Treatment of Organosolv Lignins

Ethanol organosolv lignin suspension at 1 mg/mL in aqueous HEPES (Sigma-Aldrich, St. Louis, MO, USA), buffer (50 mM, pH 8.0) with added 2 mM H₂O₂ was treated with 10 µM of ScDyP1A, ScDyP2A, or ScDyPB, incubated for 24 h, at 28 °C. For turbidity, the reaction mixtures were agitated at 200 rpm. The reaction mixtures and controls were centrifuged, and the insoluble portions were lyophilized for storage. The supernatants were extracted with ethyl acetate for further analysis. The water-insoluble portions of lignin

were analyzed via gel permeation chromatography (GPC) and water-soluble portions with gas chromatography-mass spectrometry (GC-MS).

3. Results

3.1. The Ensemble of DyP-Peroxidases of *Streptomyces coelicolor*

The genome of *S. coelicolor* A3(2) (*Sc*) carries three genes encoding for DyPs: two type-A DyPs, *ScDyP1A* (SCO2276) and *ScDyP2A* (SCO3963), and a type-B DyP, *ScDyPB* (SCO7193) with molecular weights of 45 kDa, 47 kDa, and 34 kDa, respectively. The three genes are located in three distinct loci on the single linear chromosome of *S. coelicolor*. Regarding the operonic context, it is not entirely clear what specific biological role *ScDyPB* might be involved with. However, in the case of *ScDyP1A*, the annotations of the neighboring genes in its operon suggest its role in iron homeostasis (i.e., iron permease, high-affinity iron-transporter, etc.). In contrast, in the case of *ScDyP2A*, the operon contains a putative prephenate dehydrogenase and an aminoacyl-tRNA synthetase, thus suggesting a role in the biosynthesis of aromatic amino acids, which is well aligned with lignin biochemistry (Table 1). The genes of *ScDyP1A* and *ScDyP2A* contain an N-terminal Tat secretion tag, suggesting a role outside of the cytosole, whereas *ScDyPB* lacks the secretion signal, suggesting a biochemical role inside the cell.

Table 1. The annotations of DyP-type peroxidases of *S. coelicolor* A3(2) and their corresponding operon neighbors, as assigned in the public databases.

ScDyP	Locus Tag	Annotation ¹
ScDyPB	SCO7193	putative iron-dependent peroxidase
	SCO7192	sigma factor
	SCO7194	putative polysaccharide biosynthesis protein
ScDyP1A	SCO2276	ferrous iron transport peroxidase
	SCO2272, SCO2274	heme ABC transporter
	SCO2273	hemin transport system permease
	SCO2275	ferrous iron transport periplasmic protein
	SCO2277	ferrous iron transport permease
	SCO2278	hypothetical protein
ScDyP2A ²	SCO3963	DyP-type peroxidase family protein
	SCO3971	conserved hypothetical protein
	SCO3970	Xaa-Pro aminopeptidase
	SCO3969	possible ATP/GTP-binding protein
	SCO3968	putative integral membrane protein
	SCO3967	putative membrane protein
	SCO3966, SCO3965	putative copper metallochaperone
	SCO3964	copper transport protein
	SCO3962	prephenate dehydratase
	SCO3961	seryl-tRNA synthetase
SCO3960	hydrolase (HAD superfamily)	

¹ Annotation is based on JGI IMG/M and the SEED databases. ² The operon for *ScDyP2A* is encoded on the complement strand.

3.2. Production and Purification of Recombinant *ScDyPs*

ScDyPs were expressed as His-tagged fusion proteins in *E. coli*, purified, and the concentration of apo- and holo-enzymes determined using spectrophotometry. The *ScDyPs* showed the typical heme-peroxidase spectrum with a Soret band maxima at 408 nm, 405 nm and 401 nm for *ScDyP1A*, *ScDyP2A*, and *ScDyPB*, respectively (Figure S1). The heme content of peroxidases was evaluated by Rz value (Table 2). Before reconstitution with hemin, the highest heme content was observed with *ScDyPB* followed by *ScDyP1A* and *ScDyP2A* (Table 2). The reconstitution improved the proportion of holo-enzyme (Table 2)—1.7-fold for *ScDyP1A* and 2.2-fold for *ScDyP2A*—while for *ScDyPB*, the Rz ratio remained relatively the same. In order to tackle the low expression yields of *ScDyPAs* (about 1 mg of protein from 1 L culture) from plasmids containing inserts of PCR-amplified genomic DNA

(i.e., 1 mg of protein for ScDyP1A/ScDyP2A from 1 L culture), synthetic genes that were codon-optimized for expression from an *E. coli* host, were obtained. The proteins were then expressed and purified, where ScDyP1A had an Rz value of 2.01 and ScDyP2A 2.02 before reconstitution with hemin. The reconstitution of DyPAs from the codon-optimized system with hemin did not show a particular effect, as the Rz values remained the same. The codon-optimization of genes considerably improved the protein expression yield for both ScDyP1A and ScDyP2A.

Table 2. Reinheitszahl values of ScDyPs before and after the heme reconstitution.

Rz Value	ScDyP1A	ScDyP2A	ScDyPB	ScDyP1A ^{CO}	ScDyP2A ^{CO}
Before reconstitution with hemin	0.78 ± 0.02	0.51 ± 0.02	2.36 ± 0.04	2.01 ± 0.11	2.02 ± 0.01
After reconstitution with hemin	1.33 ± 0.08	1.14 ± 0.02	2.32 ± 0.07	1.92 ± 0.03	2.17 ± 0.03

^{CO} Codon optimized genes for the expression out of *E. coli* BL21 (DE3).

3.3. Biochemical Characterization

3.3.1. Optimal pH for ScDyPs

The pH dependency of the oxidation of ABTS is shown in Figure 2. ScDyP1A and ScDyP2A exhibited the highest activity at pH 3.5, while the optimal pH for ScDyPB was determined to be 3.0 (Figure 2). At pH 5.0, all ScDyPs showed almost no activity with ABTS. Contrary to ABTS, the oxidation of phenolic substrate (2,6-DMP) by ScDyP2A and ScDyPB had a pH optimum around 8.5 (data not shown). ScDyP1A did not catalyze the oxidation of 2,6-DMP.

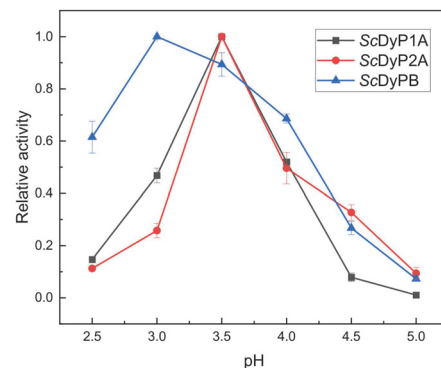


Figure 2. Optimum pH of dye-decolorizing peroxidases of *S. coelicolor* toward oxidation of ABTS. Data are average values of three independent measurements.

3.3.2. Temperature Dependency

The temperature dependency on enzyme activity was measured at pH 3.5 using ABTS as the substrate. Peroxidase activity for all DyPs were at a decline or started decreasing already at 30 °C and decreased with further temperature increase (Figure 3).

3.3.3. Thermostability

To further estimate the temperature stability of ScDyPs, the enzyme solutions were incubated, at 30 °C, for 48 h, and at fixed time intervals, sample aliquots were withdrawn, and tested for activity. Within 2 h, ScDyP2A had lost most activity compared to other ScDyPs, approximately one-third (Figure 4). After 24 h, ScDyP1A and ScDyPB had lost ~20% of activity, and ScDyP2A had around half of its activity. ScDyP1A is the most thermoresistant ScDyP and had retained ~70% of its activity within 48 h, wherein ScDyP2A had lost ~70% of its activity.

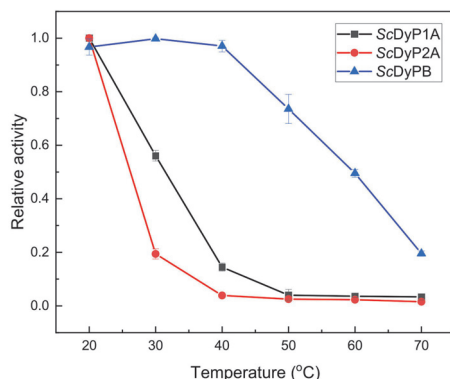


Figure 3. The temperature dependency of ScDyPs. Peroxidase activity was measured at pH 3.5 (50 mM sodium citrate) using ABTS as substrate. 1 mM H₂O₂ was used as a co-substrate. Experiments were conducted in triplicate.

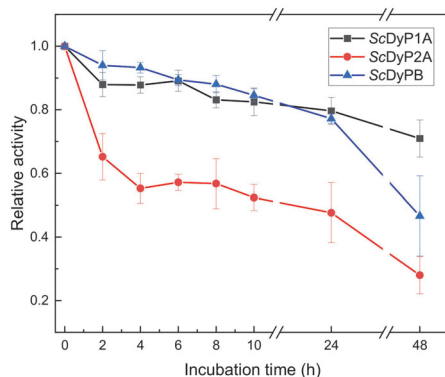


Figure 4. Thermostability of ScDyPs. The enzyme stocks were incubated in 50 mM sodium citrate (pH 3.5), at 30 °C. At selected times, the activities were measured using ABTS and 1 mM H₂O₂. Experiments were conducted in triplicate.

3.3.4. Steady-State Kinetics

Steady-state kinetic measurements were conducted at pH 3.5, varying the concentration of ABTS and using 1 mM H₂O₂ as a co-substrate. All ScDyPs displayed non-Michaelis-Menten kinetics (Figure S2), and the results were analyzed using the equation accounting for substrate inhibition (Equation (S1) in the Supplementary Materials). Kinetic parameters are summarized in Table 3. Highest k_{cat} was measured with ScDyPB, followed by ScDyP2A and ScDyP1A. The ScDyPB had also the lowest apparent K_M values for ABTS. Owing to its high k_{cat} and low K_M value, the ScDyPB had by far the highest catalytic efficiency (k_{cat}/K_M) in oxidation of ABTS (Table 3). All three DyPs are inhibited by increased substrate concentrations, wherein ScDyPB is more prone to inhibition by ABTS with a K_i of 0.4 mM (Table 3; Figure S2). 2,6-DMP was also tested as a substrate but proved to be a poor substrate for ScDyPs, especially for ScDyP1A, which did not oxidize this substrate (data not shown). However, the apparent specificities (k_{cat}/K_M) were approximately 140-fold lower for ScDyP2A ($\sim 0.1 \text{ mM}^{-1}\cdot\text{s}^{-1}$) and approximately 200-fold lower for ScDyPB ($\sim 3.1 \text{ mM}^{-1}\cdot\text{s}^{-1}$). Similarly, substrate inhibition was seen with 2,6-DMP (Figure S3).

Table 3. Kinetic parameters for the oxidation of soluble model substrate ABTS by ScDyPs. Apparent steady-state kinetic parameters were measured at pH 3.5 using 1 mM H₂O₂ as a co-substrate. Data are average values of three independent measurements.

	ScDyP1A	ScDyP2A	ScDyPB
K_M (mM)	1.4 ± 0.15	2.3 ± 0.9	0.08 ± 0.02
k_{cat} (s ⁻¹)	7.6 ± 1.1	31.7 ± 14.6	48.6 ± 5.7
k_{cat}/K_M (mM ⁻¹ ·s ⁻¹)	5.4 ± 0.2	13.8 ± 1.3	607 ± 95.2
K_i (mM)	4.3 ± 1.4	1.6 ± 1.0	0.4 ± 0.1

3.4. Lignin Remodeling Activity of ScDyPs

3.4.1. Identification of Molecular Weight Distribution of Lignin Samples by GPC Analysis

GPC analysis was utilized to observe the changes in the relative size distribution of ScDyPs-treated organosolv Mxg- and aspen lignins. Lignins were incubated in the presence of ScDyPs for 24 h, then centrifuged, and the pellets were lyophilized. For the GPC analysis, the lyophilized pellets were dissolved in THF, and the molecular weights of lignins were observed. The number-average molecular weight (Mn) of Mxg-lignin was 1509 Da, and the weight-average molecular weight (Mw) 2435 Da (Table 4).

Table 4. Mn, Mw, and the molar-mass dispersity (\mathcal{D}_M) of Mxg- (panel A) and aspen (panel B) ethanol organosolv lignins treated with ScDyPs determined by GPC analysis. Solutions containing lignins at 1 mg/mL in HEPES buffer (pH 8.0) and 2 mM H₂O₂ without enzymatic treatment, or treated with 10 μM enzyme were incubated for 24 h. Samples were centrifuged, pellets lyophilized and dissolved, and the lignins were analyzed using GPC.

	Mxg-Lignin			Aspen Lignin		
	Mn	Mw	\mathcal{D}_M	Mn	Mw	\mathcal{D}_M
Without enzyme	1509 ± 10	2435 ± 35	1.61	2772 ± 51	5533 ± 53	2.0
+ScDyP1A	1502 ± 8	2357 ± 26	1.57	2589 ± 12	4705 ± 72	1.82
+ScDyP2A	1489 ± 11	2332 ± 45	1.57	2429 ± 106	4371 ± 258	1.8
+ScDyPB	1856 ± 21	2921 ± 28	1.57	2994 ± 33	5607 ± 79	1.87

At first, pH 3.5 was used for the lignin experiments, but the lignin treatment at acidic media did not show an effect. Acidic to alkaline pH ranges were tested for optimal lignin-remodeling activity, where a pH range of 7.5 to 8.5 was deemed the most active (data not shown). The treatment of Mxg-lignin with ScDyPB led to the polymerization of lignin polymer up to 19%. Similar behavior was seen with aspen lignin. The enzymatic treatment with ScDyPB caused the increase in lignin molecular weight, whereas ScDyPAs showed the ability to decrease the molecular weight of lignin. The Mn of Mxg organosolv lignin treated with ScDyP2A and with ScDyP1A remained the same as with untreated material. However, the Mw of aspen lignin after 24 h treatment with ScDyP2A decreased by approximately 20%. Similarly, a reduction in the average molecular weight of aspen lignin after ScDyP1A treatment could also be detected. The \mathcal{D}_M of Mxg-lignin fragments decreased from 1.61 to 1.57. The \mathcal{D}_M of aspen lignin decreased from 2.00 to 1.87 (ScDyPB), 1.80 (ScDyP2A), and 1.82 (ScDyP1A). According to these results, all three ScDyPs can remodel organosolv lignin, wherein the Mxg-lignin is a better substrate for ScDyPB and aspen lignin for ScDyPAs (Figure 5).

3.4.2. Identification of Low-Molecular-Weight Compounds in Lignin Samples by GC-MS Analysis

GC-MS analysis was used to determine the low-molecular-weight (LMW) compounds in lignin samples. The organosolv lignins were incubated with and without ScDyPs for 24 h and centrifuged; the supernatants were extracted with ethyl acetate, lyophilized, dissolved in methanol, and analyzed with GC-MS. According to the GC-MS results, the

LMW proportion of *Mxg*-lignin contains mostly H-units, fewer G-units, and a small portion of S-units, wherein aspen lignin is in the most part composed of S-units, fewer G-units, and a minute proportion of H-units (based on the integrated peak area). The treatment of both lignins with ScDyPs decreased the amount of LMW compounds found in supernatants, where ScDyPB had the highest effect (Table 5).

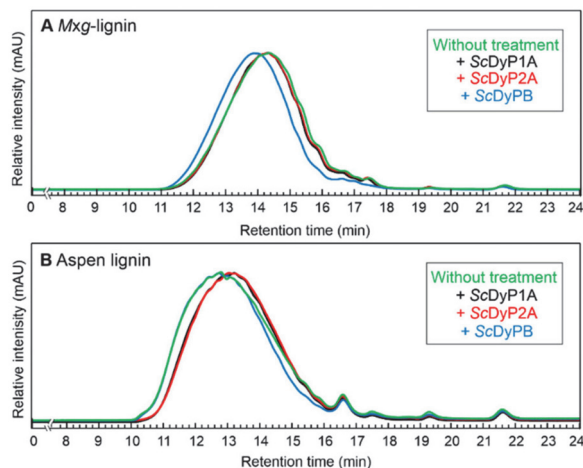


Figure 5. The characterization of lignin-remodeling activities of ScDyPs by GPC. Panel (A) *Mxg*-lignin, panel (B) aspen lignin. The treatment of *Mxg*-lignin with ScDyPB led to the polymerization of lignin polymer. The treatment of aspen lignin with ScDyPAs resulted in lignin depolymerization.

Table 5. The most prominent LMW compounds found in *Mxg*-lignin (A) and aspen lignin (B), and the influence of ScDyPs treatment to the peak area reduction. The peak areas are represented in percentages where the result from the untreated sample is set to 100%, and the treated samples are defined as the percentage peak area left after the treatment.

(A) Unit	Compound Name	Without Treatment	ScDyP1A	ScDyP2A	ScDyPB
H	<i>p</i> -Hydroxycinnamic acid, ethyl ester	100	78	78	2
G	Ethyl (E)-ferulate	100	67	75	2
G	(E)-4-(3-Hydroxyprop-1-en-1-yl)-2-methoxyphenol	100	77	69	9
G	Glyceryl ferulate	100	87	95	nd *
S	<i>trans</i> -Sinapyl alcohol	100	63	69	5
(B) Unit	Compound Name	Without Treatment	ScDyP1A	ScDyP2A	ScDyPB
S	<i>trans</i> -Sinapyl alcohol	100	53	55	37
G	(E)-4-(3-Hydroxyprop-1-en-1-yl)-2-methoxyphenol	100	44	52	16
S	<i>trans</i> -Sinapaldehyde	100	64	68	53
G	Butyrovanillone	100	92	73	nd *
G	2-Propanone, 1-hydroxy-3-(4-hydroxy-3-methoxyphenyl)-	100	nd *	nd *	nd *

* not detected.

4. Discussion

The purpose of this study was to characterize the full ensemble of DyP peroxidases from *S. coelicolor* A3(2), which consists of two A-type and one B-type DyP peroxidase in the context of enzymatic modification of organosolv lignins. The physiological roles

of DyPs are unclear to date. It has been shown previously that some type-A DyPs are components of tripartite ferrous iron transporters and serve a role in iron uptake [47,48]. There are reports of DyPs functioning as deferrochelataes by releasing heme iron without tetrapyrrole degradation, such as EfeB (class A) from *E. coli* [49]. According to the operonic context, ScDyP1A might be a ferrous iron transport peroxidase. B-type DyPs are putative cytoplasmic enzymes indicating a function in intracellular metabolism [50]. However, the operonic context of ScDyPB does not hint at its specific role for *S. coelicolor*.

For the biochemical characterization, the three DyPs from *S. coelicolor* A3(2) were heterologously expressed and purified. The efficiency of heterologous expression of proteins is often hampered by differences in the codon usage between the organism of origin and the chosen host expression organism for a particular gene. In addition to differences in the abundance of specific tRNAs, the genome of *S. coelicolor* has 72% G + C content, when compared to that of about 51% of *E. coli*. [44,51]. Although the expression of ScDyPB yielded sufficient amounts of enzyme for further experiments (20 mg per liter culture), the expression of ScDyPAs resulted in roughly 20-fold less protein. Successful protein expression in *E. coli* as the host depends on several factors, such as the choice of the expression plasmid and the strain, the optimization of expression conditions, etc. [52,53]. However, codon usage seems to have the highest impact on obtaining high protein yields from recombinant expression [54]. It is also known that *S. coelicolor* has remarkably different codon usage profile than *E. coli* [55]. Codon optimization is often used to enhance the translation efficiency of a gene of interest [56]. It has been seen that codon-optimization results in an even 140-fold improvement of protein expression yield [57]. Here, the expression with codon-optimized genes enabled the production of higher quantities of protein when compared to the non-optimized construct, resulting in a 4-fold and 43-fold increase for ScDyP1A and ScDyP2A, respectively. Additionally, DyPs require heme as a prosthetic group for its catalytic activity [29]. Recombinant bacterial expression frequently produces heme-deficient proteins [58–61], which can be combated by supplementing the growth media with extra hemin during the expression [61]. Unfortunately, the heme transport systems of most *E. coli* strains cannot efficiently uptake hemin and depend on the diffusion through the cell membrane [60,61]. The Reinheitszahl (Rz) value (from German “purity number”), the ratio of absorbances (A_{Soret}/A_{280}), is used to obtain an estimate on the extent of heme incorporation into peroxidases. Prior to supplying the DyPs with additional hemin, Rz values of ScDyP1A and ScDyP2A were below one. The reconstitution improved the Rz values by approximately 2-fold for both ScDyPAs. The Rz values for ScDyPAs obtained from codon-optimized genes and ScDyPB were over two without any extra steps. The heme reconstitution after purification did not increase the Rz values of ScDyPAs obtained from codon-optimized genes and for ScDyPB. It is fathomable that the uptake kinetics of heme by DyPAs in vivo are affected by the differences in the speed of translation between the high G + C non-optimized vs. codon-optimized DyPA constructs. Although we have no direct evidence for it, it is possible that there may be minor differences in protein folding due to ribosome stalling which may also affect the heme uptake by the purified proteins in vitro.

Having obtained sufficient amounts of heme-reconstituted ScDyPs, we set out to determine their optimal working conditions (i.e., pH and temperature). DyP-type peroxidases have demonstrated a lower pH preference than classic heme peroxidases [29,62]. Typically, rather similar pH optima for ABTS and 2,6-DMP oxidation have been identified for DyPs. Previous studies of fungal and bacterial DyPs have reported that the optimum pH for ABTS and 2,6-DMP oxidation falls in the pH range of 3–5 [63–65]. Our results of ScDyPs were consistent with the past findings for ABTS. The optimum pH of ScDyPs for ABTS oxidation was determined in the range of 3–3.5, but in contrast, for phenolic 2,6-DMP oxidation, the optimum pH was 8.5. Chaplin et al., 2017 reported that the optimum pH for 2,6-DMP oxidation is 9.0 for DyPA from *Streptomyces lividans* [66]. This kind of phenomenon has also been seen in the case of laccases, where the enzymes catalyze the oxidation of ABTS better at pH 4, but the oxidation of 2,6-DMP at alkaline pH (7–9) [67,68].

It has been shown that enzymes isolated from extremophiles can tolerate more severe conditions, such as extremes in pH, temperature, salt concentration, etc., often required for industrial processes. For instance, the optimal temperature of A-type TcDyP from a thermophilic actinomycete *Thermomonospora curvata* was also 30 °C; however, 1 h incubation of TcDyP at 60 °C resulted in ~70% retained activity [69]. Since *S. coelicolor* is a mesophilic bacterium, it was expected that ScDyPs would show only modest resistance to elevated temperatures. ScDyPB showed the highest activity at 30 °C, and the activity of all ScDyPs decreased with the rising temperature. The activities of ScDyPAs decreased more rapidly at higher temperatures compared to ScDyPB. The relative activity of ScDyPB at 40 °C was 90%, but in contrast, ScDyPAs had retained only less than 20% of activity. Further, the stability of ScDyPs at 30 °C was determined (Figure 4). The thermostability of ScDyP2A was decreasing most rapidly and, within 48 h, had lost 70% of its activity. ScDyP1A was relatively stable for 48 h with residual activity of 70%. Min et al., 2015, had a novel observation where the optimum temperature of BsDyP was dependent on the substrates the residual activity was measured with [36]. Therefore, temperature dependency and thermostability results were only compared to those where ABTS was used for the measurements.

All three DyPs possessed different apparent specificities (k_{cat}/K_M) for ABTS, 5 mM⁻¹·s⁻¹, 14 mM⁻¹·s⁻¹, and 600 mM⁻¹·s⁻¹ for ScDyP1A, ScDyP2A, and ScDyPB, respectively. Like ScDyPs, the peroxidase activities are not comparable to C- and D-type DyPs and show much lower activities. Previously characterized DypA and DypB from *Rhodococcus jostii* RHA1, a Gram-positive soil bacteria, showed lower apparent specificities with ABTS than ScDyPs, approximately 2 mM⁻¹·s⁻¹ [41]. Substrate inhibition is a frequent phenomenon and occurs in roughly 25% of known enzymes [70]. Substrate inhibition was observed in case of all ScDyPs, with both substrates, wherein with ABTS, ScDyP1A was inhibited the most and ScDyPB the least.

According to in silico analysis by Benslama et al., 2022, it was proposed that a DyP from *S. coelicolor* (ScDyP1A) has the potential to efficiently biodegrade lignin [71]. Lignin remodeling experiments with ScDyPs were conducted with organosolv lignins from aspen and *Miscanthus × giganteus*. The acidic conditions (pH 3.5) initially used in lignin remodeling experiments were unsuitable, most probably due to the aggregation of DyPs at lower pH. Additionally, alkaline pH was preferred due to the substantially increased solubility of lignin in alkaline media (deprotonation of phenolic OH-groups) [9]. A range of alkaline pHs was tested, and pH 8 was chosen as the most promising pH for lignin experiments.

GPC analysis determined that the enzymatic treatment of lignin decreased the dispersity— D_M [72] for both lignins—indicating that lignin becomes more homogeneous due to treatment with ScDyPs. Neither of the A-type ScDyPs had an effect on the molecular weight distribution of Mxg-lignin, while ScDyPB did not affect the molecular weight distribution of aspen lignin. ScDyP2A had the highest effect on lignin, and Mw of aspen lignin was reduced by ~20%. Treating Mxg-lignin with ScDyPB led to lignin polymerization and led to the increase in the molecular weight of Mxg-lignin. This is a common problem, which is brought about by several condensation and polymerization routes, such as radical coupling, vinyl condensation, generation of reactive fragments involving polymerization, and reactive functional group-induced repolymerization reactions [73]. It has been observed that the success of lignin depolymerization is highly dependent on the nature of the lignin sample. In addition to the radical species generated, the ratio of phenolic/aliphatic OH-groups in lignin determines the fate of lignin [74]. A possible strategy to combat polymerization is to combine different enzymes. For instance, Rahmanpour et al., 2017, have identified an extracellular bacterial flavoenzyme that can prevent the repolymerization of lignin [75].

GC-MS analysis was used to analyze the supernatant of enzymatically treated or untreated lignins. Although this analysis does not determine the entire monolignol content of these lignin preparations, it was used to verify the main LMW compounds solely in the supernatant. According to GC-MS, the predominant LMW peak in Mxg-lignin belongs to an H-unit (p-Hydroxycinnamic acid ethyl ester), while in aspen lignin, the spectra is

dominated mostly by S-units. Several monolignols in *Mxg*-lignin were α -ethoxylated, a distinctive feature of ethanol organosolv lignins [17]. The results from GC-MS analysis provide one possible explanation for the results obtained from GPC analysis—the tendency of aspen lignin to be depolymerized and *Mxg*-lignin to be (re)polymerized. As S-units have a higher degree of methoxylation, the steric hindrance decreases the probability of crosslinking, and therefore, the depolymerization of lignin is promoted compared to polymerization. It has been reported previously that DyPs can be applied to coupling phenolic monomers [76]. Here, we similarly observed that after the enzymatic treatment, the number of monolignols in the supernatant decreased drastically. This observation might be explained by (i) the loss of lignin solubility caused by the enzymatic treatment and (ii) the polymerization of LMW compounds of lignins remaining in the pellet fraction after centrifugation.

5. Conclusions

Streptomyces coelicolor A3(2) is a rich source of enzymes with high potential for a variety of biotechnological applications. In addition to an extensively studied small laccase, the genome of *S. coelicolor* also encodes for several lytic polysaccharide monooxygenases and glycosyl hydrolases, but also an ensemble of dye-decolorizing peroxidases—ScDyPs. Here, ScDyPs were characterized in the context of their possible biotechnological application as lignin modifying enzymes. Using ABTS as the model substrate, pH and temperature dependence as well as Michaelis–Menten kinetic parameters were determined. ScDyPB showed the highest rate of catalysis with ABTS compared to other ScDyPs. Lignin remodeling activity was demonstrated with ScDyPB, which polymerized grassy biomass derived organosolv lignin, and with ScDyPAs, which depolymerized hardwood derived organosolv lignin. In addition to that, we demonstrated that ScDyPB is an effective tool for the removal of water-soluble LMW phenolics.

Our results illustrate the relevance of ligninolytic enzyme characterization alongside characterization of lignin to understand and improve the enzymatic treatment techniques of lignin.

Supplementary Materials: The following supporting information can be downloaded at: <https://www.mdpi.com/article/10.3390/en16031557/s1>, Supplementary Materials and Methods: Gene cloning (Transformation), Enzyme Assays (Optimal pH, Temperature Dependence & Thermostability, Enzyme Kinetics), Enzymatic Treatment of Organosolv Lignin (Gel Permeation Chromatography, Gas Chromatography-Mass Spectrometry). Table S1: Oligonucleotide primers used for gene amplification. Figure S1: Spectra of ScDyPs. Figure S2: Steady-state kinetics of ScDyPs against ABTS as a substrate. Figure S3: Steady-state kinetics of ScDyP2A and ScDyPB against 2,6-DMP.

Author Contributions: Conceptualization, T.L. and H.P.; methodology, formal analysis and investigation, T.L., H.P., P.J. and M.L.B.; writing—original draft preparation, H.P., T.L. and P.J.; funding acquisition, T.L. All authors have read and agreed to the published version of the manuscript.

Funding: This work was supported by the European Regional Development Fund and the programme Mobilitas Pluss (grant number MOBTT60).

Data Availability Statement: All data underlying the results are available as part of the article and supplementary materials. No additional source data are required.

Acknowledgments: The authors would like to thank Priit Väljamäe for helpful discussions during the preparation of this manuscript. The contribution of COST Action LignoCOST (CA17128), supported by COST (European Cooperation in Science and Technology, www.cost.eu), in promoting interaction, exchange of knowledge and collaborations in the field of lignin valorization is gratefully acknowledged.

Conflicts of Interest: The authors declare no conflict of interest.

References

1. Dahmen, N.; Lewandowski, I.; Zibek, S.; Weidtmann, A. Integrated Lignocellulosic Value Chains in a Growing Bioeconomy: Status Quo and Perspectives. *GCB Bioenergy* **2019**, *11*, 107–117. [[CrossRef](#)]
2. Watkins, D.; Nuruddin, M.; Hosur, M.; Tcherbi-Narteh, A.; Jeelani, S. Extraction and Characterization of Lignin from Different Biomass Resources. *J. Mater. Res. Technol.* **2015**, *4*, 26–32. [[CrossRef](#)]
3. Chandel, A.K.; Garlapati, V.K.; Singh, A.K.; Antunes, F.A.F.; da Silva, S.S. The Path Forward for Lignocellulose Biorefineries: Bottlenecks, Solutions, and Perspective on Commercialization. *Bioresour. Technol.* **2018**, *264*, 370–381. [[CrossRef](#)]
4. Cao, L.; Yu, I.K.M.; Liu, Y.; Ruan, X.; Tsang, D.C.W.; Hunt, A.J. Lignin Valorization for the Production of Renewable Chemicals: State-of-the-Art Review and Future Prospects. *Bioresour. Technol.* **2018**, *269*, 465–475. [[CrossRef](#)] [[PubMed](#)]
5. Zoghalmi, A.; Paës, G. Lignocellulosic Biomass: Understanding Recalcitrance and Predicting Hydrolysis. *Front. Chem.* **2019**, *7*, 874. [[CrossRef](#)] [[PubMed](#)]
6. Kumar, A.; Anushree; Kumar, J.; Bhaskar, T. Utilization of Lignin: A Sustainable and Eco-Friendly Approach. *J. Energy Inst.* **2020**, *93*, 235–271. [[CrossRef](#)]
7. Ragauskas, A.J.; Beckham, G.T.; Bidy, M.J.; Chandra, R.; Chen, F.; Davis, M.F.; Davison, B.H.; Dixon, R.A.; Gilna, P.; Keller, M.; et al. Lignin Valorization: Improving Lignin Processing in the Biorefinery. *Science* **2014**, *344*, 1246843. [[CrossRef](#)]
8. Li, C.; Zhao, X.; Wang, A.; Huber, G.W.; Zhang, T. Catalytic Transformation of Lignin for the Production of Chemicals and Fuels. *Chem. Rev.* **2015**, *115*, 11559–11624. [[CrossRef](#)]
9. Schutyser, W.; Renders, T.; Van Den Bosch, S.; Koelewijn, S.F.; Beckham, G.T.; Sels, B.F. Chemicals from Lignin: An Interplay of Lignocellulose Fractionation, Depolymerisation, and Upgrading. *Chem. Soc. Rev.* **2018**, *47*, 852–908.
10. Becker, J.; Wittmann, C. A Field of Dreams: Lignin Valorization into Chemicals, Materials, Fuels, and Health-Care Products. *Biotechnol. Adv.* **2019**, *37*, 107360.
11. Vanholme, R.; Demedts, B.; Morreel, K.; Ralph, J.; Boerjan, W. Lignin Biosynthesis and Structure. *Plant Physiol.* **2010**, *153*, 895–905. [[CrossRef](#)] [[PubMed](#)]
12. Chio, C.; Sain, M.; Qin, W. Lignin Utilization: A Review of Lignin Depolymerization from Various Aspects. *Renew. Sustain. Energy Rev.* **2019**, *107*, 232–249. [[CrossRef](#)]
13. Koranyi, T.I.; Fridrich, B.; Pineda, A.; Barta, K. Development of “Lignin-First” Approaches for the Valorization of Lignocellulosic Biomass. *Molecules* **2020**, *25*, 2815. [[CrossRef](#)] [[PubMed](#)]
14. Dessbesell, L.; Paleologou, M.; Leitch, M.; Pulkki, R.; Xu, C. Global Lignin Supply Overview and Kraft Lignin Potential as an Alternative for Petroleum-Based Polymers. *Renew. Sustain. Energy Rev.* **2020**, *123*, 109768. [[CrossRef](#)]
15. Bajwa, D.S.; Pourhashem, G.; Ullah, A.H.; Bajwa, S.G. A Concise Review of Current Lignin Production, Applications, Products and Their Environment Impact. *Ind. Crops Prod.* **2019**, *139*, 111526. [[CrossRef](#)]
16. Joul, P.; Ho, T.T.; Kallavus, U.; Konist, A.; Leiman, K.; Salm, O.S.; Kulp, M.; Lukk, T. Characterization of Organosolv Lignins and Their Application in the Preparation of Aerogels. *Materials* **2022**, *15*, 2861. [[CrossRef](#)]
17. Bauer, S.; Sorek, H.; Mitchell, V.D.; Ibáñez, A.B.; Wemmer, D.E. Characterization of Miscanthus Giganteus Lignin Isolated by Ethanol Organosolv Process under Reflux Condition. *J. Agric. Food Chem.* **2012**, *60*, 8203–8212. [[CrossRef](#)]
18. Tribot, A.; Amer, G.; Abdou Alio, M.; de Baynast, H.; Delattre, C.; Pons, A.; Mathias, J.D.; Callois, J.M.; Vial, C.; Michaud, P.; et al. Wood-Lignin: Supply, Extraction Processes and Use as Bio-Based Material. *Eur. Polym. J.* **2019**, *112*, 228–240. [[CrossRef](#)]
19. Chan, J.C.; Paice, M.; Zhang, X. Enzymatic Oxidation of Lignin: Challenges and Barriers Toward Practical Applications. *ChemCatChem* **2020**, *12*, 401–425. [[CrossRef](#)]
20. Fache, M.; Boutevin, B.; Caillol, S. Vanillin Production from Lignin and Its Use as a Renewable Chemical. *ACS Sustain. Chem. Eng.* **2016**, *4*, 35–46. [[CrossRef](#)]
21. Van Den Bosch, S.; Renders, T.; Kennis, S.; Koelewijn, S.F.; Van Den Bossche, G.; Vangeel, T.; Deneyer, A.; Depuydt, D.; Courtin, C.M.; Thevelein, J.M.; et al. Integrating Lignin Valorization and Bio-Ethanol Production: On the Role of Ni-Al₂O₃ Catalyst Pellets during Lignin-First Fractionation. *Green Chem.* **2017**, *19*, 3313–3326. [[CrossRef](#)]
22. Shuai, L.; Talebi Amiri, M.; Questell-Santiago, Y.M.; Héroguel, F.; Li, Y.; Kim, H.; Meilan, R.; Chapple, C.; Ralph, J.; Luterbacher, J.S. Formaldehyde Stabilization Facilitates Lignin Monomer Production during Biomass Depolymerization. *Science* **2016**, *354*, 329–334. [[CrossRef](#)]
23. Bugg, T.D.H.; Ahmad, M.; Hardiman, E.M.; Rahmanpour, R. Pathways for Degradation of Lignin in Bacteria and Fungi. *Nat. Prod. Rep.* **2011**, *28*, 1883–1896. [[CrossRef](#)]
24. Tian, J.; Pourcher, A.; Bouchez, T.; Gelhaye, E.; Peu, P. Occurrence of Lignin Degradation Genotypes and Phenotypes among Prokaryotes. *Appl. Microbiol. Biotechnol.* **2014**, *98*, 9527–9544. [[CrossRef](#)] [[PubMed](#)]
25. Majumdar, S.; Lukk, T.; Solbiati, J.O.; Bauer, S.; Nair, S.K.; Cronan, J.E.; Gerlt, J.A. Roles of Small Laccases from Streptomyces in Lignin Degradation. *Biochemistry* **2014**, *53*, 4047–4058. [[CrossRef](#)]
26. Janusz, G.; Pawlik, A.; Sulej, J.; Świdarska-Burek, U.; Jarosz-Wilkolazka, A.; Paszczyński, A. Lignin Degradation: Microorganisms, Enzymes Involved, Genomes Analysis and Evolution. *FEMS Microbiol. Rev.* **2017**, *41*, 941–962. [[CrossRef](#)] [[PubMed](#)]
27. Li, C.; Chen, C.; Wu, X.; Tsang, C.; Mou, J.; Yan, J.; Liu, Y.; Sze, C.; Lin, K. Recent Advancement in Lignin Biorefinery: With Special Focus on Enzymatic Degradation and Valorization. *Bioresour. Technol.* **2019**, *291*, 121898. [[CrossRef](#)] [[PubMed](#)]
28. Zámocky, M.; Hofbauer, S.; Schaffner, I.; Gasselhuber, B.; Nicolussi, A.; Soudi, M.; Pirker, K.F.; Furtmüller, P.G.; Obinger, C. Independent Evolution of Four Heme Peroxidase Superfamilies. *Arch. Biochem. Biophys.* **2015**, *574*, 108–119. [[CrossRef](#)] [[PubMed](#)]

29. Kim, S.J.U.N.; Shoda, M. Purification and Characterization of a Novel Peroxidase from *Geotrichum Candidum* Dec 1 Involved in Decolorization of Dyes. *Appl. Environ. Microbiol.* **1999**, *65*, 1029–1035. [[CrossRef](#)]
30. Sugano, Y.; Muramatsu, R.; Ichiyanagi, A.; Sato, T.; Shoda, M. Dyp, a Unique Dye-Decolorizing Peroxidase, Represents a Novel Heme Peroxidase Family: ASP171 Replaces the Distal Histidine of Classical Peroxidases. *J. Biol. Chem.* **2007**, *282*, 36652–36658. [[CrossRef](#)]
31. Kim, S.J.; Ishikawa, K.; Hirai, M.; Shoda, M. Characteristics of a Newly Isolated Fungus, *Geotrichum Candidum* Dec 1, Which Decolorizes Various Dyes. *J. Ferment. Bioeng.* **1995**, *79*, 601–607. [[CrossRef](#)]
32. Singh, R.; Eltis, L.D. The Multihued Palette of Dye-Decolorizing Peroxidases. *Arch. Biochem. Biophys.* **2015**, *574*, 56–65. [[CrossRef](#)] [[PubMed](#)]
33. Sugawara, K.; Nishihashi, Y.; Narioka, T.; Yoshida, T.; Morita, M.; Sugano, Y. Characterization of a Novel Dyp-Type Peroxidase from *Streptomyces Avermitilis*. *J. Biosci. Bioeng.* **2017**, *123*, 425–430. [[CrossRef](#)]
34. Ahmad, M.; Roberts, J.N.; Hardiman, E.M.; Singh, R.; Eltis, L.D.; Bugg, T.D.H. Identification of DypB from *Rhodococcus Jostii* RHA1 as a Lignin Peroxidase. *Biochemistry* **2011**, *50*, 5096–5107. [[CrossRef](#)] [[PubMed](#)]
35. Liers, C.; Bobeth, C.; Pecyna, M.; Ullrich, R.; Hofrichter, M. Dyp-like Peroxidases of the Jelly Fungus *Auricularia Auricula-Judae* Oxidize Nonphenolic Lignin Model Compounds and High-Redox Potential Dyes. *Appl. Microbiol. Biotechnol.* **2010**, *85*, 1869–1879. [[CrossRef](#)]
36. Min, K.; Gong, G.; Woo, H.M.; Kim, Y.; Um, Y. A Dye-Decolorizing Peroxidase from *Bacillus Subtilis* Exhibiting Substrate-Dependent Optimum Temperature for Dyes and β -Ether Lignin Dimer. *Sci. Rep.* **2015**, *5*, 8245. [[CrossRef](#)] [[PubMed](#)]
37. Fawal, N.; Li, Q.; Savelli, B.; Brette, M.; Passaia, G.; Fabre, M.; Mathé, C.; Dunand, C. PeroxiBase: A Database for Large-Scale Evolutionary Analysis of Peroxidases. *Nucleic Acids Res.* **2013**, *41*, 441–444. [[CrossRef](#)] [[PubMed](#)]
38. Yoshida, T.; Sugano, Y. A Structural and Functional Perspective of Dyp-Type Peroxidase Family. *Arch. Biochem. Biophys.* **2015**, *574*, 49–55. [[CrossRef](#)]
39. Colpa, D.I.; Fraaije, M.W.; Bloois, E. Van. Dyp-Type Peroxidases: A Promising and Versatile Class of Enzymes. *J. Ind. Microbiol. Biotechnol.* **2014**, *41*, 1–7. [[CrossRef](#)]
40. Salvachúa, D.; Prieto, A.; Martínez, Á.T.; Martínez, M.J. Enzyme from *Irpex Lacteus* and Its Application in Enzymatic Hydrolysis of Wheat Straw. *Appl. Environ. Microbiol.* **2013**, *79*, 4316–4324. [[CrossRef](#)]
41. Roberts, J.N.; Singh, R.; Grigg, J.C.; Murphy, M.E.P.; Bugg, T.D.H.; Eltis, L.D. Characterization of Dye-Decolorizing Peroxidases from *Rhodococcus Jostii* RHA1. *Biochemistry* **2011**, *50*, 5108–5119. [[CrossRef](#)] [[PubMed](#)]
42. Van Bloois, E.; Pazmiño, D.E.T.; Winter, R.T.; Fraaije, M.W. A Robust and Extracellular Heme-Containing Peroxidase from *Thermobifida Fusca* as Prototype of a Bacterial Peroxidase Superfamily. *Appl. Microbiol. Biotechnol.* **2010**, *86*, 1419–1430. [[CrossRef](#)] [[PubMed](#)]
43. Rahmanpour, R.; Bugg, T.D.H. Characterisation of Dyp-Type Peroxidases from *Pseudomonas Fluorescens* Pf-5: Oxidation of Mn(II) and Polymeric Lignin by Dyp1B. *Arch. Biochem. Biophys.* **2015**, *574*, 93–98. [[CrossRef](#)] [[PubMed](#)]
44. Bentley, S.D.; Chater, K.F.; Cerdeño-Tárraga, A.M.; Challis, G.L.; Thomson, N.R.; James, K.D.; Harris, D.E.; Quail, M.A.; Kieser, H.; Harper, D.; et al. Complete Genome Sequence of the Model Actinomycete *Streptomyces Coelicolor* A3(2). *Nature* **2002**, *417*, 141–147. [[CrossRef](#)] [[PubMed](#)]
45. Teder, T.; Löhelaïd, H.; Samel, N. Structural and Functional Insights into the Reaction Specificity of Catalase-Related Hydroperoxide Lyase: A Shift from Lyase Activity to Allene Oxide Synthase by Site-Directed Mutagenesis. *PLoS ONE* **2017**, *12*, e0185291. [[CrossRef](#)]
46. Breslmayr, E.; Hanžek, M.; Hanrahan, A.; Leitner, C.; Kittl, R.; Šantek, B.; Oostenbrink, C.; Ludwig, R. A Fast and Sensitive Activity Assay for Lytic Polysaccharide Monooxygenase. *Biotechnol. Biofuels* **2018**, *11*, 79. [[CrossRef](#)]
47. Ollinger, J.; Song, K.B.; Antelmann, H.; Hecker, M.; Helmman, J.D. Role of the Fur Regulon in Iron Transport in *Bacillus Subtilis*. *J. Bacteriol.* **2006**, *188*, 3664–3673. [[CrossRef](#)] [[PubMed](#)]
48. Biswas, L.; Biswas, R.; Nerz, C.; Ohlsen, K.; Schlag, M.; Schäfer, T.; Lamkemeyer, T.; Ziebandt, A.K.; Hantke, K.; Rosenstein, R.; et al. Role of the Twin-Arginine Translocation Pathway in *Staphylococcus*. *J. Bacteriol.* **2009**, *191*, 5921–5929. [[CrossRef](#)]
49. Létoffé, S.; Heuck, G.; Delepelaire, P.; Lange, N.; Wandersman, C. Bacteria Capture Iron from Heme by Keeping Tetrapyrrole Skeleton Intact. *Proc. Natl. Acad. Sci. USA* **2009**, *106*, 11719–11724. [[CrossRef](#)]
50. Zitare, U.A.; Habib, M.H.; Rozeboom, H.; Mascotti, M.L.; Todorovic, S.; Fraaije, M.W. Mutational and Structural Analysis of an Ancestral Fungal Dye-Decolorizing Peroxidase. *FEBS J.* **2021**, *288*, 3602–3618. [[CrossRef](#)]
51. Jeong, H.; Barbe, V.; Lee, C.H.; Vallenet, D.; Yu, D.S.; Choi, S.H.; Couloux, A.; Lee, S.W.; Yoon, S.H.; Cattolico, L.; et al. Genome Sequences of *Escherichia Coli* B Strains REL606 and BL21(DE3). *J. Mol. Biol.* **2009**, *394*, 644–652. [[CrossRef](#)] [[PubMed](#)]
52. Rosano, G.L.; Ceccarelli, E.A. Recombinant Protein Expression in *Escherichia Coli*: Advances and Challenges. *Front. Microbiol.* **2014**, *5*, 172. [[CrossRef](#)] [[PubMed](#)]
53. Rosano, G.L.; Morales, E.S.; Ceccarelli, E.A. New Tools for Recombinant Protein Production in *Escherichia Coli*: A 5-Year Update. *Protein Sci.* **2019**, *28*, 1412–1422. [[CrossRef](#)] [[PubMed](#)]
54. Lithwick, G.; Margalit, H. Hierarchy of Sequence-Dependent Features Associated with Prokaryotic Translation. *Genome Res.* **2003**, *13*, 2665–2673. [[CrossRef](#)] [[PubMed](#)]
55. Gustafsson, C.; Govindarajan, S.; Minshull, J. Codon Bias and Heterologous Protein Expression. *Trends Biotechnol.* **2004**, *22*, 346–353. [[CrossRef](#)]

56. Al-Hawash, A.B.; Zhang, X.; Ma, F. Strategies of Codon Optimization for High-Level Heterologous Protein Expression in Microbial Expression Systems. *Gene Rep.* **2017**, *9*, 46–53. [[CrossRef](#)]
57. Johansson, A.S.; Bolton-Grob, R.; Mannervik, B. Use of Silent Mutations in CDNA Encoding Human Glutathione Transferase M2-2 for Optimized Expression in Escherichia Coli. *Protein Expr. Purif.* **1999**, *17*, 105–112. [[CrossRef](#)]
58. Jung, Y.; Kwak, J.; Lee, Y. High-Level Production of Heme-Containing Holoproteins in Escherichia Coli. *Appl. Microbiol. Biotechnol.* **2001**, *55*, 187–191. [[CrossRef](#)]
59. Chouchane, S.; Lippai, I.; Magliozzo, R.S. Catalase-Peroxidase (Mycobacterium Tuberculosis KatG) Catalysis and Isoniazid Activation. *Biochemistry* **2000**, *39*, 9975–9983. [[CrossRef](#)]
60. Sudhamsu, J.; Kabir, M.; Airola, M.V.; Patel, B.A.; Yeh, S.R.; Rousseau, D.L.; Crane, B.R. Co-Expression of Ferrochelatase Allows for Complete Heme Incorporation into Recombinant Proteins Produced in E. Coli. *Protein Expr. Purif.* **2010**, *73*, 78–82. [[CrossRef](#)]
61. Varnado, C.L.; Goodwin, D.C. System for the Expression of Recombinant Hemoproteins in Escherichia Coli. *Protein Expr. Purif.* **2004**, *35*, 76–83. [[CrossRef](#)] [[PubMed](#)]
62. Sugano, Y.; Nakano, R.; Sasaki, K.; Shoda, M. Efficient Heterologous Expression in Aspergillus Oryzae of a Unique Dye-Decolorizing Peroxidase, DyP, of Geotrichum Candidum Dec 1. *Appl. Environ. Microbiol.* **2000**, *66*, 1754–1758. [[CrossRef](#)] [[PubMed](#)]
63. Sugawara, K.; Yoshida, T.; Hirashima, R.; Toriumi, R.; Akiyama, H.; Kakuta, Y.; Ishige, Y.; Sugano, Y. Characterization of Class V DyP-Type Peroxidase SaDyP1 from Streptomyces Avermitilis and Evaluation of SaDyPs Expression in Mycelium. *Int. J. Mol. Sci.* **2021**, *22*, 8683. [[CrossRef](#)] [[PubMed](#)]
64. Linde, D.; Ayuso-Fernández, I.; Laloux, M.; Aguiar-Cervera, J.E.; de Lacey, A.L.; Ruiz-Dueñas, F.J.; Martínez, A.T. Comparing Ligninolytic Capabilities of Bacterial and Fungal Dye-Decolorizing Peroxidases and Class-Ii Peroxidase-Catalases. *Int. J. Mol. Sci.* **2021**, *22*, 2629. [[CrossRef](#)]
65. Rodrigues, C.F.; Borges, P.T.; Scocozza, M.F.; Silva, D.; Taborda, A.; Brissos, V.; Frazão, C.; Martins, L.O. Loops around the Heme Pocket Have a Critical Role in the Function and Stability of Bsdyp from Bacillus Subtilis. *Int. J. Mol. Sci.* **2021**, *22*, 10862. [[CrossRef](#)]
66. Chaplin, A.K.; Wilson, M.T.; Worrall, J.A.R. Kinetic Characterisation of a Dye Decolourising Peroxidase from Streptomyces Lividans: New Insight into the Mechanism of Anthraquinone Dye Decolourisation. *Dalt. Trans.* **2017**, *46*, 9420–9429. [[CrossRef](#)]
67. Liu, Y.; Huang, L.; Guo, W.; Jia, L.; Fu, Y.; Gui, S.; Lu, F. Cloning, Expression, and Characterization of a Thermostable and PH-Stable Laccase from Klebsiella Pneumoniae and Its Application to Dye Decolorization. *Process Biochem.* **2017**, *53*, 125–134. [[CrossRef](#)]
68. Arregui, L.; Ayala, M.; Gómez-Gil, X.; Gutiérrez-Soto, G.; Hernández-Luna, C.E.; Herrera De Los Santos, M.; Levin, L.; Rojo-Domínguez, A.; Romero-Martínez, D.; Saparrat, M.C.N.; et al. Laccases: Structure, Function, and Potential Application in Water Bioremediation. *Microb. Cell Fact.* **2019**, *18*, 200. [[CrossRef](#)]
69. Chen, C.; Shrestha, R.; Jia, K.; Gao, P.F.; Geisbrecht, B.V.; Bossmann, S.H.; Shi, J.; Li, P. Characterization of Dye-Decolorizing Peroxidase (DyP) from Thermomonospora Curvata Reveals Unique Catalytic Properties of A-Type DyPs. *J. Biol. Chem.* **2015**, *290*, 23447–23463. [[CrossRef](#)]
70. Kokkonen, P.; Beier, A.; Mazurenko, S.; Damborsky, J.; Bednar, D.; Prokop, Z. Substrate Inhibition by the Blockage of Product Release and Its Control by Tunnel Engineering. *RSC Chem. Biol.* **2021**, *2*, 645–655. [[CrossRef](#)]
71. Benslama, O.; Mansouri, N.; Arhab, R. In Silico Investigation of the Lignin Polymer Biodegradation by Two Actinomycetal Peroxidase Enzymes. *Mater. Today Proc.* **2022**, *53*, 1–5. [[CrossRef](#)]
72. Gilbert, R.G.; Hess, M.; Jenkins, A.D.; Jones, R.G.; Kratochvil, P.; Stepto, R.F.T. Dispersity in Polymer Science (IUPAC Recommendations 2009). *Pure Appl. Chem.* **2009**, *81*, 351–353.
73. Kim, K.H.; Kim, C.S. Recent Efforts to Prevent Undesirable Reactions from Fractionation to Depolymerization of Lignin: Toward Maximizing the Value from Lignin. *Front. Energy Res.* **2018**, *6*, 92. [[CrossRef](#)]
74. Vignali, E.; Gigli, M.; Cailotto, S.; Pollegioni, L.; Rosini, E.; Crestini, C. The Laccase-Lig Multienzymatic Multistep System in Lignin Valorization. *ChemSusChem* **2022**, *15*, e202201147. [[CrossRef](#)]
75. Rahmanpour, R.; King, L.D.W.; Bugg, T.D.H. Identification of an Extracellular Bacterial Flavoenzyme That Can Prevent Re-Polymerisation of Lignin Fragments. *Biochem. Biophys. Res. Commun.* **2017**, *482*, 57–61. [[CrossRef](#)]
76. Musengi, A.; Durrell, K.; Prins, A.; Khan, N.; Agunbiade, M.; Kudanga, T.; Kirby-McCullough, B.; Pletschke, B.I.; Burton, S.G.; Le Roes-Hill, M. Production and Characterisation of a Novel Actinobacterial DyP-Type Peroxidase and Its Application in Coupling of Phenolic Monomers. *Enzyme Microb. Technol.* **2020**, *141*, 109654. [[CrossRef](#)]

Disclaimer/Publisher's Note: The statements, opinions and data contained in all publications are solely those of the individual author(s) and contributor(s) and not of MDPI and/or the editor(s). MDPI and/or the editor(s) disclaim responsibility for any injury to people or property resulting from any ideas, methods, instructions or products referred to in the content.

Supplementary Materials

Supplementary Materials and Methods

Gene cloning

Transformation

The recombinant plasmids containing dye-decolorizing peroxidase (DyP) genes were transformed by electroporation into One Shot *E. coli* TOP10 competent cells (ThermoFisher Scientific, USA). The transformed cells were selected on an LB-agar plate containing appropriate antibiotics (37 °C overnight). The recombinant plasmids were transformed into *E. coli* BL21(DE3) strain by electroporation, and the transformed cells were grown in LB supplemented with the appropriate antibiotics at 37 °C overnight. Colonies containing the plasmid were confirmed by restriction digestion with NdeI and Xho and by Sanger sequencing (University of Tartu, Institute of Genomics, Estonia).

Enzyme Assays

Optimal pH

The optimal pH for 2,2'-azino-bis(3-ethylbenzothiazoline-6-sulfonic acid (ABTS) and 2,6-dimethoxyphenol (2,6-DMP) oxidation was determined for each DyP from *Streptomyces coelicolor* (ScDyP) using 1 mM ABTS for ScDyP1A and ScDyP2A, 0.1 mM ABTS for ScDyPB, and sodium citrate (50 mM, pH 2.5–3.5), sodium acetate (50 mM, pH 4.0–5.0), HEPES (50 mM, pH 7.0–8.0), Tris-HCl (50 mM, pH 8.5), and glycine (50 mM, pH 9.0–9.5) buffers. 2 mM 2,6-DMP, 1 mM H₂O₂, 500 nM ScDyP2A, and 100 nM ScDyPB were used for 2,6-DMP oxidation.

Temperature Dependence & Thermostability

Substrates were added to sodium citrate buffer (50 mM, pH 3.5) that was adjusted to a desired temperature and the reaction was started by the addition of the enzyme. The final concentrations of enzymes and substrates in each of the reaction mixtures were as follows: 100 nM ScDyP1A (1 mM ABTS), 50 nM ScDyP2A (1 mM ABTS), 15 nM ScDyPB (0.1 mM ABTS), and 1 mM H₂O₂. For assessing the stability of DyPs, the enzymes were pre-incubated in Tris-HCl (20 mM, pH 7.5), 100 mM NaCl buffer at 30 °C. At selected times, aliquots were drawn and the ABTS oxidizing activity was measured using the concentration of the reagents outlined above. Concentrations of the enzymes in pre-incubation were 10 μM, 5 μM, and 1.5 μM for ScDyP1A, ScDyP2A, and, ScDyPB, respectively.

Enzyme Kinetics

100 nM ScDyP1A (0.1–5 mM ABTS), 50 nM ScDyP2A (0.1–5 mM ABTS), 15 nM ScDyPB (0.01–0.5 mM ABTS), 1 mM H₂O₂, sodium citrate buffer (50 mM, pH 3.5) were used for determining the apparent kinetic constants with ABTS. 500 nM ScDyP2A (0–10 mM 2,6-DMP) and 100 nM ScDyPB (0–10 mM 2,6-DMP), 1 mM H₂O₂, Tris-HCl buffer (50 mM, pH 8.5) were utilized for enzyme kinetics with 2,6-DMP. The observed rates were plotted against substrate concentrations and V_{max} , K_M , and K_i values were found using non-linear regression according to equation 1.

$$\frac{v}{E_0} = \frac{k_{cat}^{app} [S]}{K_M^{app} + [S] + \frac{[S]^2}{K_i^{app}}} \quad (\text{Eq. 1})$$

The curve fit and data analysis were carried out using OriginPro 2021 software.

Enzymatic Treatment of Organosolv Lignin

Gel Permeation Chromatography

Gel permeation chromatography (GPC) was used to follow changes in the molecular weight distribution of lignins. Prior to the GPC analysis, the samples were dissolved in tetrahydrofuran (THF). GPC analysis was carried out with a Prominence LC-20A Modular HPLC System (Shimadzu, Japan) equipped with a photodiode array detector. A GPC/SEC Guard Column (50 x 7.5 mm, Agilent Technologies, USA) and two Organic GPC/SEC PLgel MesoPore columns connected in tandem (300 mm x 7.5 mm, inner diameter, 3 µm, Agilent Technologies) were calibrated using the EasiVial PS-L polystyrene standards for GPC/SEC (Agilent Technologies). The following conditions were used – mobile phase: THF stabilized with 250 ppm butylated hydroxytoluene in isocratic mode; flowrate: 1 mL/min; column oven temperature: 40 °C and UV detection: 254 nm. Each analysis was performed in triplicate. The number average molecular weight (Mn), weight average molecular weight (Mw), and the molar-mass dispersity (Đ_M) were determined with GPC post-run software (Shimadzu). Statistical significance was determined by analysis of variance (ANOVA), which was established at p ≤ 0.05.

Gas Chromatography-Mass Spectrometry

To analyze low molecular weight compounds (LMW) in Mxg- and aspen lignins treated with ScDyPs, and without enzymatic treatment, gas chromatography-mass spectrometry (GC-MS) was used. The reactions were centrifuged, and the supernatant was extracted with ethyl acetate, lyophilized, and dissolved in methanol. 1 µL of the sample was injected in splitless mode at 250 °C to a 7890A gas chromatograph coupled to a 5975C mass spectrometer (Agilent Technologies) with an electron ionization source and a quadrupole mass analyzer. The flow rate of carrier gas (helium, 6.0 purity) was kept constant at 1.3 mL/min. LMW compounds in lignin were separated in a ZB-5plus capillary column (30 m x 0.25 mm x 0.25 µm, Agilent Technologies). The following oven temperature program was used: the initial temperature was 35 °C (1 min), then increased to 300 °C (10 °C min⁻¹, held for 2 min). The total run time was 29.5 min. The analyte ionization was performed in electron ionization mode using the electron energy of 70 eV. The interface, ion source, and mass analyzer temperatures were set at 280, 230, and 150 °C, respectively. Scan mode in the range of 30–500 m/z was used for monitoring all analytes. LMW compounds of lignin were determined by the National Institute of Standards and Technology 17 (NIST 17) library. Agilent MassHunter Qualitative Analysis was used for data analysis. The fragment (m/z) with the highest intensity characteristic for each compound was used for quantification.

Table S1. Oligonucleotide primers used for gene amplification.

	forward	reverse
SCO2276 (ScDyP1A)	5'-GAC CGC GCC GGT GCC CAT ATG GAC CCG GCC GGT GCC-3'	5'-GAT CAG GTA GCT CGA GAA CAC CGT TAC GCC TCC TTG-3'
SCO3963 (ScDyP2A)	5'-CGC AGC CGC CCC CTC GCA TAT GGC GAC CCC CCT CAC-3'	5'-CCG CGG GGT GAT ACG CCC CTC GAG TCA CCC CTC CAG-3'
SCO7193 (ScDyPB)	5'-GGA GGA TGT TCG CAT ATG GGC GGA GAA GTC-3'	5'-CGG GTC GGG TCG CTC GAG GCT CAG GGC CGA G-3'

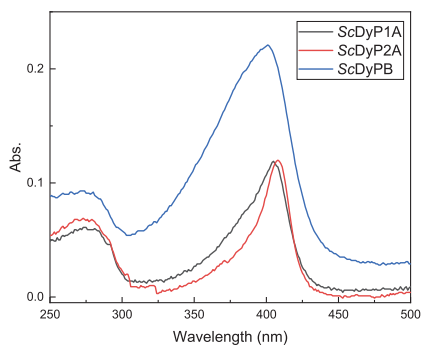


Figure S1. Spectra of ScDyPs. The enzymes were diluted in Tris-HCl (20 mM, pH 7.5), 100 mM NaCl buffer, and the spectrum of each ScDyP was recorded (250–500 nm). ScDyP1A showed the Soret band maximum at 408 nm, ScDyP2A at 405 nm, and ScDyPB at 401 nm.

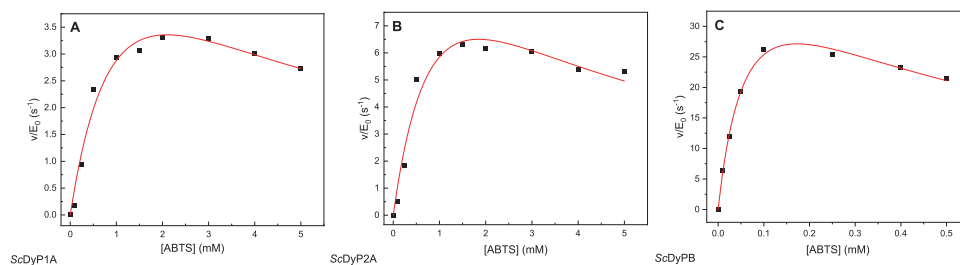


Figure S2. Steady-state kinetics of ScDyPs against ABTS as a substrate: ScDyP1A (panel A), ScDyP2A (panel B), and ScDyPB (panel C). Experiments were performed using sodium citrate (50 mM, pH 3.5) buffer and 1 mM H₂O₂ as a co-substrate. In red, fitted curves are shown employing the substrate inhibition equation (Eq 1).

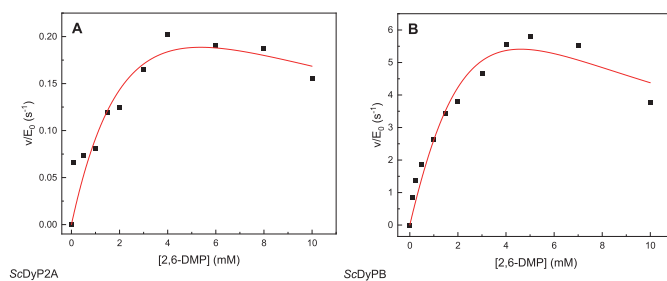


Figure S3. Steady-state kinetics of *ScDyP2A* and *ScDyPB* against 2,6-DMP: *ScDyP2A* (panel A), *ScDyPB* (panel B). Experiments were performed using Tris-HCl (50 mM, pH 8.5) buffer and 1 mM H_2O_2 as a co-substrate. In red, fitted curves are shown employing substrate inhibition equation (Eq 1).

Appendix 2

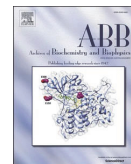
Publication II

Pupart, H.; Lukk, T.; Väljamäe, P. Dye-decolorizing peroxidase of *Thermobifida halotolerance* displays complex kinetics with both substrate inhibition and apparent positive cooperativity. *Arch Biochem Biophys* **2024**, *754*, 109931. <https://doi.org/10.1016/j.abb.2024.109931>.



Contents lists available at ScienceDirect

Archives of Biochemistry and Biophysics

journal homepage: www.elsevier.com/locate/yabbi

Dye-decolorizing peroxidase of *Thermobifida halotolerance* displays complex kinetics with both substrate inhibition and apparent positive cooperativity

Hegne Pupart^a, Tiit Lukk^a, Priit Väljamäe^{b,*}

^a Department of Chemistry and Biotechnology, Tallinn University of Technology, Akadeemia tee 15, 12618, Tallinn, Estonia

^b Institute of Molecular and Cell Biology, University of Tartu, Rõita 23b-202, 51010, Tartu, Estonia

ARTICLE INFO

Keywords:

Peroxidase
Cooperativity
Substrate inhibition
Hydrogen peroxide
Inactivation

ABSTRACT

Dye-decolorizing peroxidases (DyPs) have been intensively investigated for the purpose of industrial dye decolorization and lignin degradation. Unfortunately, the characterization of these peroxidases is hampered by their non-Michaelis-Menten kinetics, exemplified by substrate inhibition and/or positive cooperativity. Although often observed, the underlying mechanisms behind the unusual kinetics of DyPs are poorly understood. Here we studied the kinetics of the oxidation of 2,2'-azino-bis(3-ethylbenzothiazoline-6-sulfonic acid) (ABTS), hydroquinones, and anthraquinone dyes by DyP from the bacterium *Thermobifida halotolerans* (*ThDyP*) and solved its crystal structure. We also provide rate equations for different kinetic mechanisms explaining the complex kinetics of heme peroxidases. Kinetic studies along with the analysis of the structure of *ThDyP* suggest that the substrate inhibition is caused by the non-productive binding of ABTS to the enzyme resting state. Strong irreversible inactivation of *ThDyP* by H₂O₂ in the absence of ABTS suggests that the substrate inhibition by H₂O₂ may be caused by the non-productive binding of H₂O₂ to compound I. Positive cooperativity was observed only with the oxidation of ABTS but not with the two electron-donating substrates. Although the conventional mechanism of cooperativity cannot be excluded, we propose that the oxidation of ABTS assumes the simultaneous binding of two ABTS molecules to reduce compound I to the enzyme resting state, and this causes the apparent positive cooperativity.

1. Introduction

Dye-decolorizing peroxidases (DyPs, EC 1.11.1.19) are heme-dependent peroxidases that catalyze the oxidation of various compounds, such as anthraquinones, azo dyes, and lignin-related compounds using H₂O₂ as a co-substrate [1–5]. However, their native substrates as well as biological functions are yet to be identified [6]. DyPs are found in bacterial and fungal species and based on primary sequence and structural topology are divided into four subfamilies (A–D) [3,7–9]. DyPs are ferredoxin like proteins with a size ranging from monomers to hexamers [2,10–14]. The monomer of a DyP consists of two similar domains, both containing antiparallel β -sheets and peripheral α -helices connected by surrounding loop regions. The heme cofactor rests in the C-terminal domain [5,10,14,15]. H₂O₂ co-substrate and smaller reducing substrates can directly enter the heme pocket through an access channel [16,17]. Bulky substrates cannot access the heme and are oxidized on the enzyme surface through long-range electron transfer [18–22]. Long-range electron transfer pathways involve

surface-exposed aromatic amino acid residues like Trp and Tyr [23]. The existence of surface binding sites has been demonstrated for several DyPs [18,19,21].

DyPs obey ping-pong mechanism where the enzyme bounces back and forth between its resting state and reactive intermediates, compound I (Cpd I; [Fe⁴⁺=O Por⁺]) and compound II (Cpd II; [Fe⁴⁺=O] Por) [24–26]. Catalysis is initiated by the oxidation of resting state heme by H₂O₂ leading to the formation of Cpd I. Cpd I is reduced back to the resting state by two electron transfer from the reducing substrate [24, 27]. When delivered sequentially, the first electron transfer reduces Cpd I to Cpd II while the second electron transfer reduces Cpd II to the resting state. In some DyPs the Cpd II is not observed leading to the hypothesis that Cpd I is directly reduced to the resting-state through simultaneous two electron transfer [26]. It has proposed that propensity of sequential one-electron- or a direct two-electron reduction is determined by the hydration of the heme [26,28,29]. In the case of so-called dry heme (without water molecules in the distal heme pocket), the Cpd I is more susceptible to direct two-electron reduction whereas wet heme (with

* Corresponding author.

E-mail addresses: hegne.pupart@taltech.ee (H. Pupart), tiit.lukk@taltech.ee (T. Lukk), priit.valjamae@ut.ee (P. Väljamäe).

<https://doi.org/10.1016/j.abbi.2024.109931>

Received 27 November 2023; Received in revised form 15 February 2024; Accepted 16 February 2024

Available online 19 February 2024

0003-9861/© 2024 The Authors. Published by Elsevier Inc. This is an open access article under the CC BY license (<http://creativecommons.org/licenses/by/4.0/>).

water molecules in the distal heme pocket) is reduced by two sequential single-electron transfer steps [26,29,30].

Although of great biotechnological interest [4–6,31,32], the interpretation of the kinetic data of DyPs is hampered by their complex, non-Michaelis-Menten kinetics. The most often observed deviation from Michaelis-Menten kinetics occurs with substrate inhibition [3,17,33–38] by reducing substrate [3,17,34,38], by H₂O₂ [33,35,36], or by both [3]. Many peroxidases are also irreversibly inactivated by H₂O₂ [39,40]. Inactivation is often initiated by the binding of H₂O₂ to Cpd I [39–43] followed by different possible pathways that may lead to the bleaching of heme [40,43–45] or damage of enzyme protein [46,47]. Such a suicide inactivation can be relieved by the presence of reducing substrate that competes with H₂O₂ for reacting with Cpd I and/or Cpd II [45,48]. In the case of some peroxidases, the inactivation by H₂O₂ is relieved by their catalase activity [39,42,49]. An apparent positive cooperativity has also been reported for DyPs [3,19,50,51]. Positive cooperativity is a phenomenon that is usually associated with multimeric enzymes or monomeric enzymes with more than one active site. Many DyPs are multimeric enzymes with some of them showing positive cooperativity [19,50] while others are not [52–54]. Furthermore, there are also monomeric DyPs showing positive cooperativity [3]. Although of importance, our knowledge about the mechanisms underlying the non-conventional kinetics of DyP peroxidases is limited and studies addressing these issues are scarce.

Here, we studied the kinetics of an A-type DyP from a bacterium *Thermobifida halotolerans* (*ThDyP*) and solved its crystal structure. *ThDyP* showed complex kinetics with substrate inhibition by both H₂O₂ and reducing substrate, and positive cooperativity with single-electron donating substrate, ABTS (2,2'-azino-bis(3-ethylbenzothiazoline-6-sulfonic acid)). Although dimeric structure of *ThDyP* allows for conventional explanation of cooperativity, we propose a simple kinetic mechanism whereby non-productive complexes with H₂O₂ and reducing substrate are responsible for the substrate inhibition, and productive complex with two single-electron donating substrate is responsible for an apparent positive cooperativity.

2. Materials & methods

2.1. Materials

All reagents and substrates were purchased from Sigma-Aldrich with some exceptions: hemin from porcine (Acros Organics), 30 % (w/w) hydrogen peroxide solution (Honeywell), Chelex 100 Chelating Resin (50–100 mesh, sodium form) (Bio-Rad). Double deionized ultrapure (type 1) water was further purified by passing it through a column filled with Chelex 100 resin.

2.2. Protein overexpression

Codon-optimized gene encoding the dye-decolorizing peroxidase (DyP) from *Thermobifida halotolerans* (accession number: WP_068693896) was cloned into pET28a expression vector, carrying Kan resistance cassette, N-terminal His₆-tag, and an N-terminal thrombin cleavage site (Twist Bioscience). The recombinant *ThDyP* missing the N-terminal 40-amino acid twin-arginine translocation (Tat) signal was overproduced in *E. coli* BL21(DE3). The culture media (LB prepared in tap water) supplemented with Kan was incubated at 37 °C until the OD₆₀₀ reached 0.6–0.8. The recombinant protein overexpression was induced by adding isopropyl β-D-1-thiogalactopyranoside (to 0.8 mM). The culture was grown overnight at 30 °C, 180 rpm. The cells and debris were harvested by centrifugation at 4000 g for 15 min at 4 °C.

2.3. Protein purification

The harvested cells were re-suspended in buffer A (20 mM Tris-HCl, 0.5 M NaCl, 5 mM imidazole, pH 7.5), lysed using a high-pressure

homogenization (Avestin EmulsiFlex-C5), and centrifuged at 35,000 g for 1 h at 4 °C. HisTrap FF column (GE Healthcare) was equilibrated with buffer A and the lysate was loaded. The column was washed with 10 column volumes (CV) of 10% buffer B (20 mM Tris-HCl, 0.5 M NaCl, 0.5 M imidazole, pH 7.5). The His₆-tagged protein was eluted by applying a linear imidazole gradient of 10–100% of buffer B (20 CV), and the fractions were analyzed with SDS-PAGE. The fractions containing the protein of interest were pooled, and His₆-tag was cleaved by overnight incubation with thrombin (2 U per 1 mg protein) at 4 °C. The buffer was exchanged for Tris-HCl (20 mM, pH 7.5) using HiPrep 26/10 desalting column (GE Healthcare). For reconstitution with heme, the enzyme was incubated with a twofold molar excess of hemin (using 20 mg/mL stock solution in DMSO) at room temperature for 2 h. The excess heme was removed by exchanging the buffer for Tris-HCl (20 mM, pH 7.5) on HiPrep 26/10 desalting column. All purification steps were performed using ÄKTA pure system (GE Healthcare). Finally, the heme reconstituted *ThDyP* was concentrated (using centrifugal filters with a molecular weight cutoff of 10 kDa, Sartorius), frozen in liquid nitrogen and stored at –80 °C. 1 L expression yielded approximately 65 mg of *ThDyP*.

2.4. Determination of enzyme concentration

The absorbance at 280 nm and 406 nm were measured (Shimadzu UV-2700 UV-Vis spectrophotometer) before and after the reconstitution with heme to determine the total protein and heme concentrations, respectively. The Reinheitszahl values (Rz, A₄₀₆/A₂₈₀) of *ThDyP* were 1.06 and 1.63 before and after reconstitution with heme, respectively. The extinction coefficient of *ThDyP* at 280 nm (45,950 M⁻¹cm⁻¹) was calculated using the Expsy ProtParam tool and ε_{406nm} = 100,000 M⁻¹cm⁻¹ was used for the absorption of heme. The heme-based concentration of *ThDyP* was used in all experiments of enzyme kinetics.

2.5. Crystallization, data collection, structure determination, and refinement

Sitting-drop vapor diffusion crystallization screens were set up on 96-well plates (Intelliplate Rigaku) with a Crystal Gryphon crystallization robot (Art Robbins Instruments). Droplets containing 0.5 μL of 15 mg/mL *ThDyP* in Tris-HCl (20 mM, pH 7.5) and 0.5 μL of mother liquor solution from PACT Premier, Structure Screen, and JCSG + screens (Molecular Dimensions) were mixed and equilibrated against 40 μL of reservoir solution in vibration free crystallization incubators (Molecular Dimensions) at 9 and 20 °C.

Crystals were obtained from PACT premier G5 condition (0.2 M sodium nitrate, 0.1 M Bis-Tris propane, pH 7.5, 20% (w/v) PEG3350) at 9 °C. A crystal was soaked in a cryo-protectant solution, containing the corresponding crystallization solution supplemented with 20% (v/v) glycerol prior to vitrification in liquid nitrogen. The X-ray diffraction data were collected at 100 K at the BL13-XALOC beamline equipped with a PILATUS 6 M detector at the ALBA synchrotron light source (Barcelona, Spain) [55].

The crystal structure of *ThDyP* was solved by molecular replacement using MOLREP [56] in the CCP4 program suite [57], utilizing the coordinates of DyP from *Thermobifida cellulositytica* (PDB 4GS1) as the search model. The diffraction images were analyzed and integrated with IMOSflm [58] and scaled with AIMLESS [59]. Initial model refinement was performed with REFMAC5 [60]. Iterative model building and refinement was carried out with COOT [61] and phenix.refine [62]. Figures of structures were generated with UCSF Chimera molecular graphics system [63]. Structure factors and associated structure coordinates of *ThDyP* were deposited in the Protein Data Bank with PDB code 8CK9. CASTp analysis [64] and CAVER [65] plugin for PyMOL were used for identifying putative substrate channels in *ThDyP* monomer. For CAVER calculations, the heme iron was set as the starting point. PISA server was utilized to assess the macromolecular interfaces [66].

2.6. Oligomerization analysis of *ThDyP*

The oligomerization state of *ThDyP* was estimated by gel filtration chromatography on a Superdex 75 Increase 10/300 GL column (GE Healthcare) equilibrated with sodium acetate (50 mM, pH 5.0) buffer. *ThDyP* (22 mg/mL in 20 mM, pH 7.5) was diluted 2x with sodium acetate (100 mM, pH 5.0), incubated for 30 min at room temperature, and centrifuged. 100 μ L of the supernatant was injected into the column and eluted with 50 mM sodium acetate pH 5.0 at a flow rate of 0.5 mL/min. High molecular weight Gel Filtration Calibration Kit (Cytiva) containing ovalbumin (43 kDa), conalbumin (75 kDa), aldolase (158 kDa), and ferritin (440 kDa) were dissolved in PBS buffer (pH 7.2) and used for obtaining the calibration curve.

2.7. Enzyme assays

All enzyme assays were performed with a Shimadzu UV-1900i UV-Vis spectrophotometer at 25 °C. The concentration of H₂O₂ was determined spectrophotometrically at 240 nm using an extinction coefficient of 39.4 M⁻¹ cm⁻¹ [67]. Sodium acetate (50 mM, pH 5.0) buffer supplemented with 0.1 g L⁻¹ bovine serum albumin (BSA) was used for making *ThDyP* working stocks. Before the activity measurements, the working stocks of *ThDyP* were incubated at 25 °C for 30 min. All reactions were made in 50 mM sodium acetate (pH 5.0, supplemented with 0.1 g L⁻¹ BSA) at 25 °C in 1 mL total volume. Reducing substrate and H₂O₂ were mixed in the cuvette and the reactions were started by the adding of *ThDyP* working stock. ABTS, methylhydroquinone (MHQ), 2,6-dimethoxyhydroxyquinone (DMHQ), reactive blue 4 (RB4), and reactive blue 19 (RB19) were used as reducing substrates, and their oxidation was followed by the absorbance using following molar extinction coefficients, ϵ_{420} ABTS = 36,000 M⁻¹ cm⁻¹, ϵ_{251} MHQ = 21,450 M⁻¹ cm⁻¹ [68] ϵ_{292} DMHQ = 13,680 M⁻¹ cm⁻¹ [68], ϵ_{610} RB4 = 4200 M⁻¹ cm⁻¹ [5], ϵ_{595} , RB19 = 10,000 M⁻¹ cm⁻¹ [51]. The concentration of *ThDyP* was 10 nM in the experiments with ABTS and 100 nM in the experiments with other reducing substrates. The non-enzymatic oxidation of substrates was tested by performing the measurements in the absence of enzyme. All measurements were made at least in duplicate. The data were analyzed using STATISTICA 8.

2.8. Inactivation of *ThDyP*

For the time dependency of inactivation 0.9 μ M *ThDyP* was pre-incubated with H₂O₂ (0.1–50 μ M) or ABTS (10–1000 μ M) in sodium acetate (50 mM, pH 5.0, supplemented with 0.1 g L⁻¹ BSA) at 25 °C for selected time. After pre-incubation the residual ABTS oxidizing activity of *ThDyP* was measured using 1 mM ABTS, 1 mM H₂O₂, and 9 nM total *ThDyP*. Before the addition of H₂O₂/ABTS, 1.0 μ M *ThDyP* was incubated in sodium acetate (50 mM, pH 5.0, supplemented with 0.1 g L⁻¹ BSA) at 25 °C for 30 min. After that, an aliquot was withdrawn for measurement of zero-time pre-incubation activity.

For the end-point inactivation 1.0 μ M *ThDyP* was pre-incubated with H₂O₂ for 1 h or ABTS for 24 h, before measuring the residual ABTS oxidizing activity (1 mM ABTS, 1 mM H₂O₂, and 9 nM total *ThDyP*).

For the oxidation of ABTS in the absence of H₂O₂, ABTS (1.0 mM) was incubated with 1.0 μ M *ThDyP* in sodium acetate (50 mM, pH 5.0, supplemented with 0.1 g L⁻¹ BSA) at 25 °C for selected time and oxidation of ABTS was followed by the increase in absorbance at 420 nm. Control reactions with inactivated *ThDyP* (incubated at 95 °C for 10 min) were made in parallel.

2.9. Absorbance spectra

The UV-Vis absorption spectrum of *ThDyP* was recorded at 300 nm–700 nm range using a Shimadzu UV-1900i UV-Vis spectrophotometer. *ThDyP* in sodium acetate buffer (50 mM, pH 5.0) was pre-incubated with 0, 1, 2, 5, or 50 molar equivalents of H₂O₂ for 30 min before recording the spectra.

2.10. SDS-PAGE

The molecular mass of *ThDyP* was estimated after incubation with H₂O₂ by SDS-PAGE using a 10% separation gel. 5 μ M of *ThDyP* was incubated with 0, 1, 2, 4, 10, 25, and 100 equivalents of H₂O₂ at room temperature for 20 min. The reaction was stopped by adding 5X Laemmli buffer (without reducing agent) followed by heating at 95 °C for 5 min. Pierce Unstained Protein Molecular Weight Marker (Thermo Fisher) was used as a size standard. Protein bands were visualized using InstantBlue Coomassie Protein Stain (Abcam).

3. Results

3.1. *ThDyP* displays complex kinetics

Dependency of the initial rates of the oxidation of ABTS on the concentration of substrates revealed complex kinetics of *ThDyP* with substrate inhibition by both, H₂O₂ and ABTS (Fig. 1). Furthermore, the dependency of initial rates on the concentration of ABTS followed an apparent positive cooperativity (Fig. 1A). In the concentration range of ABTS studied (0.05–5.0 mM) the positive cooperativity was not observed (we note that it may appear in the region of ABTS concentrations far below 0.05 mM) at low H₂O₂ concentrations (1.0–10 μ M) and the kinetics was analyzed using an empirical equation for the substrate inhibition (eq (1)).

$$\frac{v}{E_0} = \frac{k_{cat}^{app} [S]}{K_m^{app} + [S] + \frac{[S]^2}{K_i^{app}}} \quad (1)$$

In eq (1), v is the initial rate, E_0 is total concentration of the enzyme, $[S]$ is the concentration of the substrate that was varied, and k_{cat}^{app} , K_m^{app} and K_i^{app} are apparent catalytic constant, apparent Michaelis constant, and apparent inhibition constant, respectively. Substrate inhibition by ABTS appeared stronger at lower H₂O₂ concentrations. Stronger substrate inhibition at lower concentrations of the other substrate is a kinetic signature of ping-pong kinetic mechanism where substrate inhibition is caused by the non-productive binding of substrates to the “wrong form of the enzyme”. At higher H₂O₂ concentrations (above 10 μ M) the positive cooperativity was evident, and the kinetics was analyzed using an empirical equation of Hill (eq (2)).

$$\frac{v}{E_0} = \frac{k_{cat}^{app} [ABTS]^h}{K_{0.5}^h + [ABTS]^h} \quad (2)$$

In eq (2), $K_{0.5}$ is the concentration of ABTS at which the rate is half-maximal, and h is Hill coefficient. In analyses according to eq (2), the datasets were limited with the highest concentration of ABTS of 2 mM (i. e., data points showing substrate inhibition were not included). The value of h seemed to be independent on [H₂O₂] and the average value of 2.0 ± 0.1 was found for the series made with [H₂O₂] 25–1000 μ M (Fig. S1).

In Fig. 1B the data are reorganized to show the dependency of initial rates on [H₂O₂]. The positive cooperativity was not observed with H₂O₂. However, substrate inhibition by H₂O₂ was evident, showing increase in the apparent strength with decreasing [ABTS] (Fig. 1B). According to eq (1), the optimal substrate concentration ($[S]_{opt}$, substrate concentration at which the rate is at its maximum) is given by eq (3) where K_m^{app} and K_i^{app} are as defined in eq (1).

$$[S]_{opt} = \sqrt{K_m^{app} K_i^{app}} \quad (3)$$

Using K_m^{app} and K_i^{app} values obtained from nonlinear regression analysis of the data in Fig. 1B we found that [H₂O₂]_{opt} scales linearly with [ABTS] (Fig. S2). The values of kinetic parameters for H₂O₂ and ABTS are listed in supplementary tables Table S1 and Table S2, respectively.

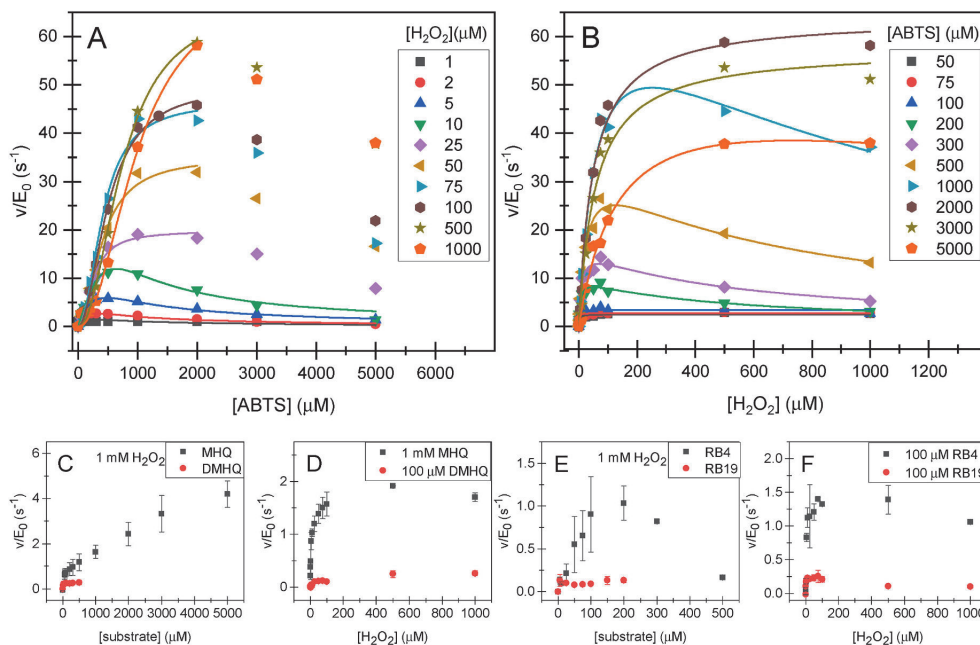
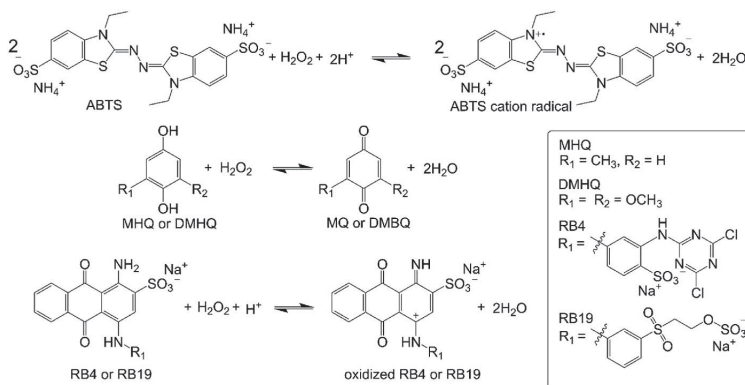


Fig. 1. Kinetics of *ThDyP* with different substrates. Reactions were made in sodium acetate (50 mM, pH 5.0, supplemented with 0.1 g L⁻¹ BSA) at 25 °C. Dependency of initial rates of the oxidation of ABTS on the concentration of (A) ABTS and (B) H₂O₂. Dependency of initial rates of the oxidation of hydroquinones and anthraquinone dyes on the concentration of (C) hydroquinone, (E) anthraquinone dye, and (D, F) H₂O₂. Solid lines in A show non-linear regression of the data according to eq (1) (for the series with [H₂O₂] 1.0–10 μM) or to eq (2) (for the series with [H₂O₂] of 25 μM and higher). In latter case the datasets were limited with the highest concentration of ABTS of 2 mM. Solid lines in B show non-linear regression of the data according to the 1. The nature and the concentration of the substrate that has been kept constant within the series is shown in the plot. Shown are average values of two experiments.

We also tested the oxidation of hydroquinones (MHQ and DMHQ) and anthraquinone dyes (RB4 and RB19). The activity of *ThDyP* with these substrates was much lower than that with ABTS and there was no positive cooperativity (Fig. 1 C–F). At the conditions tested, inhibition by reducing substrate was observed only with RB4 (Fig. 1E). With DMHQ as an exception, the inhibition by H₂O₂ was observed with all reducing substrates (Fig. 1 D and F). The structure of the substrates and stoichiometry of the reactions studied here are shown in Scheme 1.

3.2. Substrate inhibition

It is well known that H₂O₂-driven catalysis by heme-peroxidases follows ping-pong kinetics. H₂O₂ binds to the enzyme in its resting state (E-Fe³⁺) followed by the formation of reactive intermediate referred to as Compound I (Cpd I, Fig. 2A) [69]. Cpd I is reduced by two consecutive electron transfer steps from the substrate to recover the resting state of the enzyme. With the enzymes obeying a ping-pong mechanism the substrate inhibition is expected when substrate(s) bind to a “wrong form of the enzyme” [70]. The simplest mechanism that can



Scheme 1. Peroxidation reactions of *ThDyP* studied here. ABTS is a single electron donating substrate and two molecules of ABTS are needed to reduce H₂O₂ to water. Oxidation of hydroquinones (MHQ and DMHQ) and anthraquinone dyes (RB4 and RB19) takes place via two electron transfer to H₂O₂.

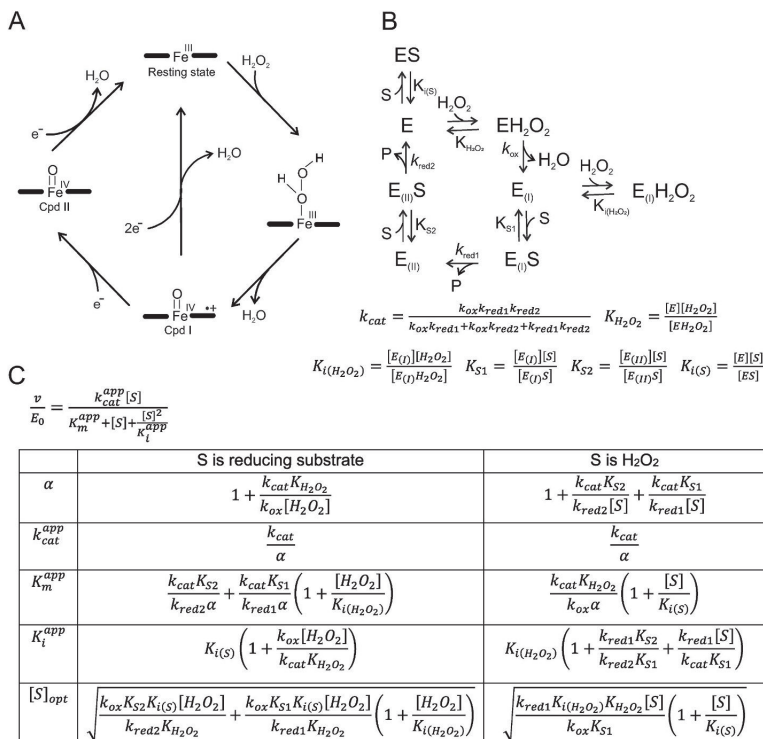


Fig. 2. Reaction mechanism and analysis of the catalysis by heme peroxidase. (A) Catalysis by heme peroxidases follows ping-pong mechanism. H₂O₂ binds to the enzyme in its resting state (E(FeIII) = E) followed by the formation of reactive intermediate known as Compound I (E(IV)•⁺ = Cpd I = E_(IV)). Cpd I is reduced by two consecutive electron transfer steps from the reducing substrate (S). In the first step Cpd I is reduced to the Compound II (E(IV) = Cpd II = E_(II)) and in the second step the Cpd II is reduced to restore the resting state. (B) Simplest kinetic mechanism explaining the substrate inhibition of heme peroxidase by both reducing substrate (S) and H₂O₂. E, E_(IV), and E_(II), stand for the enzyme resting state, Cpd I, and Cpd II, respectively. The k_{cat} , and the equilibrium dissociation constants used for deriving the rate equations are defined in the panel. (C) Dependency of apparent kinetic parameters of eq (1) (also shown in the figure) on the concentration of the substrate (the one which concentration is constant within the experiment series) and on the rate- and equilibrium constant defined in panel B. The term α is the factor by which an apparent k_{cat} is reduced compared to its true value and it is introduced for convenience of representation of equations.

account for the inhibition of heme-peroxidase by both, electron donating substrate and H₂O₂, is depicted in Fig. 2B. Binding to a “wrong form of the enzyme” is modeled by allowing the binding of H₂O₂ and ABTS to the Cpd I and to the resting state, respectively (Fig. 2B). In deriving the rate equation (eq (4)) all chemical reactions were considered irreversible and the mechanism in Fig. 2B was solved using an equilibrium assumption for all complexes.

steady-state assumption and kinetic shortcuts outlined before [25,71]. Derivations of steady-state rate equations are given in the Supplementary results. The steady-state solution to the kinetic mechanism in Fig. 2B (eq S7) was equivalent to eq (4), which was derived using rapid equilibrium assumption, but the binding constants, $K_{\text{H}_2\text{O}_2}$, K_{S1} , and K_{S2} , had different expressions in terms of individual rate constants (Table S3).

$$\frac{v}{E_0} = -\frac{d[\text{H}_2\text{O}_2]}{dt} = 2\frac{d[\text{P}]}{dt} = \frac{k_{\text{cat}}[\text{S}][\text{H}_2\text{O}_2]}{[\text{S}][\text{H}_2\text{O}_2] + \frac{k_{\text{cat}}K_{\text{H}_2\text{O}_2}}{k_{\text{ox}}}[\text{S}]\left(1 + \frac{[\text{S}]}{K_{\text{I}(\text{S})}}\right) + \frac{k_{\text{cat}}K_{\text{S1}}}{k_{\text{red1}}}[\text{H}_2\text{O}_2]\left(1 + \frac{[\text{H}_2\text{O}_2]}{K_{\text{I}(\text{H}_2\text{O}_2)}}\right) + \frac{k_{\text{cat}}K_{\text{S2}}}{k_{\text{red2}}}[\text{H}_2\text{O}_2]} \quad (4)$$

Equilibrium binding constants and the k_{cat} in eq (4) are defined in Fig. 2B. E_0 is the total concentration of the enzyme and [P] is the concentration of one electron oxidized product. Measurements of the heme peroxidase kinetics under single-turnover conditions often show no saturation of the rate of the formation of the Cpd I with [H₂O₂] [26,29,50,51] or the rate of the reduction of Cpd I with the concentration of reducing substrate [26,29,30,51]. This suggests that the rates of the chemical steps are fast and rapid equilibrium assumption may not hold for these enzymes. Therefore, we also derived the rate equations using

In practice the kinetics of enzyme reactions involving two substrates are measured so that only the concentration of one substrate is varied and that of the other is kept constant [70]. Resulting v/E_0 versus [substrate] curves can then be analyzed using the rate equations derived for a single substrate reaction like eq (1). Therefore, we rearranged eq (4) to the form of eq (1) that is often used for the analysis of the peroxidase kinetics with substrate inhibition. The dependency of the kinetic parameters of eq (1) from the concentration of the substrate that was kept constant and from the constants defined in Fig. 2B are shown in Fig. 2C.

In the absence of reducing substrate many heme peroxidases are inactivated by H_2O_2 [40,42,49,72–75]. Such an inactivation is indicative to the formation of non-productive complex between H_2O_2 and Cpd I. Therefore, we also tested a possible inactivation of *ThDyP* by H_2O_2 . For that we pre-incubated *ThDyP* with H_2O_2 before testing the residual activity with ABTS (1 mM ABTS and 1 mM H_2O_2). The residual activity of *ThDyP* decreased with pre-incubation time but, after 30 min, remained at the plateau value with the height dependent on the concentration of H_2O_2 (Fig. S3A). Analysis of the stoichiometry of inactivation revealed that only $4.6 \pm 0.9H_2O_2$ molecules was needed for complete inactivation of *ThDyP* (Fig. 3A). Titration of *ThDyP* with H_2O_2 resulted in decrease, and finally a complete loss of the absorbance of Soret band at 405 nm (Fig. S4). Collectively these data indicate the formation of some kind of non-productive complex between Cpd I and H_2O_2 as assumed in Fig. 2B.

Substrate inhibition by ABTS appeared stronger at lower concentrations of H_2O_2 (Fig. 1A) suggesting that both substrates compete for the binding to the resting state of the enzyme. Therefore, we also tested the effect of pre-incubation of *ThDyP* with ABTS in the absence of H_2O_2 to the following ABTS oxidation activity. Pre-incubation with ABTS also resulted in time dependent decrease of the residual activity of *ThDyP* (Fig. S3B). However, the inactivation of *ThDyP* by ABTS was far less efficient than that by H_2O_2 and complete inactivation of *ThDyP* was achieved only at ABTS to *ThDyP* ratio of 250 (Fig. 3B). As judged by the increase in absorbance at 420 nm, there was also a slow oxidation of ABTS in the experiments without added H_2O_2 (Fig. S5). However, the residual peroxidase activity of *ThDyP* (Fig. S3B) decayed much faster than the rate of apparent oxidation of ABTS in the absence of H_2O_2 (Fig. S5). Furthermore, maximum of about 10 oxidized ABTS molecules were produced per one molecule of *ThDyP* in the experiments without added H_2O_2 (Fig. S5) while complete inactivation of *ThDyP* occurred only at ABTS/*ThDyP* ratios over 250 (Fig. 3B). These results suggest that oxidation of ABTS in the absence of added H_2O_2 and inactivation of *ThDyP* are not coupled. High ABTS/*ThDyP* ratios needed for inactivation of *ThDyP* indicate that minor impurities in ABTS preparation may be responsible for the inactivation of *ThDyP* as recently shown for horseradish peroxidase [76]. Nevertheless, inactivation of *ThDyP* by ABTS suggest the existence of some kind of non-productive complexes between ABTS (or minor components in its preparation) and *ThDyP* resting state (note that there is no Cpd I in the experiments without H_2O_2) as assumed in Fig. 2B. It is also worth noting that, while irreversible inactivation of *ThDyP* by ABTS in the absence of H_2O_2 suggest the presence of complex between ABTS and enzymes resting state the absence of such inactivation does not rule it out (non-productive ABTS *ThDyP* complex may not cause the inactivation of the enzyme).

3.3. Structure of *ThDyP*

The structure of *ThDyP* was solved at 1.6 Å resolution and is displayed in Fig. 4A. Crystal parameters, data collection, and refinement statistics are summarized in Supplementary Table S4. The first 17 N-terminal residues of *ThDyP* were highly disordered and were therefore not modeled. The structure of *ThDyP* is comprised of two similar domains. Much like all DyPs, *ThDyP* confers to a ferredoxin-like fold, composed of two four-stranded antiparallel β -sheets and peripheral α -helices, which are joined by loop regions. The hexa-coordinated heme is located within the C-terminal domain of the *ThDyP* monomer. The heme iron is ligated by the conserved proximal axial His residue (H300) at a Ne2-iron distance of 2.1 Å (Fig. 4B). A highly conserved Asp (D360) is found within hydrogen bonding distance of H300, the carboxylate of D360 forms a hydrogen bond with H300 N δ 1 (2.8 Å), constituting the Fe-His-Asp triad. The distal face of the heme is occupied by Asp (D204), Arg (R316), and Phe (F337) residues, which are conserved among DyPs. Additionally, a nitrate ion at the distance of 2.4 Å from heme iron is found at the distal side of the heme. Most probably, this nitrate is derived from the crystallization mother liquor.

The direct accessibility of substrates to heme is determined by the architecture of heme-access channels [18] which for *ThDyP* is shown in Fig. 4A. Heme is accessible to solvent from several directions from the surface of *ThDyP*, wherein three main channels are present per monomer. Channel 1 is the largest among the channels found in *ThDyP* with a bottleneck radius of 2.0 Å. This channel is leading to the propionate group of heme pyrrole ring D, also known as the propionate pocket. Channel 2 is located on the distal face of heme with a bottleneck radius of 1.8 Å. Channel 3 is directing towards pyrrole ring C. This channel is the smallest with a bottleneck radius of 1.6 Å. It is suggested that channel 2 serves as an access channel for H_2O_2 , channels 1 and 3 are used by smaller reducing substrates as the access routes to the heme and the oxidation is catalyzed directly in the heme cavity [19]. Based on channel calculations, the heme-access channel 1 of *ThDyP* is sufficiently wide and open to allow direct interaction of ABTS with heme (Fig. 4A). This suggests that the substrate inhibition of *ThDyP* by ABTS may be caused by the competitive binding of ABTS and H_2O_2 to the resting state heme of *ThDyP* (Fig. 2B).

Although not demonstrated experimentally it is plausible that *ThDyP* may use long-range electron transfer to catalyze the oxidation of larger substrates whose size prevents direct interaction with heme. Amino acid residues responsible for the oxidation at surface sites are Trp and Tyr, and there are eight surface exposed Trp/Tyr residues in *ThDyP*. For some peroxidases that use surface binding sites and long-range electron transfer, it has been demonstrated that incubation with H_2O_2 in the

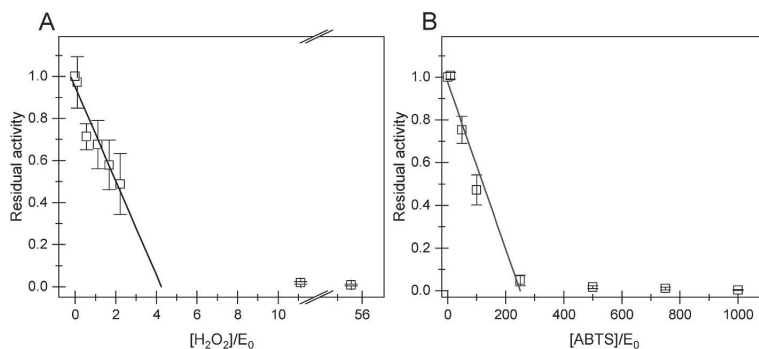


Fig. 3. *ThDyP* is inactivated by both substrates, H_2O_2 and ABTS. Reactions were made in sodium acetate (50 mM, pH 5.0, supplemented with 0.1 g L⁻¹ BSA) at 25 °C. *ThDyP* (1.0 μ M) was pre-incubated with (A) H_2O_2 for 1 h, or (B) ABTS for 24 h, before measuring the residual ABTS oxidizing activity (1 mM ABTS, 1 mM H_2O_2 , and 9 nM total *ThDyP*). Residual activity is defined as the ratio of activities in the experiments made, with and without given substrate in pre-incubation. Solid line show linear regression of the data in the range of the residual activity above 0.1. Shown are average values and SD from three independent experiments.

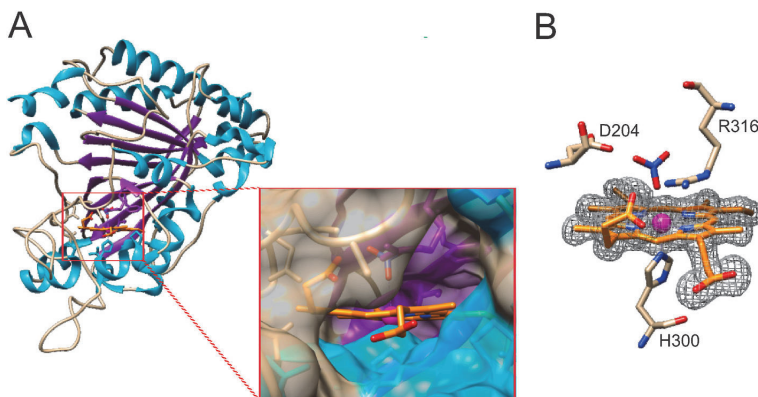


Fig. 4. Structure of DyP-type peroxidase from *T. halotolerans* (*ThDyP*). (A) Overall structure of *ThDyP* monomer (PDB ID: 8CK9). α -helices, β -sheets, and loops are shown in cyan, purple, and tan, respectively. The heme is in stick representation (orange-red-blue) and the iron is shown as a sphere (magenta). The nitrate ion (derived from mother liquor) is shown at the distal side of the heme at the distance of 2.4 Å from heme iron. The inset shows the propionate pocket of *ThDyP*. This main heme-access channel is proposed as the access route for reducing substrates. (B) The key residues surrounding heme in *ThDyP*. The omit difference ($F_o - F_c$) electron density map for the heme is shown as a grey mesh (contoured at 3σ level). The heme, iron, and nitrate ion are depicted in the same colors as in panel A.

absence of reducing substrate may lead to the covalent coupling of subunits [19,52]. No such covalent coupling was observed upon incubation of *ThDyP* with H_2O_2 (Fig. S6).

Although the asymmetric unit contains only a single polypeptide, PISA analysis suggests that the native form of the enzyme is a dimer. Contact (buried) area between subunits was 2082.5 Å², which indicates that *ThDyP* exists as a dimer with a head-to-tail configuration of monomers interacting via non-covalent interactions. Heme is not located in the oligomerization interface and the access to heme is not blocked by oligomerization suggesting that *ThDyP* can also function as a monomer. Gel filtration chromatography analyses of *ThDyP* revealed a dominant peak with an apparent molecular weight of 76 kDa (Fig. S7). This number is higher than the theoretical molecular weight of 45 kDa suggesting the presence of dimers.

3.4. Positive cooperativity

Dimeric structure of *ThDyP* and possible binding of ABTS to different sites allows for multiple potential mechanisms of positive cooperativity.

Even with one binding site, the binding of substrate to one subunit of dimeric enzyme may increase its binding affinity (or turnover number) in adjacent subunit. The same is true for the monomeric enzyme with two “cooperating” binding sites. However, to the best of our knowledge there is no experimental evidence for the existence of true cooperation between binding sites in DyP peroxidases.

In 2017 Shrestha et al. demonstrated that in DyP of *Enterobacter lignolyticus*, the Cpd II is not formed and Cpd I is directly reduced to the enzyme resting state via two electron oxidation [26]. While direct two electron oxidation of Cpd I is plausible within the complex of Cpd I with substrates capable of donating two electrons, this is not possible for substrates capable of donating single electron only. In peroxidase studies ABTS is almost exclusively considered as a single electron donating substrate (Scheme 1). However, using strong oxidants it is possible to abstract electron from $ABTS^{+ \cdot}$ and oxidize it to $ABTS^{++}$ [77,78]. $ABTS^{++}$ has an absorbance maximum at 520 nm but it is highly unstable at pH above 0 [78]. Second electron abstraction from ABTS takes place with the redox potential of $E^\circ = 1.09$ V which is considerably higher than that for the first electron abstraction ($E^\circ = 0.69$ V) [78]. The redox

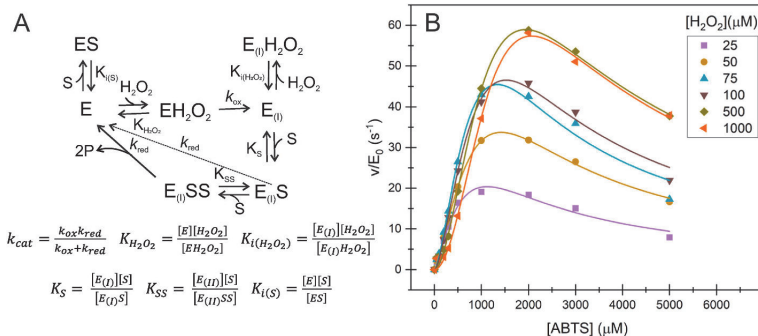


Fig. 5. Simplest kinetic mechanism explaining the kinetics of *ThDyP*. (A) In this mechanism Cpd II is not formed and Cpd I is reduced to the resting state through simultaneous two electron transfer from substrate. For single electron donating substrates (like ABTS), this assumes the existence of the Cpd I complex with two substrate molecules ($E(1)SS$) (k_{red} route shown with solid arrow). There is no need for $E(1)SS$ complex for two electrons donating substrates (like hydroquinones and anthraquinone dyes) (k_{red} route shown with dashed arrow). The rate- and equilibrium dissociation constants used for deriving the rate equations (eqs (5) and (6) for single- and two electrons donating substrate, respectively) are defined in the panel. (B) Non-linear regression analysis of the dependency of the rates of ABTS oxidation on [ABTS] according to eq (5) (solid lines). Shown are the data from Fig. 1A but the data where positive cooperativity was not observed (the series with $[H_2O_2] \leq 10$ μM) are omitted for clarity.

potentials of the reactive intermediates Cpd I and Cpd II in DyPs are in the range of 1.2–1.5 V with Cpd I being stronger oxidant than Cpd II [21]. Thus, in principle DyPs are capable to catalyze the oxidation of $\text{ABTS}^{\bullet+}$ to ABTS^{++} . To test this possibility we incubated 0.1 μM *ThDyP* with 100 μM H_2O_2 and ABTS (5, 10 and 20 μM). In all cases there was a stoichiometric conversion of ABTS to $\text{ABTS}^{\bullet+}$ and there was no further oxidation of $\text{ABTS}^{\bullet+}$ to ABTS^{++} even after addition of fresh portion of *ThDyP* (Fig. S8).

Simultaneous binding of two single electron donating substrates to Cpd I is necessary for its direct reduction to the resting state. Such kinetic mechanism is shown in Fig. 5A. Solving the mechanism in Fig. 5A results in eq (5).

$$\frac{v}{E_0} = -\frac{d[\text{H}_2\text{O}_2]}{dt} = 2\frac{d[\text{P}]}{dt} = \frac{k_{\text{cat}}[\text{S}]^2[\text{H}_2\text{O}_2]}{[\text{S}]^2[\text{H}_2\text{O}_2] + \frac{k_{\text{cat}}K_{\text{H}_2\text{O}_2}}{k_{\text{ox}}}[\text{S}]^2\left(1 + \frac{[\text{S}]}{K_{\text{S}}}\right) + \frac{k_{\text{cat}}K_{\text{SS}}K_{\text{S}}}{k_{\text{red}}}[\text{H}_2\text{O}_2]\left(1 + \frac{[\text{H}_2\text{O}_2]}{K_{\text{H}_2\text{O}_2}}\right) + \frac{k_{\text{cat}}K_{\text{SS}}}{k_{\text{red}}}[\text{S}][\text{H}_2\text{O}_2]} \quad (5)$$

In eq (5) the [P] stands for the concentration of one electron oxidized product. Rate constants and equilibrium constants in eq (5) are defined in Fig. 5A. Steady-state solution (eq S8) can be arranged to the form of eq (5) but the meaning of the binding constants, $K_{\text{H}_2\text{O}_2}$, K_{S} , and K_{SS} , is different with apparent K_{S} depending on a substrate concentration (Table S3). In the series made with H_2O_2 concentrations of 25 μM and higher (i.e. in the range where positive cooperativity with ABTS was observed) eq (5) described our results with the oxidation of ABTS reasonably well (Fig. 5B). However, because of the over-parametrization it was not possible to derive the values of kinetic parameters. The squared term of substrate concentration in the nominator is responsible for the ability of eq (5) to account for the apparent positive cooperativity and defines the value of Hill coefficient equal to 2, a value that was indeed observed experimentally (Fig. S1). As shown in the route designated with dashed arrow in Fig. 5A, there is no need for the enzyme complex with two substrate molecules in the case of two electron donating substrates and eq (5) reduces to eq (6).

$$\frac{v}{E_0} = -\frac{d[\text{H}_2\text{O}_2]}{dt} = \frac{d[\text{P}]}{dt} = \frac{k_{\text{cat}}[\text{S}][\text{H}_2\text{O}_2]}{[\text{S}][\text{H}_2\text{O}_2] + \frac{k_{\text{cat}}K_{\text{H}_2\text{O}_2}}{k_{\text{ox}}}\left[\text{S}\left(1 + \frac{[\text{S}]}{K_{\text{S}}}\right) + \frac{k_{\text{cat}}K_{\text{S}}}{k_{\text{red}}}[\text{H}_2\text{O}_2]\left(1 + \frac{[\text{H}_2\text{O}_2]}{K_{\text{H}_2\text{O}_2}}\right)\right]} \quad (6)$$

Note that in eq (6) the [P] stands for the concentration of two electron oxidized product. Rate constants and equilibrium constants in eq (6) are defined in Fig. 5. Steady-state solution (eq S9) is equivalent to eq (6) but the expressions of $K_{\text{H}_2\text{O}_2}$ and K_{S} contain the rate constants of chemical steps (Table S3). There is no squared term of substrate concentration in the numerator of eq (6) and it cannot account for the positive cooperativity. Consistent with this, there was no positive cooperativity in oxidation of two electrons donating substrates (MHQ, DMHQ, RB4, and RB19) by *ThDyP* (Fig. 1C & E).

4. Discussion

Many DyPs have been shown to display complex kinetics. The most often observed deviation from the Michaelis-Menten kinetics is the inhibition by reducing substrate and/or H_2O_2 [3,17,33–38] but positive cooperativity has also been observed [3,19,50,51]. The DyP studied

here, *ThDyP*, displayed both substrate inhibition and positive cooperativity. *ThDyP* shares sequence similarity to DyPs from *Thermobifida alba* (80.5%), *T. cellulositytica* (80.7%), and *T. fusca* (78.4%, *TfuDyP*). The structure and the substrate scope has been previously determined for *TfuDyP* [4,11,79]. *TfuDyP* can oxidase several phenolic substrates, such as guaiacol, 2,6-dimethoxyphenol, and pyrogallol [11,79] as well as anthraquinone dyes RB4 and RB19 [4,11], and ABTS [79]. An apparent k_{cat} and K_{m} for ABTS (measured with 1.0 mM H_2O_2 at pH 5.5 and 25 °C) of 28 s^{-1} and 0.86 mM, respectively, have reported for *TfuDyP* [79]. These figures are in the same order with k_{cat} (72 s^{-1}) and $K_{0.5}$ (0.98 mM) values measured here for *ThDyP* (Table S2). With 1.0 mM H_2O_2 there was no substrate inhibition of *TfuDyP* by ABTS but the highest con-

centration of ABTS was limited with 2.0 mM in this study [79]. Of note, with 1.0 mM H_2O_2 , the substrate inhibition of *ThDyP* by ABTS revealed only in the case of ABTS concentrations above 2.0 mM (see Fig. 1A). Although not so clearly revealed as with *ThDyP* here, it seems that *TfuDyP* also has a positive cooperativity with ABTS but not with two electron donating substrates like phenol and RB4 [79]. In following, we try to find a simplest mechanistic interpretation for the peculiar kinetics of *ThDyP* (and possibly of other DyPs).

Substrate inhibition is well-known phenomenon in enzyme catalysis, but it mostly occurs at substrate concentrations that are far above the physiological range. The *ThDyP* studied here contains Tat signal suggesting that the enzyme is targeted to the extracellular milieu. Unfortunately, the biological role of *ThDyP* nor the nature of its native reducing substrate is not known. In fact, this is true for most of the enzymes in the DyP family [80] although possible functioning in copper transport and H_2O_2 scavenging have been reported [81]. In this study, the inhibition by H_2O_2 became evident at H_2O_2 concentrations above 50 μM (Fig. 1B). H_2O_2 is a reactive molecule and its concentrations in native environments hardly accumulate to high micromolar range suggesting

that inhibition of *ThDyP* by H_2O_2 may not be biologically relevant. However, strong irreversible suicide inactivation of *ThDyP* by H_2O_2 in the absence of reducing substrate (Fig. 3A) suggests possible biological role. In some peroxidases, the inactivation by H_2O_2 is relieved by their catalase activity [42,49] whereas others like ascorbate peroxidase lack catalase activity and are strongly inactivated by H_2O_2 [40]. In the absence of reducing substrate, the inactivation of *ThDyP* by H_2O_2 was fast (half-life around 5 min with 56 eqv H_2O_2 , Fig. S3A) and efficient (Fig. 3A). It has been shown that inactivation by H_2O_2 is often caused by oxidation of active site cysteine and/or methionine residues [47]. There are three methionine residues in the vicinity of heme in *ThDyP* (Fig. S9). Although the oxidation of these methionines cannot be excluded, a significant bleaching of the absorbance of Soret band already at low H_2O_2 concentrations (5 equivalents, Fig. S4) suggests that the inactivation of *ThDyP* is a result of the degradation of heme. The kinetics of H_2O_2 inactivation of *ThDyP* is similar to that of ascorbate peroxidase [40,82]. Ascorbate peroxidase is functioning in the chloroplasts of plant

cells and its inactivation by H_2O_2 in the absence of ascorbate has been associated to the regulatory roles [83]. Unknown biological role of *ThDyP* does not allow to draw similar conclusions for this enzyme.

Differently from native environments, the H_2O_2 concentrations in industrial applications of peroxidase catalysis are often in the millimolar range. In this case, the substrate inhibition by H_2O_2 may be serious drawback. Potential inhibition by a reducing substrate depends on its ability to interact with enzyme's resting state (Fig. 2B). On the other hand, inhibition by H_2O_2 stems from the binding of H_2O_2 to the Cpd I (Fig. 2B) which is a common intermediate that does not depend on the reducing substrate. Therefore, one may think that, when present, the substrate inhibition by H_2O_2 is independent of the nature of reducing substrate. However, when the true binding affinity of H_2O_2 to Cpd I ($K_{I(H_2O_2)}$, Fig. 2C) is independent of the nature of reducing substrate, the strength of the H_2O_2 inhibition (K_1^{app} , Fig. 2C) also depends on the relative abundance of Cpd I which in turn depends on the kinetic properties of reducing substrate. When the efficiency of the reduction of Cpd I to Cpd II is much higher than reduction of Cpd II to resting state ($k_{red1}/K_{S1} \gg k_{red2}/K_{S2}$) then $K_1^{app} \gg K_{I(H_2O_2)}$ and inhibition by H_2O_2 is weak (Fig. 2C). We note that, for simplicity, the possible binding of H_2O_2 to Cpd II was omitted in kinetic mechanism in Fig. 2B. Studies of inactivation of heme-peroxidases have shown that upon reduction of Cpd I to Cpd II by H_2O_2 , Cpd II further reacts with H_2O_2 in the reactions that may lead to restoration of resting state [42,49,72,75] or enzyme inactivation [72,75]. When the binding of H_2O_2 is plausible, the substrate inhibition by H_2O_2 depends on the relative binding strengths of H_2O_2 to Cpd I and Cpd II and relative abundances of these intermediates in the presence of a given reducing substrate.

Conventional mechanisms of cooperativity assume the presence of more than one active site in mono-/multimeric enzyme. Binding of the substrate to one binding site influences the binding affinity and/or turnover of substrate in another binding site, i. e. there is a cooperation between binding sites. Positive cooperativity is often associated with enzymes that catalyze regulatory reactions of metabolic pathways. The activity of cooperative enzymes is often regulated by allosteric inhibitors and activators. Although an apparent positive cooperativity has been observed with DyP family peroxidases [3,19,50,51], to the best of our knowledge, the existence of allosteric regulators of DyP peroxidases has not reported so far. Although the lack of such information may simply reflect unknown biological role of DyP peroxidases, it may also stem from different, non-conventional, mechanisms underlying an apparent positive cooperativity of these enzymes.

Dimeric structure of *ThDyP*, revealed by X-ray crystallography (Fig. 4) and size exclusion chromatography (Fig. S7) leaves open the possibility that conventional mechanisms of true positive cooperativity are operational in oxidation of ABTS. Alternative explanation of our data with *ThDyP* would be the mechanism whereby Cpd I is directly reduced to the resting state via simultaneous two-electron transfer from a reducing substrate (Fig. 5A). Since ABTS can donate only single electron to *ThDyP* (Fig. S8), at least two ABTS molecules must be bound to the enzyme to enable simultaneous two-electron reduction of Cpd I. Such a mechanism will result in a positive cooperativity with the value of Hill coefficient of 2 (see equation (5)) that was also seen experimentally (Fig. S1). The heme access channel of *ThDyP* is wide enough to enable direct interaction between heme and ABTS (Fig. 4). Direct interaction between heme and ABTS is also supported by the substrate inhibition with ABTS (Fig. 1A). Whether the second ABTS molecule also directly interacts with heme or uses surface binding site and long-range electron transfer is not known.

Different from ABTS, the substrates with capability of transferring two electrons, like hydroquinones and anthraquinone dyes used here, did not show positive cooperativity (Fig. 1C & E). This is consistent with the proposed mechanism of cooperativity with ABTS since there is no need for simultaneous binding of two substrate molecules in case of two electron donating substrates. It must be noted that apparent positive cooperativity may also stem from enzyme-independent reactions that

are necessary for the formation of detectable products [51]. Chaplin et al. have demonstrated that positive cooperativity in oxidation of RB19 by DyP of *Streptomyces lividans* is caused by rate-limiting disproportionation of products necessary for decolorization of RB19 [51]. The absence of positive cooperativity with RB19 (Fig. 1E) suggest that the possible disproportionation of products is faster than oxidation of RB19 by *ThDyP*.

In 2001 the propensity of Cpd I to two electron reduction has been associated with heme-water interactions. So called "dry heme" is amenable to direct two electron oxidation without Cpd II intermediate, whereas "wet heme" is oxidized by two consecutive one electron oxidation steps (Fig. 2A) [28]. Type A DyPs, like *ThDyP* studied here, are proposed to have "wet heme", whereas type B DyPs have "dry heme" [84]. A recent study by Lučić et al. demonstrated that the apparent absence of Cpd II in the case of "dry heme" is a consequence of the slow formation and rapid decomposition of Cpd II intermediate (i.e. $k_{red2}/K_{S2} \gg k_{red1}/K_{S1}$ in Fig. 2C) [30]. The presence of Cpd II in DyPs seems to contradict the need for the ternary complex of Cpd I with two single-electron donating substrate molecules, as proposed here, to explain the positive cooperativity with ABTS (Fig. 5A). However, the nature of the reducing substrate along with the nature of its binding site (s) (direct/remote) may influence the e^-/H^+ transfer steps involved in reduction of Cpd I.

Funding

This work was supported by grants from European Regional Development Fund, Estonian Research Council [PRG1540] to PV, and Estonian Research Council [RETA11] to TL.

Data statement

All data are available within the article and its Supporting Information File and from the corresponding author upon reasonable request.

CRedit authorship contribution statement

Hegne Pupart: Writing – original draft, Visualization, Investigation, Formal analysis. **Tiit Lukk:** Writing – review & editing, Supervision, Funding acquisition. **Priit Väljamäe:** Writing – original draft, Supervision, Methodology, Funding acquisition, Formal analysis, Conceptualization.

Declaration of competing interest

The authors declare no conflict of interest.

Abbreviations

ABTS	2,2'-azino-bis(3-ethylbenzothiazoline-6-sulfonic acid)
BSA	bovine serum albumin
Cpd I	compound I
Cpd II	compound II
DMHQ	2,6-dimethoxyhydroxyquinone
DyP	dye-decolorizing peroxidase
MHQ	methylhydroquinone
RB4	reactive blue 4
RB19	reactive blue 19
Tat	twin-arginine translocation
<i>ThDyP</i>	dye-decolorizing peroxidase of <i>Thermobifida halotolerans</i>

Appendix A. Supplementary data

Supplementary data to this article can be found online at <https://doi.org/10.1016/j.abb.2024.109931>.

References

- [1] Y. Sugano, K. Sasaki, M. Shoda, cDNA cloning and genetic analysis of a novel decolorizing enzyme, peroxidase gene *dyp* from *Geotrichum candidum* Dec 1, *J. Biosci. Bioeng.* 87 (1999) 411–417, [https://doi.org/10.1016/S1389-1723\(99\)80087-5](https://doi.org/10.1016/S1389-1723(99)80087-5).
- [2] S.J. Kim, M. Shoda, Purification and characterization of a novel peroxidase from *Geotrichum candidum* Dec 1 involved in decolorization of dyes, *Appl. Environ. Microbiol.* 65 (1999) 1029–1035, <https://doi.org/10.1128/aem.65.3.1029-1035.1999>.
- [3] U.A. Zitare, M.H. Habib, H. Rozeboom, M.L. Mascotti, S. Todorovic, M.W. Fraaije, Mutational and structural analysis of an ancestral fungal dye-decolorizing peroxidase, *FEBS J.* 288 (2021) 3602–3618, <https://doi.org/10.1111/febs.15687>.
- [4] N. Loncar, D.I. Colpa, M.W. Fraaije, Exploring the biocatalytic potential of a *Dyp*-type peroxidase by profiling the substrate acceptance of *Thermobifida fusca* *Dyp* peroxidase, *Tetrahedron* 72 (2016) 7276–7281, <https://doi.org/10.1016/j.tet.2015.12.078>.
- [5] J.N. Roberts, R. Singh, J.C. Grigg, M.E.P. Murphy, T.D.H. Bugg, L.D. Eltis, Characterization of dye-decolorizing peroxidases from *Rhodococcus jostii* RHA1, *Biochemistry* 50 (2011) 5108–5119, <https://doi.org/10.1021/bi200427h>.
- [6] Y. Sugano, T. Yoshida, *Dyp*-type peroxidases: recent advances and perspectives, *Int. J. Mol. Sci.* 22 (2021) 5556, <https://doi.org/10.3390/ijms22115556>.
- [7] T. Paysan-Lafosse, M. Blum, S. Chuguransky, T. Grego, B.L. Pinto, G.A. Salazar, M. L. Bileschi, P. Bork, A. Bridge, L. Colwell, J. Gough, D.H. Haft, I. Letunic, A. Marchler-Bauer, H. Mi, D.A. Natale, C.A. Orengo, A.P. Pandurangan, C. Rivoire, C.J.A. Sigrist, I. Sillitoe, N. Thanki, P.D. Thomas, S.C.E. Tosatto, C.H. Wu, A. Bateman, InterPro in 2022, *Nucleic Acids Res.* 51 (2023) D418–D427, <https://doi.org/10.1093/nar/gkac993>.
- [8] G. Janusz, A. Pawlik, J. Sulej, U. Świdarska-Burek, A. Jarosz-Wilkolazka, A. Paszczynski, Lignin degradation: microorganisms, enzymes involved, genomes analysis and evolution, *FEMS Microbiol. Rev.* 41 (2017) 941–962, <https://doi.org/10.1093/femsre/fux049>.
- [9] N. Fawal, Q. Li, B. Savelli, M. Brette, G. Passaia, M. Fabre, C. Mathé, C. Dunand, PeroxiBase: a database for large-scale evolutionary analysis of peroxidases, *Nucleic Acids Res.* 41 (2013) 441–444, <https://doi.org/10.1093/nar/gks1083>.
- [10] Y. Sugano, R. Muramatsu, A. Ichinyanagi, T. Sato, M. Shoda, *Dyp*, a unique dye-decolorizing peroxidase, represents a novel heme peroxidase family: ASP171 replaces the distal histidine of classical peroxidases, *J. Biol. Chem.* 282 (2007) 36652–36658, <https://doi.org/10.1074/jbc.M706996200>.
- [11] E. van Bloois, D.E. Torres Pazmiño, R.T. Winter, M.W. Fraaije, A robust and extracellular heme-containing peroxidase from *Thermobifida fusca* as prototype of a bacterial peroxidase superfamily, *Appl. Microbiol. Biotechnol.* 86 (2010) 1419–1430, <https://doi.org/10.1007/s00253-009-2369-x>.
- [12] M. Scheibner, B. Hülsdau, K. Zelena, M. Nimtz, L. de Boer, R.G. Berger, H. Zorn, Novel peroxidases of *Marasmius scorodionius* degrade β -carotene, *Appl. Microbiol. Biotechnol.* 77 (2008) 1241–1250, <https://doi.org/10.1007/s00253-007-1261-9>.
- [13] H.J.O. Ogola, T. Kamiike, N. Hashimoto, H. Ashida, T. Ishikawa, H. Shibata, Y. Sawa, Molecular characterization of a novel peroxidase from the cyanobacterium *Anabaena* sp. strain PCC 7120, *Appl. Environ. Microbiol.* 75 (2009) 7509–7518, <https://doi.org/10.1128/AEM.01121-09>.
- [14] C. Zubietta, S.S. Krishna, M. Kapoor, P. Kozbial, D. McMullan, H.L. Axelrod, M. D. Miller, P. Abdubek, E. Ambing, T. Astakhova, D. Carlton, H.-J. Chiu, T. Clayton, M.C. Deller, L. Duan, M.-A. Eslsiger, J. Feuerhelm, S.K. Grzechnik, J. Hale, E. Hampton, G.W. Han, L. Jaroszewski, K.K. Jin, H.E. Klock, M.W. Knuth, A. Kumar, D. Marciano, A.T. Morse, E. Nigoghossian, L. Okach, S. Oommachen, R. Reyes, C.L. Rife, P. Schimmel, H. van den Bedem, D. Weekes, A. White, Q. Xu, K. O. Hodgson, J. Wooley, A.M. Deacon, A. Godzik, S.A. Lesley, I.A. Wilson, Crystal structures of two novel dye-decolorizing peroxidases reveal a β -barrel fold with a conserved heme-binding motif, *Proteins* 69 (2007) 223–233, <https://doi.org/10.1002/prot.21550>.
- [15] C. Zubietta, R. Joseph, S.S. Krishna, D. McMullan, M. Kapoor, H.L. Axelrod, M. D. Miller, P. Abdubek, C. Acosta, T. Astakhova, D. Carlton, H.-J. Chiu, T. Clayton, M.C. Deller, L. Duan, Y. Elias, M.-A. Eslsiger, J. Feuerhelm, S.K. Grzechnik, J. Hale, G.W. Han, L. Jaroszewski, K.K. Jin, H.E. Klock, M.W. Knuth, P. Kozbial, A. Kumar, D. Marciano, A.T. Morse, K.D. Murphy, E. Nigoghossian, L. Okach, S. Oommachen, R. Reyes, C.L. Rife, P. Schimmel, C. V. Trout, H. van den Bedem, D. Weekes, A. White, Q. Xu, K.O. Hodgson, J. Wooley, A.M. Deacon, A. Godzik, S.A. Lesley, I. A. Wilson, Identification and structural characterization of heme binding in a novel dye-decolorizing peroxidase, *TyrA*, *Proteins* 69 (2007) 234–243, <https://doi.org/10.1002/prot.21673>.
- [16] P. Dhanekar, V. Dalal, V. Singh, A.K. Sharma, P. Kumar, Structure of dye-decolorizing peroxidase from *Bacillus subtilis* in complex with veratryl alcohol, *Int. J. Biol. Macromol.* 193 (2021) 601–608, <https://doi.org/10.1016/j.ijbiomac.2021.10.100>.
- [17] T. Yoshida, H. Tsuge, T. Hisabori, Y. Sugano, Crystal structures of dye-decolorizing peroxidase with ascorbic acid and 2,6-dimethoxyphenol, *FEBS Lett.* 586 (2012) 4351–4356, <https://doi.org/10.1016/j.febslet.2012.10.049>.
- [18] E. Strittmatter, K. Serrer, C. Liers, R. Ullrich, M. Hofrichter, K. Piontek, E. Schleicher, D.A. Plattner, The toolbox of Auricularia auricula-judae dye-decolorizing peroxidase - identification of three new potential substrate-interaction sites, *Arch. Biochem. Biophys.* 574 (2015) 75–85, <https://doi.org/10.1016/j.abb.2014.12.016>.
- [19] R. Shrestha, X. Chen, K.X. Ramyar, Z. Hayati, E.A. Carlson, S.H. Bossmann, L. Song, B.V. Geisbrecht, P. Li, Identification of surface-exposed protein radicals and a substrate oxidation site in A-class dye-decolorizing peroxidase from *Thermomonospora curvata*, *ACS Catal.* 6 (2016) 8036–8047, <https://doi.org/10.1021/acscatal.6b01952>.
- [20] A.K. Chaplin, T.M. Chicano, B.V. Hampshire, M.T. Wilson, M.A. Hough, D. A. Svistunenko, J.A.R. Worrall, An aromatic dyad motif in dye decolorizing peroxidases has implications for free radical formation and catalysis, *Chem. Eur J.* 25 (2019) 6141–6153, <https://doi.org/10.1002/chem.201806290>.
- [21] D. Linde, I. Ayuso-Fernández, M. Laloux, J.E. Aguiar-Cervera, A.L. de Lacey, F. J. Ruiz-Duenas, A.T. Martínez, Comparing ligninolytic capabilities of bacterial and fungal dye-decolorizing peroxidases and class-II peroxidase-catalases, *Int. J. Mol. Sci.* 22 (2021) 2629, <https://doi.org/10.3390/ijms22052629>.
- [22] K. Nys, P.G. Furtmüller, C. Obinger, S. Van Doorslaer, V. Pfanagl, On the track of long-range electron transfer in B-type dye-decolorizing peroxidases: identification of a tyrosyl radical by computational prediction and electron paramagnetic resonance spectroscopy, *Biochemistry* 60 (2021) 1226–1241, <https://doi.org/10.1021/acs.biochem.1c00129>.
- [23] E. Strittmatter, S. Wachter, C. Liers, R. Ullrich, M. Hofrichter, D.A. Plattner, K. Piontek, Radical formation on a conserved tyrosine residue is crucial for *Dyp* activity, *Arch. Biochem. Biophys.* 537 (2013) 161–167, <https://doi.org/10.1016/j.abb.2013.07.007>.
- [24] T.L. Poulos, J. Kraut, The stereochemistry of peroxidase catalysis, *J. Biol. Chem.* 255 (1980) 8199–8205, [https://doi.org/10.1016/s0021-9258\(19\)70630-9](https://doi.org/10.1016/s0021-9258(19)70630-9).
- [25] J. Zhao, C. Lu, S. Franzen, Distinct enzyme-substrate interactions revealed by two dimensional kinetic comparison between dehaloperoxidase-hemoglobin and horseradish peroxidase, *J. Phys. Chem. B* 119 (2015) 12828–12837, <https://doi.org/10.1021/acs.jpbc.5b07126>.
- [26] R. Shrestha, G. Huang, D.A. Meekins, B.V. Geisbrecht, P. Li, Mechanistic insights into dye-decolorizing peroxidase revealed by solvent isotope and viscosity effects, *ACS Catal.* 7 (2017) 6352–6364, <https://doi.org/10.1021/acscatal.7b01861>.
- [27] E. Strittmatter, C. Liers, R. Ullrich, S. Wachter, M. Hofrichter, D.A. Plattner, K. Piontek, First crystal structure of a fungal high-redox potential dye-decolorizing peroxidase substrate interaction sites and long-range electron transfer, *J. Biol. Chem.* 288 (2013) 4095–4102, <https://doi.org/10.1074/jbc.M112.400176>.
- [28] P. Jones, Roles of water in heme peroxidase and catalase mechanisms, *J. Biol. Chem.* 276 (2001) 13791–13796, <https://doi.org/10.1074/jbc.M011413200>.
- [29] R. Shrestha, K. Jia, S. Khadka, L.D. Eltis, P. Li, Mechanistic insights into *DypB* from *Rhodococcus jostii* RHA1 via kinetic characterization, *ACS Catal.* 11 (2021) 5486–5495, <https://doi.org/10.1021/acscatal.1c00703>.
- [30] M. Lucić, M.T. Wilson, T. Tosha, H. Sugimoto, A. Shilova, D. Axford, R.L. Owen, M. A. Hough, J.A.R. Worrall, Serial femtosecond crystallography reveals the role of water in the one- or two-electron redox chemistry of Compound I in the catalytic cycle of the B-type dye-decolorizing peroxidase *DtpB*, *ACS Catal.* 12 (2022) 13349–13359, <https://doi.org/10.1021/acscatal.2c03754>.
- [31] M.E. Brown, T. Barros, M.C.Y. Chang, Identification and characterization of a multifunctional dye peroxidase from a lignin-reactive bacterium, *ACS Chem. Biol.* 7 (2012) 2074–2081, <https://doi.org/10.1021/cb300383y>.
- [32] C. Liers, C. Bobeth, M. Pecyna, R. Ullrich, M. Hofrichter, *Dyp*-like peroxidases of the jelly fungus *Auricularia auricula-judae* oxidize nonphenolic lignin model compounds and high-redox potential dyes, *Appl. Microbiol. Biotechnol.* 85 (2010) 1869–1879, <https://doi.org/10.1007/s00253-009-2173-7>.
- [33] A. Avram, A. Sengupta, P.H. Pfromm, H. Zorn, P. Lorenz, T. Schwarz, K.Q. Nguyen, P. Czermak, Novel *Dyp* from the basidiomycete *Pleurotus sapidus*: substrate screening and kinetics, *Biochemistry* 4 (2018) 1–13, <https://doi.org/10.1515/bocaa-2018-0001>.
- [34] H. Pupart, P. Jöul, M.I. Bramanis, T. Lukk, Characterization of the ensemble of lignin-remodeling *Dyp*-type peroxidases from *Streptomyces coelicolor* A3(2), *Energies* 16 (2023) 1557, <https://doi.org/10.3390/en16031557>.
- [35] V. Brissos, D. Tavares, A.C. Sousa, M.P. Robalo, L.O. Martins, Engineering a bacterial *Dyp*-type peroxidase for enhanced oxidation of lignin-related phenolics at alkaline pH, *ACS Catal.* 7 (2017) 3454–3465, <https://doi.org/10.1021/acscatal.6b03331>.
- [36] C.F. Rodrigues, P.T. Borges, M.F. Scocozza, D. Silva, A. Taborda, V. Brissos, C. Frazão, L.O. Martins, Loops around the heme pocket have a critical role in the function and stability of *BsDyp* from *Bacillus subtilis*, *Int. J. Mol. Sci.* 22 (2021) 10862, <https://doi.org/10.3390/ijms221910862>.
- [37] A. Santos, S. Mendes, V. Brissos, L.O. Martins, New dye-decolorizing peroxidases from *Bacillus subtilis* and *Pseudomonas putilla* MET94 - towards biotechnological applications, *Appl. Microbiol. Biotechnol.* 98 (2014) 2053–2065, <https://doi.org/10.1007/s00253-013-5041-4>.
- [38] H. Pupart, D. Vastjónok, T. Lukk, P. Väljamäe, Dye-decolorizing peroxidase of *Streptomyces coelicolor* (*ScDYPB*) exists as a dynamic mixture of kinetically different oligomers, *ACS Omega* 9 (2024) 3866–3876, <https://doi.org/10.1021/acscomega.3c07963>.
- [39] M.B. Arnao, M. Acosta, J.A. del Río, R. Varón, F. García-Cánovas, A kinetic study on the suicide inactivation of peroxidase by hydrogen peroxide, *Biochim. Biophys. Acta* 1041 (1990) 43–47, [https://doi.org/10.1016/0167-4838\(90\)90120-5](https://doi.org/10.1016/0167-4838(90)90120-5).
- [40] A.N.P. Hiner, J.N. Rodríguez-López, M.B. Arnao, E. Lloyd Raven, F. García-Cánovas, M. Acosta, Kinetic study of the inactivation of ascorbate peroxidase by hydrogen peroxide, *Biochem. J.* 348 (2000) 321–328, <https://doi.org/10.1042/0264-6021:3480321>.
- [41] A.N.P. Hiner, J. Hernández-Ruiz, F. García-Cánovas, A.T. Smith, M.B. Arnao, M. Acosta, A comparative study of the inactivation of wild-type, recombinant and two mutant horseradish peroxidase isoenzymes C by hydrogen peroxide and *m*-chloroperoxybenzoic acid, *Eur. J. Biochem.* 234 (1995) 506–512, <https://doi.org/10.1111/j.1432-1033.1995.506.b.x>.
- [42] A.N.P. Hiner, J. Hernández-Ruiz, J.N. Rodríguez-López, F. García-Cánovas, N. C. Brisset, A.T. Smith, M.B. Arnao, M. Acosta, Reactions of the class II peroxidases,

- lignin peroxidase and Arthromyces ramosus peroxidase, with hydrogen peroxide. Catalase-like activity, compound III formation, and enzyme inactivation, *J. Biol. Chem.* 277 (2002) 26879–26885, <https://doi.org/10.1074/jbc.M200002200>.
- [43] A. Samuni, E. Maimon, S. Goldstein, Nitroxides protect horseradish peroxidase from H₂O₂-induced inactivation and modulate its catalase-like activity, *Biochim. Biophys. Acta Gen. Subj.* 1861 (2017) 2060–2069, <https://doi.org/10.1016/j.bbagen.2017.03.021>.
- [44] R. Nakajima, I. Yamazaki, The conversion of horseradish peroxidase C to a verdohemoprotein by a hydroperoxide derived enzymatically from indole-3-acetic acid and m-nitroperoxybenzoic acid, *J. Biol. Chem.* 255 (1980) 2067–2071, [https://doi.org/10.1016/S0021-9258\(19\)85994-X](https://doi.org/10.1016/S0021-9258(19)85994-X).
- [45] H. Wariishi, M.H. Gold, Lignin peroxidase compound III: formation, inactivation, and conversion to the native enzyme, *FEBS Lett.* 243 (1989) 165–168, [https://doi.org/10.1016/0014-5793\(89\)80122-X](https://doi.org/10.1016/0014-5793(89)80122-X).
- [46] B. Valderrama, M. Ayala, R. Vazquez-Duhalt, Suicide inactivation of peroxidases and the challenge of engineering more robust enzymes, *Chem. Biol.* 9 (2002) 555–565, [https://doi.org/10.1016/S1074-5521\(02\)00149-7](https://doi.org/10.1016/S1074-5521(02)00149-7).
- [47] H.J.O. Ogola, N. Hashimoto, S. Miyabe, H. Ashida, T. Ishikawa, H. Shibata, Y. Sawa, Enhancement of hydrogen peroxide stability of a novel *Anabaena* sp. DyP-type peroxidase by site-directed mutagenesis of methionine residues, *Appl. Microbiol. Biotechnol.* 87 (2010) 1727–1736, <https://doi.org/10.1007/s00253-010-2603-6>.
- [48] M.B. Arnao, M. Acosta, J.A. del Río, F. García-Cánovas, Inactivation of peroxidase by hydrogen peroxide and its protection by a reductant agent, *Biochim. Biophys. Acta* 1038 (1990) 85–89, [https://doi.org/10.1016/0167-4838\(90\)90014-7](https://doi.org/10.1016/0167-4838(90)90014-7).
- [49] J. Hernández-Ruiz, M.B. Arnao, A.N.P. Hiner, F. García-Cánovas, M. Acosta, Catalase-like activity of horseradish peroxidase: relationship to enzyme inactivation by H₂O₂, *Biochem. J.* 354 (2001) 107–114, <https://doi.org/10.1042/0264-6021.3540107>.
- [50] C. Chen, R. Shrestha, K. Jia, P.F. Gao, B.V. Geisbrecht, S.H. Bossmann, J. Shi, P. Li, Characterization of dye-decolorizing peroxidase (DyP) from *Thermomonospora curvata* reveals unique catalytic properties of A-type DyPs, *J. Biol. Chem.* 290 (2015) 23447–23463, <https://doi.org/10.1074/jbc.M115.658807>.
- [51] A.K. Chaplin, M.T. Wilson, J.A.R. Worrall, Kinetic characterisation of a dye decolorising peroxidase from *Streptomyces lividans*: new insight into the mechanism of anthraquinone dye decolorisation, *Dalton Trans.* 46 (2017) 9420–9429, <https://doi.org/10.1039/c7dt01144j>.
- [52] T. Uchida, M. Sasaki, Y. Tanaka, K. Ishimori, A dye-decolorizing peroxidase from *Vibrio cholerae*, *Biochemistry* 54 (2015) 6610–6621, <https://doi.org/10.1021/acs.biochem.5b00952>.
- [53] A. Rai, J.P. Klare, P.Y.A. Reinke, F. Englmaier, J. Fohrer, R. Fedorov, M.H. Taft, I. Chizhov, U. Curth, O. Plettenburg, D.J. Manstein, Structural and biochemical characterization of a dye-decolorizing peroxidase from *Dictyostelium discoideum*, *Int. J. Mol. Sci.* 22 (2021) 6265, <https://doi.org/10.3390/ijms22126265>.
- [54] Y. Tang, A. Mu, Y. Zhang, S. Zhou, W. Wang, Y. Lai, X. Zhou, F. Liu, X. Yang, H. Gong, Q. Wang, Z. Rao, Cryo-EM structure of *Mycobacterium smegmatis* DyP-loaded encapsulin, *Proc. Natl. Acad. Sci. U.S.A.* 118 (2021) e2025658118, <https://doi.org/10.1073/pnas.2025658118>.
- [55] J. Juanhuix, F. Gil-Ortiz, G. Cuni, C. Colldelram, J. Nicolás, J. Lidón, E. Boter, C. Ruget, S. Ferrer, J. Benach, Developments in optics and performance at BL13-XALOC, the macromolecular crystallography beamline at the ALBA Synchrotron, *J. Synchrotron Radiat.* 21 (2014) 679–689, <https://doi.org/10.1107/S160057751400825X>.
- [56] A. Vagin, A. Teplyakov, MOLREP: an automated program for molecular replacement, *J. Appl. Crystallogr.* 30 (1997) 1022–1025, <https://doi.org/10.1107/S0021889897006766>.
- [57] E.J. Dodson, M. Winn, A. Ralph, A Collaborative Computational Project, number 4: providing programs for protein crystallography, *Methods Enzymol.* 277 (1997) 620–633, [https://doi.org/10.1016/S0076-6879\(97\)77034-4](https://doi.org/10.1016/S0076-6879(97)77034-4).
- [58] H.R. Powell, O. Johnson, A.G.W. Leslie, Autoindexing diffraction images with iMosflm, *Acta Crystallogr. D Biol. Crystallogr.* 69 (2013) 1195–1203, <https://doi.org/10.1107/S0907444912048524>.
- [59] M.D. Winn, C.C. Ballard, K.D. Cowtan, E.J. Dodson, P. Emsley, P.R. Evans, R. M. Keegan, E.B. Krissinel, A.G.W. Leslie, A. McCoy, S.J. McNicholas, G. N. Murshudov, N.S. Pannu, E.A. Potterton, H.R. Powell, R.J. Read, A. Vagin, K. S. Wilson, Overview of the CCP4 suite and current developments, *Acta Crystallogr. D Biol. Crystallogr.* 67 (2011) 235–242, <https://doi.org/10.1107/S0907444910045749>.
- [60] G.N. Murshudov, A.A. Vagin, E.J. Dodson, Refinement of macromolecular structures by the maximum-likelihood method, *Acta Crystallogr. D Biol. Crystallogr.* 53 (1997) 240–255, <https://doi.org/10.1107/S0907444996012255>.
- [61] P. Emsley, B. Lohkamp, W.G. Scott, K. Cowtan, Features and development of Coot, *Acta Crystallogr. D Biol. Crystallogr.* 66 (2010) 486–501, <https://doi.org/10.1107/S0907444910007493>.
- [62] P.D. Adams, R.W. Grosse-Kunstleve, L.W. Hung, T.R. Ioerger, A.J. McCoy, N. W. Moriarty, R.J. Read, J.C. Sacchettini, N.K. Sauter, T.C. Terwilliger, PHENIX: building new software for automated crystallographic structure determination, *Acta Crystallogr. D Biol. Crystallogr.* 58 (2002) 1948, <https://doi.org/10.1107/S0907444902016657>. –1954.
- [63] E.F. Pettersen, T.D. Goddard, C.C. Huang, G.S. Couch, D.M. Greenblatt, E.C. Meng, T.E. Ferrin, UCSF Chimera - a visualization system for exploratory research and analysis, *J. Comput. Chem.* 25 (2004) 1605–1612, <https://doi.org/10.1002/jcc.20084>.
- [64] W. Tian, C. Chen, X. Lei, J. Zhao, J. Liang, CASTp 3.0: computed atlas of surface topography of proteins, *Nucleic Acids Res.* 46 (2018) W363–W367, <https://doi.org/10.1093/nar/gky473>.
- [65] E. Chovancova, A. Pavelka, P. Benes, O. Strnad, J. Brezovsky, B. Kozlikova, A. Gora, V. Sustr, M. Klvana, P. Medek, L. Biedermannova, J. Sochor, J. Damborsky, Caver 3.0: a tool for the analysis of transport pathways in dynamic protein structures, *PLoS Comput. Biol.* 8 (2012) e1002708, <https://doi.org/10.1371/journal.pcbi.1002708>.
- [66] E. Krissinel, K. Henrick, Inference of macromolecular assemblies from crystalline state, *J. Mol. Biol.* 372 (2007) 774–797, <https://doi.org/10.1016/j.jmb.2007.05.022>.
- [67] D.P. Nelson, L.A. Kiesow, Enthalpy of decomposition of hydrogen peroxide by catalase at 25° C (with molar extinction coefficients of H₂O₂ solutions in the UV), *Anal. Biochem.* 49 (1972) 474–478, [https://doi.org/10.1016/0003-2697\(72\)90451-4](https://doi.org/10.1016/0003-2697(72)90451-4).
- [68] D. Kracher, S. Scheiblbrandner, A.K.G. Felice, E. Breslmayr, M. Preims, K. Ludwicka, D. Haltrich, V.G.H. Eijsink, R. Ludwig, Extracellular electron transfer systems fuel cellulose oxidative degradation, *Science* 352 (2016) 1098–1101, <https://doi.org/10.1126/science.1250663>.
- [69] P.C.E. Moody, E. Lloyd Raven, The nature and reactivity of ferryl heme in Compounds I and II, *Acc. Chem. Res.* 51 (2018) 427–435, <https://doi.org/10.1021/acs.accounts.7b00463>.
- [70] A. Cornish-Bowden, *Fundamentals of Enzyme Kinetics*, revised ed., Portland Press Ltd., London, 1999.
- [71] A. Fersht, *Structure and Mechanism in Protein Science: A Guide to Enzyme Catalysis and Protein Folding*, W.H. Freeman and Company, New York, 1999.
- [72] M. Paumann-Page, P.G. Fürtmüller, S. Hofbauer, L.N. Paton, C. Obinger, A. J. Kettle, Inactivation of human myeloperoxidase by hydrogen peroxide, *Arch. Biochem. Biophys.* 539 (2013) 51–62, <https://doi.org/10.1016/j.abb.2013.09.004>.
- [73] X. Bao, X. Huang, X. Lu, J.-J. Li, Improvement of hydrogen peroxide stability of *Pleurotus eryngii* versatile ligninolytic peroxidase by rational protein engineering, *Enzym. Microb. Technol.* 54 (2014) 51–58, <https://doi.org/10.1016/j.enzmictec.2013.10.003>.
- [74] V. Sáez-Jiménez, S. Acebes, V. Guallar, A.T. Martínez, F.J. Ruiz-Dueñas, Improving the oxidative stability of a high redox potential fungal peroxidase by rational design, *PLoS One* 10 (2015) e0124750, <https://doi.org/10.1371/journal.pone.0124750>.
- [75] P. Pérez Galende, N. Hidalgo Cuadrado, E.Y. Kostetsky, M.G. Roig, E. Villar, V. L. Shnyrov, J.F. Kennedy, Kinetics of Spanish broom peroxidase obeys a Ping-Pong Bi-Bi mechanism with competitive inhibition by substrates, *Int. J. Biol. Macromol.* 81 (2015) 1005–1011, <https://doi.org/10.1016/j.ijbiomac.2015.09.042>.
- [76] Y. Zhang, H. Hess, Inhibitors in commercially available 2,2'-azino-bis(3-ethylbenzothiazoline-6-sulfonate) affect enzymatic assays, *Anal. Chem.* 92 (2020) 1502–1510, <https://doi.org/10.1021/acs.analchem.9b04751>.
- [77] S.L. Scott, W.J. Chen, A. Bakac, J.H. Espenson, Spectroscopic parameters, electrode potentials, acid ionization constants, and electron exchange rates of the 2,2'-azino-bis(3-ethylbenzothiazoline-6-sulfonate) radicals and ions, *J. Phys. Chem.* 97 (1993) 6710–6714, <https://doi.org/10.1021/j100127a022>.
- [78] B. Branchi, C. Galli, P. Gentili, Kinetics of oxidation of benzyl alcohols by the dication and radical cation of ABTS. Comparison with laccase-ABTS oxidations: an apparent paradox, *Org. Biomol. Chem.* 3 (2005) 2604–2614, <https://doi.org/10.1039/b504199f>.
- [79] R. Rahmampour, D. Rea, S. Jamshidi, V. Fülöp, T.D.H. Bugg, Structure of *Thermobifida fusca* DyP-type peroxidase and activity towards Kraft lignin and lignin model compounds, *Arch. Biochem. Biophys.* 594 (2016) 54–60, <https://doi.org/10.1016/j.abb.2016.02.019>.
- [80] C. Schmidt-Dannert, Biocatalytic portfolio of basidiomycota, *Curr. Opin. Chem. Biol.* 31 (2016) 40–49, <https://doi.org/10.1016/j.cbpa.2016.01.002>.
- [81] M.L.C. Petrus, E. Vijgenboom, A.K. Chaplin, J.A.R. Worrall, G.P. van Wezel, D. Claessen, The DyP-type peroxidase DtpA is a Tat-substrate required for GlxA maturation and morphogenesis in *Streptomyces*, *Open Biol* 6 (2016) 150149, <https://doi.org/10.1098/rsob.150149>.
- [82] S. Kitajima, M. Kitamura, N. Koja, Triple mutation of Cys26, Trp35, and Cys126 in stromal ascorbate peroxidase confers H₂O₂ tolerance comparable to that of the cytosolic isoform, *Biochem. Biophys. Res. Commun.* 372 (2008) 918–923, <https://doi.org/10.1016/j.bbrc.2008.05.160>.
- [83] S. Kitajima, Hydrogen peroxide-mediated inactivation of two chloroplasmic peroxidases, ascorbate peroxidase and 2-Cys peroxidoredoxin, *Photochem. Photobiol.* 84 (2008) 1404–1409, <https://doi.org/10.1111/j.1751-1097.2008.00452.x>.
- [84] M. Lucić, M.T. Wilson, D.A. Svistunenko, R.L. Owen, M.A. Hough, J.A.R. Worrall, Aspartate or arginine? Validated redox state X-ray structures elucidate mechanistic subtleties of Fe^V = O formation in bacterial dye-decolorizing peroxidases, *J. Biol. Inorg. Chem.* 26 (2021) 743–761, <https://doi.org/10.1007/s00775-021-01896-2>.

Supplementary material to:

Dye-decolorizing peroxidase of *Thermobifida halotolerance* displays complex kinetics with both substrate inhibition and apparent positive cooperativity

Hegne Pupart^a, Tiit Lukk^a, and Priit Väljamäe^{b*}

^a Department of Chemistry and Biotechnology, Tallinn University of Technology, Akadeemia tee 15, 12618 Tallinn, Estonia

^b Institute of Molecular and Cell Biology, University of Tartu, Riia 23b-202, 51010 Tartu, Estonia.

Correspondence

Priit Väljamäe; E-mail: priit.valjamae@ut.ee

TABLE OF CONTENTS

	Page
Supplementary figures	
Figure S1. Dependency of the Hill coefficient for the oxidation of ABTS on the concentration of H ₂ O ₂ .	2
Figure S2. Dependency of the optimal concentration of H ₂ O ₂ ([H ₂ O ₂] _{opt}) for the oxidation of ABTS on the concentration of ABTS.	2
Figure S3. Time dependency of the inactivation of <i>ThDyP</i> by H ₂ O ₂ and ABTS.	3
Figure S4. Changes in absorbance spectrum of <i>ThDyP</i> upon titration with H ₂ O ₂ .	3
Figure S5. Oxidation of ABTS by <i>ThDyP</i> in the absence of added H ₂ O ₂ .	4
Figure S6. SDS-PAGE analysis of <i>ThDyP</i> pre-incubated with H ₂ O ₂ .	4
Figure S7. Gel filtration chromatography analysis of <i>ThDyP</i> .	5
Figure S8. <i>ThDyP</i> is not capable of two electron oxidation of ABTS.	6
Figure S9. Cysteine and methionine residues in <i>ThDyP</i> .	7
Supplementary tables	
Table S1. Values of apparent kinetic parameters for H ₂ O ₂ .	8
Table S2. Values of apparent kinetic parameters for ABTS.	8
Table S3. Definitions of binding constants.	9
Table S4. Data collection and refinement statistics for DyP from <i>Thermobifida halotolerans</i> .	10
Supplementary results	
Derivation of steady-state rate equations:	11
For the kinetic mechanism in Figure 2B of the main article.	11
For the kinetic mechanism in Figure 5A of the main article (k_{red} route shown with solid arrow in Figure 5A of the main article).	13
For the kinetic mechanism in Figure 5A of the main article (k_{red} route shown with dashed arrow in Figure 5A of the main article).	14

Supplementary figures

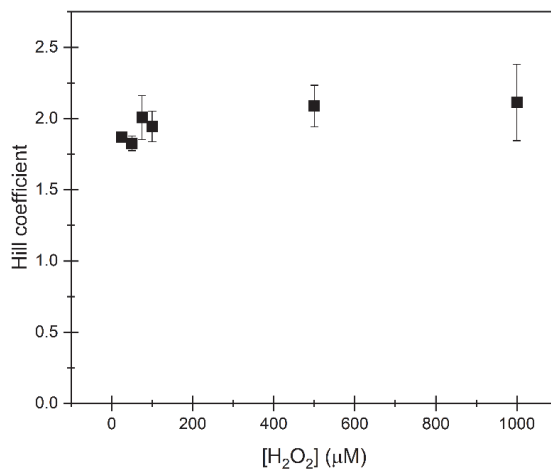


Figure S1. Dependency of the Hill coefficient for the oxidation of ABTS on the concentration of H₂O₂. The values of Hill coefficient (h) were determined using non-linear regression analysis of the data on Figure 1A according to the eq 2. In analyses according to eq 2, the datasets were limited with the highest concentration of ABTS of 2 mM (i.e., data points showing substrate inhibition were not included).

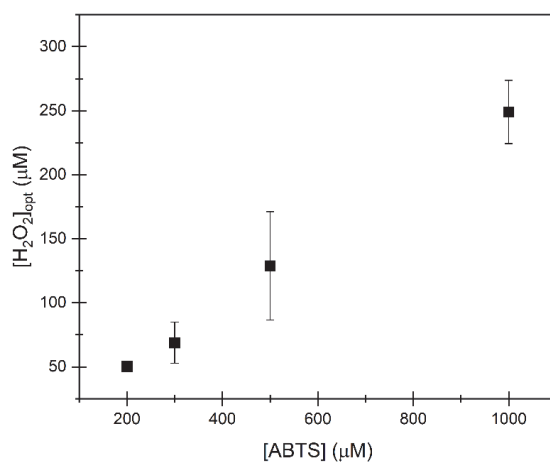


Figure S2. Dependency of the optimal concentration of H₂O₂ ([H₂O₂]_{opt}) for the oxidation of ABTS on the concentration of ABTS. The value of [H₂O₂]_{opt} was found using the eq 3 and K_m^{app} and K_i^{app} values for H₂O₂ obtained from non-linear regression analysis of the data in Figure 1B according to the eq 1.

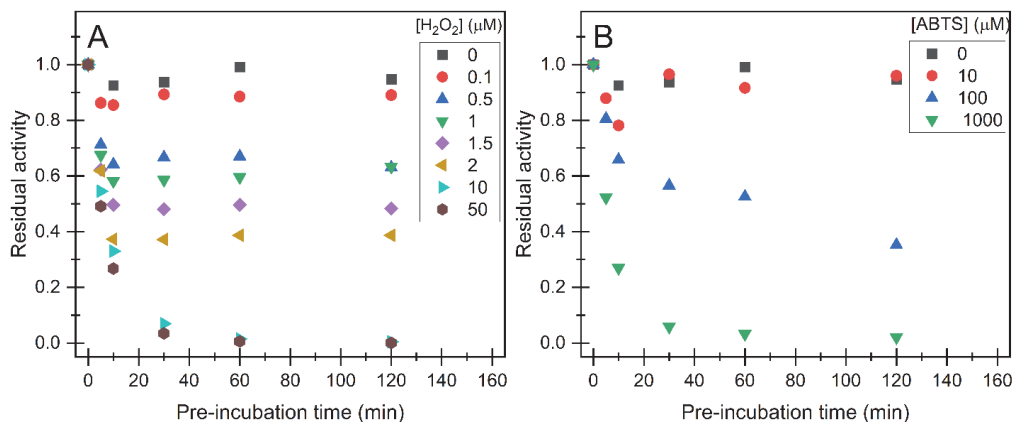


Figure S3. Time dependency of the inactivation of *ThDyP* by H₂O₂ and ABTS. *ThDyP* (0.9 μM) was pre-incubated with (A) H₂O₂ (0.1–50 μM) or (B) ABTS (10–1000 μM) in sodium acetate (50 mM, pH 5.0, supplemented with 0.1 g L⁻¹ BSA) at 25 °C. After pre-incubation the residual ABTS oxidizing activity of *ThDyP* was measured using 1 mM ABTS, 1 mM H₂O₂, and 9 nM total *ThDyP*. Before the addition of H₂O₂/ABTS, 1.0 μM *ThDyP* was incubated in sodium acetate (50 mM, pH 5.0, supplemented with 0.1 g L⁻¹ BSA) at 25 °C for 30 min. After that, an aliquot was withdrawn for measurement of zero-time pre-incubation activity. Residual activity is defined as the ratio of activity at defined pre-incubation time to the zero-time pre-incubation activity (see above). Concentrations of H₂O₂ and ABTS in pre-incubation are defined in the plot. These pre-incubation time screening experiments were made in single parallel.

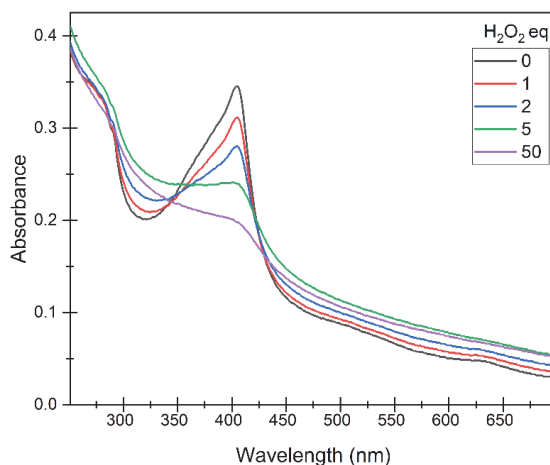


Figure S4. Changes in absorbance spectrum of *ThDyP* upon titration with H₂O₂. The absorbance of *ThDyP* (3.135 μM) was measured in 50 mM sodium acetate, pH 5.0 (absorbance of buffer is subtracted). H₂O₂ was added as aliquots of 313.5 μM stock solution (5 μL per 1 mole equivalent of *ThDyP*) and spectrums were recorded 30 min after the addition of H₂O₂. The initial volume before the addition of H₂O₂ was 500 μL and final volume (after the addition of 50 equivalents of H₂O₂) was 750 μL. The color code of added H₂O₂ equivalents is given in the plot.

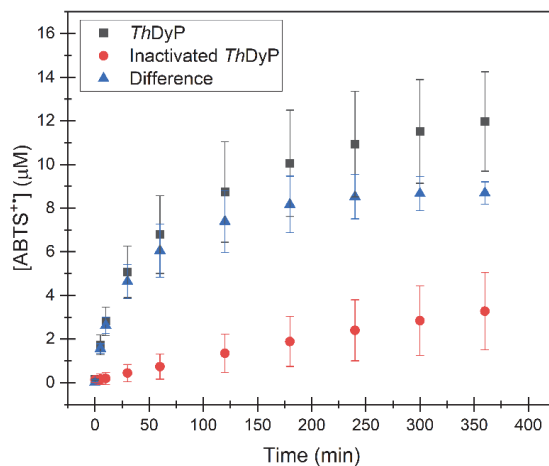


Figure S5. Oxidation of ABTS by *ThDyP* in the absence of added H₂O₂. ABTS (1.0 mM) was incubated with 1.0 μM *ThDyP* in sodium acetate (50 mM, pH 5.0, supplemented with 0.1 g L⁻¹ BSA) at 25 °C. Product (ABTS^{•+}) formation was quantified by the increase in absorbance at 420 nm using extinction coefficient of 36.0 mM⁻¹ cm⁻¹. Shown are average values of two independent experiments. In one series (designated as “Inactivated-*ThDyP*”) the *ThDyP* was inactivated by heating at 95 °C for 10 min before using in the experiment. Shown are also the difference between series made with active and inactivated *ThDyP* (designates as “Difference”).

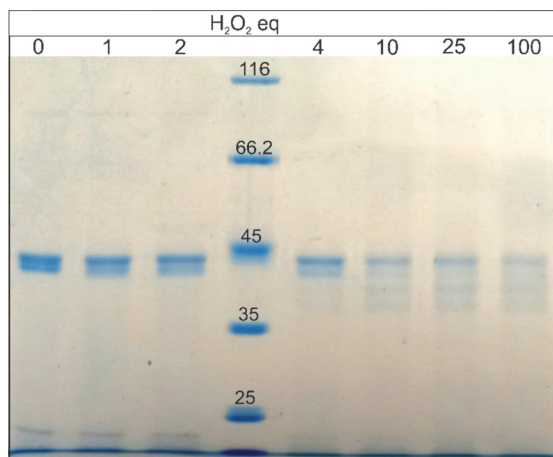


Figure S6. SDS-PAGE analysis of *ThDyP* pre-incubated with H₂O₂. 5 μM *ThDyP* in 50 mM sodium acetate pH 5.0 was incubated with 0–500 μM H₂O₂ (H₂O₂ equivalents are shown on the image) for 10 min before the analysis with SDS-PAGE.

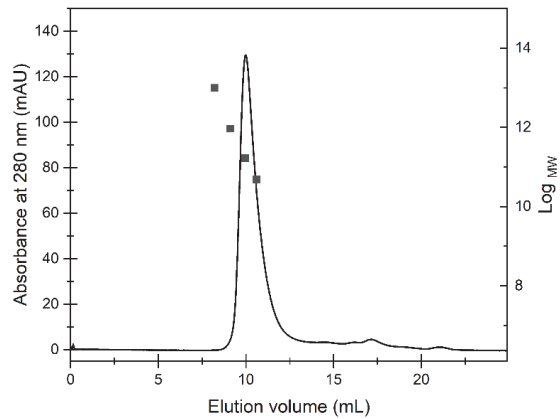


Figure S7. Gel filtration chromatography analysis of *ThDyP*. 0.1 mL *ThDyP* in 50 mM sodium acetate pH 5.0 was applied to a Superdex™ 75 Increase 10/300 GL column equilibrated with the same buffer. The mobility of standard proteins (Ovalbumin, 44 kDa; Conalbumin, 75 kDa, Aldolase, 158 kDa; and Ferritin, 440 kDa) was used to construct the calibration curve (shown in a secondary y-axes). *ThDyP* eluted as a single dominant peak with an apparent molecular weight of 75 kDa. Theoretical molecular weight of the monomeric *ThDyP* is 45.4 kDa.

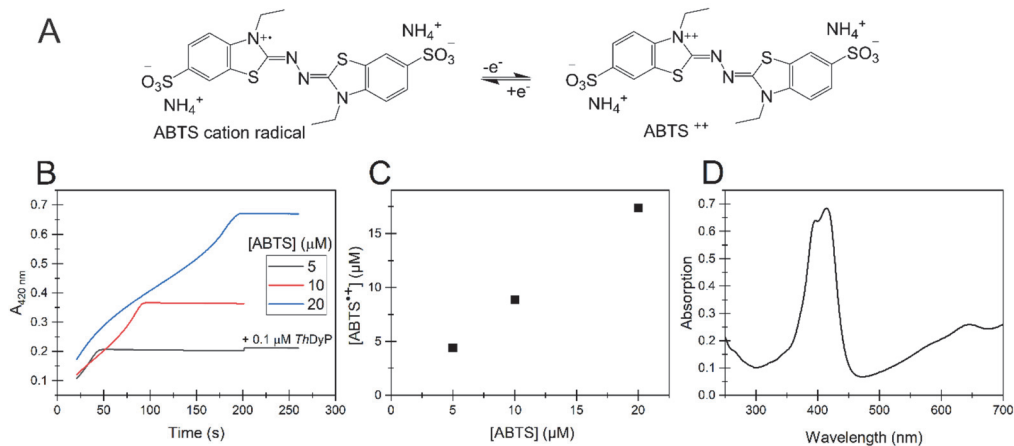


Figure S8. *ThDyP* is not capable of two electron oxidation of ABTS. (A) Schematic representation of the oxidation of one electron oxidized ABTS (ABTS^{•••}) to two electron oxidized ABTS (ABTS^{•••}). ABTS^{•••} has absorbance maximum at 420 nm while ABTS^{•••} has no significant absorbance at 420 nm. 0.1 μM *ThDyP* was incubated with 100 μM H₂O₂ and 5, 10, and 20 μM ABTS in 50 mM sodium acetate pH 5.0 (supplemented with 0.1 g L⁻¹ BSA) at 25 °C. (B) Time curves showing oxidation of ABTS to ABTS^{•••} (absorbance maximum at 420 nm). In series with 5 μM ABTS, a fresh portion (equal to the first one) of *ThDyP* was added after 200 s. No changes in absorbance at 420 nm was observed upon addition of fresh portion of *ThDyP* indicating that ABTS was depleted and ABTS^{•••} was not further oxidized to ABTS^{•••} (note that the small increase in the absorbance upon addition of the fresh portion of *ThDyP* is caused by the absorbance of the heme at 420 nm). (C) Correlation between the concentration of ABTS^{•••} formed upon oxidation of ABTS by *ThDyP* (calculated from the plateau values of the absorbance at 420 nm in panel B using $\epsilon_{420} = 36,000 \text{ M}^{-1} \text{ cm}^{-1}$ for ABTS^{•••}) and initial concentration of ABTS in the cuvette. (D) Absorbance spectrum of the reaction mixture with 20 μM ABTS (from panel B) measured after 10 min of the reaction. Panels B and C show average results from three independent experiments. Spectrum in panel D is measured in single parallel.

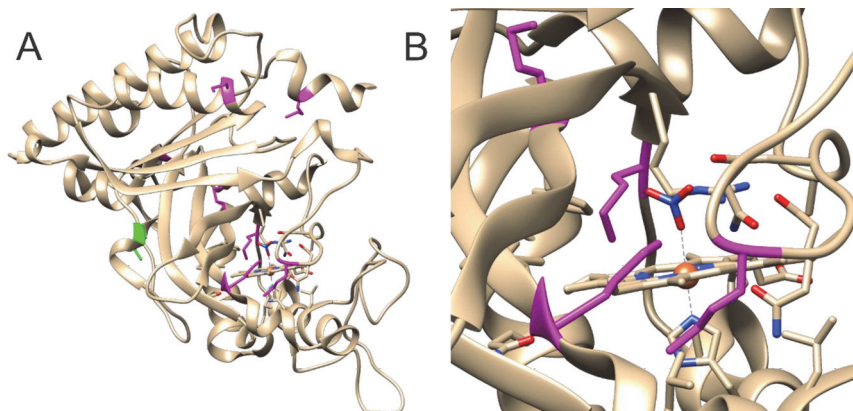


Figure S9. Cysteine and methionine residues in *ThDyP*. (A) Structure of *ThDyP* monomer (PDB ID: 8CK9). The heme is in stick representation and iron is shown as sphere (brown). The nitrate ion is located at the distal side of the heme. There is one cysteine (green) and several methionine (magenta) residues in the structure of *ThDyP*, of which three of them are in the proximity of the heme. (B) Zoom in of the heme in the structure of *ThDyP*. The heme molecule, iron and nitrate ions, and methionine residues are depicted in the same colors as is panel A.

Supplementary tables

Table S1. Values of apparent kinetic parameters for H₂O₂ at different concentrations of ABTS. Parameter values were obtained from nonlinear regression analysis of the data in Figure 1B according to eq 1. Error bars show fitting errors.

ABTS (μM)	$k_{\text{cat}}^{\text{app}}$ (s^{-1})	$K_{\text{m}(\text{H}_2\text{O}_2)}^{\text{app}}$ (μM)	$K_{\text{i}(\text{H}_2\text{O}_2)}^{\text{app}}$ (μM)	$k_{\text{cat}}^{\text{app}}/K_{\text{m}(\text{H}_2\text{O}_2)}^{\text{app}}$ ($\mu\text{M}^{-1} \text{s}^{-1}$)
50	2.5 ± 0.1	2.0 ± 0.6	poorly defined	1.27 ± 0.38
75	2.8 ± 0.1	0.9 ± 0.3	poorly defined	3.0 ± 1.0
100	3.4 ± 0.2	1.0 ± 0.4	poorly defined	3.5 ± 1.4
200	9.8 ± 0.6	5.2 ± 1.0	491 ± 112	1.90 ± 0.37
300	16 ± 1	9.0 ± 2.1	507 ± 127	1.82 ± 0.42
500	35 ± 3	25 ± 5	632 ± 125	1.40 ± 0.28
1000	73 ± 8	61 ± 13	1033 ± 281	1.20 ± 0.26
2000	64 ± 2	49 ± 6	poorly defined	1.30 ± 0.16
3000	58 ± 2	57 ± 8	poorly defined	1.00 ± 0.14
5000	53 ± 7	138 ± 29	poorly defined	0.39 ± 0.08

Table S2. Values of apparent kinetic parameters for ABTS at different concentrations of H₂O₂. Parameter values were obtained from nonlinear regression analysis of the data in Figure 1A according to eq 1 or eq 2 as defined in the table. Error bars show fitting errors. In analyses according to eq 2 the datasets were limited with the highest concentration of ABTS of 2 mM.

H ₂ O ₂ (μM)	Model	$k_{\text{cat}}^{\text{app}}$ (s^{-1})	$K_{\text{m}(\text{ABTS})}^{\text{app}}$ (μM)	$K_{\text{i}(\text{ABTS})}^{\text{app}}$ (μM)	h	$K_{0.5(\text{ABTS})}$ (μM)
1	eq 1	2.0 ± 0.1	33 ± 8	1283 ± 218		
2	eq 1	4.7 ± 0.5	110 ± 23	856 ± 172		
5	eq 1	16 ± 2	392 ± 66	595 ± 99		
10	eq 1	156 ± 182	poorly defined	105 ± 131		
25	eq 2	20 ± 1			1.9 ± 0.2	255 ± 23
50	eq 2	35 ± 2			1.8 ± 0.3	404 ± 43
75	eq 2	47 ± 3			2.0 ± 0.3	417 ± 44
100	eq 2	50 ± 2			1.9 ± 0.2	502 ± 42
500	eq 2	67 ± 5			2.1 ± 0.2	745 ± 75
1000	eq 2	72 ± 7			2.1 ± 0.3	981 ± 122

Table S3. Definitions of binding constants. Definitions of binding constants appearing in the rate equations in the main article (derived using rapid equilibrium assumption) in terms of rate constants (defined in Schemes S1–S3) for the rapid equilibrium and steady-state solutions of the kinetic mechanisms in Schemes S1–S3.

Apparent binding constant	Rapid equilibrium (no. of eq)	Steady-state (no. of eq)
$K_{\text{H}_2\text{O}_2}$	k_{-1}/k_1 (eq 4)	$(k_{-1}+k_{\text{ox}})/k_1$ (eq S7)
$K_{\text{S}1}$	k_{-2}/k_2 (eq 4)	$(k_{-2}+k_{\text{red}1})/k_2$ (eq S7)
$K_{\text{S}2}$	k_{-3}/k_3 (eq 4)	$(k_{-3}+k_{\text{red}2})/k_3$ (eq S7)
$K_{\text{H}_2\text{O}_2}$	k_{-1}/k_1 (eq 5)	$(k_{-1}+k_{\text{ox}})/k_1$ (eq S8)
K_{S}	k_{-2}/k_2 (eq 5)	$k_{-2}/k_2 + k_3k_{\text{red}}[\text{S}]/k_2(k_{-3}+k_{\text{red}})$ (eq S8)
K_{SS}	k_{-3}/k_3 (eq 5)	$(k_{-3}+k_{\text{red}})/k_3$ (eq S8)
$K_{\text{H}_2\text{O}_2}$	k_{-1}/k_1 (eq 6)	$(k_{-1}+k_{\text{ox}})/k_1$ (eq S9)
K_{S}	k_{-2}/k_2 (eq 6)	$(k_{-2}+k_{\text{red}})/k_2$ (eq S9)

Table S4. Data collection and refinement statistics for DyP from *Thermobifida halotolerans*

<i>ThDyP</i>	
Data collection	
Wavelength (Å)	0.97926
Space group	C222 ₁
Unit Cell (a,b,c) (Å)	70.36, 78.37,135.65
Resolution range (Å) ¹	29.6-1.6 (1.63-1.60)
Total reflections	338025
Unique reflections	49674
Multiplicity	6.8 (4.7)
Completeness (%)	99.9 (99.8)
Mean I/sigma (I)	11.5 (4.7)
R-merge (%) ²	10.0 (27.7)
R-meas (%)	10.8 (30.2)
CC ½	0.993 (0.954)
Refinement	
Resolution (Å)	29.61-1.60
Number of reflections	49628
R-work	15.8
R-free ³	18.7
Number of atoms	3333
Protein	2867
Heme	43
Water	423
NO ₃	4
Average B-factor	
Macromolecules	18.2
Heme	10.0
Solvent	28.5
NO ₃	25.9
RMS (bond lengths)	0.006
RMS (bond angles)	0.829
Favored (%)	98.66
Allowed (%)	1.34
Outliers (%)	0
Rotamer outliers (%)	0.35
Clashscore	0.52
PDB code	8CK9

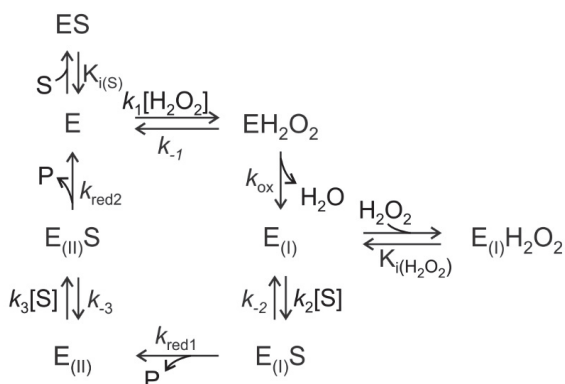
Supplementary results

Derivation of steady-state rate equations

Kinetic mechanism in Figure 2B of the main article

In the main article the kinetic mechanisms were solved using an assumption that all binding steps are in equilibrium (rapid equilibrium assumption). Here we solve the same kinetic mechanisms using more general, steady-state assumption. The equilibrium assumption is used only for the dead-end complexes as these can be only at equilibrium.

The kinetic mechanism of Figure 2B of the main article is shown in Scheme S1 below but the equilibrium dissociation constants of non-dead-end complexes are replaced with corresponding rate constants.



Scheme S1. Shown is the scheme in the figure 2B of the main article but equilibrium dissociation constants are replaced with the rate constants as follows: $K_{H_2O_2} = k_{-1}/k_1$, $K_{S1} = k_{-2}/k_2$, and $K_{S2} = k_{-3}/k_3$. P is the single electron oxidized product. E, E(I), and E(II), stand for the enzyme resting state, Cpd I, and Cpd II, respectively. The steady-state concentration of dead-end complexes, ES and E(II)H₂O₂, is given by corresponding equilibrium dissociation constants as in figure 2B of the main article.

To derive the steady-state rate equation the reversible steps in Scheme S1 were first converted to the first order net rate constants which are as follows.

For:

$$E \xrightarrow{k_1'} EH_2O_2 \quad k_1' = \frac{k_1[H_2O_2]k_{ox}}{k_{-1} + k_{ox}} \quad (S1)$$

$$E(I) \xrightarrow{k_2'} E(I)S \quad k_2' = \frac{k_2[S]k_{red1}}{k_{-2} + k_{red1}} \quad (S2)$$

$$E(II) \xrightarrow{k_3'} E(II)S \quad k_3' = \frac{k_3[S]k_{red2}}{k_{-3} + k_{red2}} \quad (S3)$$

The steady-state rate of the formation of single electron oxidized product (P) is given by

$$v = -\frac{d[H_2O_2]}{dt} = 2\frac{d[P]}{dt} = k_{ox}[EH_2O_2] \quad (S4)$$

Steady-state concentration of EH_2O_2 complex can be found as a product of total enzyme concentration (E_0) and the ratio of its transit time ($1/k_{ox}$) to the total transit time.

$$[EH_2O_2] = \frac{E_0 \frac{1}{k_{ox}}}{\frac{1}{k_1} \left(1 + \frac{[S]}{K_{i(S)}}\right) + \frac{1}{k_{ox}} + \frac{1}{k_2} \left(1 + \frac{[H_2O_2]}{K_{i(H_2O_2)}}\right) + \frac{1}{k_{red1}} + \frac{1}{k_3} + \frac{1}{k_{red2}}} \quad (S5)$$

Combining equations S4 and S5 results in:

$$v = -\frac{d[H_2O_2]}{dt} = 2\frac{d[P]}{dt} = k_{ox}[EH_2O_2] = \frac{E_0}{\frac{1}{k_1} \left(1 + \frac{[S]}{K_{i(S)}}\right) + \frac{1}{k_{ox}} + \frac{1}{k_2} \left(1 + \frac{[H_2O_2]}{K_{i(H_2O_2)}}\right) + \frac{1}{k_{red1}} + \frac{1}{k_3} + \frac{1}{k_{red2}}} \quad (S6)$$

Replacing the first order net rate constants in eq S6 with eq-s S1–S3 and rearranging results in the steady-state rate equation for the mechanism depicted in Scheme S1.

$$\frac{v}{E_0} = \frac{k_{cat}[S][H_2O_2]}{[S][H_2O_2] + \frac{k_{cat}(k_{-1} + k_{ox})}{k_{ox}k_1}[S] \left(1 + \frac{[S]}{K_{i(S)}}\right) + \frac{k_{cat}(k_{-2} + k_{red1})}{k_{red1}k_2}[H_2O_2] \left(1 + \frac{[H_2O_2]}{K_{i(H_2O_2)}}\right) + \frac{k_{cat}(k_{-3} + k_{red2})}{k_{red2}k_3}[H_2O_2]} \quad (S7)$$

For convenient comparison, the rate equation obtained using rapid equilibrium treatment (eq 4 of the main article) is reiterated below.

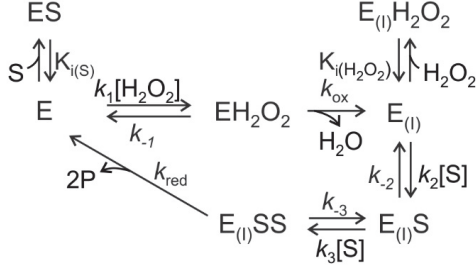
$$\frac{v}{E_0} = \frac{k_{cat}[S][H_2O_2]}{[S][H_2O_2] + \frac{k_{cat}K_{H_2O_2}}{k_{ox}}[S] \left(1 + \frac{[S]}{K_{i(S)}}\right) + \frac{k_{cat}K_{S1}}{k_{red1}}[H_2O_2] \left(1 + \frac{[H_2O_2]}{K_{i(H_2O_2)}}\right) + \frac{k_{cat}K_{S2}}{k_{red2}}[H_2O_2]} \quad (\text{eq 4 of the main article})$$

As in the eq 4 of the main article the k_{cat} in eq S7 is defined as:

$$k_{cat} = \frac{k_{ox}k_{red1}k_{red2}}{k_{ox}k_{red1} + k_{ox}k_{red2} + k_{red1}k_{red2}}$$

Note that the eq S7 is the same as eq 4 that was derived using rapid equilibrium assumption but the equilibrium dissociation constants have different expressions in terms of individual rate constants (Table S3).

Kinetic mechanism in Figure 5A of the main article (k_{red} route shown with solid arrow in Figure 5A of the main article).



Scheme S2. Shown is the scheme in the figure 5A of the main article (k_{red} route shown with solid arrow) but equilibrium dissociation constants are replaced with the rate constants as follows: $K_{H_2O_2}=k_{-1}/k_1$, $K_S=k_{-2}/k_2$, and $K_{SS}=k_{-3}/k_3$. P is the single electron oxidized product. E, and $E_{(1)}$ stand for the enzyme resting state, and Cpd I, respectively. The steady-state concentration of dead-end complexes, ES and $E_{(1)}H_2O_2$, is given by corresponding equilibrium dissociation constants as in figure 5A of the main article.

Like for Scheme S1 the reversible steps in Scheme S2 were first converted to the first order net rate constants which are as follows.

$$E \xrightarrow{k'_1} EH_2O_2 \quad k'_1 = \frac{k_1[H_2O_2]k_{ox}}{k_{-1}+k_{ox}}$$

$$E_{(1)} \xrightarrow{k'_2} E_{(1)}S \quad k'_2 = \frac{k_2[S]k'_3}{k_{-2}+k'_3}$$

$$E_{(1)}S \xrightarrow{k'_3} E_{(1)}SS \quad k'_3 = \frac{k_3[S]k_{red}}{k_{-3}+k_{red}}$$

Using the net first order rate constants defined above and similar treatment used in deriving the rate equation for Scheme 1 (see eq-s S4 and S5) resulted in the steady-state rate equation S8.

$$\frac{v}{E_0} = -\frac{d[H_2O_2]}{dt} = 2 \frac{d[P]}{dt} = \frac{k_{cat}[S]^2[H_2O_2]}{[S]^2[H_2O_2] + \frac{k_{cat}(k_{-1}+k_{ox})}{k_{ox}k_1}[S]^2 \left(1 + \frac{[S]}{K_i(S)}\right) + \frac{k_{cat}(k_{-3}+k_{red}) \left(\frac{k_{-2} + \frac{k_3 k_{red} [S]}{k_2}}{k_2(k_{-3}+k_{red})}\right)}{k_{red}k_3} [H_2O_2] \left(1 + \frac{[H_2O_2]}{K_i(H_2O_2)}\right) + \frac{k_{cat}(k_{-3}+k_{red})}{k_{red}k_3} [S][H_2O_2]}$$

(S8)

For convenient comparison, the rate equation obtained using rapid equilibrium treatment (eq 4 of the main article) is reiterated below.

$$\frac{v}{E_0} = -\frac{d[H_2O_2]}{dt} = 2 \frac{d[P]}{dt} = \frac{k_{cat}[S]^2[H_2O_2]}{[S]^2[H_2O_2] + \frac{k_{cat}K_{H_2O_2}}{k_{ox}}[S]^2 \left(1 + \frac{[S]}{K_i(S)}\right) + \frac{k_{cat}K_{SS}K_S}{k_{red}}[H_2O_2] \left(1 + \frac{[H_2O_2]}{K_i(H_2O_2)}\right) + \frac{k_{cat}K_{SS}}{k_{red}}[S][H_2O_2]}$$

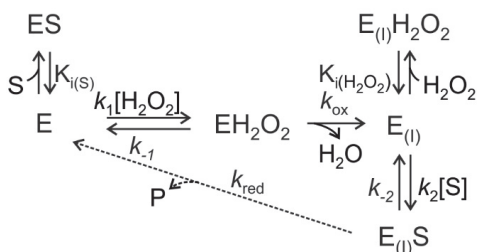
(eq5 of the main article)

As in the eq 5 of the main article the k_{cat} in eq S8 is defined as:

$$k_{cat} = \frac{k_{ox}k_{red}}{k_{ox}+k_{red}}$$

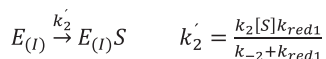
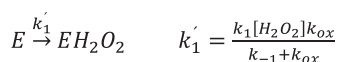
Eq S8 is in the form of eq 5 that was derived using rapid equilibrium assumption but the apparent binding constants have different expressions in terms of individual rate constants and K_S depends on the concentration of the substrate (Table S3).

Kinetic mechanism in Figure 5A of the main article (k_{red} route shown with dashed arrow in Figure 5A of the main article)



Scheme S3. Shown is the scheme in the figure 5A of the main article (k_{red} route shown with dashed arrow) but equilibrium dissociation constants are replaced with the rate constants as follows: $K_{H_2O_2}=k_{-1}/k_1$, and $K_S=k_{-2}/k_2$. P is the two-electron oxidized product. E, and $E_{(I)}$ stand for the enzyme resting state, and Cpd I, respectively. The steady-state concentration of dead-end complexes, ES and $E_{(I)}H_2O_2$, is given by corresponding equilibrium dissociation constants as in figure 5A of the main article.

Again, the reversible steps in Scheme S3 were first converted to the first order net rate constants which are as follows.



Using the same treatment outlined in deriving the rate equation for the Scheme S1 resulted in following rate equation.

$$\frac{v}{E_0} = -\frac{d[H_2O_2]}{dt} = \frac{d[P]}{dt} = \frac{k_{cat}[S][H_2O_2]}{[S][H_2O_2] + \frac{k_{cat}(k_{-1}+k_{ox})}{k_{ox}k_1}[S] \left(1 + \frac{[S]}{K_{i(S)}}\right) + \frac{k_{cat}(k_{-2}+k_{red})}{k_{red}k_2}[H_2O_2] \left(1 + \frac{[H_2O_2]}{K_{i(H_2O_2)}}\right)} \quad (S9)$$

For convenient comparison, the rate equation obtained using rapid equilibrium treatment (eq 6 of the main article) is reiterated below.

$$\frac{v}{E_0} = -\frac{d[H_2O_2]}{dt} = \frac{d[P]}{dt} = \frac{k_{cat}[S][H_2O_2]}{[S][H_2O_2] + \frac{k_{cat}K_{H_2O_2}}{k_{ox}}[S]\left(1 + \frac{[S]}{K_{i(S)}}\right) + \frac{k_{cat}K_S}{k_{red}}[H_2O_2]\left(1 + \frac{[H_2O_2]}{K_{i(H_2O_2)}}\right)} \quad (\text{eq 6 of the main article})$$

The k_{cat} in the eq S9 (and eq 6 of the main article) is defined exactly as in eq S8 (and eq 5 of the main article). Note that in eq S9 (and eq 6 of the main article) the P denotes two electron oxidized product.

The steady-state equation S9 is the same as the one derived using rapid equilibrium treatment (eq 6 of the main article) but apparent binding constants depend on the rate constants of chemical steps (Table S3).

Appendix 3

Publication III

Pupart, H.*; Vastšjonok, D.*; Lukk, T. and Väljamäe, P. Dye-Decolorizing Peroxidase of *Streptomyces coelicolor* (ScDyPB) Exists as a Dynamic Mixture of Kinetically Different Oligomers. *ACS Omega* **2024**, *9*, 3866–3876. <https://doi.org/10.1021/acsomega.3c07963>.

*These authors contributed equally.

Dye-Decolorizing Peroxidase of *Streptomyces coelicolor* (ScDyPB) Exists as a Dynamic Mixture of Kinetically Different Oligomers

Hegne Pupart,[§] Darja Vastšjonok,[§] Tiit Lukk, and Priit Väljamäe*Cite This: *ACS Omega* 2024, 9, 3866–3876

Read Online

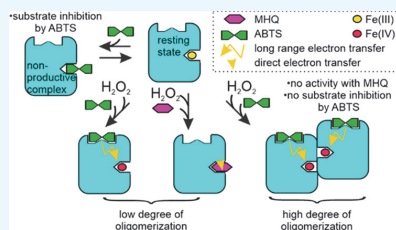
ACCESS |

Metrics & More

Article Recommendations

Supporting Information

ABSTRACT: Dye-decolorizing peroxidases (DyPs) are heme-dependent enzymes that catalyze the oxidation of various substrates including environmental pollutants such as azo dyes and also lignin. DyPs often display complex non-Michaelis–Menten kinetics with substrate inhibition or positive cooperativity. Here, we performed in-depth kinetic characterization of the DyP of the bacterium *Streptomyces coelicolor* (ScDyPB). The activity of ScDyPB was found to be dependent on its concentration in the working stock used to initiate the reactions as well as on the pH of the working stock. Furthermore, the above-listed conditions had different effects on the oxidation of 2,2'-azino-di(3-ethylbenzothiazoline-6-sulfonic acid) (ABTS) and methylhydroquinone, suggesting that different mechanisms are used in the oxidation of these substrates. The kinetics of the oxidation of ABTS were best described by the model whereby ScDyPB exists as a mixture of two kinetically different enzyme forms. Both forms obey the ping-pong kinetic mechanism, but one form is substrate-inhibited by the ABTS, whereas the other is not. Gel filtration chromatography and dynamic light scattering analyses revealed that ScDyPB exists as a complex mixture of molecules with different sizes. We propose that ScDyPB populations with low and high degrees of oligomerization have different kinetic properties. Such enzyme oligomerization-dependent modulation of the kinetic properties adds further dimension to the complexity of the kinetics of DyPs but also suggests novel possibilities for the regulation of their catalytic activity.



INTRODUCTION

Dye-decolorizing peroxidases (EC 1.11.1.19, DyPs) are enzymes that catalyze the oxidation of various substrates using H₂O₂ as an electron acceptor. Although the physiological substrate has not been identified yet, these peroxidases are known to oxidize anthraquinone and azo dyes,¹ β -carotene,² and different phenolic compounds³ including lignin. There has been a growing interest in DyPs due to their biotechnological potential in bioremediation of industrial dyes and valorization of lignin.⁴

To date, over 50 different DyPs have been characterized.^{5,6} These heme-dependent peroxidases are present in both fungal and bacterial species, and the family of DyPs is divided into four subfamilies (type A, B, and C/D) according to their primary sequences (RedOxiBase) with a sequence identity less than 15% between the subfamilies.^{7–10} All DyPs adopt a similar dimeric ferredoxin-like fold consisting of β -sheets and peripheral α -helices, distinct from well-known peroxidases, such as horseradish peroxidase.¹¹ DyPs belong to the CDE superfamily, a part of the “dimeric $\alpha + \beta$ barrel superfamily”.^{12–14} Heme is held in the heme cavity, positioned in the C-terminal domain of the monomer, where it is ligated by a proximal conserved histidine residue.^{9,15}

Being able to degrade bulky textile dyes and even polymeric lignin, DyPs differ from classic peroxidases.^{4,8,9,16} However, like other heme peroxidases, DyPs obey the ping-pong kinetic mechanism, by cycling between the ferric resting state and its

high-valent intermediates compound I (Cpd I) and compound II (Cpd II).⁸ Smaller reducing substrates as well as the H₂O₂ cosubstrate can access the heme through channels that connect heme with the protein exterior.^{17,18} To catalyze the oxidation of substrates with a bulkier size, DyPs are known to apply long-range electron transfer pathways. In this case, the electrons are first transferred from the reducing substrate to the solvent-accessible amino acid residues at the surface (usually Trp or Tyr residues) from where they are further transferred to the high-valent intermediate of heme.^{19,20}

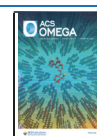
Like for other heme peroxidases, the general ping-pong kinetic mechanism of DyPs is well studied and generally accepted. At the same time, the molecular mechanisms behind the non-Michaelis–Menten kinetics that are often observed with DyPs and characterized by the presence of substrate inhibition^{18,21–26} and cooperative effects^{15,22,27,28} remain largely unknown. The oligomeric state of DyPs varies from monomers to hexamers. Most of the fungal DyPs are monomeric;^{1,22,29–33} however, the existence of dimers has

Received: October 11, 2023

Revised: December 19, 2023

Accepted: December 21, 2023

Published: January 8, 2024



also been described.^{2,34} It has been suggested that loop insertions and the increasing complexity of fungal DyPs favor the monomeric form by hindering the oligomerization.^{11,35} In contrast to their fungal counterparts, the bacterial DyPs exist mostly as oligomers, including dimers,^{11,28,35–41} tetramers,^{26,42,43} pentamers,⁴⁴ and hexamers.^{11,45,46} Nevertheless, some bacterial DyPs have been shown to exist as monomers^{3,26,36,47} or as a mixture of enzyme populations with different degrees of oligomerization such as monomer and dimer^{48–50} and monomer and oligomer ($n = 4–6$).^{51–53} The DyP from *Thermomonospora curvata* was shown to exist as a mixture of dimer, tetramer, and octamer.²⁷ Furthermore, many bacterial DyPs are often loaded as cargo proteins into the encapsulin nanoparticles,^{45,46,53–55} where they exist at an even higher degree of oligomerization.⁵⁴ Although it has been shown that the DyP–encapsulin complex has higher lignin degrading activity compared to nonencapsulated DyP⁴⁵ and that monomeric forms may be deficient in the binding of heme,^{50,52,53} little is known about the relations between the degree of oligomerization of DyPs and their catalytic activity.

Here, we performed an in-depth kinetic characterization of the subfamily B DyP of the bacterium *Streptomyces coelicolor* (ScDyPB) along with analyses of its size distribution. Our results suggest that ScDyPB exists as a mixture of enzyme forms with different degrees of oligomerization, which differed in their catalytic properties.

MATERIALS AND METHODS

ABTS (lot no. SLBT0759) and methylhydroquinone MHQ (lot no. BCBH9920 V) were purchased from Sigma-Aldrich. BSA (lot no. K00113-2235, Fraction V) was obtained from GE Healthcare. The concentration of the H₂O₂ stock solution (Honeywell, lot # SZBG2070) was determined spectrophotometrically at 240 nm using an extinction coefficient of 39.4 M⁻¹ cm⁻¹.⁵⁶ Dilutions of a H₂O₂ stock solution were prepared in water before use. Milli-Q (mQ) ultrapure (type 1) water was used in all experiments.

Recombinant ScDyPB. Dye-decolorizing peroxidase from *S. coelicolor* A3(2) (ScDyPB, UniProtKB Q9FBY9) was overexpressed in *Escherichia coli* BL21 (DE3), purified, and reconstituted with heme as described in Pupart et al.²³ The concentration of ScDyPB was determined by the absorbance of the heme at 406 nm using an extinction coefficient of 100,000 M⁻¹ cm⁻¹ or by the absorbance at 280 nm using an extinction coefficient of 18,450 M⁻¹ cm⁻¹. The concentration of the enzyme storage stock was 18.1 ± 0.6 μM (based on the absorbance at 406 nm) and 39.0 ± 1.6 μM (based on the absorbance at 280 nm). In all experiments, the enzyme was dosed based on its concentration measured by the absorbance of heme. ScDyPB was stored at -80 °C as frozen aliquots in 20 mM Tris-HCl (pH 7.5) containing 0.1 M NaCl. ScDyPB working stocks were made by the dilution of the storage stock to the appropriate buffer containing 0.1 g L⁻¹ BSA and 0.1 M NaCl.

Measuring the Activity of ScDyPB. ABTS and MHQ were used for the kinetic characterization. If not stated otherwise, the activity measurements were performed in 50 mM sodium acetate (pH 4.0) in a spectrophotometer (Shimadzu UV-1900i UV-vis) cuvette at 25 °C in a total volume of 1.0 mL. The oxidation of ABTS was measured by the increase in the absorbance at 420 nm ($\epsilon_{420} = 36,000$ M⁻¹ cm⁻¹) and that of MHQ by the increase in the absorbance at 251 nm ($\epsilon_{251} = 21,450$ M⁻¹ cm⁻¹).⁵⁷ Reactions were started by

the addition of the enzyme from its working stock to a cuvette containing a mixture of the reducing substrate and H₂O₂. The nonenzymatic oxidation of substrates was measured in the experiments without the enzyme, and all activity measurements were corrected for this background. If not stated otherwise, the oxidation of ABTS was measured using 1 mM ABTS and 100 μM H₂O₂, and the oxidation of MHQ was measured using 1 mM MHQ and 1 mM H₂O₂. The oxidation of textile dyes reactive blue 4 (RB4) and 19 (RB19) was tested using 0.15 μM ScDyPB, 0.1 mM dye, and 1.0 mM H₂O₂ in 50 mM NaAc (pH 4.0) at 25 °C. Oxidation of the RB4 was measured by the decrease of the absorbance at 610 nm using an ϵ_{610} of 4200 M⁻¹ cm⁻¹ and by that of RB19 at 595 nm using an ϵ_{595} of 10,000 M⁻¹ cm⁻¹. The data were analyzed by using STATISTICA 8.0 and GraphPad Prism 5 software.

Inactivation of ScDyPB by H₂O₂. 1.5 μM ScDyPB in 50 mM NaAc (pH 4.0) or 20 mM Tris-HCl (pH 7.5) (both supplemented with 0.1 g L⁻¹ BSA) was preincubated with H₂O₂ (0–5 mM) at 25 °C. At selected times, a 10 μL aliquot was withdrawn and added to the cuvette containing 990 μL of the mixture of 1 mM ABTS and 0.1 mM H₂O₂ and the activity was measured by the increase in the absorbance at 420 nm.

Gel Filtration Chromatography. A Superdex 75 Increase 10/300 GL column (GE Healthcare) was equilibrated with 20 mM Tris-HCl and 0.1 M NaCl, pH 7.5. 100 μL of 18.1 μM ScDyPB was injected, and the column was eluted with equilibration buffer at a flow rate of 0.5 mL min⁻¹. Elution of the proteins was monitored by the absorbance at 280 nm. The high-molecular weight gel filtration calibration kit (Cytiva) contained ovalbumin (43 kDa), conalbumin (75 kDa), aldolase (158 kDa), and ferritin (440 kDa). The standard proteins were dissolved in Tris-HCl buffer (20 mM, pH 7.5, supplemented with 0.1 M NaCl) and used for calibration.

Dynamic Light Scattering. Dynamic light scattering (DLS) analyses were performed using a Zetasizer Nano S particle size analyzer (Malvern Panalytical) with a constant 173 °C scattering angle at 25 °C and the laser wavelength of 633 nm. Before DLS analysis, the buffers (20 mM Tris-HCl, pH 7.5, 0.1 M NaCl, or 50 mM NaAc mM, pH 4.0) were filtered through a sterile syringe filter with 0.22 μm pore size. The sample volume used for analysis was 80 μL, and the concentration of ScDyPB was 1.5 μM. The scattering intensity data were processed using instrumental software to obtain the hydrodynamic diameter (D_h) and the size distribution of scatterers in each sample.

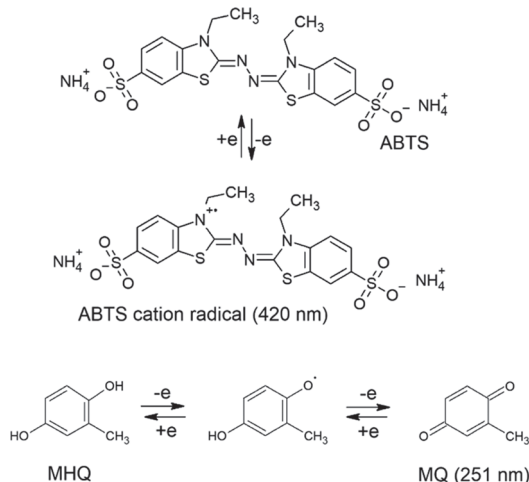
Spectra of ScDyPB. The UV-vis absorption spectra of ScDyPB were recorded at 250–700 nm using a Shimadzu UV-1900i UV-vis spectrophotometer at 25 °C. After recording the spectrum of 3.6 μM ScDyPB in 4 mM Tris-HCl (pH 7.5, supplemented with 20 mM NaCl) in 0.5 mL total volume, the pH was brought to 4.0 by the addition of 26 μL of 1.0 M NaAc (pH 4.0) and spectra were recorded again. Finally, 150 μL of 1.0 M Tris-HCl (pH 7.5) was added, and spectra were recorded.

RESULTS

Measuring the Activity of ScDyPB. Kinetic characterization of ScDyPB was performed using two reducing substrates: a conventional peroxidase substrate, 2,2'-azino-di(3-ethyl-benzothiazoline-6-sulfonic acid) (ABTS), and a phenolic substrate, methylhydroquinone (MHQ). ABTS is a one electron-donating substrate, and its oxidation can be

followed by the absorbance of the ABTS cation radical product (ABTS^{•+}) at 420 nm. MHQ is a two electron-donating substrate, and its oxidation can be followed by the absorbance of the methylquinone (MQ) product at 251 nm (Scheme 1).

Scheme 1. Oxidation of 2,2'-Azino-di-(3-ethyl-benzothiazoline-6-sulfonic acid) (ABTS) and methylhydroquinone (MHQ)^a



^aOne-electron oxidation of ABTS to the ABTS cation radical and two-electron oxidation of MHQ to methylquinone (MQ) (absorption maxima at 420 and 251 nm, respectively).

All peroxidase reactions were carried out in a spectrophotometer cuvette at 25 °C. Reactions were started by the addition of the enzyme from its working stock to the cuvette containing the mixture of the reducing substrate and H₂O₂, and all rates correspond to the initial rates (measured between 30 and 60 s, Figure 1A,B). The pH optima of the oxidation of both substrates were around 4 (Figure 1C), and all further

activity measurements were made in 50 mM sodium acetate (NaAc), pH 4.0.

Dependency of the Activity on the Concentration of ScDyPB. As expected for the enzyme-catalyzed reactions, the rate of the oxidation of both ABTS and MHQ scaled linearly with the concentration of the ScDyPB in the cuvette (Figure 2A,B). However, we found that the activity of ScDyPB was dependent on its concentration in the working stock used for the initiation of the enzyme reactions in the cuvette as well as on the pH of the working stock. Furthermore, the presence and the direction of these effects were dependent on the substrate used for the activity measurements. With ABTS as the substrate, the activity of the enzyme from the working stock made in NaAc pH 4.0 was about 1.5–2.5-fold (depending on the concentration of ScDyPB in the working stock) higher than that from the working stock made in Tris pH 7.5 (Figure 2A). The opposite was true for the activity measured with MHQ where the reactions that started from the working stock made in NaAc pH 4.0 had about sixfold lower activity compared to those made in Tris pH 7.5 (Figure 2B).

With ABTS as the substrate, we made a series of activity measurements using different ScDyPB concentrations in the working stock. The activity seemed to reach a plateau value with an increasing concentration of ScDyPB in the working stock (Figure 2C). An apparent half-saturating concentration of ScDyPB in the working stock made in 20 mM Tris pH 7.5 was about 0.38 μM, whereas the corresponding figure for the working stock made in 50 mM NaAc pH 4.0 was below 0.03 μM (Figure 2C). We note that in all cases, the concentration of ScDyPB in the cuvette was 15 nM. The simplest explanation for this phenomenon would be a nonspecific binding of ScDyPB to the laboratory plastics, like microcentrifuge tubes used for preparing enzyme working stocks. The results of the preliminary experiments, indeed, suggested that such nonspecific binding exists but not in the presence of BSA that was present (at 0.1 g L⁻¹) in the working stocks of ScDyPB used in all experiments shown in this work. Furthermore, one may expect that the nonspecific binding to laboratory plastics would have similar effects on the activities measured using different

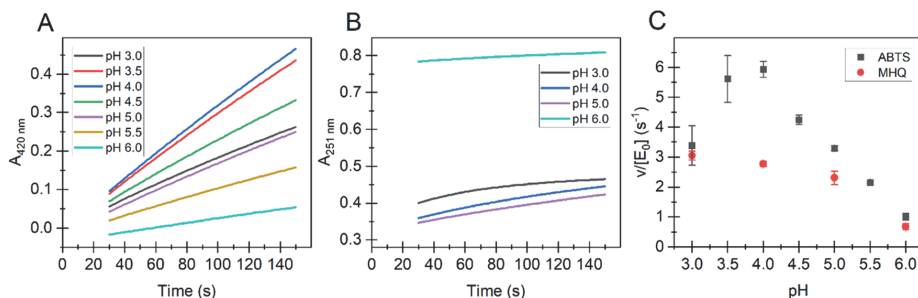


Figure 1. Dependency of initial rates of reducing substrate oxidation on pH by ScDyPB. The time curves of the oxidation of (A) ABTS and (B) MHQ. The pH values are given in the plot. (C) Dependency of the initial rates (measured between 30 and 60 s) of the oxidation of ABTS and MHQ on pH. All reactions were performed at 25 °C. Buffers were 50 mM sodium citrate (for pH 3.0 and 3.5), 50 mM sodium acetate (for pH 4.0–5.0), and 50 mM Bis-Tris-HCl (for pH 5.5 and 6.0). Reactions were initiated by the addition of the ScDyPB from its working stock (1.5 μM ScDyPB in 20 mM Tris-HCl pH 7.5 supplemented with 0.1 g L⁻¹ BSA and 0.1 M NaCl) to the cuvette containing the mixture of the substrate and H₂O₂. The final concentration of the ScDyPB in the cuvette was 15 nM. The oxidation of ABTS was measured using 1 mM ABTS and 100 μM H₂O₂. The oxidation of MHQ was measured using 1 mM MHQ (note that MHQ preparation had a high background absorbance at pH 6.0) and 1 mM H₂O₂. Data are presented as average values (*n* = 3, independent experiments), and error bars show SD. For clarity, the error bars are not shown for the traces in panels (A) and (B).

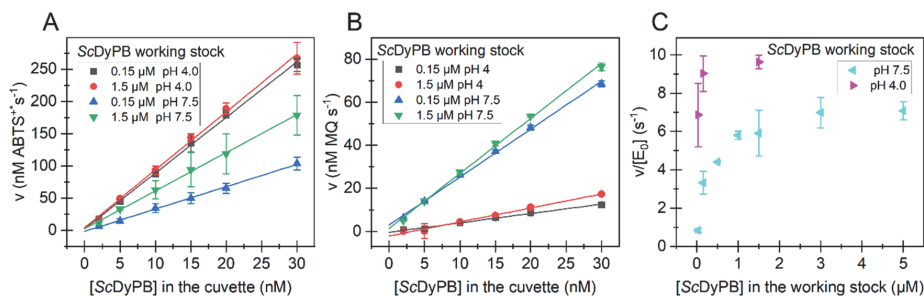


Figure 2. Dependency of the activity on the concentration of ScDyPB in the cuvette and in its working stock. All reactions were performed in NaAc buffer (50 mM, pH 4.0) at 25 °C. The oxidation of ABTS was measured using 1 mM ABTS and 100 μ M H₂O₂ and the oxidation of MHQ with 1 mM MHQ and 1 mM H₂O₂. The rates of oxidation of (A) ABTS and (B) MHQ at different concentrations of ScDyPB in the cuvette. The concentration of ScDyPB in its working stock and the pH of the working stock are shown in the figure. Solid lines show the linear regression of the data. (C) Dependency of the ABTS oxidizing activity of ScDyPB on its concentration in the working stock. The pH of the ScDyPB working stock is shown in the figure. The concentration of the ScDyPB in the cuvette was 15 nM. The working stocks of ScDyPB, with concentrations of 30 nM–5 μ M, were prepared in 20 mM Tris pH 7.5, 0.1 M NaCl, or 50 mM NaAc pH 4.0 buffers (both supplemented with 0.1 g L⁻¹ BSA). Data are presented as average values ($n = 3$, independent experiments), and error bars show SD.

substrates such as ABTS and MHQ, which was clearly not the case in this study (Figure 2A,B).

The higher activity measured in the reactions that started from the working stocks with higher enzyme concentrations can be explained by the enzyme being active as an oligomer. In the case of reversible binding, the relative concentration of the oligomeric form is expected to increase with an increasing total concentration of the enzyme. However, the relaxation to a possible binding equilibrium between different oligomeric states must be slow enough not to be achieved during the activity measurements in the cuvette. The results of several control experiments made using different preincubation times of ScDyPB working stocks suggested that the establishment of the possible new equilibrium upon the dilution of ScDyPB working stocks was relatively slow (compared to the time frame of the activity measurement). Furthermore, higher activity was observed when ABTS was present in preincubation of the ScDyPB working stock (Figure S1). These results suggest that equilibrium between different possible oligomeric forms of ScDyPB that has been established in its working stock is at least partly retained during the activity measurement in the cuvette. Since higher total enzyme concentration is expected to favor the association, the higher activity observed in the case of higher concentration of ScDyPB in its working stock (Figure 2C) suggests that higher oligomeric forms have higher ABTS oxidizing activity. If that is the case, the lower pH of the working stock seems to favor the higher oligomeric forms of ScDyPB (Figure 2A,C). Although there was little dependency between the MHQ oxidizing activity and the concentration of ScDyPB in its working stock, the lower activity observed with working stocks made at pH 4.0 (compared to those made in pH 7.5) (Figure 2B) suggests that contrary to the ABTS, the higher oligomeric forms have lower MHQ oxidizing activity. We also tested the oxidation of two textile dyes, RB4 and RB19, by ScDyPB (using 0.1 mM dye and 1.0 mM H₂O₂), but the activity with these substrates was low with apparent rates of 0.66 ± 0.04 and 0.58 ± 0.02 s⁻¹ for RB4 and RB 19, respectively.

Effects of Additives on the Activity of ScDyPB. As shown above, the pH of the ScDyPB working stock had differential effects depending on which substrate, ABTS or MHQ, was used for the activity measurement (Figure 2A,B).

Here, we tested the effects of different additives (ammonium sulfate, DMSO, methanol, Tween-20, and ethylene glycol) in the ScDyPB working stock (1.5 μ M ScDyPB in 20 mM Tris-HCl pH 7.5 supplemented with 0.1 g L⁻¹ BSA and 0.1 M NaCl) to the ABTS and MHQ oxidizing activity. Among the compounds tested, only the presence of ammonium sulfate in the working stock of ScDyPB had a significant effect on the activity (Figure 3). The presence of 1.0 M ammonium sulfate in the working stock resulted in about a twofold increase in

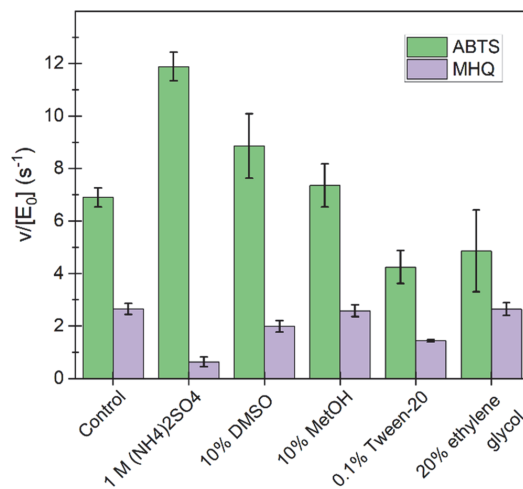


Figure 3. Effects of different additives in the working stock of ScDyPB on the ABTS and MHQ oxidizing activity. Prior to the activity measurements, the ScDyPB working stock (1.5 μ M ScDyPB in 20 mM Tris-HCl pH 7.5 supplemented with 0.1 g L⁻¹ BSA and 0.1 M NaCl) was incubated for 30 min at 25 °C in the presence of different compounds as indicated in the figure. The activity was measured in 50 mM NaAc at pH 4.0 using 15 nM ScDyPB (100-fold dilution of the working stock to the cuvette). The activity was measured using 1 mM ABTS and 100 μ M H₂O₂ or 1 mM MHQ and 1 mM H₂O₂. Data are presented as average values ($n = 3$, independent experiments), and error bars show SD.

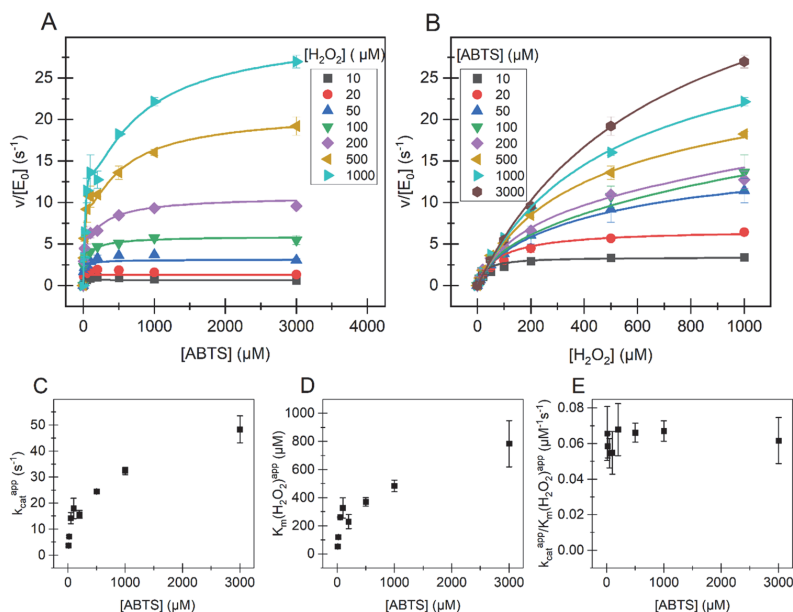


Figure 4. Kinetics of the oxidation of ABTS by ScDyPB. Dependency of initial rates of the oxidation of ABTS on the concentration of (A) ABTS and (B) H_2O_2 , and the dependency of apparent parameters (C) $k_{\text{cat}}^{\text{app}}$, (D) $K_{\text{M}}(\text{H}_2\text{O}_2)^{\text{app}}$, and (E) $k_{\text{cat}}^{\text{app}}/K_{\text{M}}(\text{H}_2\text{O}_2)^{\text{app}}$ on the concentration of ABTS. Reactions were made in 50 mM NaAc (pH 4.0) at 25 °C. The concentration of ScDyPB was 15 nM, and the reactions were initiated by the addition of ScDyPB from the working stock with 1.5 μM ScDyPB in 20 mM Tris pH 7.5 (supplemented with 0.1 g L^{-1} BSA and 0.1 M NaCl). Solid lines in (A) and (B) show the global nonlinear regression of the data according to eq 2. The concentration of the substrate that has been kept constant within the series is indicated in the plot. The values of apparent kinetic parameters for H_2O_2 shown in panels (C–E) were derived by nonlinear regression analysis of the data in panel (B) according to the Michaelis–Menten equation (eq S1, for the fit, see Figure S2B). Data are presented as average values ($n = 3$, independent experiments), and error bars show SD.

ABTS oxidizing activity, whereas there was about a fourfold decrease in the MHQ oxidizing activity (Figure 3). Control experiments made with 0.01 M ammonium sulfate in the cuvette showed no effect on the activity (data not shown), confirming that the observed effects were caused by the presence of ammonium sulfate in the working stock of ScDyPB. The opposite effects of ammonium sulfate on the activity with ABTS and MHQ corroborate with the effects of the pH of the working stock (Figure 2A,B) and suggest that different oligomeric forms of ScDyPB may be responsible for the oxidation of ABTS and MHQ.

Kinetics of the Oxidation of ABTS. All experiments described above were performed using ABTS and H_2O_2 concentrations of 1.0 and 0.1 mM, respectively. Here, we performed experiments with varied concentrations of ABTS (0.01–3.0 mM) and H_2O_2 (0.01–1.0 mM). The concentration of ScDyPB in the cuvette was 15 nM, and the reactions were started by the addition of ScDyPB from the working stock with 1.5 μM ScDyPB in 20 mM Tris pH 7.5 (supplemented with 0.1 g L^{-1} BSA and 0.1 M NaCl). The dependency of the rates on the concentration of ABTS shows substrate inhibition by ABTS with the effect being more prominent at low concentration of H_2O_2 (Figure 4A, see Figure S2A for the zoom-in of the data at the region of low H_2O_2 concentrations). Substrate inhibition by one substrate at a low concentration of the other substrate is a kinetic signature of the enzymes obeying a ping-pong kinetic mechanism such as heme peroxidases. There was no substrate inhibition by H_2O_2 at

any concentration of ABTS (Figure 4B). However, when incubated with H_2O_2 in the absence of ABTS, the ScDyPB was irreversibly inactivated (Figure S3). The rate of inactivation increased with increasing concentration of H_2O_2 , and the second order rate constants of 4.9 ± 0.3 and $6.2 \pm 0.9 \text{ M}^{-1} \text{ s}^{-1}$ were found for H_2O_2 -driven inactivation of ScDyPB at pH 4.0 and 7.5, respectively (Figure S3).

When the concentration of H_2O_2 was treated as a variable, the rate of ABTS oxidation was well in line with the simple Michaelis–Menten equation (Figure S2B and eq S1). However, the dependency of apparent parameters for H_2O_2 ($k_{\text{cat}}^{\text{app}}$, $K_{\text{M}}(\text{H}_2\text{O}_2)^{\text{app}}$, and $k_{\text{cat}}^{\text{app}}/K_{\text{M}}(\text{H}_2\text{O}_2)^{\text{app}}$) on the concentration of ABTS (Figure 4C–E) was more complex than expected for ping-pong peroxidase kinetics with substrate inhibition by ABTS. The dependency of $k_{\text{cat}}^{\text{app}}$ (Figure 4C) on [ABTS] does not follow simple saturation with ABTS according to the hyperbola (eq S2) but shows a drop in the parameter value between 0.1 mM and 0.2 mM ABTS. Furthermore, an apparent $k_{\text{cat}}/K_{\text{M}}(\text{H}_2\text{O}_2)$ does not approach zero with increasing [ABTS] (eq S3) but levels to a constant value of $65.7 \pm 2.7 \text{ mM}^{-1} \text{ s}^{-1}$ after the initial drop with increasing [ABTS] (Figure 4E). When the concentration of ABTS was treated as a variable, both the Michaelis–Menten equation and the equation accounting for the substrate inhibition failed to describe the kinetics. The characteristic feature of the kinetics of ABTS oxidation was a slight drop or retardation in the rates observed around ABTS concentrations of 0.1–0.2 mM, which was followed by the increase in rates with a further increase in

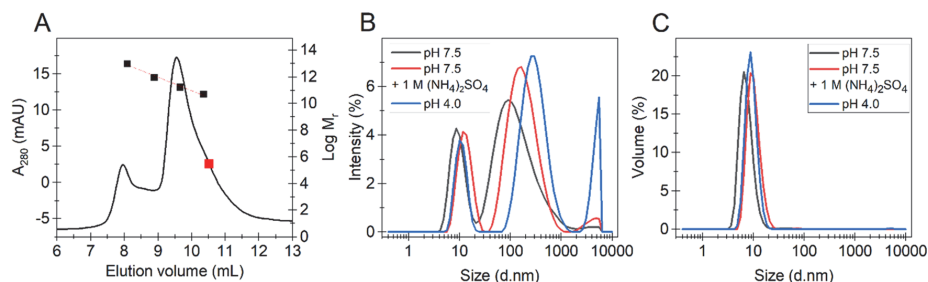


Figure 5. Analysis of the size distribution of ScDyPB. (A) Gel filtration chromatogram of ScDyPB in 20 mM Tris-HCl (pH, 7.5) (supplemented with 100 mM NaCl). Black squares show the elution volume of standard proteins: ferritin (440 kDa), aldolase (158 kDa), conalbumin (75 kDa), and ovalbumin (44 kDa). The red line shows linear regression analysis of the mobility of the standard proteins used for calibration. The red square shows the expected elution volume of the ScDyPB monomer. (B, C) Dynamic light scattering (DLS) analysis of 1.5 μM ScDyPB in 50 mM NaAc pH 4.0, in 20 mM Tris pH 7.5, and in 20 mM Tris pH 7.5 supplemented with 1.0 M ammonium sulfate (as indicated in the plot). Size distribution based on the intensity (B) or volume (C). Traces show the average of at least four consecutive scans.

[ABTS]. This kinetic phenomenon was best revealed in the series made at higher H_2O_2 concentrations (Figure 4A).

The simplest kinetic mechanism that can account for the above-described phenomenon assumes the enzyme to be active as two independent, kinetically different forms. One form of the enzyme (form II, E^{II}) is a subject of substrate inhibition by ABTS, whereas the other form (form I, E^{I}) follows the Michaelis–Menten saturation kinetics. Assuming that the two forms are independent, the rate equation can be written as a sum of the two steady-state rate equations (eq 1)

$$\frac{v_i}{[E]_0} = \frac{\frac{[E^{\text{I}}]}{[E]_0} k_{\text{cat}}^{\text{I}} [\text{ABTS}] [\text{H}_2\text{O}_2]}{K_{\text{M}(\text{ABTS})}^{\text{I}} [\text{H}_2\text{O}_2] + K_{\text{M}(\text{H}_2\text{O}_2)}^{\text{I}} [\text{ABTS}] + [\text{ABTS}] [\text{H}_2\text{O}_2]} + \frac{\frac{[E^{\text{II}}]}{[E]_0} k_{\text{cat}}^{\text{II}} [\text{ABTS}] [\text{H}_2\text{O}_2]}{K_{\text{M}(\text{ABTS})}^{\text{II}} [\text{H}_2\text{O}_2] + K_{\text{M}(\text{H}_2\text{O}_2)}^{\text{II}} [\text{ABTS}] \left(1 + \frac{[\text{ABTS}]}{K_{\text{i}(\text{ABTS})}}\right) + [\text{ABTS}] [\text{H}_2\text{O}_2]} \quad (1)$$

In eq 1, the enzyme forms I and II and corresponding kinetic parameters are designated with superscripts I and II, respectively. The enzyme form I follows ping-pong kinetics, whereas form II follows ping-pong kinetics with substrate inhibition by ABTS. This equation was able to account for experimentally observed kinetic peculiarities, like a “kink in the curve” observed after 0.1 mM ABTS (Figure 4A). Global nonlinear regression analysis of the data in Figure 4A according to eq 1 predicted the $[E^{\text{I}}]/[E]_0$, $K_{\text{M}(\text{ABTS})}^{\text{I}}$, and $K_{\text{M}(\text{H}_2\text{O}_2)}^{\text{I}}$ values of $59 \pm 3 \text{ s}^{-1}$, $1.0 \pm 0.12 \text{ mM}$, and $0.89 \pm 0.06 \text{ mM}$, respectively (for the fit, see Figure S4A). However, because of the interdependency between the parameters, the values of the kinetic parameters for enzyme form II came with a large standard deviation. Precise determination of the parameter values for two different enzyme forms apparently assumes measurements under the experimental conditions where one of the forms is predominant and the contribution by the other is insignificant. Since the activity of ScDyPB was higher (with 1.0 mM ABTS and 0.1 mM H_2O_2) when the reactions were started from the working stock made in 50 mM NaAc pH 4.0 (Figure 2C) instead of 20 mM Tris pH 7.5, we also tested the 1.5 μM ScDyPB working stock made in pH 4.0 in making the series with varying [ABTS] and $[\text{H}_2\text{O}_2]$. Although the general activity was higher, apparent biphasic kinetics persisted also in these experiments, suggesting that ScDyPB existed in two

kinetically different forms also in 50 mM NaAc pH 4.0 (data not shown).

In order to evaluate the relative abundance of enzyme forms, we further assume that the two enzyme forms have the same values of kinetic parameters and they differ only by the presence of substrate inhibition in the case of form E^{II} . In this case, eq 1 simplifies to

$$\frac{v_i}{[E]_0} = \frac{\frac{[E^{\text{I}}]}{[E]_0} k_{\text{cat}} [\text{ABTS}] [\text{H}_2\text{O}_2]}{K_{\text{M}(\text{ABTS})} [\text{H}_2\text{O}_2] + K_{\text{M}(\text{H}_2\text{O}_2)} [\text{ABTS}] + [\text{ABTS}] [\text{H}_2\text{O}_2]} + \frac{\left(1 - \frac{[E^{\text{I}}]}{[E]_0}\right) k_{\text{cat}} [\text{ABTS}] [\text{H}_2\text{O}_2]}{K_{\text{M}(\text{ABTS})} [\text{H}_2\text{O}_2] + K_{\text{M}(\text{H}_2\text{O}_2)} [\text{ABTS}] \left(1 + \frac{[\text{ABTS}]}{K_{\text{i}(\text{ABTS})}}\right) + [\text{ABTS}] [\text{H}_2\text{O}_2]} \quad (2)$$

Global nonlinear regression analysis of the data in Figure 4A according to eq 2 predicted the relative abundance of forms I ($[E^{\text{I}}]/[E]_0$) and II ($1 - [E^{\text{I}}]/[E]_0$) of 0.18 ± 0.01 and 0.82 ± 0.01 , respectively. The estimates of common parameter values for both forms were $327 \pm 28 \text{ s}^{-1}$, $0.95 \pm 0.09 \text{ mM}$, and $0.89 \pm 0.06 \text{ mM}$, for k_{cat} , $K_{\text{M}(\text{ABTS})}$, and $K_{\text{M}(\text{H}_2\text{O}_2)}$, respectively. The estimate of the $K_{\text{i}(\text{ABTS})}$ was $4.12 \pm 0.36 \mu\text{M}$. Despite having two parameters less, the fitting according to eq 2 was not significantly worse than that according to eq 1 with R^2 values of 0.9957 and 0.9962, respectively (for the comparison of fits, see Figure S4A,B). The high k_{cat} value obtained from the analysis according to eq 2 is a result of the low abundance of the nonsubstrate inhibited form. Despite strong substrate inhibition, the enzyme form E^{II} has significant contribution to the overall activity at [ABTS] below 0.1 mM (Figure S4C,D).

ScDyPB Exists in Oligomeric Forms with Different Sizes. The results of the kinetic studies described above suggested that ScDyPB may exist as a mixture of different oligomeric forms. Here, we analyzed the size distribution of ScDyPB using gel filtration chromatography and dynamic light scattering (DLS). Analysis using a Superdex-75 column showed that at pH 7.5, the ScDyPB eluted as two peaks. A dominant peak with an apparent molecular weight of 91 kDa and a smaller peak eluted close to the void volume of the column (MW of about 450 kDa) (Figure 5A). Considering the molecular weight of ScDyPB of 34 kDa, the dominant peak corresponds to an apparent trimer. The shoulder in the region of the expected elution of the ScDyPB monomer suggests that

the dominant peak may correspond to the mixture of mono- and trimeric ScDyPB. Unfortunately, the gel permeation chromatographic analysis at pH 4.0 but also at pH 7.5 but in the presence of 1.0 M ammonium sulfate was not possible. At pH 4.0, ScDyPB precipitated at high concentrations necessary for this analysis (14.5 μM) and at pH 7.5, but in the presence of 1.0 M ammonium sulfate, the elution of ScDyPB was retarded because of the interaction with the column matrix.

DLS analyses were also applicable at pH 4.0 and 7.5 in the presence of 1.0 M ammonium sulfate. In the case of all conditions tested, the ScDyPB existed as a complex mixture of particles with different sizes with the diameter ranging from 9 nm to more than 4 μm . However, although intensity-based size distribution revealed the presence of large aggregates (Figure 5B), the relative contribution of ScDyPB engaged in these aggregates was less than 1% as judged by the volume-based size distribution analysis (Figure 5C). The majority of ScDyPB appeared in the population of oligomers with an average size of around 10 nm (Figure 5C and Table 1). The lowest average

Table 1. DLS Analysis of the Mean Size and Relative Contribution of ScDyPB Oligomers^a

experiment conditions	intensity-based size (nm)	volume-based size (nm)	volume-based contribution (%)
pH 7.5	9.8 \pm 0.7	7.6 \pm 0.3	99.6 \pm 0.4
pH 7.5 + 1 M (NH ₄) ₂ SO ₄	13.2 \pm 0.4	10.4 \pm 0.4	99.1 \pm 0.2
pH 4.0	10.9 \pm 0.4	9.3 \pm 0.3	99.3 \pm 0.2

^aCalculated based on the size distribution of intensity (Figure 5B) and volume (Figure 5C). Mean sizes are calculated from at least four DLS scans, and error bars show SD.

size of ScDyPB oligomers was observed at pH 7.5 followed by pH 4.0 and pH 7.5 but in the presence of 1.0 M ammonium sulfate (Figure 5B,C and Table 1). Although the average size of oligomers depends on which distribution, intensity, or volume was used for the size calculation, the trends were the same. Addition of ammonium sulfate led to the increase in the average size of ScDyPB oligomers, and higher oligomers were observed at pH 4.0 compared to pH 7.5 (Table 1).

We also recorded the UV–vis spectra of ScDyPB at pH 7.5 and pH 4.0 (Figure S5). At both pH values, there was a clear absorbance of the Soret band around 400 nm, characteristic for heme proteins. Changing the pH from 7.5 to 4.0 resulted in an increase in the absorbance at all wavelengths, but the effect was more prominent at shorter wavelengths, suggesting the contribution of the light scattering. This observation is corroborated by the higher abundance of large particles observed in DLS spectra at pH 4.0 compared to pH 7.5 (Figure 5B,C). Of note, the pH-dependent changes in the UV–vis spectrum were reversible as the adjustment of pH from 4.0 back to 7.5 restored the initial absorbance spectrum measured at pH 7.5 (Figure S5).

DISCUSSION

DyP peroxidases often display complex, non-Michaelis–Menten kinetics with substrate inhibition by H₂O₂,^{21,24,25} by the reducing substrate,^{18,22,23} or by both.²² An apparent positive cooperativity with the reducing substrate has also been observed with many DyP peroxidases.^{15,22,27,28} Kinetics of heme peroxidases are well studied, and they obey a ping-pong kinetic mechanism. Catalysis is initiated by the binding of

H₂O₂ to the heme in its resting state (Fe³⁺) followed by two-electron oxidation of the heme and formation of the reactive intermediate known as compound I (Cpd I).⁵⁸ Cpd I is reduced back to the resting state via two consecutive one-electron transfer steps from the reducing substrate. Electrons may be transferred directly from the reducing substrate to Cpd I, but many DyPs have shown to employ long-range electron transfer where the reducing substrate is oxidized at surface binding sites.^{19,28,59–61} The latter strategy is used in the oxidation of bulky substrates that cannot pass through the heme access channel(s).

Substrate inhibition is a phenomenon that is often observed with enzymes obeying a ping-pong kinetic mechanism, and it happens when substrates bind to the “wrong form” of the enzyme. In the case of DyP peroxidases, it assumes the binding of the reducing substrate to the enzyme resting state in a way that competes with the binding of H₂O₂. The substrate inhibition by H₂O₂ occurs when H₂O₂ binds to Cpd I and restricts its reduction by the reducing substrate. The ScDyPB studied here was substrate-inhibited by ABTS but not by H₂O₂ (Figure 4A,B). Analysis of the structure of ScDyPB (PDB: 4GU7) reveals the presence of one heme access channel, a propionate pocket with a bottleneck radius of 2.45 Å that can possibly accommodate ABTS (Figure 6A). The heme access channel of ScDyPB is similar to the well-studied DtpB of the bacterium *Streptomyces lividans*.⁶² Thus, it seems plausible that substrate inhibition of ScDyPB involves the entrance of the ABTS through the propionate pocket and binding to the heme resting state. Inactivation of ScDyPB upon incubation with H₂O₂ (Figure S3) in the absence of ABTS suggests that H₂O₂ can interact with Cpd I. Such binding would compete with the direct binding of ABTS to the heme but not with the possible binding to the surface site. In latter case, the oxidation of ABTS would be kinetically favored by the factor of more than 10⁴ ($k_{\text{cat}}^{\text{app}}/K_{\text{M}}^{\text{app}}(\text{H}_2\text{O}_2)$) for the oxidation of ABTS of 65.7 \pm 2.7 mM⁻¹ s⁻¹ (Figure 4E), versus rate constant for inactivation by H₂O₂ of 0.0049 \pm 0.0003 mM⁻¹ s⁻¹, (Figure S3) and provides possible explanation for the absence of substrate inhibition by H₂O₂.

Characteristic to the enzyme catalyzed reactions, the rate of the oxidation of ABTS and MHQ was proportional to the concentration of the ScDyPB in the reaction (Figure 2A,B). However, we found that the rates of ABTS oxidation were dependent on the concentration of ScDyPB in its working stock used to initiate the reactions. Higher rates were observed at higher concentrations of ScDyPB in the working stock (Figure 2C). The in-depth kinetic characterization of the oxidation of ABTS (Figures 4 and S4) suggests that ScDyPB exists as a mixture of at least two kinetically different enzyme forms, with one being inhibited by ABTS but not the other one. Size exclusion chromatography and DLS analyses revealed that ScDyPB, indeed, exists as a complex mixture of oligomers and aggregates with different sizes (Figure 5). Furthermore, the lower pH (pH 4.0 versus 7.5) and supplementation with ammonium sulfate seemed to favor a higher degree of oligomerization (Figure 5B,C and Table 1). It is also important to note that while ScDyPB working stocks made at pH 4.0 resulted in higher ABTS oxidizing activity when compared to the working stocks made at pH 7.5 (Figure 2A), the opposite was true for the oxidation of MHQ (Figure 2B). Similarly, the presence of 1.0 M ammonium sulfate in the working stock of ScDyPB increased the ABTS oxidizing activity but decreased

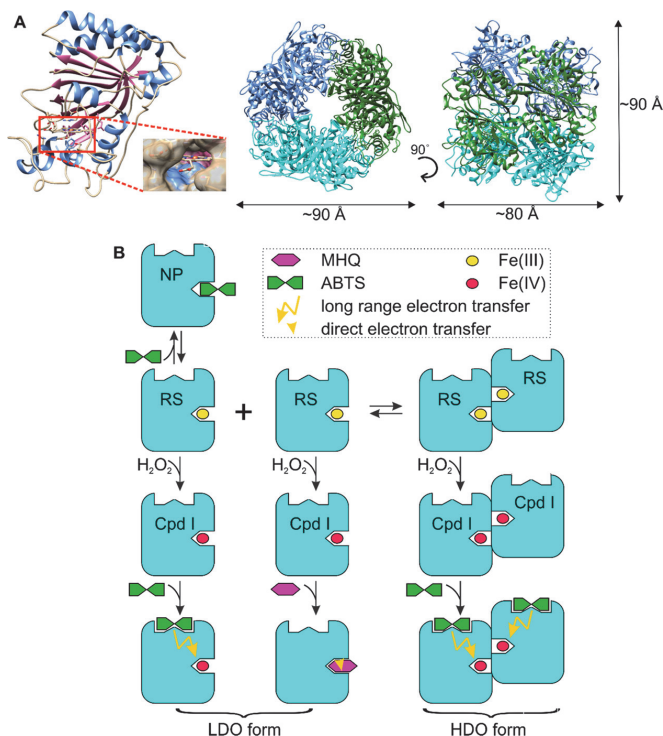


Figure 6. Structure of ScDyPB and simplest possible mechanism of the formation of kinetically different forms of the enzyme. (A) Structure of ScDyPB (PDB: 4GU7). The structure of the ScDyPB monomer, where α -helices, β -sheets, and loops are colored blue, pink, and tan, respectively. The heme is shown as a stick model. Nitrogen, oxygen, and iron atoms are colored blue, red, and brown, respectively. The inset shows the heme access channel of ScDyPB, the propionate pocket (left). The ScDyPB hexamer (trimer of dimers), with dimers shown in different colors and the approximate dimensions of the hexamer (right). (B) Simplest mechanism of the catalysis by ScDyPB that explains the experimental observations of this study. ScDyPB exists as an equilibrium (slow compared with the time frame used for the activity measurements) of the enzyme forms with low (LDO form) and high degrees of oligomerization (HDO form). For the simplicity of visualization of the concept, the LDO- and HDO forms are represented by the monomer and dimer, respectively (in a real system, the degree of oligomerization of both forms is much higher). In their resting state (RS), both forms of the enzyme can be oxidized by H_2O_2 to form an active intermediate, compound I (Cpd I). In the case of ABTS as the reducing substrate, the RS is restored by the long-range electron transfer to Cpd I. For MHQ, there is no surface binding site, and Cpd I is reduced via direct electron transfer to the heme iron. The heme access channel is assumed to be inaccessible for the reducing substrate in the enzyme in its HDO form. Therefore, the oxidation of MHQ occurs only with the enzyme in its LDO form. Substrate inhibition by ABTS results from the nonproductive binding of ABTS to the heme (NP) and is possible only with the enzyme in its LDO form. Thus, the conditions that favor the HDO form of ScDyPB will decrease the MHQ oxidizing activity through blockage of the access to the heme and increase ABTS oxidizing through relieving substrate inhibition. Note that possible substrate inhibition by MHQ and oxidation of ABTS through direct electron transfer do not change the general outcome of the model and are omitted for simplicity.

the MHQ oxidizing activity (Figure 3). Collectively, these results suggest that different mechanisms are used in the oxidation of ABTS and MHQ and that these mechanisms are differently affected by the degree of oligomerization of ScDyPB.

The simplest mechanism that would explain the results of this study is depicted in Figure 6B, and it relies on the four following assumptions. (i) ScDyPB exists as a mixture of two enzyme forms (we note that assuming just two enzyme forms may be an oversimplification, but including more forms leads to the overparametrization of the rate equations that do not permit quantitative analyses) with different degrees of oligomerization. One form has a high degree of oligomerization (HDO form), whereas the other form has a low degree of oligomerization (LDO form). (ii) ABTS can be oxidized at the surface binding site through the long-range electron transfer,

but there is no such possibility with smaller substrate MHQ. Oxidation of MHQ takes place in a direct contact with Cpd I (note that there is no need to exclude this possibility for the oxidation of ABTS). (iii) Substrate inhibition by ABTS involves the binding of ABTS to the heme resting state competing with the binding of H_2O_2 and Cpd I formation. (iv) Direct access of ABTS and MHQ to the heme and Cpd I is possible only with the LDO form of ScDyPB, but H_2O_2 has access to the heme of ScDyPB in its both LDO and HDO forms.

Relative contribution of the HDO form increases with an increasing concentration of ScDyPB in its working stocks. Since the direct access of reducing substrates to heme in the HDO form is blocked, the substrate inhibition by ABTS is relieved, while the oxidation through long-range electron transfer is unaffected. The net result is increased ABTS

oxidizing activity with increasing concentration of ScDyPB in its working stocks (Figure 2). Without long-range electron transfer, as proposed for the MHQ substrate, the blockage of the heme access channel in the HDO form will abolish the MHQ oxidizing activity, and it decreases with increasing concentration of ScDyPB in its working stocks (Figure 2). As indicated by the increased average size of ScDyPB oligomers, the lower pH of the ScDyPB working stock as well as the presence of ammonium sulfate in it also seems to increase the relative concentration of the HDO form (Table 1). The result is increased ABTS but decreased MHQ oxidizing activity in the experiments with the ScDyPB working stock made at pH 4.0 (Figure 2) but also at pH 7.5 in the presence of 1.0 M ammonium sulfate (Figure 3).

Long-range electron transfer involves accessible Trp or Tyr residues at the surface of the enzyme. There are two Trp and five Tyr residues in ScDyPB, and all of them, except Tyr 141, are in the solvent-accessible surface. Although the use of surface binding site(s) by ScDyPB remains to be experimentally validated, its ability to oxidize bulky dyes RB4 and RB19 and polymeric lignin²³ suggests the presence of this possibility. The core dimensions of a ScDyPB (PDB: 4GU7) dimer in the crystal structure are $6 \times 8 \times 4$ nm³. Assessment of the structure of ScDyPB using PISA analysis revealed that the most probable multimeric state of ScDyPB would be a hexamer (trimer of dimers) with a buried surface area of 23,290 Å² (27.5% of the total surface area of six monomers, Figure 6A). The hexamer had a diameter of 8 nm \times 8 nm \times 9 nm (Figure 6A). The maximum particle dimensions D_{\max} and the radius of gyration R_g are 86 and 27 Å for the dimer and 99 and 36 Å for the hexamer, respectively, as calculated with GNOM based on the theoretical solution small-angle X-ray scattering curves generated with FoXS.^{63,64} Thus, the ScDyPB population with the diameter of around 10 nm observed in DLS scans (Figure 5B,C and Table 1) may well correspond to a hexamer. However, considering the heterogeneity of enzyme populations revealed in consecutive DLS scans and relatively big differences between intensity- and volume distribution-based sizes (Table 1), identification of this population as a dimer cannot be excluded. Since more than 99% of ScDyPB appears in this peak (Table 1), it is evident that both LDO and HDO forms are merged to this single peak. Unfortunately, our data do not enable us to derive the sizes of LDO and HDO forms separately as we see only an average size of the mixture of different oligomers (Table 1). All in all, the structural as well as biophysical analyses (Figure 5) suggest that ScDyPB exists as a mixture of enzyme populations with different degrees of oligomerization. Our results suggest that lower pH (pH 4.0 compared to pH 7.5) supports the formation of the HDO form. The most probable candidate for changing its protonation state upon shifting from pH 7.5 to 4.0 would be a histidine with a pK_a value of 6.0–7.0. Although there is one His residue (His 137) in the contact area of adjacent ScDyPB monomers, this residue is not involved in salt bridge formation. Increased contribution of the HDO form in the presence of 1.0 M ammonium sulfate suggests that hydrophobic interactions may be involved in the formation of oligomers. An important assumption of our model was that the heme access channel is not accessible for the reducing substrates, ABTS and MHQ, in the HDO form of ScDyPB (Figure 6B). Similar to the observations made with the oligomerization of other DyPs,^{11,35} the heme access channel in the ScDyPB hexamer is not located in the subunit interface and seems to be accessible. However, a

possible blockage of heme access channels upon formation of oligomers with a higher degree of oligomerization that were observed in both gel filtration and DLS analyses (Figure 5) cannot be excluded. Further studies are needed to judge the plausibility of the assumptions underlying the mechanism in Figure 6B.

The biological role of DyP peroxidases and the nature of their native reducing substrates are not known. Many DyP peroxidases are secreted as cargo proteins in the interior of the shell made from encapsulins.^{45,46,53,54} As an example, the DyP of *Mycobacterium smegmatis* is loaded into the encapsulin shell as a dodecamer made from two hexamers.⁵⁴ However, there are no encapsulin-coding genes in the genome of *S. coelicolor*, suggesting that oligomerization of ScDyPB is not related to the packing into encapsulin nanoparticles. Although the exact mechanism and biological role remain to be revealed, the enzyme oligomerization-dependent modulation of the kinetic properties observed here expands the complexity of the kinetics of DyP peroxidases but also suggests novel possibilities for the regulation of their catalytic activity.

■ ASSOCIATED CONTENT

Supporting Information

The Supporting Information is available free of charge at <https://pubs.acs.org/doi/10.1021/acsomega.3c07963>.

Effects of preincubation time of ScDyPB working stocks before the measurement of the activity with ABTS, kinetics of the oxidation of ABTS, inactivation of ScDyPB by H₂O₂, comparison of the fitting of the data of ABTS oxidation according to eqs 1 and 2, contribution of the enzyme forms EI and EII, and absorbance spectra of ScDyPB (PDF)

Accession Codes

Type B dye-decolorizing peroxidase from *Streptomyces coelicolor*, Q9FBY9.

■ AUTHOR INFORMATION

Corresponding Author

Priit Väljamäe – Institute of Molecular and Cell Biology, University of Tartu, Tartu 51010, Estonia; orcid.org/0000-0002-1035-9493; Email: priit.valjamae@ut.ee

Authors

Hegne Pupart – Department of Chemistry and Biotechnology, Tallinn University of Technology, Tallinn 12618, Estonia

Darja Vastšjonok – Institute of Molecular and Cell Biology, University of Tartu, Tartu 51010, Estonia

Tiit Lukk – Department of Chemistry and Biotechnology, Tallinn University of Technology, Tallinn 12618, Estonia; orcid.org/0000-0001-7765-1707

Complete contact information is available at: <https://pubs.acs.org/10.1021/acsomega.3c07963>

Author Contributions

[§]H.P. and D.V. contributed equally to this work. H.P. performed experiments and wrote the article; D.V. performed experiments; T.L. wrote the article; P.V. conceived and coordinated the study and wrote the article. All authors have given approval to the final version of the article.

Funding

This work was funded by the Estonian Research Council (Grant PRG1540, to P.V.), the ERDF, and the Estonian Research Council via project RESTA11 (to T.L.).

Notes

The authors declare no competing financial interest.

ACKNOWLEDGMENTS

The authors thank Vitali Sõritski from the Tallinn University of Technology for the assistance with DLS analyses and Silja Kuusk from the University of Tartu for the assistance with preparing Figure 6B.

ABBREVIATIONS

ABTS, 2,2'-azino-di(3-ethyl-benzothiazoline-6-sulfonic acid); Cpd I, compound I; Cpd II, compound II; DLS, dynamic light scattering; DyP, dye-decolorizing peroxidase; HDO, high degree of oligomerization; LDO, low degree of oligomerization; MHQ, methylhydroquinone; MQ, methylquinone; NaAc, sodium acetate; ScDyPB, type B dye-decolorizing peroxidase of *Streptomyces coelicolor*

REFERENCES

- (1) Kim, S. J.; Shoda, M. Purification and characterization of a novel peroxidase from *Geotrichum candidum* Dec 1 involved in decolorization of dyes. *Appl. Environ. Microbiol.* **1999**, *65*, 1029–1035.
- (2) Scheibner, M.; Hülsdau, B.; Zelena, K.; Nimtz, M.; de Boer, L.; Berger, R. G.; Zorn, H. Novel peroxidases of *Marasmius scorodoni* degrade β -carotene. *Appl. Microbiol. Biotechnol.* **2008**, *77*, 1241–1250.
- (3) van Bloois, E.; Pazmiño, D. E. T.; Winter, R. T.; Fraaije, M. W. A robust and extracellular heme-containing peroxidase from *Thermobifida fusca* as prototype of a bacterial peroxidase superfamily. *Appl. Microbiol. Biotechnol.* **2010**, *86*, 1419–1430.
- (4) Singh, R.; Eltis, L. D. The multihued palette of dye-decolorizing peroxidases. *Arch. Biochem. Biophys.* **2015**, *574*, 56–65.
- (5) Yoshida, T.; Sugano, Y. Unexpected diversity of dye-decolorizing peroxidases. *Biochem. Biophys. Rep.* **2023**, *33*, No. 101401.
- (6) Sugano, Y.; Yoshida, T. Dyp-type peroxidases: Recent advances and perspectives. *Int. J. Mol. Sci.* **2021**, *22*, 5556.
- (7) Savelli, B.; Li, Q.; Webber, M.; Jemmat, A. M.; Robitaille, A.; Zamocky, M.; Mathé, C.; Dunand, C. RedoxBase: A database for ROS homeostasis regulated proteins. *Redox Biol.* **2019**, *26*, No. 101247.
- (8) Shrestha, R.; Jia, K.; Khadka, S.; Eltis, L. D.; Li, P. Mechanistic insights into DyPB from *Rhodococcus jostii* RHA1 via kinetic characterization. *ACS Catal.* **2021**, *11*, 5486–5495.
- (9) Colpa, D. I.; Fraaije, M. W.; van Bloois, E. DyP-type peroxidases: a promising and versatile class of enzymes. *J. Ind. Microbiol. Biotechnol.* **2014**, *41*, 1–7.
- (10) Sugano, Y.; Matsushima, Y.; Tsuchiya, K.; Aoki, H.; Hirai, M.; Shoda, M. Degradation pathway of an anthraquinone dye catalyzed by a unique peroxidase DyP from *Thanatephorus cucumeris*. *Biodegradation* **2009**, *20*, 433–440.
- (11) Zubieta, C.; Krishna, S. S.; Kapoor, M.; Kozbial, P.; McMullan, D.; Axelrod, H. L.; Miller, M. D.; Abdubek, P.; Ambing, E.; Astakhova, T.; et al. Crystal structures of two novel dye-decolorizing peroxidases reveal a β -barrel fold with a conserved heme-binding motif. *Proteins* **2007**, *69*, 223–233.
- (12) Hofbauer, S.; Pfanzagl, V.; Michlits, H.; Schmidt, D.; Obinger, C.; Furtmüller, P. G. Understanding molecular enzymology of porphyrin-binding $\alpha + \beta$ barrel proteins - One fold, multiple functions. *Biochim. Biophys. Acta* **2021**, *1869*, No. 140536.
- (13) Celis, A. L.; DuBois, J. L. Substrate, product, and cofactor: The extraordinarily flexible relationship between the CDE superfamily and heme. *Arch. Biochem. Biophys.* **2015**, *574*, 3–17.
- (14) Goblirsch, B.; Kurker, R. C.; Streit, B. R.; Wilmot, C. M.; Dubois, J. L. Chlorite dismutases, DyPs, and EfeB: 3 microbial heme enzyme families comprise the CDE structural superfamily. *J. Mol. Biol.* **2011**, *408*, 379–398.
- (15) Chaplin, A. K.; Wilson, M. T.; Worrall, J. A. R. Kinetic characterisation of a dye decolorising peroxidase from *Streptomyces lividans*: new insight into the mechanism of anthraquinone dye decolorisation. *Dalton Trans.* **2017**, *46*, 9420–9429.
- (16) Sugano, Y. DyP-type peroxidases comprise a novel heme peroxidase family. *Cell. Mol. Life Sci.* **2009**, *66*, 1387–1403.
- (17) Rahmanpour, R.; Rea, D.; Jamshidi, S.; Füllöp, V.; Bugg, T. D. H. Structure of *Thermobifida fusca* DyP-type peroxidase and activity towards Kraft lignin and lignin model compounds. *Arch. Biochem. Biophys.* **2016**, *594*, 54–60.
- (18) Yoshida, T.; Tsuge, H.; Hisabori, T.; Sugano, Y. Crystal structures of dye-decolorizing peroxidase with ascorbic acid and 2,6-dimethoxyphenol. *FEBS Lett.* **2012**, *586*, 4351–4356.
- (19) Nys, K.; Furtmüller, P. G.; Obinger, C.; van Doorslaer, S.; Pfanzagl, V. On the track of long-range electron transfer in B-type dye-decolorizing peroxidases: identification of a tyrosyl radical by computational prediction and electron paramagnetic resonance spectroscopy. *Biochemistry* **2021**, *60*, 1226–1241.
- (20) Strittmatter, E.; Wachter, S.; Liers, C.; Ullrich, R.; Hofrichter, M.; Plattner, D. A.; Piontek, K. Radical formation on a conserved tyrosine residue is crucial for DyP activity. *Arch. Biochem. Biophys.* **2013**, *537*, 161–167.
- (21) Avram, A.; Sengupta, A.; Pfromm, P. H.; Zorn, H.; Lorenz, P.; Schwarz, T.; Nguyen, K. Q.; Czermak, P. Novel DyP from the basidiomycete *Pleurotus sapidus*: substrate screening and kinetics. *Biocatalysis* **2018**, *4*, 1–13.
- (22) Zitare, U. A.; Habib, M. H.; Rozeboom, H.; Mascotti, M. L.; Todorovic, S.; Fraaije, M. W. Mutational and structural analysis of an ancestral fungal dye-decolorizing peroxidase. *FEBS J.* **2021**, *288*, 3602–3618.
- (23) Pupart, H.; Jöul, P.; Bramanis, M. I.; Lukk, T. Characterization of the ensemble of lignin-remodeling DyP-type peroxidases from *Streptomyces coelicolor* A3(2). *Energies* **2023**, *16*, 1557.
- (24) Brissos, V.; Tavares, D.; Sousa, A. C.; Robalo, M. P.; Martins, L. O. Engineering a bacterial DyP-type peroxidase for enhanced oxidation of lignin-related phenolics at alkaline pH. *ACS Catal.* **2017**, *7*, 3454–3465.
- (25) Rodrigues, C. F.; Borges, P. T.; Scocozza, M. F.; Silva, D.; Tabora, A.; Brissos, V.; Frazão, C.; Martins, L. O. Loops around the heme pocket have a critical role in the function and stability of BsDyP from *Bacillus subtilis*. *Int. J. Mol. Sci.* **2021**, *22*, 10862.
- (26) Santos, A.; Mendes, S.; Brissos, V.; Martins, L. O. New dye-decolorizing peroxidases from *Bacillus subtilis* and *Pseudomonas putida* MET94: towards biotechnological applications. *Appl. Microbiol. Biotechnol.* **2014**, *98*, 2053–2065.
- (27) Chen, C.; Shrestha, R.; Jia, K.; Gao, P. F.; Geisbrecht, B. V.; Bossmann, S. H.; Shi, J.; Li, P. Characterization of dye-decolorizing peroxidase (DyP) from *Thermomonospora curvata* reveals unique catalytic properties of A-type DyPs. *J. Biol. Chem.* **2015**, *290*, 23447–23463.
- (28) Shrestha, R.; Chen, X.; Ramyar, K. X.; Hayati, Z.; Carlson, E. A.; Bossmann, S. H.; Song, L.; Geisbrecht, B. V.; Li, P. Identification of surface-exposed protein radicals and a substrate oxidation site in A-class dye-decolorizing peroxidase from *Thermomonospora curvata*. *ACS Catal.* **2016**, *6*, 8036–8047.
- (29) Liers, C.; Bobeth, C.; Pecyna, M.; Ullrich, R.; Hofrichter, M. DyP-like peroxidases of the jelly fungus *Auricularia auricula-judae* oxidize nonphenolic lignin model compounds and high-redox potential dyes. *Appl. Microbiol. Biotechnol.* **2010**, *85*, 1869–1879.
- (30) Duan, Z.; Shen, R.; Liu, B.; Yao, M.; Jia, R. Comprehensive investigation of a dye-decolorizing peroxidase and a manganese peroxidase from *Irpex lacteus* F17, a lignin-degrading basidiomycete. *AMB Express* **2018**, *8*, 119.
- (31) Salvachúa, D.; Prieto, A.; Martínez, Á. T.; Martínez, M. J. Characterization of a novel dye-decolorizing peroxidase (DyP)-type

- enzyme from *Irpex lacteus* and its application in enzymatic hydrolysis of wheat straw. *Appl. Environ. Microbiol.* **2013**, *79*, 4316–4324.
- (32) Liers, C.; Pecyna, M. J.; Kellner, H.; Worrlich, A.; Zorn, H.; Steffen, K. T.; Hofrichter, M.; Ullrich, R. Substrate oxidation by dye-decolorizing peroxidases (DyPs) from wood- and litter-degrading agaricomycetes compared to other fungal and plant heme-peroxidases. *Appl. Microbiol. Biotechnol.* **2013**, *97*, 5839–5849.
- (33) Johjima, T.; Ohkuma, M.; Kudo, T. Isolation and cDNA cloning of novel hydrogen peroxide-dependent phenol oxidase from the basidiomycete *Termitomyces albuminosus*. *Appl. Microbiol. Biotechnol.* **2003**, *61*, 220–225.
- (34) Lauber, C.; Schwarz, T.; Nguyen, Q. K.; Lorenz, P.; Lochnit, G.; Zorn, H. Identification, heterologous expression and characterization of a dye-decolorizing peroxidase of *Pleurotus sapidus*. *AMB Express* **2017**, *7*, 164.
- (35) Zubietta, C.; Joseph, R.; Krishna, S. S.; McMullan, D.; Kapoor, M.; Axelrod, H. L.; Miller, M. D.; Abdubek, P.; Acosta, C.; Astakhova, T.; et al. Identification and structural characterization of heme binding in a novel dye-decolorizing peroxidase, TyrA. *Proteins* **2007**, *69*, 234–243.
- (36) Sturm, A.; Schierhorn, A.; Lindenstrauß, U.; Lilie, H.; Brüser, T. YcdB from *Escherichia coli* reveals a novel class of Tat-dependently translocated hemoproteins. *J. Biol. Chem.* **2006**, *281*, 13972–13978.
- (37) Uchida, T.; Sasaki, M.; Tanaka, Y.; Ishimori, K. A dye-decolorizing peroxidase from *Vibrio cholerae*. *Biochemistry* **2015**, *54*, 6610–6621.
- (38) Musengi, A.; Durrell, K.; Prins, A.; Khan, N.; Agunbiade, M.; Kudanga, T.; Kirby-McCullough, B.; Pletschke, B. I.; Burton, S. G.; Le Roes-Hill, M. Production and characterisation of a novel actinobacterial DyP-type peroxidase and its application in coupling of phenolic monomers. *Enzyme Microb. Technol.* **2020**, *141*, No. 109654.
- (39) Pfanzagl, V.; Nys, K.; Bellei, M.; Michlits, H.; Mlynek, G.; Battistuzzi, G.; Djinovic-Carugo, K.; van Doorslaer, S.; Furtmüller, P. G.; Hofbauer, S.; Obinger, C. Roles of distal aspartate and arginine of B-class dye-decolorizing peroxidase in heterolytic hydrogen peroxide cleavage. *J. Biol. Chem.* **2018**, *293*, 14823–14838.
- (40) Habib, M. H.; Rozeboom, H. J.; Fraaije, M. W. Characterization of a new DyP-peroxidase from the alkaliphilic Cellulomonad, *Cellulomonas bogoriensis*. *Molecules* **2019**, *24*, 1208.
- (41) Shrestha, R.; Huang, G.; Meekins, D. A.; Geisbrecht, B. V.; Li, P. Mechanistic insights into dye-decolorizing peroxidase revealed by solvent isotope and viscosity effects. *ACS Catal.* **2017**, *7*, 6352–6364.
- (42) Ogola, H. J. O.; Kamiike, T.; Hashimoto, N.; Ashida, H.; Ishikawa, T.; Shibata, H.; Sawa, Y. Molecular characterization of a novel peroxidase from the cyanobacterium *Anabaena* sp. strain PCC 7120. *Appl. Environ. Microbiol.* **2009**, *75*, 7509–7518.
- (43) Yoshida, T.; Ogola, H. J.; Amano, Y.; Hisabori, T.; Ashida, H.; Sawa, Y.; Tsuge, H.; Sugano, Y. *Anabaena* sp. DyP-type peroxidase is a tetramer consisting of two asymmetric dimers. *Proteins* **2016**, *84*, 31–42.
- (44) Ebihara, A.; Okamoto, A.; Kousumi, Y.; Yamamoto, H.; Masui, R.; Ueyama, N.; Yokoyama, S.; Kuramitsu, S. Structure-based functional identification of a novel heme-binding protein from *Thermus thermophilus* HB8. *J. Struct. Funct. Genomics* **2005**, *6*, 21–32.
- (45) Rahmanpour, R.; Bugg, T. D. H. Assembly *in vitro* of *Rhodococcus jostii* RHA1 encapsulin and peroxidase DypB to form a nanocompartment. *FEBS J.* **2013**, *280*, 2097–2104.
- (46) Sutter, M.; Boehringer, D.; Gutmann, S.; Günther, S.; Prangishvili, D.; Loessner, M. J.; Stetter, K. O.; Weber-Ban, E.; Ban, N. Structural basis of enzyme encapsulation into a bacterial nanocompartment. *Nat. Struct. Mol. Biol.* **2008**, *15*, 939–947.
- (47) Sugawara, K.; Nishihashi, Y.; Narioka, T.; Yoshida, T.; Morita, M.; Sugano, Y. Characterization of a novel DyP-type peroxidase from *Streptomyces avermitilis*. *J. Biosci. Bioeng.* **2017**, *123*, 425–430.
- (48) Dhankhar, P.; Dalal, V.; Mahto, J. K.; Gurjar, B. R.; Tomar, S.; Sharma, A. K.; Kumar, P. Characterization of dye-decolorizing peroxidase from *Bacillus subtilis*. *Arch. Biochem. Biophys.* **2020**, *693*, No. 108590.
- (49) Li, J.; Liu, C.; Li, B.; Yuan, H.; Yang, J.; Zheng, B. Identification and molecular characterization of a novel DyP-type peroxidase from *Pseudomonas aeruginosa* PKE117. *Appl. Biochem. Biotechnol.* **2012**, *166*, 774–785.
- (50) Liu, X.; Du, Q.; Wang, Z.; Zhu, D.; Huang, Y.; Li, N.; Wei, T.; Xu, S.; Gu, L. Crystal structure and biochemical features of EfeB/YcdB from *Escherichia coli* O157: ASP235 plays divergent roles in different enzyme-catalyzed processes. *J. Biol. Chem.* **2011**, *286*, 14922–14931.
- (51) Cagide, C.; Marizcurrena, J. J.; Vallés, D.; Alvarez, B.; Castro-Sowinski, S. A bacterial cold-active dye-decolorizing peroxidase from an Antarctic *Pseudomonas* strain. *Appl. Microbiol. Biotechnol.* **2023**, *107*, 1707–1724.
- (52) Brown, M. E.; Barros, T.; Chang, M. C. Identification and characterization of a multifunctional dye peroxidase from a lignin-reactive bacterium. *ACS Chem. Biol.* **2012**, *7*, 2074–2081.
- (53) Contreras, H.; Joens, M. S.; McMath, L. M.; Le, V. P.; Tullius, M. V.; Kimmey, J. M.; Bionghi, N.; Horwitz, M. A.; Fitzpatrick, J. A.; Goulding, C. W. Characterization of a *Mycobacterium tuberculosis* nanocompartment and its potential cargo proteins. *J. Biol. Chem.* **2014**, *289*, 18279–18289.
- (54) Tang, Y.; Mu, A.; Zhang, Y.; Zhou, S.; Wang, W.; Lai, Y.; Zhou, X.; Liu, F.; Yang, X.; Gonga, H.; et al. Cryo-EM structure of *Mycobacterium smegmatis* DyP-loaded encapsulin. *Proc. Natl. Acad. Sci. U.S.A.* **2021**, *118*, No. e2025658118.
- (55) Putri, R. M.; Allende-Ballesterro, C.; Luque, D.; Klem, R.; Rousou, K. A.; Liu, A.; Traulsen, C. H.; Rurup, W. F.; Koay, M. S. T.; Castón, J. R.; Cornelissen, J. J. L. M. Structural Characterization of Native and Modified Encapsulins as Nanoplatforams for *in Vitro* Catalysis and Cellular Uptake. *ACS Nano* **2017**, *11*, 12796–12804.
- (56) Nelson, D. P.; Kiesow, L. A. Enthalpy of decomposition of hydrogen peroxide by catalase at 25° C (with molar extinction coefficients of H₂O₂ solutions in the UV). *Anal. Biochem.* **1972**, *49*, 474–478.
- (57) Kracher, D.; Scheiblbrandner, S.; Felice, A. K. G.; Breslmayr, E.; Preims, M.; Ludwicka, K.; Haltrich, D.; Eijnsink, V. G. H.; Ludwig, R. Extracellular electron transfer systems fuel cellulose oxidative degradation. *Science* **2016**, *352*, 1098–1101.
- (58) Moody, P. C. E.; Raven, E. L. The nature and reactivity of ferryl heme in compounds I and II. *Acc. Chem. Res.* **2018**, *51*, 427–435.
- (59) Strittmatter, E.; Serrer, K.; Liers, C.; Ullrich, R.; Hofrichter, M.; Piontek, K.; Schleider, E.; Platter, D. A. The toolbox of *Auricularia auricula-judae* dye-decolorizing peroxidase – Identification of three new potential substrate-interaction sites. *Arch. Biochem. Biophys.* **2015**, *574*, 75–85.
- (60) Chaplin, A. K.; Chicano, T. M.; Hampshire, B. V.; Wilson, M. T.; Hough, M. A.; Svistunenko, D. A.; Worrall, J. A. R. An aromatic dyad motif in dye decolorising peroxidases has implications for free radical formation and catalysis. *Chem. – Eur. J.* **2019**, *25*, 6141–6153.
- (61) Linde, D.; Ayuso-Fernandez, I.; Laloux, M.; Aguiar-Cervera, J. E.; de Lacey, A. L.; Ruiz-Duenas, F. J.; Martinez, A. T. Comparing ligninolytic capabilities of bacterial and fungal dye-decolorizing peroxidases and class-II peroxidase-catalase. *Int. J. Mol. Sci.* **2021**, *22*, 2629.
- (62) Lučić, M.; Wilson, M. T.; Svistunenko, D. A.; Owen, R. L.; Hough, M. A.; Worrall, J. A. R. Aspartate or arginine? Validated redox state X-ray structures elucidate mechanistic subtleties of Fe^{IV} = O formation in bacterial dye-decolorizing peroxidases. *J. Biol. Inorg. Chem.* **2021**, *26*, 743–761.
- (63) Svergun, D. I. Determination of the regularization parameter in indirect-transform methods using perceptual criteria. *J. Appl. Crystallogr.* **1992**, *25*, 495–503.
- (64) Schneidman-Duhovny, D.; Hammel, M.; Tainer, J. A.; Sali, A. FoXS, FoXSDock and MultiFoXS: Single-state and multi-state structural modeling of proteins and their complexes based on SAXS profiles. *Nucleic Acids Res.* **2016**, *44*, W424–W429.

Supporting information to:

Dye-decolorizing peroxidase of *Streptomyces coelicolor* (ScDyPB) exists as a dynamic mixture of kinetically different oligomers

Hegne Pupart^{a§}, Darja Vastšjonok^{b§}, Tiit Lukk^a, and Priit Väljamäe^{b*}

^aDepartment of Chemistry and Biotechnology, Tallinn University of Technology, 15 Akadeemia tee, Tallinn, 12618, Estonia

^bInstitute of Molecular and Cell Biology, University of Tartu, Riia 23b-202, Tartu, 51010, Estonia

*Email: priit.valjamae@ut.ee

§H.P. and D.V. contributed equally to this work.

KEYWORDS

dye-decolorizing peroxidase, substrate inhibition, enzyme oligomers, *Streptomyces coelicolor*

Supplementary figures:

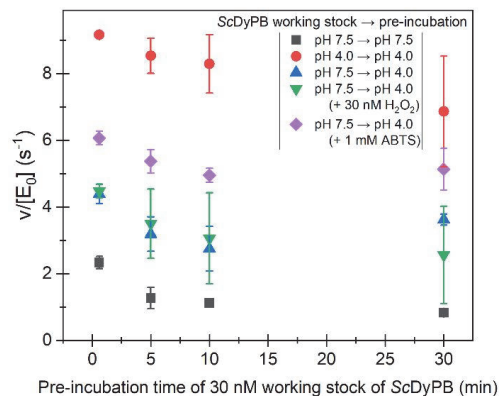


Figure S1. Effects of pre-incubation time of ScDyPB working stocks before the measurement of the activity with ABTS. 1.5 μM ScDyPB working stock (supplemented with 0.1 g L⁻¹ BSA) was prepared in NaAc pH 4.0 or Tris-HCl pH 7.5, 0.1 M NaCl buffer. 10 μL of this working stock was added to the cuvette containing 490 μL of 50 mM NaAc pH 4.0 or 5 mM Tris-HCl pH 7.5 (supplemented with 25 mM NaCl) and the resulting 30 nM ScDyPB was pre-incubated at 25 °C for selected times before activity measurement with 1 mM ABTS and 0.1 mM H₂O₂. Activity measurements were started by adding 0.5 mL of the mixture of ABTS and H₂O₂ (at appropriate concentrations in 100 mM or 50 mM NaAc pH 4.0 for pre-incubations at pH 7.5 or pH 4.0, respectively) to the cuvette containing 0.5 mL pre-incubated 30 nM ScDyPB. In one series the 30 nM ScDyPB was pre-incubated in the presence of 1 mM ABTS or 30 nM H₂O₂ as shown in the plot. The pH of the 1.5 μM ScDyPB working stock as well as the pH of the pre-incubation mixture is also indicated in the plot. Data are presented as average values ($n = 3$, independent experiments) and error bars show SD.

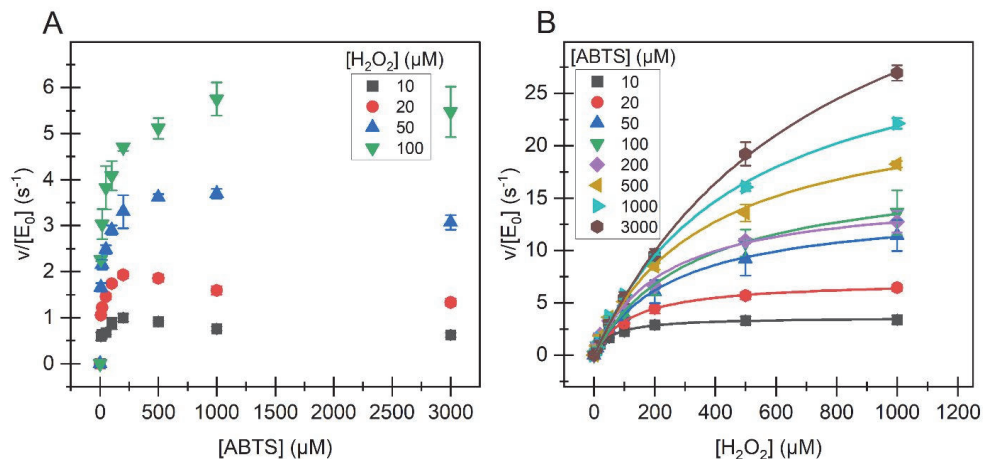


Figure S2. Kinetics of the oxidation of ABTS. Dependency of the initial rates of the oxidation of ABTS on the concentration of (A) ABTS and (B) H₂O₂. Reactions were made in 50 mM NaAc (pH 4.0) at 25 °C. Concentration of ScDyPB was 15 nM and the reactions were initiated by the addition of ScDyPB from the working stock with 1.5 μM ScDyPB in 20 mM Tris pH 7.5 (supplemented with 0.1 g L⁻¹ BSA and 0.1 M NaCl). Shown are the same data as in the Figure 3 A and B of the main article but in panel A the data with H₂O₂ concentrations above 100 μM are omitted for better visual inspection of the substrate inhibition by ABTS. Solid lines in panel B show non-linear regression of the data according to the Michaelis Menten equation (equation S1 below). The concentration of the substrate that was constant within the series is indicated in the plot. The data are presented as the average values ($n = 3$, independent measurements), and the error bars show the SD.

$$\frac{v_i}{E_0} = \frac{k_{cat}^{app} [H_2O_2]}{[H_2O_2] + K_M^{app}(H_2O_2)} \quad (S1)$$

In equation S1 the k_{cat}^{app} and $K_M^{app}(H_2O_2)$ stand for the apparent (*i.e.* depends on [ABTS]) catalytic constant and Michaelis constant for H₂O₂, respectively. Following relationships between apparent k_{cat} and k_{cat}/K_M for H₂O₂ and the concentration of ABTS are expected for the enzyme obeying ping-pong kinetics with substrate inhibition by ABTS:

$$k_{cat}^{app} = \frac{k_{cat}[ABTS]}{[ABTS] + K_M(ABTS)} \quad (S2)$$

$$\frac{k_{cat}^{app}}{K_M^{app}(H_2O_2)} = \frac{k_{cat}}{K_M(H_2O_2)} \left(\frac{K_{i(ABTS)}}{K_{i(ABTS)} + [ABTS]} \right) \quad (S3)$$

k_{cat} and $K_M(H_2O_2)$ in equations S2 and S3 are the true catalytic constant and Michaelis constant for H₂O₂, respectively, whereas $K_{i(ABTS)}$ stands for the substrate inhibition constant by ABTS.

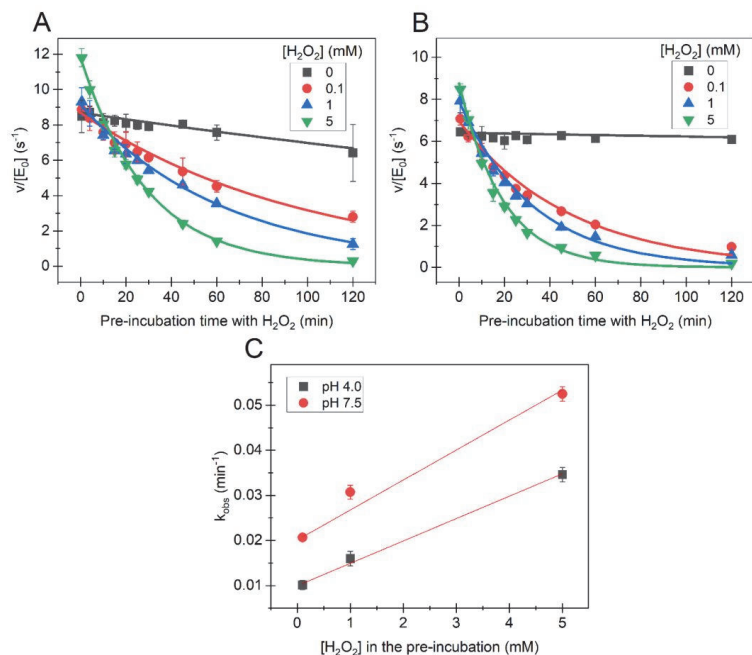


Figure S3. Inactivation of *ScDyPB* by H₂O₂. 1.5 μM *ScDyPB* (supplemented with 0.1 g L⁻¹ BSA) in (A) 50 mM NaAc (pH 4.0) or (B) 20 mM Tris-HCl (pH 7.5) was pre-incubated with different concentrations of H₂O₂ (as indicated in the figure) at 25 °C. At selected times 10 μL aliquot was withdrawn and added to the cuvette containing 990 μL of the mixture of 1 mM ABTS and 0.1 mM H₂O₂ and the activity was measured by the increase in the absorbance at 420 nm. Solid lines show non-linear regression of the data according to the equation for the first-order reaction (equation S4 below). (C) The dependency of the observed first order rate constant of inactivation of *ScDyPB* (k_{obs}) on the concentration of H₂O₂ in the pre-incubation at pH 4.0 and pH 7.5 (shown in the plot). The dotted line shows linear regression of the data according to the equation S5 below. Data are presented as average values ($n = 3$, independent experiments) and error bars show SD.

$$\frac{v_i}{E_0} = \left(\frac{v_i}{E_0}\right)_{max} e^{-k_{obs}t} \quad (S4)$$

In equation S4 the $(v_i/E_0)_{max}$ is the value of v_i/E_0 at pre-incubation time zero and the k_{obs} is the observed first order rate constant for the decay of activity during pre-incubation with H₂O₂. Note that a slight increase in the value of v_i/E_0 in the experiments with high (5 mM) concentration of H₂O₂ in pre-incubation is caused by the increase in the concentration of H₂O₂ in activity measurements.

$$k_{obs} = k_i[H_2O_2] + k_0 \quad (S5)$$

The k_i and k_0 in equation S5 stand for the second order rate constant of the inactivation by H₂O₂ and first order rate constant of the inactivation in the absence of added H₂O₂, respectively.

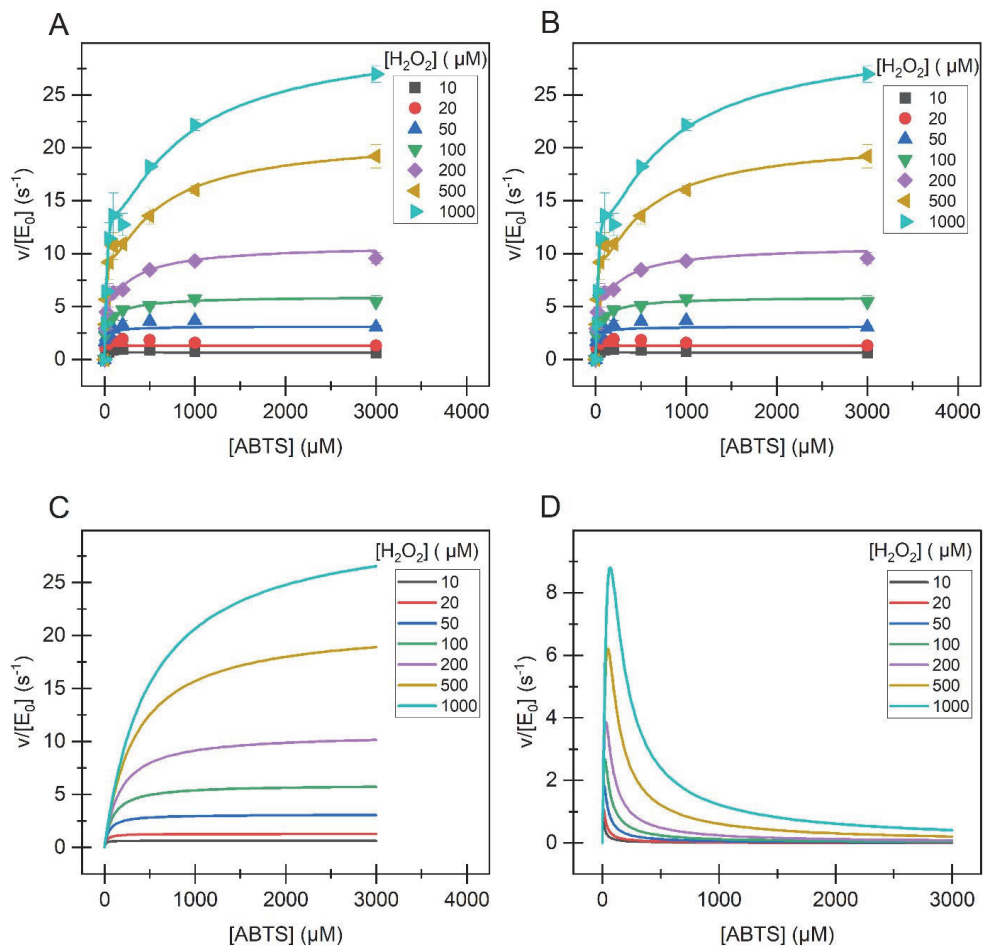


Figure S4. Comparison of the fitting of the data of ABTS oxidation according to the equations 1 and 2, and contribution of the enzyme forms E^I and E^{II} . The experiment data are the same as those in Fig. 4A of the main article. Solid lines show the result of the global non-linear regression analysis according to equation 1 (A) or equation 2 (B) of the main article. Contribution of the two enzyme forms E^I (C) and E^{II} (D) in ABTS oxidizing activity. The activity of enzyme forms was calculated using the parameter values obtained from the global non-linear regression analysis according to equation 2 and leftmost and rightmost side of sum in the equation 2 for the form E^I and E^{II} , respectively.

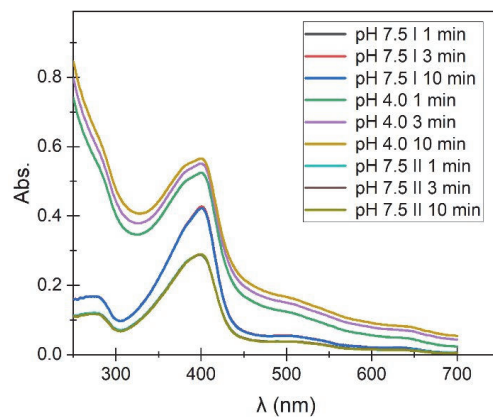


Figure S5. Absorbance spectra of *ScDyPB*. After recording the spectrum of 3.6 μM *ScDyPB* in 4 mM Tris-HCl (pH 7.5, supplemented with 20 mM NaCl) in 0.5 mL total volume (designated as pH 7.5 I) the pH was brought to 4.0 by the addition of 26 μL of 1.0 M NaAc (pH 4.0) and spectra were recorded again (designated as pH 4.0). Finally, 150 μL of 1.0 M Tris-HCl (pH 7.5) was added and spectra were recorded (designated as pH 7.5 II). In the case of each condition, the spectra were recorded 1, 3, and 10 min after changing the condition (as indicated in the plot). Note that in the case of pH 7.5 the spectra recorded at different times after changing the condition overlap.

Curriculum vitae

Personal data

Name: Hegne Pupart
Date of birth: 2 July 1994
Place of birth: Kuressaare, Estonia
Citizenship: Estonian

Contact data

E-mail: hegne.pupart@taltech.ee

Education

2019–... Tallinn University of Technology, Chemistry, PhD
2017–2019 Tallinn University of Technology, Applied Chemistry and Biotechnology, MSc
2013–2017 University of Tartu, Chemistry, BSc
2010–2013 Saaremaa Co-Educational Gymnasium

Language competence

Estonian native language
English fluent
German intermediate
Russian beginner
French beginner

Professional employment

2019–... early-stage researcher, Department of Chemistry and Biotechnology, Tallinn University of Technology, Estonia
June–Aug. 2018 intern, Division of Biology and Chemistry, Paul Scherrer Institute, Switzerland
July–Aug. 2015 intern, Icosagen Cell Factory, Estonia

Other administrative and professional activities

2019–... Estonian Biochemical Society, member

Publications

Pupart, H.; Lukk, T.; Väljamäe, P. Dye-decolorizing peroxidase of *Thermobifida halotolerance* displays complex kinetics with both substrate inhibition and apparent positive cooperativity. *Arch Biochem Biophys* **2024**, *754*, 109931. <https://doi.org/10.1016/j.abb.2024.109931>.

Pupart, H.; Vastšjonok, D.; Lukk, T. and Väljamäe, P. Dye-Decolorizing Peroxidase of *Streptomyces coelicolor* (ScDyPB) Exists as a Dynamic Mixture of Kinetically Different Oligomers. *ACS Omega* **2024**, *9*, 3866–3876. <https://doi.org/10.1021/acsomega.3c07963>.

Pupart, H.; Jõul, P.; Bramanis, M. I.; Lukk, T. Characterization of the Ensemble of Lignin Remodeling DyP-Type Peroxidases from *Streptomyces coelicolor* A3(2). *Energies* **2023**, *16*, 1557. <https://doi.org/10.3390/en16031557>.

Zovo, K.; **Pupart, H.**; Van Wieren, A.; Gillilan, R. E.; Huang, Q.; Majumdar, S.; Lukk, T. Substitution of the Methionine Axial Ligand of the T1 Copper for the Fungal-like Phenylalanine Ligand (M298F) Causes Local Structural Perturbations that Lead to Thermal Instability and Reduced Catalytic Efficiency of the Small Laccase from *Streptomyces coelicolor* A3(2). *ACS Omega* **2022**, *7*, 6184–6194. <https://doi.org/10.1021/acsomega.1c06668>.

Smirnova, J.; Gavrilova, J.; Noormägi, A.; Valmsen, K.; **Pupart, H.**; Luo, J.; Tõugu, V.; Palumaa, P. Evaluation of Zn²⁺- and Cu²⁺-Binding Affinities of Native Cu, Zn-SOD1 and Its G93A Mutant by LC-ICP MS. *Molecules* **2022**, *27*, 3160. <https://doi.org/10.3390/molecules27103160>.

Wu, J.; Österlund, N.; Wang, H.; Sterneke-Hoffmann, R.; **Pupart, H.**; Ilag, L. L.; Gräslund, A.; Luo, J. Identifying the role of co-aggregation of Alzheimer's amyloid- β with amorphous protein aggregates of non-amyloid proteins. *Cell Reports Physical Science* **2022**, *3*, 101028. <https://doi.org/10.1016/j.xcrp.2022.101028>.

Elulookirjeldus

Isikuandmed

Nimi: Hegne Pupart
Sünniaeg: 2. juuli 1994
Sünnikoht: Kuressaare, Eesti
Kodakondsus: eestlane

Kontaktandmed

E-post: hegne.pupart@taltech.ee

Hariduskäik

2019–... Tallinna Tehnikaülikool, Keemia, PhD
2017–2019 Tallinna Tehnikaülikool, Rakenduskeemia ja biotehnoloogia, MSc
2013–2017 Tartu Ülikool, Keemia, BSc
2010–2013 Saaremaa Ühisgümnaasium

Keelteoskus

eesti keel emakeel
inglise keel kõrgtase
saksa keel keskase
vene keel algtase
prantsuse keel algtase

Teenistuskäik

2019–... doktorant-nooremteadur, Keemia ja Biotehnoloogia Instituut, Tallinna Tehnikaülikool, Eesti
juuni–august 2018 praktikant, Bioloogia ja Keemia Osakond, Paul Scherrer Institute, Šveits
juuli–august 2015 praktikant, Icosagen Cell Factory OÜ, Eesti

Muu teaduslik organisatsiooniline ja erialane tegevus

2019–... Eesti Biokeemia Selts, liige

Publikatsioonid

Pupart, H.; Lukk, T.; Väljamäe, P. Dye-decolorizing peroxidase of *Thermobifida halotolerance* displays complex kinetics with both substrate inhibition and apparent positive cooperativity. *Arch Biochem Biophys* **2024**, *754*, 109931. <https://doi.org/10.1016/j.abb.2024.109931>.

Pupart, H.; Vastšjonok, D.; Lukk, T. and Väljamäe, P. Dye-Decolorizing Peroxidase of *Streptomyces coelicolor* (ScDyPB) Exists as a Dynamic Mixture of Kinetically Different Oligomers. *ACS Omega* **2024**, *9*, 3866–3876. <https://doi.org/10.1021/acsomega.3c07963>.

Pupart, H.; Jõul, P.; Bramanis, M. I.; Lukk, T. Characterization of the Ensemble of Lignin Remodeling DyP-Type Peroxidases from *Streptomyces coelicolor* A3(2). *Energies* **2023**, *16*, 1557. <https://doi.org/10.3390/en16031557>.

Zovo, K.; **Pupart, H.**; Van Wieren, A.; Gillilan, R. E.; Huang, Q.; Majumdar, S.; Lukk, T. Substitution of the Methionine Axial Ligand of the T1 Copper for the Fungal-like Phenylalanine Ligand (M298F) Causes Local Structural Perturbations that Lead to Thermal Instability and Reduced Catalytic Efficiency of the Small Laccase from *Streptomyces coelicolor* A3(2). *ACS Omega* **2022**, *7*, 6184–6194. <https://doi.org/10.1021/acsomega.1c06668>.

Smirnova, J.; Gavrilova, J.; Noormägi, A.; Valmsen, K.; **Pupart, H.**; Luo, J.; Tõugu, V.; Palumaa, P. Evaluation of Zn²⁺- and Cu²⁺-Binding Affinities of Native Cu, Zn-SOD1 and Its G93A Mutant by LC-ICP MS. *Molecules* **2022**, *27*, 3160. <https://doi.org/10.3390/molecules27103160>.

Wu, J.; Österlund, N.; Wang, H.; Sterneke-Hoffmann, R.; **Pupart, H.**; Ilag, L. L.; Gräslund, A.; Luo, J. Identifying the role of co-aggregation of Alzheimer's amyloid- β with amorphous protein aggregates of non-amyloid proteins. *Cell Reports Physical Science* **2022**, *3*, 101028. <https://doi.org/10.1016/j.xcrp.2022.101028>.

ISSN 2585-6901 (PDF)
ISBN 978-9916-80-239-7 (PDF)